Fermions, criticality and superconductivity

She, J.H.

Fermions, Criticality and Superconductivity

PROEFSCHRIFT

ter verkrijging van de graad
van Doctor aan de Universiteit Leiden, op gezag van
Rector Magnificus Prof. mr. P. F. van der Heijden,
volgens besluit van het College voor Promoties
te verdedigen op dinsdag 3 mei 2011
te klokke 13.45 uur

door

Jian-Huang She

geboren te Rudong, China,
in 1981

Promotiecommissie:

Promotor:	Prof. dr. J. Zaanen
Overige leden:	Prof. dr. J. M. van Ruitenbeek (Universiteit Leiden)
	Prof. dr. A. V. Balatsky (Los Alamos National Laboratory)
	Prof. dr. D. van der Marel (University of Geneva)
	Prof. dr. ir. H. Hilgenkamp (Universiteit Leiden en Universiteit Twente)
	Prof. dr. C. W. J. Beenakker (Universiteit Leiden)
	Dr. K. E. Schalm (Universiteit Leiden)

Casimir PhD Series, Delft-Leiden, 2011-06
ISBN 978-90-8593-095-2

The research described in this thesis was supported by the Netherlands Organisation for Scientific Research (NWO) through a Spinoza Prize grant.

To my family

Contents

Chapter 1

Introduction

In the early days of quantum physics, the study of many-body systems was regarded as messy, ugly and undignified. The solution of the Schrödinger equation for the hydrogen atom was the hallmark of modern physics. But trying to generalize this procedure to 10^{23} atoms interacting with each other, as is the case in real materials, seems pointless. A huge number of approximations need to be made before one can arrive at any concrete conclusions. Pauli, himself one of the pioneers of the field, had called the study of many-body systems 'dirt physics'.

Thanks to the hard work of several generations of researchers, including the greatest names of all time, such as Lev Landau, John Bardeen, Ken Wilson, Phil Anderson and Bob Laughlin, it has become clear today that many-body physics, under the name *Condensed Matter Physics* replacing the old one *Solid State Physics*, is indeed governed by deep and simple physical principles, which are different from those governing the individual atoms constituting the system. The symmetry of the macroscopic system can be different from that of the microscopic Hamiltonian. The excitations of the macroscopic system can have different charge, spin and statistics as compared to the constituent microscopic particles. These new principles operating at the macroscopic scale are called *emergent*. The appearance of this theme led Anderson to coin the phrase 'More is Different', emphasizing that the study of many-body physics is as equal and fundamental as, say the study of the elementary particles. Sometimes these new principles are written in terms of the sophisticated and beautiful language of higher mathematics, and the Einstein-Dirac type thinking can lead to fruitful discoveries in many-body physics.

The two most important organizing principles that came out of the several decades' investigation of emergent phenomena are spontaneous symmetry breaking (SSB) and adiabatic continuity. SSB refers to the fact that the symmetry of the ground state is different from the symmetry of space or the Hamiltonian describing the system. This is actually something we meet constantly in our everyday life: our desk does not have the translational and rotational symmetry that the Schrödinger equation describing its atomic degrees of freedom possesses. Nevertheless this principle is extremely powerful: instead of describing the system using 10^{23} variables, which is an impossible task, we can now use only one or a few. These few variables are called order parameters (OP). SSB is a quite universal principle, capturing the physics of diverse phenomena, ranging from simple crystals to various density waves, smectic and nematic ordering, from magnetism to superfluidity and superconductivity, even generation of mass. The order parameters can fluctuate in space and time, and field-theoretical methods can be employed. This has opened the door to a whole new world. Later on gauge fields were incorporated, and very recently even gravitational fields have been used to model condensed matter systems.

The prototype of adiabatic continuity is Landau's theory of Fermi liquids. It describes strongly interacting electron systems, for which naive perturbation theory obviously breaks down. The basic insight is that the low energy and low temperature properties of such systems are governed by Fermi-Dirac statistics. The simplest system that possesses this statistics is the free Fermi gas. One can imagine the following process: start from the non-interacting free Fermi gas, and gradually turn on interactions. As long as the system stays away from any phase transitions, the qualitative behavior of the system does not change. For Fermi liquids at low temperature, the specific heat has a linear temperature dependence, the resistivity is quadratic and the spin susceptibility nearly constant, as is the case for free Fermi gas. The main focus here are the excitations. Let us think about the energy levels of the system during this process. There is a shift in each energy level, but they do not cross each other. In other words, the labeling of the energy levels does not change. In this framework, such strongly interacting many-body systems can again be characterized by a rather small number of parameters.

These two principles are so powerful that they have dominated the landscape of condensed matter physics for years, leaving most theorists doing just engineering work: bosonic order parameters + Fermi gas + perturbations around them. However, as always, dark clouds appear in the perfect sky. In 1982, a new state of matter was discovered in the two-dimensional electron gases under a strong magnetic field, the so-called fractional quantum hall states. These states can not be adiabatically continued to free fermions. They do not break any continuous symmetry and can not be described by a conventional order parameter. They are actually topological in nature. Investigations in this direction lead to fruitful outcomes, with groundbreaking wavefunctions, beautiful field theories and even predictions of new states of matter.

The second dark cloud that has develpoed into a serious intellectual crisis over the last twenty years or so is in the condensed matter physics enterprise dealing with strongly interacting electrons in solids. This field is flourishing right now and there is a general perception that after a slump in the 1990's the field has reinvented itself. What is this intellectual crisis about? Substantial progress has been made on the experimental side, both with regard to the discovery of electron systems in solids that behave in very interesting and puzzling ways (high-T_c superconductors [1] and other oxides [2], heavy fermion intermetallics [3], organics [4], 2DEG's in semiconductors [5]), and in the rapid progress of new instruments that make it possible to probe deeper and farther in these mysterious electron worlds (scanning tunneling spectroscopy [6], photoemission [7], neutron- [8] and resonant X-ray scattering [9]). On the theoretical side there is also much action. This is energized by the 'quantum field theory' (QFT) revolution that started in the 1970's in high energy physics, and is still in the process of unfolding its full potential in the low energy realms, as exemplified by topological quantum computation, quantum criticality and so forth. However, the QFT approach still lies within the framework of bosonic order parameters + Fermi gas + perturbations.

We are forced by experimentalists to face the problem of building a theory for the system of strongly interacting fermions that can neither be adiabatically continued to a free Fermi gas, nor be described in terms of bosonic order parameters. And this will be the target of this thesis. In our opinion, the key point that hinders this task is the fermion sign problem. Via the Euclidean path integral, the theory of interacting bosons boils down to exercises in equilibrium statistical physics. It is about computing probabilistic partition sums in euclidean spacetime following the recipe of Boltzmann and this seems to have no secrets left. However, this Boltzmannian path integral logic does not work at all when one wants to describe problems characterized by a finite density of fermionic particles. The culprit is that the path integral is suffering from the fermion sign problem. The Boltzmannian computation is spoiled by 'negative probabilities' rendering the approach to be mathematically ill-defined. In fact, the mathematics is as bad as can be: Troyer and Wiese [10] showed recently that the sign problem falls in the mathematical complexity class 'NP hard', and the Clay Mathematics Institute has put one of its seven one million dollar prizes on the proof that such problems cannot be solved in polynomial time.

Although not always appreciated, the fermion sign problem is quite consequential for the understanding of the physical world. Understanding matter revolves around the understanding of the emergence principles prescribing how a large number of simple constituents (like elementary particles) manage to acquire very different properties when they form a wholeness. The path integral is telling us that in the absence of the signs these principles are the same for quantum matter as they are for classical matter. But these classical emergence principles are in turn resting on Bolzmannian statistical physics. When this fails because of the fermion signs, we can no longer be confident regarding our un-

derstanding of emergence. To put it positively, dealing with fermionic quantum matter there is room for surprises that can be very different from anything we know from the classical realms that shape our intuition. In fact, we have only comprehended one such form of fermionic matter: the Fermi gas, and its 'derivative' the Fermi liquid. The embarrassment is that we are completely in the dark regarding the nature of other forms of fermionic matter, although we know that they exist because the experiments are telling us so.

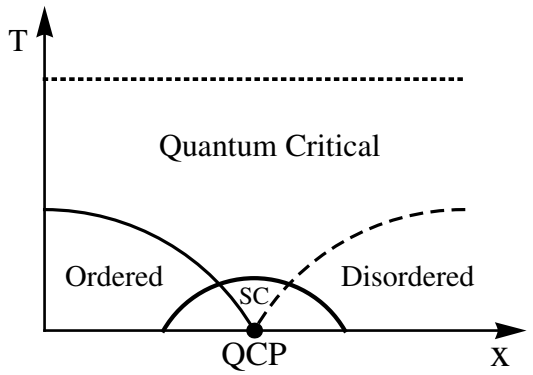

Figure 1.1: Illustration of the interplay of quantum criticality and superconductivity. x is the tuning parameter, which can be pressure, magnetic field or doping. The superconducting temperature usually has the highest value right above the QCP.

This thesis explores the emergent phenomena in the signful fermionic matters. In section 1.1, we introduce the two prototype materials of this thesis: cuprates and heavy fermions. The theme coming out the experimental findings is the phase diagram (1.1). By applying pressure, magnetic field, or doping, a second-order phase transition can be tuned to zero temperature, producing a quantum critical point (QCP). Such a singular point spreads out influence over a wide region in the phase diagram. Anomalous scaling behaviors thus emerge in various finite-temperature properties of the system, such as specific heat, resistivity and magnetic susceptibility, which go far beyond our conventional understanding of metals. Moreover, the QCP is a highly degenerate state. On approach to the QCP, a perturbation that was deemed irrelevant initially, takes over and dominates at low temperature, replacing the QCP by an alternative stable phase. In this way new states of matter that can not be constructed from stable states like normal metals or superconductors can be built. One common way to avoid the critical singularity is that the electrons organize themselves collectively into a superconducting state before they reach the critical point.

In section 1.2, we give a somewhat unconventional discussion of Fermi liq-

uids. To get the problem sharply in focus, we step back from the usual textbook viewpoint and instead consider the Fermi liquid from the perspective of the emergence principles governing classical and bosonic matter. We then proceed in two opposite directions. One direction is to go microscopic and try to deconstruct the existing principles of emergence. We explore the worldline formulation of many particle systems initiated by Feynman. A simple introduction is given in section 1.3. The other direction is to go macroscopic and search for new organizing principles. The keyword here is quantum criticality, which will be introduced in section 1.4. In section 1.5, we outline the basic structure of the remainder of this thesis and summarize the main results.

1.1 The prototype materials of this thesis

1.1.1 Cuprates

Cuprates are a kind of transition metal oxides with layered structure made up of one or more copper oxygen planes. The initial interest in cuprates was triggered by the fact that they can become superconducting at anomalously high temperatures [11]. After more than 20 years' extensive study, with sample preparation sufficiently advanced and nearly all possible experimental tools applied, it has become clear that cuprates means much more than a high transition temperature, a number that can be as large as 160. Their properties in the normal state above the superconducting temperature are even more exotic, and that may also account for the unusually high T_c (see [12] for a comprehensive review).

It is now generally agreed that the active physics of cuprates lies in the CuO_2 plane, and the effect of the c-axis is basically to tune the electronic structure of the CuO_2 plane. For the parent compound without doping, each copper is surrounded by 4 oxygens in the planes, with the copper ion in the d^9 configuration, providing per unit cell a single 3d hole, and the oxygen ion in the p^6 configuration. The tetragonal environment promotes the $d_{x^2-y^2}$ orbital of the copper ions to higher energy level, which further mixes with the oxygen p_x and p_y orbitals, forming a strong covalent bond. The question is then where the holes reside. A crucial insight is that there is a strong repulsion when two electrons or two holes are placed on the same ion. The energy to doubly occupy the copper d orbital is actually the largest energy scale in the problem. It also costs more energy for the holes to be placed at the oxygen p orbitals than at the copper d orbitals. When this energy difference is large enough, as is the case for cuprates, the holes will mainly just stay at the lattice sites of copper atoms, forming a charge transfer insulator with localized moments [13]. Virtual hopping to nearby oxygen p orbitals induces an exchange interaction between these local moments, and the insulator is actually in an antiferromagnetic ground state.

When replacing, say some La by Sr, more holes are added to the CuO_2 plane. These extra holes will occupy the oxygen p orbitals at the first place. A metallic

state is formed when these holes hop around among the oxygen p orbitals. However, the Cu-O hybridization creates a new low lying resonate state, in which the local moment on the copper lattice site forms a local spin singlet with the spin of the doped hole residing on the neighboring square of the oxygen atoms [14]. These singlets can hop from one site to another, and the low energy physics is captured by a one-band tight-binding model on the square lattice. This way, cuprates present an almost perfect realization of the simple single-band Hubbard model, with the energy difference between the oxygen p orbital and copper d orbital playing the role of the Hubbard U. When this energy difference is large, the problem is further reduced to the t-J model,

$$H = -P\left[\sum_{<ij>,\sigma} t_{ij} c^{\dagger}_{i\sigma} c_{i\sigma}\right] P + \sum_{<ij>} J_{ij}\mathbf{S}_i \cdot \mathbf{S}_j, \tag{1.1}$$

where $c^{\dagger}_{i\sigma}$ and $c_{i\sigma}$ are the fermion creation and annihilation operators, and $\mathbf{S}_i$ the spin operator. The crucial part is the Gutzwiller projection operator P which eliminates double occupancies. The essential physics of the t-J model is encapsulated by the trial wavefunctions proposed by Anderson: $\Psi_{tJ}(\mathbf{r}_1, \cdots, \mathbf{r}_N) = P\Phi_{\mathrm{HF}}(\mathbf{r}_1, \cdots, \mathbf{r}_N)$, with Φ_{HF} a Hatree-Fock wavefunction for either conventional Fermi liquid or BCS superconductor. The projection operator is a singular transformation. Thus Ψ_{tJ} and Φ_{HF} can not be adiabatically continued to each other.

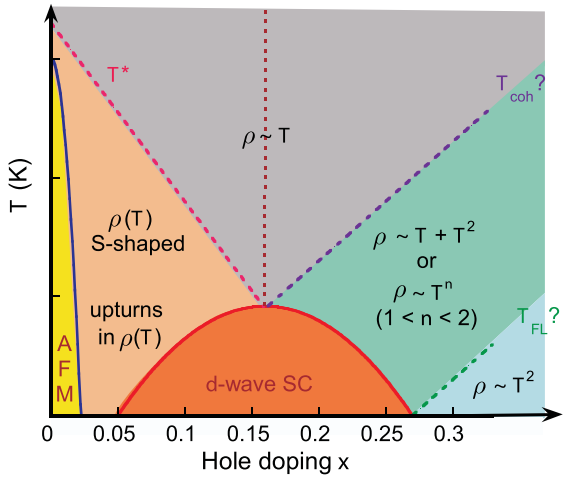

Figure 1.2: Phase diagram of cuprates as determined by transport measurements (from Hussey [15]).

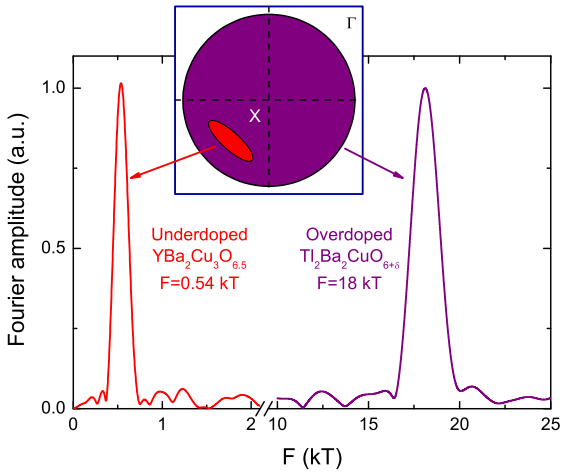

Figure 1.3: Change of the cuprate Fermi surface between the overdoped and underdoped regions deduced from quantum oscillation (from Jaudet et al. [16]).

Now let us look at the phase diagram of cuprates [15]. A large variety of emergent phenomena flourish in the underdoped region, such as stripes, vertex liquids, quantum liquid crystals and the intra-unit cell spontaneous diamagnetic currents. This part of the phase diagram is still attracting most of the attentions of the researchers in the field. There is ample evidence that at large doping (the so-called overdoped region), cuprates gradually conform to the laws of Landau Fermi liquid, with the T^2 component of the resistivity dominating over the T-linear component.

The arguably most mysterious part of the phase diagram is the strange metal phase above the superconducting dome. The behavior in this region is actually extremely simple and universal, of mathematical purity. The defining property of such states is the linear temperature dependence of the resistivity for a wide temperature range. The optical conductivity measurement (in optimally doped $Bi_2Sr_2Ca_{0.92}Y_{0.08}Cu_2O_{8+\delta}$) also shows clear scaling behavior. The absorptive and reactive parts combine to produce a nearly perfect power law behavior in the complex optical conductivity, with $\sigma(\omega) \sim (-i\omega)^{\gamma-2}$, where the exponent is determined to be $\gamma \simeq 1.35$.

So one would suspect that the strange metal phase is in some critical state. And with temperature the most prominent energy scale in this regime, one would be tempted to further associate this state with a zero temperature quantum critical point near optimal doping. We notice that, different from the quantum critical states in many heavy fermion systems, which will be the topic of the next subsection, the electronic specific heat of this state displays an ordinary Fermi liquid type behavior, $C = \gamma T$, with γ nearly constant for a wide range of

temperature and doping. There is no evidence for quasiparticle mass divergence. Neither is it inconsistent with quantum criticality. Anyhow, it is clear that the stange metal phase is not a conventional Fermi liquid. It is well established by ARPES measurements that in the normal state at optimal doping, although there is well defined Fermi surface in momentum space, sharp quasi-particle peaks cease to exist near the $(\pi, 0)$ point of the Brillouin zone.

An immediate question would be what is changing across such a QCP. In the overdoped regime, a large closed Fermi surface characteristic of a normal metal is observed. In the underdoped regime, ARPES sees only disconnected arcs shape residues of Fermi surface, while quantum oscillations reveal small closed pockets of Fermi surface. It has also been proposed by Zaanen and Overbosch that such QCP actually corresponds to a statistics changing transition [17]. The crucial insight is that in the underdoped regime, the t-J model actually encodes a completely different quantum statistical principle, which is fundamentally different from the Fermi-Dirac statistics governing the overdoped regime. It is a great theoretically challenge to reconcile such abrupt change with the second order nature of the transition as expected from the scaling behavior in the normal state. To our knowledge, up to now, we do not even have a simple proof-of-principle model demonstrating such compatibility.

1.1.2 Heavy fermions

The term 'heavy fermions' stands for a class of rare earth or actinide compounds, the electronic excitations of which can be as much as thousand times heavier than that in copper. These systems show a diversity of orderings, including ferromagnetism, antiferromagnetism and unconventional superconductivity. The conventional wisdom of mutual exclusion of magnetism and superconductivity was invalidated by the discovery of superconductivity in such f-electron systems, first in the compound $CeCu_2Si_2$ by Steglich, Aarts et al. in 1976 [18] and confirmed in 1983 in UBe_{13} [19]. In 1994, von Lohneyson et al. discovered that by changing pressure or the gold concentration, the heavy fermion alloy $CeCu_{6-x}Au_x$ can be tuned through an antiferromagnetic quantum phase transition [20]. The finite temperature properties of the system above the critical point show pronounced deviations from the predictions of conventional Landau Fermi liquid theory (for a comprehensive review see [21]).

The basic picture of the heavy fermion systems is that of a dense lattice of magnetic moments immersed in the sea of conduction electrons. The f-electrons associated with the rare earth or actinide ions have strong on-site Coulomb repulsion and they localize into magnetic moments, as in the Mott insulators. The local moments interact antiferromagnetically with the spin density of the conduction electron fluid, generating a lattice analog of the single ion Kondo effect. A heavy electron band is thus formed out of the resonances created in each unit cell. Resistivity drops down at low temperature when coherence develops. The f-electrons are effectively dissolved in the conduction electron fluid, with the net

effect that the Fermi surface volume counts the number of both conduction electrons and f-electrons.

The local moments also induce Friedel oscillations in the spin density of the conduction electron liquid. These oscillations again couple to the other local moments, resulting in an effective magnetic interaction between the local moments. Such conduction-electron-mediated interactions between magnetic moments are called RKKY interactions, named after Ruderman, Kittel, Kasuya and Yosida. The RKKY interaction favors an antiferromagnetic ground state for the local moments. When the f-electrons are locked into the local moments, the Fermi surface volume just counts the number of conduction electrons.

All these ingredients can be grouped together into the following Hamiltonian, usually called the Kondo lattice model,

$$\mathcal{H} = \sum_{\mathbf{k}\alpha} \varepsilon_{\mathbf{k}} c^{\dagger}_{\mathbf{k}\alpha} c_{\mathbf{k}\alpha} + \frac{J_K}{2} \sum_i \mathbf{S}_i \cdot c^{\dagger}_{i\alpha} \sigma_{\alpha\beta} c_{i\beta} + \sum_{i,j} J^{\mathrm{RKKY}}_{ij} \mathbf{S}_i \cdot \mathbf{S}_j, \tag{1.2}$$

where $c_{\mathbf{k}\alpha}$ represents the conduction electrons and $\mathbf{S}_i$ the local moments. J_K parameterizes the Kondo coupling between the conduction electrons and the local moments, and J^{RKKY}_{ij} the RKKY interaction between the local moments. The Kondo coupling is proportional to the square of the hybridization matrix element V between the conduction electrons and f-electrons, $J_K \sim V^2$, and the RKKY interaction is proportional to the conduction electron density of states and the square of the Kondo coupling, $J^{\mathrm{RKKY}} \sim J_K^2 \rho$.

The canonical picture of Kondo lattice, due to Doniach, is that the competition between the Kondo coupling and RKKY interaction governs the phase diagram [22]. Daniach's reasoning is based on a comparison of energy scales. There are two characteristic energy scales in such system: the single ion Kondo temperature $T_K = De^{-1/(2J_K\rho)}$ with D the bandwidth and the RKKY temperature $T_{\mathrm{RKKY}} = J_K^2 \rho$. For $J_K\rho$ large, the Kondo temperature is the larger one and the ground state is the heavy Fermi liquid with a large Fermi surface. For $J_K\rho$ small, the RKKY temperature is larger, resulting in an antiferromagnetic ground state with a small Fermi surface.

Let us look at one example: the heavy fermion alloy $CeCu_{6-x}Au_x$. The parent compound $CeCu_6$ is a heavy fermion metal showing no long-range magnetic order above 5 mK. Antiferromagnetic fluctuations have been observed in inelastic neutron scattering. By replacing some copper atoms by gold atoms, the lattice expands, leading to a reduction in the hybridization between the Ce 4f electrons and the conduction electrons. And the RKKY interaction becomes more important. Actually in the doping range $0.1 \leqslant x \leqslant 1$, the Neel temperature is linear in x, $T_N \propto (x - 0.1)$. By decreasing x or adding pressure, the Neel temperature can be tuned to essentially zero, where we get a continuous phase transition at zero temperature. Such phase transitions will be dominated by quantum mechanical fluctuations, and are thus called quantum phase transitions (QPTs).

There are two aspects of such transitions. One is that the system goes from a

magnetically ordered state to a magnetically disordered state, for which an order parameter can be asigned that captures such a transition. The other aspect is that the Fermi surface also changes across the transition. One would expect that the Fermi surface changes continuously from the phase with a large Fermi surface to the other phase with a small Fermi surface. A spin density wave transition would give rise to such a result. However de Haas-van Alphen measurements have shown that at least for some QPTs, e.g. the pressure-tuned QPT in $CeRhIn_5$, there is a sudden change in the Fermi surface area right at the transition point (see Fig.1.4). How to reconcile the second-order nature of the phase transition with the sudden change in the Fermi surface area is a serious challenge to theorists, which obviously goes beyond the conventional paradigm of spontaneous symmetry breaking.

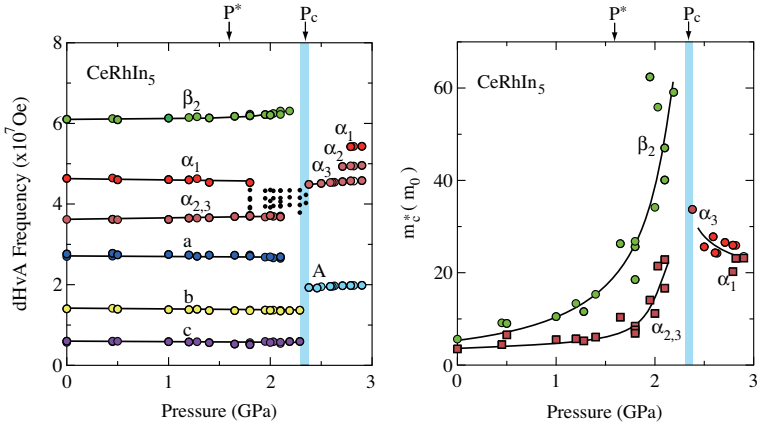

Figure 1.4: Pressure dependence of the de Haas-van Alphen frequency and cyclotron mass in $CeRhIn_5$. P_c denotes the critical pressure (from Gegenwart et al. [23], measurement by Shishido et al. [24]).

Associated with such unconventional zero-temperature phase transitions are the various exotic behaviors in the finite temperature properties of the system above the QCPs, widely known as the non-Fermi liquid behavior (see [25] and references therein), signaling our ignorance of such states. In various systems, the specific heat coefficient shows an upturn at low temperature, which is usually best fitted by a logarithmic divergence, $C_V/T \sim -\log T$, e.g. $CeCoIn_5$, $CeCu_{6-x}Au_x$, U_2Pt_2In, $U_xTh_{1-x}Cu_2Si_2$, $YbRh_2Si_2$, YbAgGe, and sometimes equally well or even better fitted by a power-law divergence, $C_V/T \sim T^{-1+\lambda}$ with $0 < \lambda < 1$, e.g. $Ce_{1-x}Th_xRhSb$, $UCu_{4-x}Pd_{1+x}$, $U_xY_{1-x}Pd_3$. Thinking Fermi liquid, this would mean that the quasiparticle effective mass diverges $m^*/m \to \infty$. The transport properties of such systems are also quite different from that of Fermi liquid. For $CeCoIn_5$ (along the c-axis), $CeCu_2Ge_2$,

$CeCu_{6-x}Au_x$, $UCu_{4-x}Pd_{1+x}$, $UCu_{4+x}Pt_{1-x}$, $U_2Cu_{12}Al_5$, $YbRh_2Si_2$, YbAgGe and $YbRh_2Si_{2-x}Ge_x$, the resistivity has a (quasi-)linear temperature dependence, reminiscent of the strange metal phase of cuprates. In many other systems, the resistivity obeys the power law $\rho = \rho_0 + AT^\alpha$, with the power α obviously smaller than 2, e.g. $CeCu_2Si_2$, $CePd_2Si_2$, $CeNi_2Ge_2$, $Ce(Ru_{1-x}Rh_x)_2Si_2$, $CeIrIn_5$, $CeRu_4Sb_{12}$, $U_2Co_2Sn_5$, UBe_{13}, UPt_{13}, UCoAl, $U_xTh_{1-x}Cu_2Si_2$ and $YbCu_{3+x}Al_{2-x}$. The Fermi-liquid-type scattering can not account for such behavior. The critical fluctuations evade the locking of the Fermi-Dirac statistics.

Another important feature of the quantum critical state in heavy fermion systems, which is also observed in cuprates, is the so-called locality. For example, for $CeCu_{6-x}Au_x$, the scale-invariant part of the dynamical spin susceptibility shows the same ω/T scaling for different momenta, which implies that the critical excitations are local.

It is surprisingly universal that as one lowers temperature, new phases appear near the QCP. Most commonly observed to date is the superconducting phase (see [26] and references therein). The phenomenon of a superconducting dome enclosing the region near the QCP is quite general (see Fig.1.1). The prototype material in heavy fermions with such a phase diagram is the intermetallic compound $CePd_2Si_2$. At ambient pressure, $CePd_2Si_2$ orders antiferromagnetically below about 10 K. Applying pressure reduces the Neel temperature, and at about 28 kbar, the Neel temperature vanishes, where one expects the existence of a QCP. However, in the immediate vicinity of the critical pressure, superconductivity appears, with highest T_c about 0.4 K. Above the superconducting dome, the electrical resistivity shows anomalous scaling behavior, with quasi-linear temperature dependence over almost two orders of magnitude in temperature. Other materials with a similar phase diagram include $CeIn_3$, $CeCu_2Si_2$, $CeCu_2Ge_2$, UGe_2, URhGe and UCoGe.

1.2 Fermions: the main target of this thesis

The new experimental findings in cuprates and heavy fermions clearly indicate the breakdown of the old paradigm of Landau. At this time, it is helpful to go back to basics, deconstruct the old laws, and get detoxified from the stubborn beliefs of the traditional way of thinking, which we have been following for decades.

The experimentalists measure systems formed from electrons and electrons are fermions. The only exactly solvable many Fermion problem is the non-interacting Fermi gas. Surely, every student in physics knows the canonical solution. Introduce creation and annihilation operators that anti-commute,

$$\{c^\dagger_{\vec{k}}, c_{\vec{k}'}\} = \delta_{\vec{k},\vec{k}'}, \tag{1.3a}$$

$$\{c^\dagger_{\vec{k}}, c^\dagger_{\vec{k}'}\} = \{c_{\vec{k}}, c_{\vec{k}'}\} = 0, \tag{1.3b}$$

and the Hamiltonian is

$$H_0 = \sum_{\vec{k}} \varepsilon_k c^\dagger_{\vec{k}} c_{\vec{k}}, \tag{1.4}$$

where $\vec{k}$ is some set of single particle quantum numbers; a representative example is the spinless gas in the continuum where $\vec{k}$ represents single particle momentum and $\varepsilon_k = \hbar^2 k^2/2m$. It follows from standard manipulations that its grand canonical free energy is

$$F_G = -\frac{1}{\beta} \sum_{\vec{k}} \ln\left(1 + e^{-\beta(\varepsilon_{\vec{k}} - \mu)}\right), \tag{1.5}$$

where $\beta = 1/(k_B T)$ and μ the chemical potential, tending to the Fermi-energy E_F when $T \to 0$. The particle number is

$$N = \sum_{\vec{k}} n_{\vec{k}}, \tag{1.6a}$$

$$n_{\vec{k}} = \frac{1}{e^{\beta(\varepsilon_{\vec{k}} - \mu)} - 1}, \tag{1.6b}$$

where $n_{\vec{k}}$ is recognized as the momentum distribution function. At zero temperature this momentum distribution function turns into a step function: $n_{\vec{k}} = 1$ for $|\vec{k}| \leq k_F$ and zero otherwise where the Fermi-momentum $k_F = \sqrt{2mE_F/\hbar^2}$. The step smears at finite temperature, and this is another way of stating the fact that only at zero temperature one is dealing with a Fermi-surface with a precise locus in single particle momentum space separating occupied- and unoccupied states.

The simplicity of the Fermi gas is deceptive. This can be highlighted by a less familiar but illuminating argument. As Landau guessed correctly [27], the Fermi gas can be adiabatically continued to the interacting Fermi liquid. The meaning of this statement is that when one considers the system at sufficiently large times and distances and sufficiently small temperatures('scaling limit') a state of interacting fermionic matter exists that is physically indistinguishable from the Fermi gas. It is characterized by a sharp Fermi surface and a Fermi energy but now these are formed from a gas of non-interacting quasiparticles that have still a finite overlap ('pole strength' $Z_{\vec{k}}$) with the bare fermions, because the former are just perturbatively dressed versions of the latter, differing from each other only on microscopic scales [27]. This is the standard lore, but let us now consider these matters with a bit more rigor. The term describing the interactions between the bare fermions will have the general form,

$$H_1 = \sum_{\vec{k},\vec{k}'\vec{q}} V(\vec{k},\vec{k}',\vec{q}) c^\dagger_{\vec{k}+\vec{q}} c_{\vec{k}} c^\dagger_{\vec{k}'-\vec{q}} c_{\vec{k}'}. \tag{1.7}$$

It is obvious that single particle momentum does not commute with the interaction term,

$$\left[c^{\dagger}_{\vec{k}}c_{\vec{k}}, H_1\right] \neq 0, \tag{1.8}$$

henceforth, single particle momentum is in the presence of interactions no longer a quantum number and single particle momentum space becomes therefore a fuzzy, quantum fluctuating entity. But according to Landau we can still point at a surface with a sharp locus in this space although this space does not exist in a rigorous manner in the presence of interactions!

In the textbook treatments of the Fermi liquid this obvious difficulty is worked under the rug. Since the above argument is rigorous, it has to be the case that the Fermi-surface does not exist when one is dealing with any finite number of particles! Since we know empirically that the Fermi liquid exists in the precise sense that interacting Fermi-systems are characterized by a Fermi-surface that is precisely localized in momentum space in the *thermodynamic limit* it has to be that this system profits from the singular nature of the thermodynamic limit, in analogy with the mechanism of spontaneously symmetry breaking that rules bosonic matter.

We refer to the peculiarity of bosonic- and classical systems that (quantum) phases of matter acquire a sharp identity only when they are formed from an infinity of constituents [28]. Consider for instance the quantum crystal, breaking spatial translations and rotations. Surely, one can employ a STM needle to find out that the atoms making up the crystal take definite positions in space but this is manifestly violating the quantum mechanical requirement that 'true' quantum objects should delocalize over all of space when it is homogeneous and isotropic. The resolution of this apparent paradox is well known. One should add to the Hamiltonian an 'order parameter' potential $V(\mathbf{R})$ where $\mathbf{R}$ refers to the dN dimensional configuration space of N atoms in d dimensional space, having little potential valleys at the real space positions of the atoms in the crystal. It is then a matter of order of limits,

$$\lim_{N\to\infty}\lim_{V\to 0}\langle\sum_i \delta(\vec{r}_i - \vec{r}_i^{\,0})\rangle = 0, \tag{1.9a}$$

$$\lim_{V\to 0}\lim_{N\to\infty}\langle\sum_i \delta(\vec{r}_i - \vec{r}_i^{\,0})\rangle \neq 0, \tag{1.9b}$$

where $\vec{r}_i$ and $\vec{r}_i^{\,0}$ are the position operator and the equilibrium position of the i-th atom forming the crystal. Henceforth, the precise positions of the atoms in the solid, violating the demands of quantum mechanical invariance, emerge in the thermodynamic limit – we know that a small number of atoms cannot form a crystal in a rigorous sense.

Returning to the Fermi liquid, the commonality with conventional symmetry breaking is that in both cases non existent quantum numbers (position of atoms in a crystal, single particle momentum in the Fermi liquid) come into existence

via an 'asymptotic' emergence mechanism requiring an infinite number of constituents, at least in principle. But this is as far the analogy goes. In every other regard, the Fermi liquid has no dealings with the classical emergence principles, that also govern bosonic matter.

Although it is unavoidable that the Fermi liquid needs the thermodynamic limit it is not at all clear what to take for the order parameter potential V. In this regard, the Fermi liquid is plainly mysterious. The textbook treatises of the Fermi liquid, including the quite sophisticated 'existence proofs', share a very perturbative attitude. The best treatments on the market are the ones based on functional renormalization and the closely related constructive field theory [29]. Their essence is as follows: start out with a Fermi gas and add an infinitesimal interaction, follow the (functional) renormalization flow from the UV to the IR to find out that all interactions are irrelevant operators. Undoubtedly, the conclusions from these tedious calculations that the Fermi gas is in a renormalization group sense stable against small perturbations are correct. The problem is that these perturbative treatments lack the mighty general emergence principles that we worship when dealing with classical and bosonic matter.

To stress this further, let us consider a rather classic problem that seems to be more or less forgotten although it was quite famous a long time ago: the puzzle of the ^{3}He Fermi liquid. The ^{3}He liquid at temperatures in the Kelvin range is not yet cohering and it is well understood that it forms a dense van der Waals liquid. Such liquids have a bad reputation; all motions in such a classical liquid are highly cooperative to an extent that all one can do is to put them into a computer and solve the equations of motions by brute force using molecular dynamics. When one cools this to the millikelvin range, quantum coherence sets in and eventually one finds the impeccable textbook version of the Fermi liquid: the macroscopic properties arise from dressed helium atoms that have become completely transparent to each other, except that they communicate via the Pauli principle, while they are roughly ten times as heavy as real ^{3}He atoms. When one now measures the liquid structure factor using neutron scattering one finds out that on microscopic scales this Helium Fermi liquid is more or less indistinguishable from the classical van der Waals fluid! Hence, at microscopic scales one is dealing with the same 'crowded disco' dynamics as in the classical liquid except that now the atoms are kept going by the quantum zero-point motions. On the microscopic scale there is of course no such thing as a Fermi surface. For sure, the idea of renormalization flow should still apply, and since one knows what is going on in the UV and IR one can guess the workings of the renormalization flow in the ^{3}He case: one starts out with a messy van der Waals ultraviolet, and when one renormalizes by integrating out short distance degrees of freedom one meets a 'relevant operator creating the Fermi-surface'. At a time scale that is supposedly coincident with the inverse renormalized Fermi-energy this relevant operator takes over and drags the system to the stable Fermi liquid fixed point. How to construct such a 'Fermi-surface creation operator'? Nobody seems to have a clue!

Although the microscopic details are quite different, the situation one encounters in interesting electron system like the ones realized in manganites [2, 30], heavy fermion intermetallics [3] and cuprate superconductors [1] is in gross outlines very similar as in ^{3}He. In various guises one finds coherent quasiparticles (or variations on the theme, like the Bogoliubons in the cuprates) only at very low energies and low temperatures. Undoubtedly the UV in these systems has much more to do with the van der Waals quantum liquid than with a free Fermi gas. Still, the only activity the theorists seem capable off is to declare the UV to be a Fermi gas that is hit by small interactions. It is not because these theorists are incompetent: humanity is facing the proverbial brick wall called the fermion sign problem that frustrates any attempt to do better.

The other 'anomaly' of the Fermi liquid appears again as rather innocent when one has just worked oneself through a fermiology textbook. However, giving this a further thought, it is actually the most remarkable and most mysterious feature of the Fermi liquid. Without exaggeration, one can call it a 'UV-IR connection', indicating the rather unreasonable way in which microscopic information is remembered in the scaling limit. It refers to the well known fermiology fact that by measuring magneto-oscillations in the electrical transport (De Haas-van Alphen, and Shubnikov- de Haas effects) one can determine directly the average distance between the microscopic fermions by executing measurements on a macroscopic scale. This is as a rule fundamentally impossible in strongly interacting classical- and sign free quantum matter. Surely, this is possible in a weakly interacting and dilute classical gas, as used with great effect by van der Waals in the 19-th century to proof the existence of molecules. But the trick does not work in dense, strongly interacting classical fluids: from the hydrodynamics of water one cannot extract any data regarding the properties of water molecules. Surely, the weakly interacting Fermi gas is similar to the van der Waals gas but a more relevant example is the strongly interacting ^{3}He, or either the heavy fermion Fermi liquid. At microscopic scales it is of course trivial to measure the inter-particle distances and the liquid structure factor of ^{3}He will directly reveal that the helium atoms are apart by 4 angstroms or so. But we already convinced the reader that there is no such thing as a Fermi surface on these scales. Descending to the scaling limit, a Fermi-surface emerges and it encloses a volume that is protected by the famous Luttinger theorem [31,32]: it has to enclose the same volume as the non-interacting Fermi gas at the same density. Using macroscopic magnetic fields, macroscopic samples and macroscopic distances between the electrical contacts one can now measure via de Haas van Alphen effect, etcetera, what k_F is and the Fermi momentum is just the inverse of the inter-particle distance modulo factors of 2π. This is strictly unreasonable. We repeat, on microscopic scales the system has knowledge about the inter-particle distance but there is no Fermi-surface; the Fermi surface emerges on a scale that is supposedly in some heavy fermion systems a factor 100 or even 1000 larger than the microscopic scale. But this emerging Fermi-surface still gets its information from somewhere, so that it knows to fix its volume satisfying Luttinger's rule! In Chapter 3 we hope to

shed some light on the 'mysteries' addressed here using Ceperley's path integral but we are still completely in the dark regarding this particular issue. It might well be that there are even much deeper meanings involved; we believe that it has dealings with the famous anomalies in quantum field theories [33]. These are tied to Dirac fermions and the bottom line is that these process in rather mysterious ways ultraviolet (Planck scale) information to the infrared, with the effect that a gauge symmetry that is manifest on the classical level is destroyed by this 'quantum effect'.

To summarize, in this section we have discussed the features of the Fermi liquid that appear to be utterly mysterious to a physicist believing that any true understanding of physics has to rest on Boltzmannian principle:
(i) What is the order parameter and order parameter potential of the zero temperature Fermi liquid?
(ii) How to construct a 'Fermi-surface creation operator', which is supposed to be the relevant operator associated with the IR stability in the renormalization group flow?
(iii) Why is it possible to retrieve microscopic information via the Luttinger sum rule by performing macroscopic magneto-transport measurements, even in the asymptotically strongly interacting Fermi liquid?

1.3 Feynmanian deconstruction of the order parameter

A better way to understand symmetry breaking is to inspect the dual representation in terms of the worldline path integral [34, 35], which will be the task of Chapters 2 and 3 of this thesis. In such first-quantized formalism, the order parameter is deconstructed, in the sense that the condensate can be expressed directly in terms of the microscopic constituents of the system. The indistinguishability of the bosons and fermions translates into the recipe that one has to trace about all possible ways the worldlines can wind around the periodic imaginary time axis. For a bosonic system, at the temperature where the average of the topological winding number w becomes macroscopic, $\lim_{N\to\infty}\langle w\rangle/N \neq 0$, a phase transition occurs either to the BEC or the superfluid. Bose condensation means that a macroscopic number of particles 'share the same worldline' and the only difference between a BEC and a superfluid is that in the latter this condensate is somewhat depleted.

What is more attractive to us is that the worldline formalism has also the merit of making the fermion sign most transparent. Fermionic worldlines with an even winding number have positive signs, while those having an odd winding number carry negative signs, and they are the origin of the fermion sign problem. It is in this formalism that a partial solution of the sign problem is proposed [Chapter 3]. The basic idea is to discard the worldlines with odd winding numbers and in compensation, some of the even winding worldlines also need to be thrown

away.

Feynman's worldline path integral formulation of many body system is now a textbook problem, although we are aware of only one textbook where it is worked out in detail: Kleinert's Path integral book [36]. Consider the partition function for Bosons or Fermions; this can be written as an integral over configuration space $\mathbf{R} = (\mathbf{r}_1, \ldots, \mathbf{r}_N) \in \mathbb{R}^{Nd}$ of the diagonal density matrix evaluated at an imaginary $\hbar\beta$,

$$\mathcal{Z} = \mathrm{Tr} e^{-\beta H} = \int \mathrm{d}\mathbf{R} \rho(\mathbf{R}, \mathbf{R}; \beta). \tag{1.10}$$

The path integral formulation of the partition function rests on a formal analogy between the quantum mechanical time evolution operator in real time $e^{-i\hat{H}t/\hbar}$ and the finite temperature quantum statistical density operator $\hat{\rho} = e^{-\beta\hat{H}}$, where the inverse temperature $\beta = 1/k_B T$ has to be identified with the imaginary time $it/\hbar$. The partition function defined as the trace of this operator and expression (1.10) simply evaluates this trace in position space. More formally this can viewed as a Wick rotation of the quantum mechanical path integral, and requires a proper analytic continuation to complex times. This rotation tells us that the path integral defining the partition function lives in D-dimensional Euclidean space, with $D = d + 1$ and d the spatial dimension of the equilibrium system. This analogy tells us that to study the equilibrium statistical mechanics of a quantum system in d space dimensions, we can study the quantum system in a Euclidean space of dimension $d + 1$, where the extra dimension is now identified as a 'thermal' circle of extent β. At finite temperature this circle is compact and world-lines of particles in the many-body path integral (1.10) then wrap around the circle, with appropriate boundary conditions for bosons or fermions. The discrete Matsubara frequencies that arise from Fourier transforming modes on this circle carry the idea of Kaluza-Klein compactification to statistical mechanics.

For distinguishable particles interacting via a potential V the density matrix can be written in a worldline path integral form as,

$$\rho_D(\mathbf{R}, \mathbf{R}'; \beta) = \int_{\mathbf{R}\to\mathbf{R}'} \mathcal{D}\mathbf{R} \exp(-\mathcal{S}[\mathbf{R}]/\hbar), \tag{1.11a}$$

$$\mathcal{S}[\mathbf{R}] = \int_0^{\hbar\beta} d\tau \left(\frac{m}{2} \dot{\mathbf{R}}^2(\tau) + V(\mathbf{R}(\tau)) \right), \tag{1.11b}$$

but for indistinguishable bosons or fermions one has also to sum over all $N!$ permutations $\mathcal{P}$ of the particle coordinates,

$$\rho_{B/F}(\mathbf{R}, \mathbf{R}; \beta) = \frac{1}{N!} \sum_{\mathcal{P}} (\pm 1)^p \rho_D(\mathbf{R}, \mathcal{P}\mathbf{R}; \beta), \tag{1.12}$$

where p is he parity of the permutation. For the bosons one gets away with the positive sign, but for fermions the contribution of a permutation with uneven

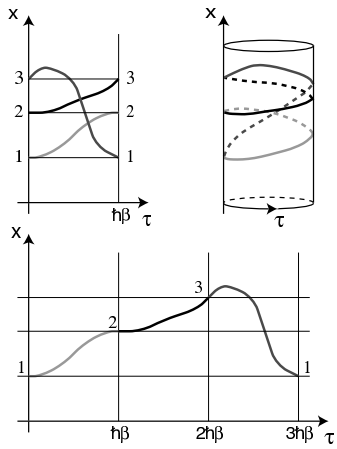

Figure 1.5: Worldline configuration corresponding to a cyclic exchange of three particles, $1 \to 2$, $2 \to 3$, and $3 \to 1$, or in short notation (123) (upper left). On a cylinder (upper right), the worldlines form a closed loop winding $w = 3$ times around the cylinder. In the extended zone scheme (bottom), the exchange process of three particles can be identified with a worldline of a single particle at an effective inverse temperature 3β.

parity to the partition sum is a 'negative probability', as required by the anti-symmetry of the fermionic density matrix. This is the origin of the fermion sign problem, which will be discussed in more detail in section 2.

The partition sum describes worldlines that 'lasso' the circle in the time direction. Every permutation in the sum is composed out of so called permutation cycles. For instance, consider three particles. One particular contribution is given by a cyclic exchange of the three particles corresponding with a single worldline that winds three times around the time direction with winding number $w = 3$ (see Fig. 1.5), a next class of contributions correspond with a 'one cycle' with $w = 1$ and a two-cycle with $w = 2$ (one particle returns to itself while the other two particles are exchanged), and finally one can have three one cycles (all particles return to their initial positions).

The crucial insight of Feynman was that quantum mechanics actually renders a strongly interacting Bose or Fermi liquid to act like a system of free particles, with renormalized parameters ([34], [35]). The main task here is to characterize the important trajectories for the partition sum. One can neglect the contributions from configurations $\mathbf{R}(0)$ and motions $\mathbf{R}(\tau)$ which give small contributions. Let us consider the contribution from moving a single particle i from its initial position $\mathbf{r}_i(0)$ to a final position $\mathbf{r}_i(\beta)$. $\mathbf{r}_i(\beta)$ might be the same as $\mathbf{r}_i(0)$, or $\mathbf{r}_j(0)$ for another particle j. As a simple model that captures the essence of the

problem, imagine the interaction to be of very short range. So the important initial configurations are those for which particles are far apart. There may be other particles in the way of the path $\mathbf{r}_i(\tau)$, and they will interact with particle i due to the potential energy V. It is also possible that as particle i moves, the other particles move out of its way, avoiding to interact with it. For some special paths $\mathbf{R}(\tau)$, it can be that the particles have adjusted their motions so well that during the whole motion, the total potential energy of all the particles is nearly equal to the potential energy of the original configuration $\mathbf{R}(0)$. Instead of increasing their potential energy, for which the time integral is proportional to β, the particles just need to pay an increase of kinetic energy for the readjustment of their coordinates, which varies as the square of the velocity of particle i and has time integral inversely proportional to β. The change in kinetic energy can be accounted for by assigning a larger mass to particle i. The net effect is that for every trajectory, the particle behaves like a free particle with a shifted effective mass.

So we can proceed by considering as fixed point theory the non-interacting Bose and Fermi gas, keeping in mind that mass m is now a renormalized quantity. The evaluation of their path integrals reduces to a combinatorial exercise. Let us first illustrate these matters for the example of $N = 3$ particles. It is straightforward to demonstrate, that the identity permutation gives a contribution $Z_0(\beta)^3$ to the partition function (here $Z_0(\beta)$ denotes the partition function of a single particle), whereas an exchange of all three particles contribute as $Z_0(3\beta)$. The meaning is simple: in the absence of interactions the 3-cycle can be identified with a single particle worldline returning to its initial position at an effective inverse temperature 3β (see Fig. 1.5). Further on, a permutation consisting of a $w = 1$ and a $w = 2$ cycle contributes with $Z_0(\beta)Z_0(2\beta)$. To write down the canonical partition function for $N = 3$ non-interacting bosons or fermions we only have to know the combinatorial factors (e.g. there are 3 permutations made out of a $w = 1$ and a $w = 2$ cycle) and the parity of the permutation to obtain

$$Z_{B/F}^{(N=3)}(\beta) = \frac{1}{3!}[Z_0(\beta)^3 \pm 3Z_0(\beta)Z_0(2\beta) + 2Z_0(3\beta)]. \tag{1.13}$$

This result can easily be generalized to N particles. We denote the number of 1-cycles, 2-cycles, 3-cycles, ... N-cycles the permutation is build of with C_1, C_2, C_3,..., C_N and denote the combinatorial factors counting the numbers of permutations with the same cycle decomposition $C_1, \dots C_N$ with $M(C_1, \dots C_N)$. For N particles we have to respect the overall constraint $N = \sum_w C_w$ and obtain

$$Z_{B/F}^{(N)}(\beta) = \frac{1}{N!} \sum_{C_1,\dots C_N}^{N=\sum_w C_w} M(C_1, \dots C_N)(\pm 1)^{\sum_w (w-1)C_w} \prod_{w=1}^{N} [Z_0(w\beta)]^{C_w}. \tag{1.14}$$

Although the combinatorial factors can be written down in closed form,

$$M(C_1, \dots C_N) = \frac{N!}{\prod_w C_w! w^{C_w}}, \tag{1.15}$$

the canonical partition function (1.14) is very clumsy to work with because of the constraint acting on the sum over cycle decompositions. The constraint problem can be circumvented by going to the grand-canonical ensemble. After simple algebraic manipulations we arrive at the grand-canonical partition function

$$\begin{aligned} Z_G(\beta,\mu) &= \sum_{N=0}^{\infty} Z_{B/F}^{(N)}(\beta) e^{\beta\mu N} \\ &= \exp\left(\sum_{w=1}^{\infty} (\pm 1)^{w-1} \frac{Z_0(w\beta)}{w} e^{w\beta\mu}\right), \end{aligned} \tag{1.16}$$

corresponding to a grand-canonical free energy

$$F_G(\beta) = -\frac{1}{\beta} \ln Z_G(\beta,\mu) = -\frac{1}{\beta} \sum_{w=1}^{\infty} (\pm 1)^{w-1} \frac{Z_0(w\beta)}{w} e^{\beta w\mu}, \tag{1.17}$$

with the $\pm$ inside the sum referring to bosons $(+)$ and fermions $(-)$, respectively. This is a quite elegant result: in the grand-canonical ensemble one can just sum over worldlines that wind w times around the time axis; the cycle combinatorics just adds a factor $1/w$ while $Z_0(w\beta)\exp(\beta w\mu)$ refers to the return probability of a single worldline of overall length $w\beta$. In the case of zero external potential we can further simplify

$$Z_0(w\beta) = \frac{V^d}{\sqrt{2\pi\hbar^2 w\beta/M}^d} = Z_0(\beta)\frac{1}{w^{d/2}}, \tag{1.18}$$

to obtain for the free energy and average particle number N_G, respectively,

$$F_G = -\frac{Z_0(\beta)}{\beta} \sum_{w=1}^{\infty} (\pm 1)^{w-1} \frac{e^{\beta w\mu}}{w^{d/2+1}}, \tag{1.19a}$$

$$N_G = -\frac{\partial F_G}{\partial \mu} = Z_0(\beta) \sum_{w=1}^{\infty} (\pm 1)^{w-1} \frac{e^{\beta w\mu}}{w^{d/2}}. \tag{1.19b}$$

To establish contact with the textbook results for the Bose and Fermi gas one just needs that the sums over windings can be written in an integral representation as,

$$\sum_{w=1}^{\infty} (\pm 1)^{w-1} \frac{e^{\beta w\mu}}{w^{\nu}} = \frac{1}{\Gamma(\nu)} \int_0^{\infty} d\varepsilon \frac{\varepsilon^{\nu-1}}{e^{\beta(\varepsilon-\mu)} \mp 1}, \tag{1.20}$$

and one recognizes the usual expressions involving an integral of the density of states ($N(\varepsilon) \sim \varepsilon^{d/2}$ in d space dimensions) weighted by Bose-Einstein or Fermi-Dirac factors.

For bosons, by using the worldline path integral formalism, the quantum mechanical problem is reduced to a purely classical equilibrium ring polymer problem. At the transition $\mu \to 0$, one directly infers from Eq. (1.19) that very long

worldlines corresponding with winding numbers $w \sim N$ are no longer penalized, while there are many more long winding- than short winding contributions in the sum. It is straightforward to show that in the thermodynamic limit worldlines with w between $\sqrt{N}$ and N have a vanishing weight above the BEC temperature, while these infinite long lines dominate the partition sum in the condensate [37]. One starts with a summation over a finite number of winding worldlines and take the infinite winding limit, or equivalently the infinite particle number limit, at the end of the day.

The number of particles contained in worldlines with winding number w is

$$N_w = \frac{e^{w\beta\mu}}{w^{d/2}} \left[\frac{D}{\lambda} W\left((\frac{D}{\lambda})^2 \frac{\pi}{w} \right) \right]^d , \tag{1.21}$$

where $W(x) = \sum_{n=-\infty}^{\infty} e^{-xn^2}$ comes from a summation over all discrete momentums, and $\lambda = \hbar\sqrt{2\pi\beta/m}$ is the de Broglie thermal wavelength. It is easy to show that for $d = 3$ the fraction of particles contained in the long loops is

$$\lim_{N\to\infty} \frac{1}{N} \sum_{w=\sqrt{N}}^{N} N_w = \begin{cases} 0 & \text{for } T > T_c \\ 1 - \left(\frac{T}{T_c}\right)^{3/2} & \text{for } T \leqslant T_c. \end{cases} \tag{1.22}$$

while for $d = 2$ the result is

$$\lim_{N\to\infty} \frac{1}{N} \sum_{w=\sqrt{N}}^{N} N_w = \begin{cases} 0 & \text{for } T > 0 \\ 1 & \text{for } T = 0. \end{cases} \tag{1.23}$$

A related issue is the well known fact that the non-interacting Bose-Einstein condensate and the superfluid that occurs in the presence of finite repulsions are adiabatically connected: when one switches on interactions the free condensate just turns smoothly into the superfluid and there is no sign of a phase transition. This can be seen easily from the canonical Bogoliubov theory. Again, although the algebra is fine matters are a bit mysterious. The superfluid breaks spontaneous $U(1)$ symmetry, thereby carrying rigidity as examplified by the fact that it carries a Goldstone sound mode while it expels vorticity. The free condensate is a non-rigid state, that does not break symmetry manifestly, so why are they adiabatically connected? The answer is obvious in the path-integral representation [38, 39]. The superfluid density ρ_S can be written in terms of the mean-squared winding number in the spatial direction,

$$\rho_S = \frac{m}{\hbar^2} \frac{\langle W^2 \rangle L^{2-d}}{d\beta}. \tag{1.24}$$

Here periodic boundary condition is imposed. d is the dimensionality, L is the size of the periodic cell, which is assumed to be the same for all spatial directions. The winding number W describes the net number of times the paths of the N

particles have wound around the periodic cell, $\mathbf{W}L = \sum_{i=1}^{N}(\mathbf{r}_{\mathcal{P}_i} - \mathbf{r}_i)$. Although interactions will hinder the free meandering of the polymers, a lot of this hindrance is required to make it impossible for worldlines to become infinitely long below some temperature. The fraction of infinitely long worldlines is just the condensate fraction ρ_S/ρ and even in the very strongly coupled ^{4}He superfluid these still make up for roughly 30% of all worldlines! The only way one can get rid of the infinite windings in the interacting system is to turn it into a static array of one cycles - the ^{4}He crystal.

1.4 Quantum criticality: a new organizing principle

Quantum criticality is an important concept that has dominated the landscape of modern condensed matter physics for the last decade [40]. The idea behind quantum criticality is simple and powerful. Imagine competing interactions that typically drive the transitions between different phases. Logically one has to allow for the possibility that the relative strength of these competing interactions is tunable as a function of the external control parameters such as pressure, magnetic field or doping; we deliberately omit temperature as a control parameter since quantum phase transitions (QPTs) will occur at T=0. The simplest route to arrive at a QPT is to consider a line of finite temperature phase transition as a function of some control parameter, such as pressure P, magnetic field B or doping x. At $T = 0$ this line will indicate a critical value of the control parameter. This specific value of the control parameter, where one expects a precise balance between tendency to different phases or states, is called a quantum critical point (QCP). Near this point, competing interactions nearly compensate each other. It is often asserted that it is the physics of frustration and competition which leads to the finite temperature transition, and that also controls and enables the interesting properties of materials as they are brought to the $T = 0$ QCP.

In this section, we intend to give a short introduction to the theoretical idea of quantum criticality. In the previous section, we have seen the experimental evidence that by applying pressure, magnetic field, or doping, a second-order phase transition can be tuned to zero temperature, producing a quantum critical point. Associated with such a singular point, ordinarily anomalous scaling behaviors emerge in various finite-temperature properties of the system, such as specific heat, resistivity and magnetic susceptibility, which goes far beyond our conventional understanding of metals. One of the basic questions arising from the experimental findings is how the zero temperature phase transition point is related to the finite temperature behavior of the system. The theoretical idea of quantum criticality states that the zero temperature QCPs actually profoundly modify finite temperature properties of the quantum critical metals.

The basic concepts of quantum criticality is best illustrated by a simple model: the 1+1-dimensional Ising chain in a transverse field. This model can be solved

exactly and it is the hydrogen atom of quantum phase transitions. One can find a comprehensive introduction to this model in Sachdev's book [40]. We will summarize the essential points here. The Hamiltonian is of the form,

$$H_I = -J \sum_i \left(\hat{\sigma}_i^z \hat{\sigma}_{i+1}^z + g \hat{\sigma}_i^x \right). \tag{1.25}$$

Here the overall coefficient $J > 0$ is an exchange constant. It sets the microscopic energy scale of the system. When temperature is much larger than J, the properties are nonuniversal. In the following, we consider temperature within the range $T \ll J$. $\hat{\sigma}$'s are the Pauli matrices. $g > 0$ is a dimensionless coupling. When $g = 0$, the ground state is a product of eigenstates of $\hat{\sigma}_i^z$. It is a ferromagnetic state, with all the spins aligned up, either all in the spin up state or all in the spin down state. The Z_2 symmetry, $\hat{\sigma}_i^z \to -\hat{\sigma}_i^z, \hat{\sigma}_i^x \to \hat{\sigma}_i^x$, is broken. For $g \to \infty$, the ground state is a product of eigenstates of $\hat{\sigma}_i^x$, $|\to\rangle_i = (|\uparrow\rangle_i + |\downarrow\rangle_i)/\sqrt{2}$. This state restores the above Z_2 symmetry. Then the question is what happens in-between the two limits.

This quantum model can be mapped to a classical model in 2 dimension. Temperature in the quantum model corresponds to the total length of the classical system in the time direction, and gap in the quantum model is mapped to the correlation length along the time direction. One can introduce the concept of dynamical critical exponent z, which relates the scaling in the time direction to the space direction, and frequency scales with momentum as $\omega \sim k^z$. In the quantum Ising model, $z = 1$.

The immediate consequence of this mapping is that the zero temperature phase transition in the quantum Ising model is second order. The Hamiltonian is invariant under the above Z_2 transformation. So this symmetry can only be broken spontaneously, which also points to a second order phase transition. For $g \gg 1$, the correlation in $\hat{\sigma}_i^z$ is short-ranged, decaying as $\langle 0|\hat{\sigma}_i^z \hat{\sigma}_j^z|0\rangle \sim \exp(-|x_i - x_j|/\xi)$ at long distance, with ξ the correlation length. For $g \ll 1$, there is spontaneous symmetry breaking, with $\langle 0|\hat{\sigma}_i^z|0\rangle$ finite.

This model can be mapped to a free fermion problem and solved exactly. By making the Jordan-Wigner transformation, with the spin axes rotated by $\pi/4$ about the y axis, $\hat{\sigma}_i^x = 1 - 2c_i^\dagger c_i$, $\hat{\sigma}_i^z = -\prod_{j<i}(1 - 2c_j^\dagger c_j)(c_i + c_i^\dagger)$, the Hamiltonian reads in momentum space

$$H_I = J \sum_k \left(2[g - \cos(ka)] c_k^\dagger c_k - i \sin(ka)[c_{-k}^\dagger c_k^\dagger + c_{-k} c_k] - g \right), \tag{1.26}$$

where a is the lattice spacing. A Bogliubov transformation $c_k = u_k \gamma_k + i v_k \gamma_{-k}^\dagger$ brings the above quadratic Hamiltonian into the simple form, $H_I = \sum_k \varepsilon_k (\gamma_k^\dagger \gamma_k - \frac{1}{2})$, with $\varepsilon_k = 2J\sqrt{1 + g^2 - 2g\cos k}$. For $g \neq 1$, there is an energy gap at $k = 0$, with amplitude $2J|1 - g|$, which vanishes at $g = 1$. So $g = 1$ is expected to be the phase transition point, at which fermions dominate the low energy properties.

Near this point, the system is described by a universal continuum field theory, with partition function

$$\begin{aligned} \mathcal{Z} &= \int \mathcal{D}\Psi\mathcal{D}\Psi^\dagger \exp\left(-\int_0^\beta d\tau dx \mathcal{L}_I\right) \\ \mathcal{L}_I &= \Psi^\dagger \frac{\partial \Psi}{\partial \tau} + \frac{c}{2}\left(\Psi^\dagger \frac{\partial \Psi^\dagger}{\partial x} - \Psi \frac{\partial \Psi}{\partial x}\right) + \Delta \Psi^\dagger \Psi, \end{aligned} \tag{1.27}$$

with higher order terms all irrelevant. Here the continuum Fermi field $\Psi(x_i) = c_i/\sqrt{a}$, and coupling constants $c = 2Ja, \Delta = 2J(1-g)$. At the critical point, $g = 1$ and $\Delta = 0$. We also notice that above the energy scale J, lattice effects will be important, and the above critical field theory is no longer adequate to describe the system. So J is the ultraviolet cutoff ω_c of the critical theory. Here Δ is the most relevant perturbation about the QCP and it has scaling dimension 1. The correlation length scales as $\xi \sim |g - g_c|^{-\nu}$, and one can read off the critical exponent $\nu = 1$.

The two-point correlation functions read for $\tau > 0$,

$$\begin{aligned} \langle \Psi(x,\tau)\Psi^\dagger(0,0)\rangle =& \frac{T}{4c}\left(\frac{1}{\sin(\pi T(\tau - ix/c))} + \frac{1}{\sin(\pi T(\tau + ix/c))}\right), \\ \langle \Psi(x,\tau)\Psi(0,0)\rangle =& i\frac{T}{4c}\left(\frac{1}{\sin(\pi T(\tau - ix/c))} - \frac{1}{\sin(\pi T(\tau + ix/c))}\right). \end{aligned} \tag{1.28}$$

The $T = 0$ result and $T > 0$ result is connected by the conformal mapping from a plane to a cylinder,

$$c\tau \pm ix \to \frac{c}{\pi T}\sin\left(\frac{\pi T}{c}(c\tau \pm ix)\right). \tag{1.29}$$

The central object of this model is the order parameter correlation function $C(x_i, t) = \langle \hat{\sigma}^z(x_i, t)\hat{\sigma}^z(0,0)\rangle$. The equal-time correlation function can be calculated from the fermion representation. At long distance, it has the scaling form

$$\lim_{|x|\to\infty} C(x,0) = ZT^{2s} G_I\left(\frac{\Delta}{T}\right)\exp\left[-\frac{T|x|}{c}F_I\left(\frac{\Delta}{T}\right)\right]. \tag{1.30}$$

The operator $\hat{\sigma}^z$ has dimension $s = 1/8$. F_I and G_I are universal scaling functions, and they are smooth across the critical point $\Delta = 0$. One can see clearly from the above expression that there is only long-range order at zero temperature. At any finite temperature, the correlation decays exponentially, with correlation length $\xi = c/(TF_I)$. With ξ behaving qualitatively differently in different regions of the parameter space, the phase diagram is divided into several different regions. This can already been seen by just comparing the two energy scales Δ and T. And the crossover lines are at $\Delta \sim T$. When $\Delta > 0, T \ll \Delta$, one has $\xi^{-1} = (2|\Delta|T/\pi c^2)^{1/2}\exp(-|\Delta|/T)$. For $\Delta < 0, T \ll |\Delta|$, the correlation length

is given by $\xi^{-1} = |\Delta|/c + (2|\Delta|T/\pi c^2)^{1/2} \exp(-|\Delta|/T)$ and reaches a finite value as $T \to 0$. In the region with $T \gg |\Delta|$, the correlation length is $\xi = 4c/\pi T$, which has the quantum critical scaling form $T^{-1/z}$, and this region is called the quantum critical region (see Fig. (1.6)).

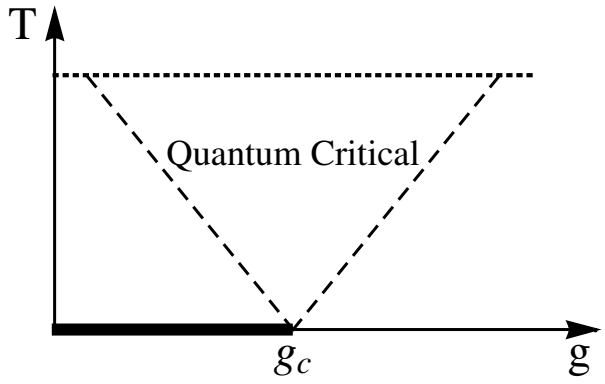

Figure 1.6: Theoretical phase diagram of the 1+1-dimensional quantum Ising model. The dashed lines are the crossover lines $|\Delta| = 2J|g - g_c| \sim T$, with the critical coupling $g_c = 1$. The dotted line represents the ultraviolet cutoff energy scale $T \sim J$. The thick solid line at $T = 0, 0 < g < g_c$ is the region in the phase diagram with long-range order. The ground state at $T = 0, g > g_c$ is a quantum paramagnet. The triangular region in the center is the quantum critical region.

In the quantum critical region, the order parameter susceptibility can be easily derived from the universal two-point correlator at an imaginary time τ. One starts from the equal-time correlator at $T = 0, \Delta = 0$,

$$C(x, 0) \sim \frac{1}{(|x|/c)^{2s}}. \tag{1.31}$$

The consideration here is quite general, not just restricted to the Ising model, which has $s = 1/8$. Due to Lorentz invariance, the time direction can be included simply,

$$C(x, \tau) \sim \frac{1}{(\tau^2 + x^2/c^2)^s}. \tag{1.32}$$

The finite temperature result can be obtained through the transformation (1.29),

$$C(x, \tau) = \tilde{Z} \frac{T^{2s}}{(\sin[\pi T(\tau - ix)] \sin[\pi T(\tau + ix)])^s}. \tag{1.33}$$

The analytical continuation to real time $\tau \to it$ yields the real time two-point

correlation function

$$C(x,t) = \tilde{Z}\frac{T^{2s}}{(i\sinh[\pi T(t-x)]i\sinh[\pi T(t+x)])^s}, \tag{1.34}$$

with a Fourier transform corresponding to the dynamic structure factor

$$S(k,\omega) = \int_{-\infty}^{\infty} dx \int_{-\infty}^{\infty} dt C(x,t) e^{-i(kx-\omega t)}. \tag{1.35}$$

A convenient way to perform the Fourier transform is by factorizing $C(x,t)$ into left-moving and right-moving modes, $C(x,t) = C_-(t-x)C_+(t+x)$, to subsequently integrate over $t \pm x$. The result is

$$S(k,\omega) = Ze^{\frac{\omega}{2T}}\frac{1}{T^{2(1-2s)}}B(s+i\frac{\omega+k}{4\pi T}, s-i\frac{\omega+k}{4\pi T})B(s+i\frac{\omega-k}{4\pi T}, s-i\frac{\omega-k}{4\pi T}), \tag{1.36}$$

where B is the beta function, and the overall numerical coefficient $Z = 2^{4s-3}\pi^{2(s-1)}\tilde{Z}$. The fluctuation-dissipation theorem

$$S(k,\omega) = \frac{2}{1-e^{-\omega/T}}\chi''(k,w) \tag{1.37}$$

then yields the imaginary part of the order parameter susceptibility,

$$\chi''(k,\omega) = Z\frac{\sinh(\frac{\omega}{2T})}{T^{2(1-2s)}}B(s+i\frac{\omega+k}{4\pi T}, s-i\frac{\omega+k}{4\pi T})B(s+i\frac{\omega-k}{4\pi T}, s-i\frac{\omega-k}{4\pi T}). \tag{1.38}$$

Indeed $\chi''(\omega) \to 0$ in a linear fashion with ω with a slope set by $1/T$, while for $\omega >> T$ the temperature dependence drops out, recovering the power law. The crossover occurs at $\omega \simeq 2k_BT/\hbar$ where $\chi''(\omega)$ has a maximum. This result will be used in the later chapters when we consider superconductivity in quantum critical metals. The real part can be computed from the Kramers-Kronig transform,

$$\chi'(k,\omega) = \frac{Z'}{T^{2(1-2s)}}\left(\frac{-i\pi}{s-i\frac{\omega+k}{4\pi T}}\frac{\sin(2s\pi-\frac{ik}{2T})}{\sinh(\frac{k}{2T})}\frac{\Gamma(2s)\Gamma(2s-\frac{ik}{2\pi T})}{\Gamma(1-\frac{ik}{2\pi T})}\right.$$
$$\left.{}_3F_2(2s, s-i\tfrac{\omega+k}{4\pi T}, 2s-\tfrac{ik}{2\pi T}; 1+s-i\tfrac{\omega+k}{4\pi T}, 1-\tfrac{ik}{2\pi T}; 1) + (k \to -k)\right) \tag{1.39}$$

where F is the generalized hypergeometric function.

In summary, we have shown that for the 1+1-dimensional quantum Ising chain in the quantum critical region $|\Delta| \ll T \ll J$, the finite temperature properties of the system are related to its property at the zero temperature critical point $\Delta = 0, T = 0$ simply by conformal mapping (1.29). As one approaches the QCP, the correlation length scales as $\xi \sim |g - g_c|^{-\nu}$, and the correlation time scales as $\xi_\tau \sim \xi^z$. Here the critical exponents are $z = 1, \nu = 1$. For higher dimensional systems, the mapping will be more complex. But the basic idea of finite size scaling in the temporal direction is the same. The critical exponents are different for different universal classes. The fact that there is only long-range order at zero temperature is the special property of 1+1 dimension. In higher dimensional systems, the ordered phase can extend to finite temperature, occupying a finite region in the phase diagram.

1.5 This thesis

This thesis is divided into two parts. The first part (Chapters 2 and 3) is about worldline path integrals and the fermion nodal structure. The second part (Chapters 4, 5, 6) is about quantum criticality and its interplay with superconductivity. There are actually intrinsic connections between the two, though they look far apart at first glance. The study of the nodal structure of the fermionic wavefunctions and density matrices serves as an antidote to the conventional Fermi gas way of thinking. What we learn from exploring the nodes is that the world of condensed matter systems is not just about the single particle Green's functions, and the many-body entanglement perspective is crucial for the understanding of emergent phenomena. Nature has already revealed this to us when the FQHE was discovered: Laughlin's wavefunction contains much more information than a single particle Green's function, or even earlier, when Schrieffer wrote down the simple wave function for the superconducting ground state. A simple step going beyond the Fermi gas way of thinking would be to consider the two particle correlation functions, e.g. charge susceptibility, spin susceptibility and pairing susceptibility, to be as fundamental as the single particle Green's functions, which is the basic idea of Chapter 5.

We start in Chapter 2 with the signful worldline path integrals. The Feynmanian deconstruction of the order parameter is shown explicitly by calculating, in the first quantized path integral formalism, the effect of the condensation of a gas of charged particles in the background magnetic field. Coupling to a bosonic condensate generates a mass term for the background magnetic field, leading to the Anderson-Higgs effect. The value of the mass is determined by the number density of the condensed particles. In this formalism, the fermionic statistics are encoded via the inclusion of additional Grassmann coordinates in a manner that leads to a manifest worldline supersymmetry. This extra symmetry is key in demonstrating the absence of the Anderson-Higgs effect for charged fermions.

In Chapter 3, we study the fermion sign problem in the worldline path integral formalism. The insightful work of Ceperley in constructing fermionic path integrals in terms of constrained world-lines is reviewed. In this representation, the minus signs associated with Fermi-Dirac statistics are self consistently translated into a geometrical constraint structure, the nodal hypersurface, acting on an effective bosonic dynamics. Working with the path integral in momentum space, we then show that the Fermi gas can be understood by analogy to a Mott insulator in a harmonic trap. Going back to real space, we discuss the topological properties of the nodal cells, and suggest a new holographic conjecture relating Fermi liquids in higher dimensions to soft-core bosons in one dimension.

We turn to the exploration of quantum criticality in Chapter 4. In this chapter, we consider the dynamics of the bosonic order parameters around the QCPs, assuming that the fermionic degrees of freedom can be integrated out. We are interested in the stability of QCPs in the presence of two competing phases. These phases near QCPs are assumed to be either classical or quantum and as-

sumed to repulsively interact via square-square interactions. We find that for any dynamical exponents and for any dimensionality strong enough interaction renders QCPs unstable, and drives transitions to become first order. We propose that this instability and the onset of first-order transitions lead to spatially inhomogeneous states in practical materials near putative QCPs. Our analysis also leads us to suggest that there is a breakdown of Conformal Field Theory (CFT) scaling in the Anti de Sitter models, and in fact these models contain first-order transitions in the strong coupling limit.

In particular, we carry out the renormalization group (RG) analysis of two coupled order parameters with different dynamical exponents, and we find a line of fixed points in such theories. The RG analysis of such models is not an easy task. The conventional picture is that in d spatial dimensions, the quantum field theory of a bosonic field with dynamical exponent z is equivalent to a classical field theory in d + z dimensions. This picture still holds when there are more than one field, but all the fields have the same dynamical exponent. However, when the coupled fields have different dynamical exponents, this picture is no longer valid: the fields are frustrated in choosing their effective dimensions. Technically, this problem arises in the RG analysis for example when one calculates the loop diagrams containing internal lines corresponding to fields with different dynamical exponents. If we think more carefully about how one arrives at the conventional way of counting effective dimensions, we will find that one has to rescale the parameters to absorb the generally dimensionfull coefficient in the frequency dependent terms, the presence of which ensures these terms to have the right dimensions. We will show explicitly such rescaling. With distinct dynamical exponents, one can no longer rescale out these coefficients. They actually lead to dramatically different scaling behavior in the RG structure.

In Chapter 5, we present a simple phenomenological scaling theory for the pairing instability of a quantum critical metal. It can be viewed as a minimal generalization of the classical BCS theory of superconductivity for normal Fermi liquid metals. We assume that attractive interactions are induced in the fermion system by an external bosonic glue that is strongly retarded. Resting on the small Migdal parameter, all the required information from the fermion system needed to address the superconductivity enters through the pairing susceptibility. Asserting that the normal state is a strongly interacting quantum critical state of fermions, the form of this susceptibility is governed by conformal invariance and one only has the scaling dimension of the pair operator as free parameter. Within this scaling framework, conventional BCS theory appears as the marginal case but it is now easily generalized to the (ir)relevant scaling regimes. In the relevant regime an algebraic singularity takes over from the BCS logarithm with the obvious effect that the pairing instability becomes stronger. However, it is more surprising that this effect is strongest for small couplings and small Migdal parameters, highlighting an unanticipated important role of retardation. Using exact forms for the finite-temperature pair susceptibility from 1+1D conformal field theory as models, we study the transition temperatures, finding that the gap

to transition temperature ratios is generically large compared to the BCS case, showing, however, an opposite trend as a function of the coupling strength compared to the conventional Migdal-Eliashberg theory. We show that our scaling theory naturally produces the superconducting domes surrounding the quantum critical points, even when the coupling to the glue itself is not changing at all. We argue that hidden relations will exist between the location of the crossover lines to the Fermi liquids away from the quantum critical points and the detailed form of the dome when the glue strength is independent of the zero-temperature control parameter. Finally, we discuss the behavior of the orbital-limited upper critical magnetic field as a function of the zero-temperature coupling constant. Compared to the variation in the transition temperature, the critical field might show a much stronger variation pending the value of the dynamical critical exponent.

In Chapter 6, we propose to use the second order Josephson effect as a direct probe of the Cooper channel of quantum critical metals, to shed light on the problem of unconventional superconductivity in such systems. We review the idea of Ferrell and Scalapino who suggested a superconductor-insulator-normal (SIN) tunneling setup in which a strong superconductor acts as an effective external probe for a normal metallic state above its superconducting transition temperature T_c. The fluctuating pair field of the metal is coupled to the rigid pair-field of the strong superconductor, and this leads to an additional contribution to the total tunneling current, on top of the well-known SIN-junction quasiparticle current. This additional tunneling current is proportional to the imaginary part of the pair(ing) susceptibility in the metallic state. We calculate the pair susceptibility for several different scenarios of the pairing mechanism for quantum critical metals, to provide templates for experimentalists. We find that different models differ qualitatively.

Chapter 2

Fermions in the Worldline Path Integral: Absence of Anderson-Higgs Mechanism

2.1 Introduction

The Meissner effect [41], the expulsion of magnetic fields from superconducting regions, is a salient feature of superconductivity which distinguishes it from perfect conductivity. It can be described in a phenomenological way via the London equations [42], but a microscopic understanding requires an accounting of the pairing mechanism [43–45] leading to condensation in the ground state, and the concomitant generation of an effective mass for the photon, [46,47]. The modern viewpoint takes the spontaneous breaking of a gauge invariance as the central idea, though of course this is strictly speaking not correct, as a gauge symmetry can never be broken, but rather serves as a good description in a perturbative expansion around the breaking of a global symmetry. The breaking of a global symmetry is also relevant to the study of Bose-Einstein condensation. An understanding of this phenomena, in the case of strongly interacting Helium and the superfluid transition, was advanced by the introduction of the methods of first quantized path integrals [48, 49], wherein it is understood as the proliferation of worldlines of bosons [50,51]. In fact, the partition function for the worldlines can be mapped onto a second quantized Euclidean path integral (over fields) of the Landau-Ginzburg type.

The idea of spontaneously broken gauge symmetry has been used to great advantage in high energy physics. It had long been assumed that a renormalizable theory of massive vector bosons could not be gauge invariant, until it was suggested [52–57] that a microscopic gauge invariant theory involving massless vector bosons could still account for massive vector bosons at low energy (like the $W^{\pm}$ and Z^0 in electroweak theory), if the symmetry gauged by such modes is spontaneously broken at some scale (assumed to be around a few hundred GeV for electroweak theory). This realization guided the construction of the electroweak theory [58, 59], now a cornerstone of the standard model of particle physics.

In electroweak theory the symmetry breaking is driven by condensation of a bosonic Higgs field, the search for which is one of the main motivations for recent efforts in experimental high energy physics. Various technical issues (such as the hierarchy problem) have led to the suggestion that the Higgs particle is not in fact elementary, but gives an effective description of some as yet unknown underlying physics (such as technicolor [60]), in much the same way that superconductivity is often described as Bose-Einstein condensation of bound Cooper pairs [61].

One might wonder if this mechanism is specific to bosons, or whether it can be realized using fermionic constituents. In relativistically invariant systems, condensation of fermionic operators would lead to a breaking of Lorentz invariance. More generaly such a condensation leads to a vacuum expectation value for the fields of the form $\langle 0|\hat{O}|0\rangle = v$, with $|0\rangle$ the vacuum state of the system, and $\hat{O}$ either a bosonic or fermionic operator. Since fermionic operators connect bosonic states to fermionic ones and vice-versa, and it assumed that the vacuum state has a definite character (in fact nearly always assumed bosonic), the vev v must necessarily vanish. This argument shows that spontaneous symmetry breaking driven by fermions (if at all possible) must take a form different from the familiar picture described in terms of bosonic order parameters. In fact this argument can also be made in the sense of superselection rules, which limit the allowed possible observations made on a quantum system by disallowing matrix elements between certain classes of states, and separating the Hilbert space into superselction sectors from which linear combinations of basis vectors can not be made. It has been suggested [62] that a superselection rule exists which obstructs the assembling of states which are superpositions of bosons and fermions. Since a coherent state of fermions would necessarily mix both bosonic and fermionic statistics, it is then not possible to construct condensates of fermions. In fact, the question of whether such a superselection rule is operative is one to be determined by experiment, and it has recently been proposed [63] that observation of coherent superpositions of even and odd numbers of fermions in mesoscopic quantum dots can be used as a test of supersymmetry.

Considering the importance of, and the many mysterious issues surrounding the mechanism of spontaneous symmetry breaking, it is valuable to have an alternative view of it. Here we will explore the formalism due to Feynmann [48, 49], where one considers a representation in terms of the worldline path integral.

The indistinguishability of the bosons translates into the recipie that one has to trace over all possible ways the worldlines can wind around the periodic imaginary time axis. At the temperature where the average of the topological winding number w becomes macroscopic, $\lim_{N\to\infty}\langle w\rangle/N \neq 0$, the system undergoes a phase transition either to a Bose-Einstein condensate, or a superfluid. Bose-Einstein condensation means that a macroscopic number of particles 'share the same worldline' with difference between BEC and superfluidity being that in the latter this condensate is somewhat depleted. This formalism turns out to be very efficient for numerical calculation of properties of strongly interacting bosonic systems such as Helium[4] [50,51], where it is also shown that the average winding number corresponds directly to the superfluid density.

It is more difficult but perhaps even more interesting to consider the fermionic particles in this formalism. One can easily show [36] that below the Fermi temperature, worldlines with macroscopic winding number also proliferate in fermionic systems; this leads to a puzzle: the macroscopic worldlines lead to a Meissner effect, via the Anderson-Higgs mechanism, in charged bosonic systems, but surely such phenomenon can not happen in charged fermionic systems [1].

It is the aim of this chapter to show in the worldline formalism, in a certain limit, that particles obeying fermionic statistics can not drive an Anderson-Higgs transition. In the next section we begin by recalling the single particle path integral for a spinless boson, which we couple to a background magnetic field, and write the partition function for the many-body system, from which we compute the second order perturbative correction to the effective action. Focusing on a special subclass of winding modes, we demonstrate the appearance of a mass for the magnetic field. We then generalize this logic to the case of a spin-1/2 particle by way of introduction of appropriate terms in the action for Grassmannian degrees of freedom coupled to the particle worldlines. Underlying our observation on the behaviour of fermionic systems in this language is the existence of a worldline (though not target space, where the particle trajectory is embedded) supersymmetry. The inclusion of the particle statistics leads to an additional term in the effective action, and this addition is shown to lead to the disappearance of the effect manifested for charged bosons.

[1] In the BCS theory of superconductivity, pairs of fermions form Cooper pairs, which have a bosonic character, and whose condensation then leads to superconductivity.

2.2 Spinless Bosons in background Magnetic Field

We begin by considering a single spinless boson, in the non-relativistic limit, whose action reads [2]

$$\mathcal{A}_{e,0} \;=\; \int_{\tau_a}^{\tau_b} d\tau\, \frac{M}{2}\dot{x}^2(\tau)\;, \tag{2.1}$$

with τ the proper time along the particle's worldline. In the presence of the electromagnetic field, one needs to add the interaction term [3]

$$\mathcal{A}_{e,\mathrm{int}} \;=\; i\,e\,\int_{\tau_a}^{\tau_b} d\tau\, \dot{x}^i(\tau)\, A_i(x(\tau))\;, \tag{2.2}$$

where the dot in $\dot{x}$ denotes a derivative with respect to proper time of the particle, which should not be confused with the Euclidean time in target space. Here $i,j = 1,\cdots,d$, with d the dimension of space. We shall only be interested in the study of particles immersed in an external magnetic field. Hence, in the following we set the electric field to zero, $E^i = 0$, and consider only the response to a magnetic field B^i. We drop the inter-particle Coulomb repulsion.

Since we are interested in using the single- and many-body path integrals in first-quantized form, we are restricted to considering non-relativistic physics. Standard problems with negative probabilities and pair production would force us to rely on the second-quantized quantum field theory language to address the relativistic problem.

We now study the condensation of bosonic particles in a background magnetic field, giving a new vantage point on the Meissner effect, before we turn to apply the same ideas to the study of fermionic systems. The partition function of N identical bosons sums over all permutations $\mathcal{P}$ of the particle coordinates (with no relative minus sign)

$$Z_N = \frac{1}{N!}\int dx_1 \cdots \int dx_N \sum_{\mathcal{P}} \prod_i \left(x_{p(i)}, \beta | x_i, 0\right)\;, \tag{2.3}$$

with

$$\left(x_{p(i)}, \beta | x_i, 0\right) \;\equiv\; \int_{x_i}^{x_{p(i)}} \mathcal{D}x\, e^{-\mathcal{A}_e^{(i)}}\;. \tag{2.4}$$

We study the system at finite temperature, which is reflected in the fact that the worldlines wrap around the imaginary (thermal) time direction, with τ running from 0 to β, i.e. the action involves $\mathcal{A} = \int_0^\beta \ldots d\tau$.

[2] As shown by Feynman [48, 49], interactions in the worldline formalism are best handled by working in a relativistic formalism, where worldlines are parameterized in terms of a local proper-time coordinate. Our approach, while non-relativistic, uses a similar parametrization of worldlines.

[3] We work throughout in units where $\hbar = c = 1$.

Consider a general partition of the orbits of N particles grouped into different winding cycles via permutation,

$$N = \sum_{w=1}^{N} w\ C_w\ . \tag{2.5}$$

In this decomposition we keep track of the number of cycles (which we denote by C_w) each of length w, so that with each permutation we associate a series of numbers C_w, with $w = 1, ..., N$. Then, a sum over all permutations can be rewritten as a sum over all integers assigned to the various C_w, subject of course to an overall constraint, this constraint being that the total length of all cycles taken together must be N (for a discussion of this point, see [4]). The number of permutations with such a decomposition is

$$M(C_1, C_2, \cdots, C_N) = \frac{N!}{\prod_{w=1}^{N} C_w! w^{C_w}}\ . \tag{2.6}$$

The partition function of N bosons is a summation over different partitions

$$Z^{(N)}(\beta) = \frac{1}{N!} \sum_{\{C_1,\cdots,C_N\}} M(C_1, \cdots, C_N) \prod_{w=1}^{N} [Z(w\beta)]^{C_w}\ , \tag{2.7}$$

where for each loop one has

$$Z(w\beta) = \int d^d x \int_{\mathcal{C}_w} \mathcal{D}x\ e^{-\int_0^{w\beta} d\tau \left(\frac{M}{2}\dot{x}^2 + i\frac{e}{c}\dot{x}_i A^i\right)}\ , \tag{2.8}$$

with the loop winding w times around the imaginary time direction.

We consider first a single winding loop with length w. To study the Meissner effects, we employ a standard procedure, namely to first expand the interaction part of the partition function $\exp(-ie\int d\tau \dot{x}_i A^i)$ as a power series, and then compute the average of each term with respect to the free particle action, which leads to corrections of the form $\langle A^n \rangle_0$, i.e. averages taken with respect to the free system. Define for this particular winding loop the correction to the effective action to be $\Delta\Gamma(w\beta) = Z(w\beta) - Z_0(w\beta)$. Here the lowest order non-trivial term is of order A^2, and its contribution to the Euclidean effective action reads

$$\Delta\Gamma(w\beta)\ =\ \frac{e^2}{2}\Big\langle \int d\tau_1 \int d\tau_2\ \dot{x}_i(\tau_1) A^i(x(\tau_1))\ \dot{x}_j(\tau_2) A^j(x(\tau_2)) \Big\rangle_0\ , \tag{2.9}$$

where by definition the average of the operator O with respect to the free action is $< O[x] >_0 \sim \int d^d x \int \mathcal{D}x e^{-A_0} O[x]$, up to a normalization factor. We will work with the Fourier transform of the gauge potential $A(x) =$

[4] See appendix of [64].

$\int \frac{d^dk}{(2\pi)^d} e^{ikx}\tilde{A}(k)$, and will have to evaluate expectation values of the form $< e^{ik_1x(\tau_1)}e^{ik_2x(\tau_2)}\dot{x}(\tau_1)\dot{x}(\tau_2) >_0$. To do so, we expand the position as the sum of an average and a fluctuation part $x(\tau) = x_0 + \delta x(\tau)$, where the average is the same for all coordinates appearing above. The desired expectation value then factorizes into $< e^{i(k_1+k_2)x_0} >_0 < \delta\dot{x}(\tau_1)e^{ik_1\delta x(\tau_1)}\delta\dot{x}(\tau_2)e^{ik_2\delta x(\tau_2)} >_0$ (indices have been suppressed in an obvious fashion). The first factor is easily shown to result in a delta function $(2\pi/L)^d\delta(k_1+k_2)$, ensuring momentum conservation, and we evaluate the second factor by applying Wick's theorem. We get that

$$\begin{aligned}\Delta\Gamma(w\beta) =& \frac{e^2}{2L^d}\prod_{\alpha=1}^{2}\int d^dk_\alpha\ \delta(k_1+k_2)\ \tilde{A}^i(k_1)\tilde{A}^j(k_2) \\ & \int_0^{w\beta} d\tau_1 \int_0^{w\beta} d\tau_2 \left[\frac{\partial^2 G}{\partial\tau_1\partial\tau_2}\delta^{ij} + k_1^i k_1^j \frac{\partial G}{\partial\tau_1}\frac{\partial G}{\partial\tau_2}\right] e^{(k_1^2+k_2^2)G'} \ .\end{aligned} \tag{2.10}$$

Note that the τ integrals now run from 0 to $w\beta$. Here we used the standard language of Green's functions, which is explained as follows: for a single particle, the Green's function is defined as

$$\delta^{ij}G_1(\tau_1,\tau_2) \equiv \left\langle x^i(\tau_1)x^j(\tau_2)\right\rangle_0 \ , \tag{2.11}$$

which in the path integral formalism reads

$$G_1(\tau_1,\tau_2) = \int d^dx \int \mathcal{D}x\, e^{-\mathcal{A}_{e,0}} x(\tau_1)x(\tau_2) \ . \tag{2.12}$$

This Green's function can be derived from the zero frequency limit of the finite temperature harmonic oscillator, after a subtraction of an infinite contribution due to the zero Matsubara frequency, yielding

$$G_1(\tau_1,\tau_2) = -\frac{\tau_1-\tau_2}{2} + \frac{(\tau_1-\tau_2)^2}{2\beta} + \frac{\beta}{12} \ . \tag{2.13}$$

For a many particle system, we define the Green's function for a particular permutation pattern as

$$\begin{aligned}G_N(\tau_1,\tau_2) \equiv & \int dx_1\cdots dx_N \int_{x_1}^{x_{p(1)}} \mathcal{D}x^{(1)} \cdots \int_{x_N}^{x_{p(N)}} \mathcal{D}x^{(N)} \\ & e^{-\left(\mathcal{A}_e^{(1)}+\cdots+\mathcal{A}_e^{(N)}\right)} x(\tau_1)x(\tau_2) \ ,\end{aligned} \tag{2.14}$$

or

$$\delta^{ij}G_N(\tau_1,\tau_2) \ \equiv\ \left\langle x^i(\tau_1)x^j(\tau_2)\right\rangle_{\mathcal{P}} \ , \tag{2.15}$$

and the result for the chosen winding loop is just the one-particle Green's function with β replaced by $w\beta$

$$G_w(\tau_1,\tau_2) = -\frac{\tau_1-\tau_2}{2} + \frac{(\tau_1-\tau_2)^2}{2w\beta} + \frac{w\beta}{12} \ . \tag{2.16}$$

Furthermore, the subtracted Green's function [5] is defined as

$$G'(\tau_i, \tau_j) \equiv G(\tau_i, \tau_j) - G(\tau_i, \tau_i). \tag{2.17}$$

We now proceed to calculate the correction to the effective action (2.10). The δ-function forces $k_1 = -k_2$, and since the integrand only depends on the difference $\tau_1 - \tau_2$, one of the τ integrals can be easily calculated, giving only an overall factor. In this way (2.10) simplifies to

$$\Delta\Gamma \;=\; \frac{w\beta e^2}{2M^2L^d} \int d^dk \; \tilde{A}^i(k)\tilde{A}^j(-k) \; \Omega_{ij}(k) \; , \tag{2.18}$$

where all the relevant information is encapsulated in the momentum dependent function

$$\Omega_{ij}(k) = (k^2\delta^{ij} - k^ik^j) \int_0^{w\beta} d\tau \left(-\frac{1}{2} + \frac{\tau}{w\beta} \right)^2 e^{\frac{k^2}{M}(-\frac{\tau}{2} + \frac{\tau^2}{2w\beta})} \; . \tag{2.19}$$

When w is finite, including the case with only a single particle, the $k^2\delta^{ij} - k^ik^j$ term will give rise to two differentials on the gauge field when transformed back to real space, giving the spatial part of the well known vacuum polarization

$$\int d^dx \; F_{ij}(x) \; \Pi(-\partial^2) \; F^{ij}(x) \; , \tag{2.20}$$

with the field strength $F_{ij}(x) = \partial_i A_j(x) - \partial_j A_i(x)$. $\Pi(-\partial^2)$ is the self-energy of the electromagnetic field, with corrections arising from polarization effects induced by the bosons which are coupled to the electromagnetic field.

In the limit $w \to \infty$, a partial integration on Eq.(2.19) leads to the result

$$\Omega_{ij}(k) = (k^2\delta^{ij} - k^ik^j)\frac{M}{k^2} \left(1 - \int_{-\frac{1}{2}}^{\frac{1}{2}} dy e^{w\beta \frac{k^2}{2M}(y^2 - 1/4)} \right), \tag{2.21}$$

with $y = \tau/w\beta - 1/2$. The second term in the bracket vanishes when $w \to \infty$. Thus the k^2 term is killed, and we get a mass term for the transverse component of the gauge field

$$\Delta\Gamma \;=\; \frac{m^2}{2} \int d^dx \; A_i^\perp A_i^\perp, \tag{2.22}$$

with $A_i^\perp = (\delta_{ij} - \partial_i\partial_j/\partial^2)A_j$. This is exactly the desired Meissner effect. The contribution to the mass term coming from a single winding loop is

$$\Delta\Gamma(w\beta) \;\propto\; \frac{e^2 n}{M} \frac{w\beta}{N} A_\perp^2, \tag{2.23}$$

[5] This Green's function can be related to the zero frequency limit of a harmonic oscillator Green's function, and the subtraction removes a divergent term arising in this limit; the divergence can be traced to the contribution of the zero Matsubara frequency.

where $n = N/L^d$ is the number density. In the following, we ignore the backreaction of $A_\perp$ on the condensate.

To get the mass of the gauge field, one needs to sum over different cycle decompositions. The correction to the effective action of the whole system is

$$\Delta\Gamma = \frac{1}{N!}\sum_{\{C_w\}} M(\{C_w\}) \prod_{w=1}^{N} [Z_0(w\beta)]^{C_w} \sum_{w=1}^{N} C_w \Delta\Gamma(w\beta) \ . \tag{2.24}$$

The mass term is gotten by taking the thermodynamic limit of the above equation and keeping only terms with infinite winding. Here we need to be careful about the order of limits to take. As shown above, only those permutation patterns containing infinitely long winding loops (in the thermodynamic limit), will contribute to the mass term. So we will first take the limit that the winding number goes to infinity. To do so, we also need to take the total number of particles N, and the size of the system L, to infinity, while keeping the particle number density $n = N/L^d$ fixed. We employ a cutoff N_c for the winding number, which goes to infinity as the particle number $N \to \infty$, and count only those winding loops longer than N_c. For example, one can take N_c to be N^α with $0 < \alpha < 1$. In a box with side length L, the partition function of free bosons for a winding loop with length w is

$$Z_0(w\beta) = \left(\frac{L}{\lambda\sqrt{w}} \sum_{n=-\infty}^{\infty} e^{-n^2 (\frac{L}{\lambda})^2 \frac{\pi}{w}} \right)^d , \tag{2.25}$$

with the thermal de Broglie wavelength $\lambda = \sqrt{2\pi\beta/M}$. Consider the case of three dimensions, where Bose-Einstein condensation is known to occur at finite temperature, and where $2/3 < \alpha < 1$. In the limit $w \to \infty$, $L/\lambda\sqrt{w}$ goes to zero and $Z_0(w\beta) \to 1$ for $w > N_c$. Thus for a particular cycle decomposition, the contribution to the mass term from the long loops reads

$$\sum_{w=N_c}^{N} C_w \Delta\Gamma(w\beta) \sim \frac{e^2 n}{MN} \left(\sum_{w=N_c}^{N} w \ C_w \right) \ A_\perp^2 \ . \tag{2.26}$$

Here $\sum_{w=N_c}^{N} wC_w$ just counts the number of long loops in this cycle decomposition, and since it is only these longs loops which contribute, the mass square becomes

$$m^2 \ = \ \frac{e^2 n}{2M} \sum_{\{C_w\}} \frac{M(\{C_w\})}{N!} \left(\prod_{w=1}^{N} [Z_0(w\beta)]^{C_w} \right) \ \left(\frac{\sum_{w'=N_c}^{N} w' C_{w'}}{N} \right) \ . \tag{2.27}$$

Since for w large, $Z_0(w\beta) \simeq 1$, the temperature dependence is fully encoded in the contributions from small w. When tempereture goes to zero, $Z_0(w\beta) \to 1$

even for small w. The mass square thus reads

$$m^2 \;=\; \frac{e^2 n}{2M} \sum_{\{C_w\}} \frac{M(\{C_w\})}{N!} \frac{\sum_{w=N_c}^{N} w C_w}{N}. \tag{2.28}$$

The combinatorial factor in the above equation can be calculated by using random permutation theory [65, 66]. It can be rewritten in the form

$$\frac{1}{N} \sum_{w=N_c}^{N} \sum_{k=1}^{[N/w]} kw P(C_w = k) \;, \tag{2.29}$$

where $P(C_w = k)$ is the probability to have k cycles of length w, and according to [65, 66], is

$$P(C_w = k) = \frac{w^{-k}}{k!} \sum_{j=0}^{[N/w]-k} (-1)^j \frac{w^{-j}}{j!} \;. \tag{2.30}$$

We can estimate the magnitude of the combinatorial factor as follows. For large winding number w, the probability to have large number k of them is extremely small. Thus we can concentrate on small k, where $P(C_w = k)$ is approximately $\frac{1}{k!} e^{-1/w} w^{-k}$. Summing over k gives roughly $\sum_k kw P(C_w = k) \simeq 1$. Taking N_c to be of order $\sqrt{N}$, the combinatorial factor is then approximately one. Thus as the temperature goes to zero, the mass square goes over to

$$m^2 \;=\; \frac{e^2 n}{M} \;. \tag{2.31}$$

With the closed-form formula given above, one can also calculate the combinatorial factor numerically and it converges to one very quickly [6]. The bottom line is that a finite value of mass can be gotten by summing over the long winding loops.

It is conceptually the same, but technically even easier to work in the grand-canonical ensemble, where the partition function for free bosons is

$$F_G(\beta) = -\frac{1}{\beta} \sum_{w=1}^{\infty} (\pm 1)^{w-1} \frac{Z_0(w\beta)}{w} e^{w\beta\mu} \;, \tag{2.32}$$

with the plus sign for bosons and the minus sign for fermions. In the presence of an electromagnetic field, one needs only to replace $Z_0(w\beta)$ by $Z(w\beta)$. The change in the free energy due to the background field is

$$\Delta F = \frac{1}{\beta} \frac{e^2 n}{M} A_\perp^2 \frac{1}{N} \sum_{w=N_c}^{\infty} \frac{e^{w\beta\mu}}{w} w\beta. \tag{2.33}$$

[6] For $N = 100, 10000, 40000$, it is correspondingly $0.91, 0.9901, 0, 995025$.

The quantity $N_L = \sum_{w=N_c}^{\infty} e^{w\beta\mu}$ is just the number of particles residing in the long loops, or equivalently the number of particles in the condensate. This can be shown by counting the number of particles

$$N = \sum_{w=1}^{\infty} Z_0(w\beta) e^{w\beta\mu} \ . \tag{2.34}$$

For small winding, $Z_0(w\beta)$ is approximately $(L/\lambda\sqrt{w})^d$, while for large winding approximately $(L/\lambda\sqrt{w})^d + 1$. Thus N can be rewritten as

$$N = \sum_{w=1}^{\infty} \left(\frac{L}{\lambda\sqrt{w}}\right)^d e^{w\beta\mu} + \sum_{w=N_c}^{\infty} e^{w\beta\mu} \ , \tag{2.35}$$

where the first term represents the number of particles N_S living in the short loops, and the second term the long loops. Consider again the case of three dimensions, where the critical temperature T_c is determined by setting the chemical potential $\mu = 0$ and equating $N = N_S$, that is $N = \sum_{w=1}^{\infty} (L/\lambda_c)^3 w^{-3/2}$, where $\lambda_c = \sqrt{2\pi/T_c M}$. In this way the ratio of the size of the system and the thermal de Broglie wavelength can be expressed as

$$\frac{L}{\lambda} = \left(\frac{N}{\zeta(3/2)}\right)^{1/3} \left(\frac{T}{T_c}\right)^{1/2} \ . \tag{2.36}$$

This result can be derived via standard statistical mechanics methods; see for example [36] and references therein. One can show that when Bose-Einstein condensation occurs (and thus $\mu = 0$), the number of particles winding in the short loops is

$$N_S = N \left(\frac{T}{T_c}\right)^{3/2} \ . \tag{2.37}$$

Thus the fraction of the particles living in the long loops is

$$\frac{N_L}{N} = 1 - \left(\frac{T}{T_c}\right)^{3/2} \ . \tag{2.38}$$

When there is no condensation (and thus $\mu < 0$), N_L/N vanishes in an obvious way. The conclusion is that the mass square of the transverse photons is determined by the number density of the condensed particles

$$m^2 = \frac{e^2 n_{\rm cod}}{M} \ . \tag{2.39}$$

It has been shown [67] using perturbation theory that for an ideal charged Bose gas, with the Coulomb interaction ignored and only the magnetic coupling $\vec{p} \cdot \vec{A}$, when there is condensation, there is a Meissner effect. The inverse screening length squared is known to be $1/\lambda^2 = (e^2/M) n_{\rm cod}$. The calculation above

agrees perfectly with this result. Inclusion of the Coulomb repulsion between the charged particles would lead to a renormalization of the superfluid density. These phenomena are well understood in quantum field theory. The above first quantized formalism gives a new picture of these well known effects.

2.3 Inclusion of Spin and Fermionic Statistics

We begin by recalling that the Hilbert space structure of a system is given by the path integral for zero Hamiltonian ($H = 0$), wherein the exponent appearing in the path integral sum consists simply of a Berry phase term of the form $p\dot{q}$, arising from overlaps of complete sets of position and momentum states at neighboring time slices. Consider a non-relativistic point particle system in three space dimensions, given by the following path integral for Grassmann variables $\theta^j(t)$ [36]

$$Z \;=\; \int \mathcal{D}\theta \; e^{i \int dt \frac{i}{4} \theta_j \dot{\theta}^j} \quad \text{for } j = 1, 2, 3, \tag{2.40}$$

which is a pure Berry phase term. This path integral takes as its starting point the classical mechanics of spin, and can be constructed via spin coherent states [68][7]. The momentum conjugate to $\theta^j(t)$ is given by $p_j = -(i/4)\theta^j$, the sign arising from the Grassmann nature of θ. The equation of motion forces the variable θ to be time independent, $\dot{\theta}^j(t) = 0$. That the momentum is proportional to the position is a reflection of the fact that systems that are first order in time derivatives (like the Dirac equation) represent constrained systems. The second-class constraints are

$$\chi_j \;=\; p_j \;+\; \frac{i}{4}\theta_j \;=\; 0 \; . \tag{2.41}$$

The origin of the constraint lies in the fact that the transformation from Lagrangian configuration space $q, \dot{q}$, to the phase space q, p, is singular with a vanishing Jacobian determinant, which means we can not invert the velocities to solve for the momenta, and results in a Hamiltonian which is defined only on the constraint surface. Dirac [70] has shown that such systems can be handled if one extends the notion of Poisson brackets to Dirac brackets, defined as

$$\{A, B\}_D \;=\; \{A, B\} \;-\; \{A, \chi_i\} \, C^{i,j} \, \{\chi_j, B\} \; , \tag{2.42}$$

and $C^{i,j}$ are the components of the matrix inverse of C, whose elements are are built from the Poisson brackets of the constraints

$$C_{i,j} \;\equiv\; \{\chi_i, \chi_j\} \; . \tag{2.43}$$

[7] See [69] for a general review of applications of worldline formalism to perturbative quantum field theory

Care must be taken that the Poisson brackets of Grassmann valued fields are defined as [71]

$$\{f(\theta_i, p_j), g(\theta_i, p_j)\} \;=\; -\left(\frac{\partial f}{\partial \theta_k}\frac{\partial g}{\partial p^k} \;+\; \frac{\partial g}{\partial \theta_k}\frac{\partial f}{\partial p^k}\right) , \tag{2.44}$$

in order to satisfy natural algebraic properties and yield a proper quantization for fermions. With these, we see that the Dirac bracket associated to (2.40) is

$$\{p_i, \theta_j\}_D \;=\; -\frac{1}{2}\delta_{i,j} \; . \tag{2.45}$$

Canonical quantization proceeds by replacing the Dirac bracket with the anti-commutator (for fermions), as $\{,\}_D \to -i\,[,]_+$. Making this substitution and enforcing the constraints (2.41), we have the operator equation

$$\left[\hat{\theta}_i \; , \; \hat{\theta}_j\right]_+ \;=\; 2\delta_{ij} \; . \tag{2.46}$$

In three dimensions, the operators θ^i can be defined via their matrix elements as

$$\langle\alpha|\hat{\theta}^i|\beta\rangle \;\equiv\; \sigma^i_{\alpha,\beta} \; , \tag{2.47}$$

with the range of the spinor indices $\alpha, \beta = 1, 2$, and the σ matrices being the standard Pauli matrices, after which (2.46) is a simple identity for the Pauli matrices. A classical spin vector can also be defined

$$S^i \;=\; -\frac{i}{4}\epsilon^{ijk}\theta^j\theta^k \; , \tag{2.48}$$

which after canonical quantization, gives an operator representation of the spin algebra

$$\left[\hat{S}^i \; , \; \hat{S}^j\right]_- \;=\; i\epsilon^{ijk}\hat{S}^k \; . \tag{2.49}$$

Now consider the addition to the zero Hamiltonian path integral a term describing the coupling of a spin to an external magnetic field $\vec{B}$, $H = -\vec{S}\cdot\vec{B}$, the spin vector having already been defined by (2.48). Taking account of (2.47), we see that [36] matrix elements of the operator

$$e^{i\int dt \vec{B}\cdot\frac{\vec{\sigma}}{2}} \; , \tag{2.50}$$

has the path integral representation

$$\int \mathcal{D}\theta \; e^{i\int dt \frac{i}{4}\left(\theta_j\dot{\theta}^j \,+\, \epsilon^{jkl}B^j\theta^k\theta^l\right)} \; . \tag{2.51}$$

The trace of the operator (2.50) can then be computed by summing the path integral (2.51) over all anti-periodic paths, for which $\theta^j(\tau_b) = -\theta^j(\tau_a)$. For zero external magnetic field this fixes the normalization of the Berry phase term

(2.40). This normalization simply counts the dimension of the relevant spinor representation in d dimensions

$$\int \mathcal{D}\theta \exp\left[\frac{i}{4}\int_{\tau_a}^{\tau_b=\tau_a} d\tau\, \theta_j \dot{\theta}^j\right] \;=\; 2^{d-2}\;, \tag{2.52}$$

which for $d = 3$ coincides with the dimension of the Pauli matrices (2.47).

The free particle action (2.1) can now be modified for the inclusion of spin degrees of freedom as follows [36]

$$\mathcal{A}_{e,0} = \int_{\tau_a}^{\tau_b} d\tau \left(\frac{M}{2}\dot{x}^2(\tau) - \frac{i}{4}\theta_j(\tau)\dot{\theta}^j(\tau)\right)\;, \tag{2.53}$$

while the coupling to the electromagnetic field becomes

$$\mathcal{A}_{e,\mathrm{int}} \;=\; i\frac{e}{c}\int_{\tau_a}^{\tau_b} d\tau \left(\dot{x}_j A^j + i\frac{1}{4M}F_{jk}\theta^j\theta^k\right)\;. \tag{2.54}$$

This action contains an "orbital" contribution associated with the particle's motion x, together with a "spin" contribution arising from the Grassmann coordinates θ. The Grassmann field obeys antiperiodic boundary condition with $\theta(\tau_b) = -\theta(\tau_a)$, in contrast to the periodic boundary condition for x.

An important property of the spinfull interacting action (2.53) and (2.54), is an underlying worldline supersymmetry, mixing the bosonic and fermionic degrees of freedom, given by [36, 72]

$$\begin{aligned}\delta x^j(\tau) &= i\alpha\theta^j(\tau)\;,\\ \delta\theta^j(\tau) &= \alpha\dot{x}^j(\tau)\;,\end{aligned} \tag{2.55}$$

with α an arbitrary Grassmann parameter. We will show that this symmetry has far reaching consequences for the properties of the fermionic system. The non-existence of the Anderson-Higgs effect can be traced to a non-renormalization resulting from this symmetry. Note that this worldline supersymmetry does not imply a supersymmetric system in the target space in which the particle is embedded, which represents just a bosonic system; it acts as a short-hand to capture the particle statistics in the target space.

We now turn our attention to the study of N spin-$\frac{1}{2}$ fermions, which follows essentially the same logic as for bosons, except that now we must deal with the action given in (2.53) and (2.54), which as already pointed out manifests a worldline supersymmetry. In the presence of many particles, the worldline can wind many times around the temporal direction, and the functional integral over the Grassman fields we introduced serves to keep track of the exchange statistics,

$$\int \mathcal{D}\theta \exp\left[\frac{i}{4}\int_0^{w\beta} d\tau\theta_j\dot{\theta}^j\right] \;\propto\; (-1)^{w-1}\;, \tag{2.56}$$

providing a minus sign for an even winding (corresponding to an odd permutation), and a plus sign for odd winding (corresponding to an even permutation), and the proportionality constant counting the number of fermionic degrees of freedom. This sign agrees with the $(-1)^{w-1}$ factor in the grand-canonical formalism (2.32).

Proceeding as we did earlier for bosons, we set the electric field to zero, pick out the long windings and expand the interaction term, and we get for the effective action the correction

$$\begin{aligned}\Delta\Gamma(w\beta) =&\frac{e^2}{2}\Big\langle \int d\tau_1 \int d\tau_2 \ \big\{\dot{x}_i(\tau_1)A^i(x(\tau_1))\ \dot{x}_j(\tau_2)A^j(x(\tau_2)) \\ &-\frac{1}{(4M)^2}F_{ij}(\tau_1)\theta^i(\tau_1)\theta^j(\tau_1)F_{kl}(\tau_2)\theta^k(\tau_2)\theta^l(\tau_2)\Big\}\Big\rangle_0 \ ,\end{aligned} \tag{2.57}$$

Here in addition to the bosonic Green's function, we also need the fermionic contribution

$$2\delta^{ij}G_w^f(\tau_1,\tau_2) \equiv \left\langle \theta^i(\tau_1)\theta^j(\tau_2)\right\rangle_{N,0} \ , \tag{2.58}$$

which is calculated to be

$$G_w^f(\tau_1,\tau_2) = \frac{1}{2}\theta(\tau_1-\tau_2) \ , \tag{2.59}$$

with $\theta(\tau)$ the step function. Carrying out the steps as before, we get the same result for the effective actions as in (2.18), with the observation that we need to add a fermionic contribution to $\Omega_{ij}(k)$, which shifts the term $(-\frac{1}{2}+\frac{\tau}{N\beta})^2$ to $(-\frac{1}{2}+\frac{\tau}{N\beta})^2-\frac{1}{4}$, that is

$$\Omega_{ij}(k) = (k^2\delta^{ij}-k^ik^j)\int_0^{w\beta} d\tau \left((-\frac{1}{2}+\frac{\tau}{w\beta})^2-\frac{1}{4}\right) e^{\frac{k^2}{M}(-\frac{\tau}{2}+\frac{\tau^2}{2w\beta})} \ . \tag{2.60}$$

and the new addition will make a critical impact.

The qualitative picture remains the same for w finite. There is still the vacuum polarization effect. However, in the limit $w\to\infty$, the picture changes completely. The integral appearing in $\Omega_{ij}(k)$ (2.60), becomes

$$\begin{aligned}&\int_0^{w\beta} d\tau \left[(-\frac{1}{2}+\frac{\tau}{w\beta})^2-\frac{1}{4}\right] e^{\frac{k^2}{M}(-\frac{\tau}{2}+\frac{\tau^2}{2w\beta})} \\ =&\frac{M}{k^2}\left(1-\frac{\sqrt{\pi}}{2}\frac{(\tilde{w}+2)}{\sqrt{\tilde{w}}}e^{-\tilde{w}/4}\mathrm{Erfi}[\sqrt{\tilde{w}}/2]\right) \ ,\end{aligned} \tag{2.61}$$

with $\tilde{w}=w\beta\frac{k^2}{2M}$, and the imaginary error function given by $\mathrm{Erfi}[x]=\frac{2}{\sqrt{\pi}}\int_0^x e^{t^2}dt$. One can see that the function (2.61) vanishes in the limit $w\to\infty$, thus

$$\lim_{w\to\infty}\Omega_{ij}(k) = 0, \tag{2.62}$$

a result that can also arrived at by making a saddle point expansion of the left-hand side. That is to say that the contribution to the effective action arising from the fermionic part cancels precisely that of the bosonic part in the limit of large N. In the Grassmannian language, it is the worldline supersymmetry between the bosonic coordinate x and the fermionic coordinate θ that destroys the Anderson-Higgs or Meissner effect. We note again that the Grassmann fields simply encapsulate the fermion signs, and it is these signs which transform the behaviour in the case of fermions in an essential way.

2.4 Conclusions

Below some finite critical temperature, infinitely long windings proliferate in both bosonic and fermionic systems. For the former this drives Bose-Einstein condensation, while for the latter it occurs at the Fermi temperature T_F. Owing to the statistics of the particles involved though, the long windings generate vastly different physics. For the Bose system, it gives rise to superfluidity for neutral systems and superconductivity for charged ones. Both are consequences of spontaneous symmetry breaking, breaking a global symmetry in the neutral superfluid and a gauge symmetry for the charged superconductor (seen as the Anderson-Higgs mechanism, and responsible for the Meissner effect).

We have attacked the question of whether fermions can drive spontaneous symmetry breaking of a local nature with the tools of the signful path integral. We managed the fermion signs by introducing a new Grassmannian coordinate, leading to a supersymmetric worldline theory. It is supersymmetry then that eliminates the Meissner effect for a gas of charged fermions. The question still remains whether one can find an order parameter for the phase transition involving fermions, even in the free case, and how to understand the sharpness of the Fermi surface.

Chapter 3

Fermions in the Constrained Path Integral: towards the Minus Sign Problem

3.1 Introduction

The 'quantum weirdness' of the Fermi-gas is obvious: how to understand the Fermi-surface, the Fermi-energy and so forth, just knowing about classical statistical physics? The interacting Fermi-liquid is a bit more than the Fermi-gas, but focusing on the emergence principles it is deep inside the same thing. As Landau pointed out, the Fermi-liquid is connected by adiabatic continuation to the Fermi-gas meaning that the two are qualitatively indistinguishable at the long times and distances where emergence is in full effect. The great framework of diagrammatic perturbation theory developed in the 1950's [27] does allow to arrive at quite non trivial statements associated with the presence of the interactions but it only works under the condition that the Fermi-liquid is adiabatically connected to the Fermi gas. But conventional Feynman diagrams are impotent with regard to revealing the nature of 'non Fermi liquids'. To complete the 'fermionic' repertoire of theoretical physics, Bardeen, Cooper and Schrieffer discovered the 'Hartree-Fock' mechanism, showing how the Fermi-gas can become unstable towards a bosonic state, like the superfluids- and conductors, charge- and spin density wave states and so forth. Despite fermionic peculiarities (like the gap function), this is eventually a recipe telling us how the fermi-gas can

turn into bosonic matter that is in turn ruled by the Ginzburg-Landau-Wilson classical emergence rules.

Given the present repertoire of theoretical physics, all we know to do with fermionic matter is to hope that it is a Fermi gas or bound in bosons. But we are facing a zoo of 'non-Fermi-liquid' states of electrons coming out of the experimental laboratories and the theorists are standing empty handed because the fermion signs render all the fancy theoretical technologies to be useless. The NP hardness of the sign problem tells us that there is no mathematically exact solution but how many features of the physical world we understand well are actually based on exact mathematics? Nearly all of it is based on an effective description, mathematics that is tractable while it does describe accurately what nature is doing although it is not derived with exact mathematics from the first principles. Is there a way to handle non-Fermi-liquid matter on this phenomenological level?

The remainder of this chapter is dedicated to the case that there is reason to be optimistic. This optimism is based on a brilliant discovery some fifteen years ago of an alternative path-integral description of the fermion problem by David Ceperley [73, 74]. This 'constrained' or 'Ceperley' path integral has a Boltzmannian structure (i.e., only positive probabilities) but the signs are traded in for another unfamiliar structure: a structure of constraints acting on a 'bosonic' configuration space that is coding for all the effects of Fermi-Dirac statistics. This is called the reach and it amounts to the requirement that for all imaginary times τ between zero and $\hbar\beta$ ($\beta = 1/(k_B T)$) the worldline configurations should not cross the hypersurface determined by the zero's of the full N-particle, imaginary time density matrix. Although the constrained path integral suffers from a self-consistency problem since the exact constrain structure is not known except for the non-interacting Fermi-gas, it appears that this path integral is quite powerful for the construction of phenomenological effective theories. The information carried by the reach lives 'inside' the functional integral and should therefore be averaged. This implies that only global- and averaged properties of this reach should matter for the physics in the scaling limit. The reach is in essence a high dimensional geometrical object, closely related to the more familiar 'nodal hypersurface' associated with the sign changes of ground state wave function. The theoretical program is to classify the geometrical and topological properties of the reach in general terms, to find out how this information is averaged over in the path integral, with the potential to yield eventually a systematic classification of phenomenological theories of fermionic matter.

Given that Ceperley derived his path integral already quite some time ago, why is it not famous affair? These path integral are not so easy to handle. Although various interesting results were obtained [75], even the attempt to reconstruct the Fermi-liquid in this language stalled. But these efforts were limited to a very small community, with a focus on large scale numerical calculations. The potential of the Ceperley path integral to address matters of principle appears to be overlooked in the past. We discovered the Ceperley path integral in an attempt to understand the scale invariant fermionic quantum critical states as

found in the heavy fermion intermetallics. We started out on the more primitive level of wave function nodal structure, discovering by accident the much more powerful Ceperley path integral approach. We believe that we have delivered proof of principle that this language gives penetrating insights in the nature of a prominent non-Fermi liquid state: the fermionic quantum critical states realized in the heavy fermion intermetallics. Since this work is still under review we will not address it in any detail. However, to make further progress, we were confronted with the need to better understand the detailed workings of the Ceperley path integral and we decided to revisit the description of the Fermi gas and the Fermi liquid. The outcomes of this pursuit are summarized in this chapter.

This remainder of this chapter is organized as follows. In section 3.2 we introduce the Ceperley path integral, reviewing it's derivation as well as various other technical issues. Section 3.3 is intended to be the highlight of this chapter. We present a quite simple solution of the Ceperley path integral for the Fermi-gas: the Fermi-gas turns out to be in one-to-one correspondence with a system of cold atoms in an harmonic trap, subjected to a deep optical lattice potential such that the atoms form a perfect Bose Mott-insulator! Finally in section 3.4 we turn to the real space description of the Fermi-gas. The presence of the reach changes radically the winding statistics as compared to the boson case and it appears that the windings of the Ceperley particles in *any* higher dimension are counted as if they are the windings associated with soft core bosons living in one space dimension.

3.2 Ceperley's constrained path integral

In this section we review Ceperley's 1991 discovery of a path integral representation for arbitrary fermion problems that is not suffering from the 'negative probabilities' of the standard formulation [73]. Surely, one cannot negotiate with the NP-hardness of the fermion problem and Ceperley's path integral is not solving this problem in a mathematical sense. However, the negative signs are transformed away at the expense of a structure of constraints limiting the Boltzmannian sum over world-line configurations. These constraints in turn can be related to a geometrical manifold embedded in configuration space: the 'reach', which is a generalization of the nodal hypersurface characterizing wave functions to the fermion density matrix. This reach should be computed self-consistently: it is governed by the constrained path integral that needs itself the reach to be computed. This is again a NP-hard problem and Ceperley's path integral is therefore not solving the sign problem. However, the reach contains all the data associated with the differences between bosonic and fermionic matter, and only its average and global properties should matter for the physics in the scaling limit since it acts on worldline configurations that themselves are averaged. Henceforth, it should be possible in principle to classify all forms of fermionic matter in a phenomenological way by classifying the average geometrical- and

topological properties of the reach, to subsequently use this data as an input to solve the resulting bosonic path integral problem. This procedure is supposedly a unique extension of the Ginzburg-Landau-Wilson paradigm for bosonic matter to fermionic matter. We do not have a mathematical proof that this procedure will yield a complete classification of fermionic matter, but we have some very strong circumferential evidences in the offering that it will work. The status of our claim is conjectural in the mathematical sense.

Let us start out presenting the answer. Ceperley proved in 1991 that the following path integral is strictly equivalent to the standard fermion path integral Eq. (1.11,1.12), as we reviewed in the introduction,

$$\rho_F(\mathbf{R},\mathbf{R};\beta) = \frac{1}{N!}\sum_{\mathcal{P},even}\int_{\gamma:\mathbf{R}\rightarrow\mathcal{P}\mathbf{R}}^{\gamma\in\Gamma_\beta(\mathbf{R})}\mathcal{D}\mathbf{R}e^{-\mathcal{S}[\mathbf{R}]/\hbar}. \tag{3.1}$$

This is quite like the standard path integral, except that one should only sum over *even* permutations (the reason to address this in section IV), while the allowed worldline configurations γ are constrained to lie 'within the reach Γ'. This reach is defined as,

$$\Gamma_\beta(\mathbf{R}) = \{\gamma : \mathbf{R}\rightarrow\mathbf{R}' | \rho_F(\mathbf{R},\mathbf{R}(\tau);\tau) \neq 0\} \tag{3.2}$$

for all imaginary times $0 < \tau < \hbar\beta$. In words, only those wordline configurations should be taken into account in Eq. (3.1) that do not cause a sign change of the full density matrix at every intermediate imaginary time between 0 and $\hbar\beta$. In outline, the proof of this result is as follows. The fermion density matrix is defined as a solution to the Bloch equation

$$\frac{\mathrm{d}\rho_F(\mathbf{R}_0,\mathbf{R};\beta)}{\mathrm{d}\beta} = -H\rho_F(\mathbf{R}_0,\mathbf{R};\beta) \tag{3.3}$$

with initial conditions

$$\rho_F(\mathbf{R}_0,\mathbf{R};\beta=0) = \frac{1}{N!}\sum_{\mathcal{P}}(-1)^p\delta(\mathbf{R}_0-\mathcal{P}\mathbf{R}). \tag{3.4}$$

In the following we fix the reference point $\mathbf{R}_0$ and define the reach $\Gamma(\mathbf{R}_0,\tau)$ as before as the set of points $\{\mathbf{R}_\tau\}$ for which there exists a continuous space-time path with $\rho_F(\mathbf{R}_0,\mathbf{R}_{\tau'};\tau') > 0$ for $0 \leq \tau' < \tau$. Suppose that the reach is known in advance. It is a simple matter to show that the problematical initial condition, Eq. (3.4), imposing the anti-symmetry can be replaced by a zero boundary condition on the surface of the reach. It follows because the fermion density matrix is a unique solution to the Bloch equation (3.3) with the zero boundary condition. One can now find a path integral solution without the minus signs. One simply restricts the paths to lie in the reach $\Gamma(\mathbf{R}_0,\tau)$ imposing the zero boundary condition on the surface of the reach. The odd permutations fall for sure out of the reach since $\rho_F(\mathbf{R}_0,\mathcal{P}_{odd}\mathbf{R}_0) = -\rho_F(\mathbf{R}_0,\mathbf{R}_0)$.

The Ceperley path integral revolves around the reach. How to think about this object? The way the path integral is constructed seems to break imaginary time translations. One has to first pick some 'reference point' $\mathbf{R}$ in configuration space at imaginary time 0 or $\hbar\beta$. Starting from this set of particle coordinates, one has to spread them out in the form of wordline configurations to check at every time slice that the density matrix does not change sign. The dimensionality of the density matrix is $2dN+1$ (twice configuration space plus a time axis) and the dimensionality of the reach is therefore $2dN$ (one overall constraint). However, when we first pick a reference point $\mathbf{R}$ and we focus on a particular imaginary time the dimensionality of this restricted reach is $dN-1$. In the limit $\tau \to \infty$ this restricted reach turns into a more familiar object: the nodal hypersurface associated with the ground state wave function. The density matrix becomes for a given $\mathbf{R}$ in this limit,

$$\rho(\mathbf{R}, \mathbf{R}'; \beta = \infty) = \Psi^*(\mathbf{R})\Psi(\mathbf{R}') \tag{3.5}$$

and the zero's of the density matrix are just coincident with the nodes of the ground-state wave function, $\Psi(\mathbf{R}) = 0$, where we have assumed that the ground state is non-degenerate. The wave function is anti-symmetric in terms of the fermion coordinates,

$$\Psi(\cdots, \mathbf{r}_i, \cdots, \mathbf{r}_j, \cdots) = -\Psi(\cdots, \mathbf{r}_j, \cdots, \mathbf{r}_i, \cdots), \tag{3.6}$$

and therefore the nodal hypersurface

$$\Omega = \{\mathbf{R} \in \mathbb{R}^{Nd} | \Psi(\mathbf{R}) = 0\} \tag{3.7}$$

is a manifold of dimensionality $\dim\Omega = Nd - 1$ embedded in Nd-dimensional configuration space. This nodal surface Ω is surely an object that is simpler than the full reach Γ and it is rather natural to train the intuition using the former. According to Ceperley's numerical results [73], it appears that at least for the Fermi gas the main features of the reach are already encoded in Ω. In a way, the dependence on imaginary time is remarkably smooth and unspectacular. A greater concern is the role of the reference point, or either the fact that the reach depends on two configuration space coordinates. In the long imaginary time limit, the reach factorizes in the nodal surfaces (Eq. (3.5)), which means that one can get away just considering the nodal surface of the ground state wave function, but this is not the case at finite imaginary times. It is not at all that clear what role the 'relative distance' $\mathbf{R} - \mathbf{R}'$ plays, although there is some evidence that it can be quite important as we will discuss in Section IX. Notice that the conventional 'fixed-node' quantum Monte-Carlo methods aim at a description of the ground state, using typically diffusion Monte-Carlo methods. As input for the 'fermionic-side', these only require the wave function nodal structure. The difference between the reach and this nodal structure is telling us eventually about the special nature of the excitations in the fermion systems since

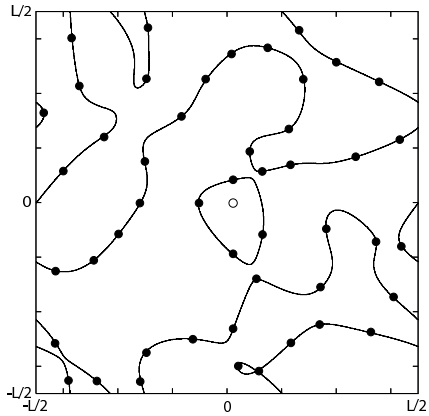

Figure 3.1: Cut through the nodal hypersurface of the ground-state wave function of $N = 49$ free, spinless fermions in a two-dimensional box with periodic boundary conditions. The cut is obtained by fixing $N - 1$ fermions at random positions (black dots) and moving the remaining particle (white dot) over the system. The lines indicate the zeros of the wave function (nodes). Note that the nodal surface cut has to connect the $N - 1$ fixed particles since the Pauli surface is a lower dimensional submanifold of dimension $Nd-d$ included in the nodal hypersurface with dimension $Nd - 1$.

the Ceperley path integral can be used to calculate dynamics, either in the form of finite temperature thermodynamics or, by Wick rotation to real time, about dynamical linear response. At this moment in time it is not well understood what the precise meaning is of these 'dynamical signs' encoded in the non-local nature of the reach.

Another useful geometrical object associated with Fermi-Dirac statistics is the Pauli surface, corresponding with the hypersurface in configuration space where the wave function vanishes because the fermions are coincident in real space,

$$\begin{aligned} P &= \bigcup_{i \neq j} P_{ij} \\ P_{ij} &= \{\mathbf{R} \in \mathbb{R}^{Nd} | \mathbf{r}_i = \mathbf{r}_j\}. \end{aligned} \tag{3.8}$$

Obviously, the Pauli surface is a submanifold of the nodal hypersurface of dimension $\dim P = Nd-d$. The specialty of one dimension is that the Pauli- and nodal hypersurfaces are coincident. This property that the nodes are 'attached' to the particles is the key to the special status of one dimensional physics as we will explain in detail in the next section.

In the next sections we will discuss in more detail the few facts that are known about the reach and nodal hypersurface geometry and topology. To complete the

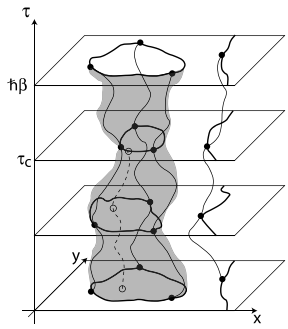

Figure 3.2: Nodal constraint structure in space-time seen by one particular particle. In the constraint path integral only world-line configurations $\{\mathbf{r}_\tau\}$ are allowed that do not cross or touch a node of the density matrix on all time slices, $\rho_F(\mathbf{R}_0, \mathbf{R}_\tau, \tau) \neq 0$ for $0 \leq \tau < \hbar\beta$. Therefore, a particular particle (white circle) is constrained by the dynamical nodal tent (grey surface) spanned by the $N-1$ remaining particles trajectories (black circles). In a Fermi liquid the nodal tent has a characteristic dimensions and particles feel the nodal constraints at an average time scale τ_c. Later we will see that these scales are in one-to-one correspondence with the Fermi degeneracy scale E_F.

discussion of the basic structure of the Ceperley Path Integral, let us once more emphasize that according to its definition Eq. (3.1) one still has to sum over *even* permutations in so far these do not violate the reach. As for the signful path integral, this translates via the sum over cycles into a sum over winding numbers that are now associated with triple exchanges of particles. We explained already in detail in section IV that this has the peculiar consequence that it codes for supersymmetry when one is dealing with the free quantum gas that just knows about the even permutation requirement. Because of the constraints, the 'particles' of the Ceperley path integral are actually very strongly interacting and it is unclear to what extent this supersymmetry is of any relevance to the final solution. In fact, we do know for the Fermi-gas that the combined effect of the constraints and the triple exchanges is to eventually give back a free gas with Fermi-Dirac statistics. As we discussed in section IV, there is a 'don't worry theorem' at work because the thermodynamics of the supersymmetric gas is quite similar to the Bose gas.

In conclusion, Ceperley has demonstrated that in principle fermion problems can be formulated in a probabilistic, Boltzmannian mathematical language, paying the prize of a far from trivial constraint structure that is a-priori not known while it cannot be exactly computed. Qualitatively, the reach is like the nodal structure of a wave function. It is obvious that the nodal structure codes for physics but this connection is largely unexplored, while the remainder of this

chapter is dedicated to the case that it is actually quite easy to make progress, at least with regard to the Fermi-liquid. One particular property is so important that it should be already introduced here. Any wave function of a system of fermions has the anti-symmetry property Eq. (3.6) and naively one could interpret this as 'any physical system of fermions has its fermionic physics encoded in a $Nd-1$ dimensional nodal surface'. This is obviously not the case. It is easy to identify a variety of fermionic systems where many more nodes are present in the fermion wave function than are required to encode the physics. A first example are Mott-insulating antiferromagnets on bipartite lattices. Because the electrons are localized they become effectively distinguishable. One can therefore transform away remnant signs in the Heisenberg spin problem by Marshall sign transformations: the bottom line is that such Mott-insulators can be handled by standard bosonic quantum Monte Carlo methods. A next example is physics in one dimensions, as we will discuss in the next section, where again the fermion signs can be transformed away completely, in a way that can be neatly understood in terms of the topology of the nodal surface. Nodal structure is therefore like a gauge field: it carries redundant information that is inconsequential for the physics. Nodal structure that is in this 'gauge volume' we call *reducible* nodal structure, while the 'gauge invariant' (physical) part of the nodal structure we call *irreducible*, and as a first step one should always first isolate the true, irreducible signs.

3.3 The Fermi gas as a cold atom Mott-insulator in momentum space

The Fermi-gas of the canonical formalism is very easy to solve exactly, and one would expect that in one or the other way this should mean that the constrained path integral is also easy to solve. This is not true at all in the position representation, as we will discuss in the next section. However, considering the derivation of the Ceperley path integral there is actually no preferred status of real space. The construction is completely independent of the representation one chooses for the single particle states. On the canonical side momentum space is the convenient representation to start from in the galilean continuum, or either any other basis that diagonalizes the single particle problem. As we will show in this section, also the Ceperley path integral of the Fermi-gas becomes very easy indeed when one chooses to formulate it in momentum space. After a couple of straightforward manipulations one finds a sign free, Boltzmannian path integral showing a most entertaining correspondence: the Fermi-gas is in one-to-one correspondence with a system of classical atoms forming a Mott insulating state in the presence of a commensurate optical lattice of infinite strength, living in a harmonic potential trap of finite strength (see Fig. 3.3a). This is literal and the only oddity is that this trap lives in momentum space instead of real space; the Fermi surface is just the boundary between the occupied optical lattice sites and

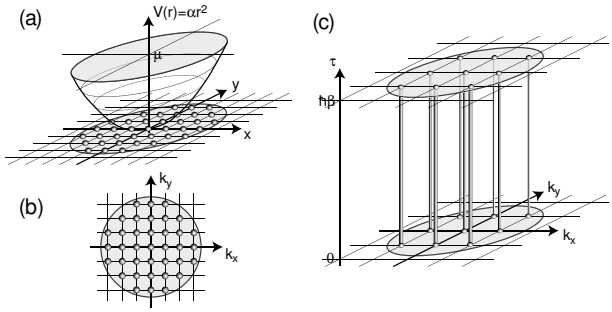

Figure 3.3: (a) a system of classical atoms forming a Mott insulating state in the presence of a commensurate optical lattice of infinite strength, living in a harmonic potential trap $V(\vec{r}) = \alpha r^2$ of finite strength; (b) the trap in momentum space k_x, k_y instead of real space; the Fermi surface is just the boundary between the occupied optical lattice sites and the empty ones; (c) a grid of allowed momentum states $k = (2\pi/L)(k_x, k_y, k_z, ...)$ where the k_i's are the usual integers and any worldline just closes on itself along the imaginary time τ direction $0 \to \beta$: single particle momentum conservations prohibit anything but the one cycles.

the empty ones. This boundary is sharp at zero temperature but it smears at finite temperature because of the entropy that can be gained by exciting atoms out of the trap! When you are quick, you should already have realized that this trap interpretation is actually consistent with everything we know about the Fermi-gas. Let us now proof it by constructing the Ceperley path integral.

The central wheel of the Ceperley path integral is the fermion density matrix. One should first guess an ansatz, use it to construct the path integral, to check if the same density matrix is produced by the path integral. Surely we know the full fermion density matrix for the Fermi gas, and in momentum space this turns out to be a remarkably simple affair. The k-space density matrix can be written as the determinant formed from imaginary time single particle propagators in the galilean continuum,

$$g(\mathbf{k}, \mathbf{k}'; \tau) = 2\pi\delta(\mathbf{k} - \mathbf{k}')e^{-\frac{|k|^2\tau}{2\hbar M}}. \tag{3.9}$$

Since we live in the space of exact single quantum numbers these propagators are diagonal; in the galilean continuum this just means the conservation of momentum, but when translational symmetry is broken one should use here just the basis diagonalizing the single particle Hamiltonian.

Consider now the full momentum configuration space $\mathbf{K} = (\mathbf{k}_1, \ldots, \mathbf{k}_N)$ imaginary time density matrix,

$$\rho_F(\mathbf{K}, \mathbf{K}'; \tau) = \frac{1}{N!}\sum_{\mathcal{P}}(-1)^p \prod_{i=1}^{N} g\left(\mathbf{k}_{p(i)}, \mathbf{k}'_i; \tau\right). \tag{3.10}$$

We find that the delta functions cause a great simplification. Substituting the single-fermion expression Eq. (3.9) in this expression for the density matrix Eq. (3.10) we obtain:

$$\begin{aligned}\rho_F(\mathbf{K},\mathbf{K}';\tau) &= \frac{1}{N!}e^{-\sum_{i=1}^{N}\frac{|\mathbf{k}_i|^2\tau}{2\hbar M}} \\ &\quad\times\sum_{\mathcal{P}}(-1)^p\prod_{i=1}^{N}2\pi\delta(\mathbf{k}_{p(i)}-\mathbf{k}'_i). \end{aligned} \tag{3.11}$$

Since the single particle propagators are eigenstates of the Hamiltonian, the momentum world lines go 'straight up' in the time direction until they arrive at the time τ where the reconnections can take place associated with the permutations. But the δ function enforces that the permuted momentum has to be the same as the non-permuted one, and the worldlines can therefore not wind except when the momenta of some pairs of fermions coincide. But now the sum of the permutations in Eq. (3.11) is zero due to the Pauli principle. Mathematically, this follows from the fact that the expression on the right hand side of Eq. (3.11) is actually a Slater determinant formed from the delta-functions $2\pi\delta(\mathbf{k}_{p(i)}-\mathbf{k}'_i)$ as the matrix elements of the $Nd\times Nd$ matrix, that are indexed by momenta $\{\mathbf{k}_{p(i)},\mathbf{k}'_i\}$. Hence, when two of the momenta coincide (e.g. $\mathbf{k}_i=\mathbf{k}_j$, $i\neq j$)there are two coinciding raws/columns in the matrix and the Slater determinant equals zero. The result is that Eq. (3.10) factorizes in $N!$ relabeling copies, associated with $N!$ nodal cells like in 1+1D, of the following simple density matrix describing distinguishable and localized particles in momentum space,

$$\rho_F(\mathbf{K},\mathbf{K}';\tau)=\prod_{\mathbf{k}_1\neq\mathbf{k}_2\neq\cdots\neq\mathbf{k}_N}^{N}2\pi\delta(\mathbf{k}_i-\mathbf{k}'_i)e^{-\frac{|\mathbf{k}_i|^2\tau}{2\hbar M}}. \tag{3.12}$$

This has the structure of a Boltzmannian partition sum of a system subjected to steric constraints: it is actually the solution of the Ceperley path integral for the Fermi gas in momentum space! Let us apply periodic boundary conditions so that on every time slice of the Ceperley path integral we find a grid of allowed momentum states $\mathbf{k}_i=(2\pi/L)(k_{i,x},k_{i,y},k_{i,z},....)$ where the $k_{i,\alpha}$'s are the usual integers (see Fig. 3.3b). We learn directly from Eq. (3.12) that we can ascribe a distinguishable particle with every momentum cell, with a worldline that just closes on itself along the time direction: single particle momentum conservation prohibits anything but the one cycles (see Fig. 3.3c). In addition, we find that the reach just collapses to the Pauli hypersurface, just as in one dimensions: per momentum space cell either zero or one worldline can be present. These worldlines are given by Eq. (3.9): since we are living in exact quantum number space these just go straight up along the time direction, since there are no quantum fluctuations: these are actually classical particles living in momentum space. We do have to remember that these world 'rods' carry a fugacity set by a potential

$\frac{|k|^2\tau}{\hbar M}$. Henceforth, we have a problem of an ensemble of classical hard core particles that live on a lattice of 'cells' in momentum space where every cell can either contain one or no particle, with an overall harmonic potential envelope centered at $\mathbf{k} = 0$: this is literally the problem of cold atoms living in a harmonic trap, subjected to an infinite strong optical lattice potential, tuned such that they form a Mott-insulating state. The ground state is simple: occupy the cells starting at $\mathbf{k} = 0$, while the particles are put into cells at increasing trap potential until the trap is filled up with the available particles. At zero temperature there are no fluctuations and when one exceeds the chemical potential the cells remain empty, and there is a sharp $(d-1)$-dimensional interface between the occupied- and unoccupied trap states. This is of course the way we explain the Fermi-gas to our undergraduate students. It invokes an odd metaphor that however turns out to express an exact identification since we learned to handle the Ceperley path integral!

Having a statistical physics interpretation, can we now address the questions posed in section II? First, what is the order parameter of the Fermi-liquid? The answer is: the same order parameter that governs the Mott-insulator. This order parameter is well understood, although it is of an unconventional kind: it is the 'stay at home' emergent $U(1)$ gauge symmetry [76], stating that at every site and at all times there is precisely one particle per site. The particle number is locally conserved and henceforth a local $U(1)$ symmetry emerges. The 'disorder operators' that govern the finite temperature fate of the order parameter are just substitutional-interstitial defects: there is a finite thermal probability to excite a particle out of the trap, and the presence of the vacancies destroys the $U(1)$ gauge symmetry. Since the disorder operators are zero-dimensional particles regardless the dimensionality of momentum space, thermal melting of the Mott-insulator occurs at any finite temperature regardless dimensionality.

We repeat, this is just a rephrasing of the standard Fermi gas wisdoms in a non-standard language. The strange powers of the Ceperley path integral become more obvious when interactions are switched on. In the presence of the interactions single-particle momentum is no longer conserved, and this means that the worldlines of the Ceperley particles in momentum states get quantized: it is analogous to making the optical potential barriers finite in the cold gas Mott-insulator with the effect that the particles acquire a finite tunneling rate between the potential wells. One gets directly a hint regarding the stability of the Fermi-liquid: Mott-insulators are stable states that need a rather large tunneling rate to get destroyed. But the story is quite a bit more interesting than that, as can be easily argued from the knowledge on the canonical side. Let's consider first what would happen in a literal cold atom Mott insulator when we start to quantize the atoms. Deep inside the trap motions are only possibly by doubly occupying the nodal cells and given that in the non-interacting limit the 'Hubbard U' is infinite (expressing the Pauli surface) such processes are strongly suppressed. In the bulk of the trap the Mott state would be very robust. However, at the boundary one

can make cheap particle-hole excitations, and at any finite t the interface would no longer be infinitely sharp on the microscopic scale: the density profile would change smoothly. Eventually one would meet the 'wedding cake' situation where the bulk is still Mott-insulating while the interface would turn into a superfluid (we live in a bosonic world). How different is the Fermi-liquid! We know how it behaves from the canonical side. The single-fermion self-energy tells us directly about the fate of the **k**-space Mott insulator. We learn that the time required to loose information on single-particle momentum is just given by the imaginary part of the self-energy and that behaves as [27] $1/\tau_k \sim (k - k_F)^2$, Henceforth, it diverges at the interface while it get shorter moving into the bulk. In the Ceperley bosonic language the Fermi-liquid is like a grilled marshmallow: It has a 'crispy', solid Mott insulating crust while it becomes increasingly fluid when one moves inside!

More precisely, the worldlines near the interface are fluctuating at short times, since we know that the momentum distribution of the bare electrons do smear around the Fermi-momentum - they do 'spill out of the trap'. However, the effect of integrating out these microscopic fluctuations is to renormalize the 'optical lattice potential' upwards. This has to be the case because in the scaling limit the renormalized worldlines represent the quasiparticles and since they produce a perfectly sharp interface (i.e. unit jump in the quasiparticle n_k), the Mottness has to be perfect. This can only be caused by infinitely high effective potential barriers. This physics is of course coming from the modifications happening in the reach when interactions are turned on. The phase space restrictions giving rise to $\Sigma'' \sim \omega^2$ are rooted in Fermi-Dirac statistics and all the statistical effects are coded in the reach when dealing with the Ceperley formalism. These aspects can be computed by controlled perturbation theory and in a future publication they will be analyzed in detail.

3.4 The Fermi-liquid in real space: holographic duality

We showed in the previous section that at least for the Fermi gas the momentum space Ceperley path integral becomes a quite simple affair. Momentum space is a natural place to be when one is dealing with a quantum gas or -liquid, but dealing with a bosonic- or statistical physics systems one invariably runs into the general notion of duality [77,78]. Dealing with conjugate degrees of freedom, like momentum and position or phase and number, one can reformulate the manifestly local order on one 'side' into some non-local topological order parameter on the dual side. An elementary example is the Bose-Einstein condensate. In the language of the previous section, one can either form a 'black hole' in the momentum space 'trap', by putting all bosons in the $\mathbf{k} = 0$ 'optical lattice cell'. But one can also view it in real space, to discover the lively world of Section III where the local order in momentum space translates into a global, topological

description revolving around the infinite windings of worldlines around the time direction. Such duality structures are ubiquitous in Bolzmannian systems, and they are at the heart of our complete understanding of such systems: when one has a complete duality 'map' one understands the system from all possible sides and there is no room for surprises. For instance, when one is dealing with a strongly interacting system like ^{4}He one prefers the real space side because it is much easier to track the effects of the interactions [38]. Also in the strongly interacting fermion systems one expects that one is better off on the real space side. In this concluding section we will address the issue of the dual, real space description of the Fermi-liquid in the Ceperley path integral formalism. This real space side is remarkably complex: despite an intense effort even Ceperley and coworkers got stuck to the degree that they even did not manage to get things working by brute computer force. They ran into a rather mysterious 'reference point glassification' problem in their quantum Monte Carlo simulations, likely related to a contrived 'energy landscape' problem associated with the workings of the reach.

This is a fascinating problem: there has to be a simple, dual real space description of the Fermi gas. The obvious difficulty as compared to straightforward bosonic duality is the presence of the reach. One has to dualize not only the 'life of the worldlines' but also the constraints coding for the Fermi-Dirac statistics. Topology is at the heart of duality constructions and in this regard Ceperley [73], and more recently Mitas [79], have obtained some remarkably deep results, which will be discussed at length in the first subsection: the topology of the reach of the Fermi-liquid in $d \geq 2$ is such that the reach is open for all cycles of Ceperley worldlines based on even permutations or triple exchange. Henceforth, there is no topological principle that prevents infinitely long worldlines to occur and in subsection B we will argue that the zero temperature order of the Fermi-liquid has to be a Bose condensate of the 'Ceperley particles'. This is conjectural but if it proves to be correct the Fermi-liquid holography we discussed in section 3.2 acquires a fascinating meaning: the scaling limit thermodynamics of the Fermi-gas in any spatial dimension $d > 1$ is governed entirely by the statistical physics associated with distributing the Ceperley worldlines over the cycles associated with even permutations, and this effective partition sum is indistinguishable from the partition sum enumerating the cycles of a soft-core boson system in one space dimension.

3.4.1 The topology of the Fermi-liquid nodal surface

To decipher the structure of constraints as needed for the real space Ceperley path integral one has to find out where the zero's of the real space density matrix are. By continuation, these should be in qualitative regards the same in the Fermi-liquid as in the Fermi gas, and in the latter case we have an expression of the full density matrix in closed form,

$$\rho_F(\mathbf{R}_0,\mathbf{R};\tau) = (4\pi\lambda\tau)^{-dN/2} \times \det \exp\left[-\frac{(\mathbf{r}_i - \mathbf{r}_{j0})^2}{4\lambda\tau}\right], \tag{3.13}$$

where $\lambda = \hbar^2/(2M)$. Henceforth, one needs to find out the zero's of this quantity for all $\mathbf{R}_0, \mathbf{R}$ in the imaginary time interval $0 < \tau < \beta$. In real space, this is not an easy task. Part of the trouble is that at low temperature the zero's of the determinant depend on all coordinates at the same time. Only in the high temperature limit ($\tau \to 0$) the nodal surface of the density matrix becomes extremely simple [73]. To see this, define first a *permutation cell* $\Delta_{\mathcal{P}}(\mathbf{R}_0)$ as the set of points closer to $\mathcal{P}\mathbf{R}_0$ than to any other $\mathcal{P}'\mathbf{R}_0$. Obviously, the configuration space is divided into $N!$ permutation cells which are convex polyhedra bounded by hyperplanes, $\mathbf{R}\cdot(\mathcal{P}\mathbf{R}_0 - \mathcal{P}'\mathbf{R}_0) = 0$. The density matrix is simply a sum over all permutations and for $\mathbf{R} \in \Delta_{\mathcal{P}}(\mathbf{R}_0)$ and sufficiently high temperatures this sum is completely dominated by the term $(-1)^p \exp[-(\mathbf{R} - \mathcal{P}\mathbf{R}_0)^2/(4\lambda\tau)]$ since all the other terms are exponentially damped relative to it. Therefore, in the high temperature limit, $\rho_F(\mathbf{R}_0,\mathbf{R};\tau)$ will have the sign of $\mathcal{P}$ inside of $\Delta_{\mathcal{P}}(\mathbf{R}_0)$ and the nodal hypersurface is simply given by the common faces shared by permutation cells of different parities.

The reach acts both in a local way, much in the same way as we learned in the (1+1)-dimensional case as a special 'steric hindrance' structure having to do with entropic interactions, etcetera. However, it also carries global, topological properties and these are now well understood because of some remarkable results by Mitas [79], who managed to proof the 'two nodal cell' (or 'nodal domain') property of the higher dimensional Fermi-gas reach [73]. The topology of the nodal surface is associated with the structure of cycles as discussed in section III but now for the Ceperley path integral. The latter can be written as

$$Z = \sum_{\mathcal{P}_e} \int d\mathbf{R}\tilde{\rho}_D(\mathbf{R}, \mathcal{P}_e\mathbf{R};\beta), \tag{3.14}$$

where $\mathcal{P}_e$ refers to even permutations, while $\tilde{\rho}_D$ refers to the density matrix of distinguishable particles that are however still subjected to the reach constraints. As in the case of the Feynman path integral, this sum over even permutations can be recasted in a sum over cycles associated with all possible ways one can reconnect the worldlines at the temporal boundary, of course limiting this sum to those cycles that are associated with even permutations. We learned in section IV that for free wordlines even permutations translate into the supersymmetric quantum gas. But the Ceperley particles are not at all free, and the topology of the nodal surface tells us about global restrictions on the cycles that can contribute to Eq. (3.14).

It is immediately clear that the counting of cycles is governed by topology: to find out how to reconnect wordlines arriving at the temporal boundary from the imaginary time past, to worldlines that depart to the imaginary time future one needs obviously *global* data. This global information residing in the reach is

just the division of the reach in nodal cells we already encountered in the (1+1)-dimensional context and the momentum space Fermi gas. There we found that the space of all permutations got divided in $N!$ nodal cells, with the ramification that the sum in Eq. (3.14) is actually reduced to one cycles. Mitas has delivered the proof that in $d \geq 2$ the reach carries a two nodal cell topology, implying that all cycles based on even permutations lie within the reach. Since only this topological property of the reach can impose that certain cycles have to rigorously disappear from the cycle sum, this does imply that all cycles based on even permutations can contribute to the partition sum, including the cycles containing macroscopic winding numbers. Henceforth, the Ceperley worldlines can Bose condense in principle and it is now just matter of finding out what the distributions of the winding numbers are as function of temperature. This is what really matters for the main line of this story. Finding out the the way that Mitas determined the two-cell property is quite interesting and we will sketch it here for those who are interested. When you just want to understand the big picture, you might want to skip the remainder of this subsection.

Quite recently Mitas [79] proved a conjecture due to Ceperley [73], stating that the reach of the higher dimensional Fermi gas is 'maximal' in the sense that, for a given $\mathbf{R}_0$ and τ, the nodal surface of $\rho_F(\mathbf{R}_0, \mathbf{R}; \tau)$ separates the configuration space in just two nodal cells, corresponding with ρ_F being positive- and negative respectively. This is a quite remarkable property: for every pair $\mathbf{R}$ and $\mathbf{R}'$ in the same domain (lets say $\rho_F > 0$), one can change $\mathbf{R}$ into $\mathbf{R}'$ without encountering a zero crossing of ρ_F.

The easy way to prove this property goes as follows [79]. First, it can be demonstrated [73] that once there are only two nodal cells at some initial τ_0 than this property has to hold for any $\tau > \tau_0$. This follows straightforwardly from the imaginary time Bloch equation for the density matrix,

$$-\frac{\partial \rho(\mathbf{R}, \mathbf{R}'; \tau)}{\partial \tau} = H\rho(\mathbf{R}, \mathbf{R}'; \tau) \tag{3.15}$$

with initial condition,

$$\rho(\mathbf{R}, \mathbf{R}'; 0) = \det\left[\delta(\mathbf{r}_i - \mathbf{r}'_j)\right] \tag{3.16}$$

and the Bloch equation is a linear equation. This is a very powerful result because it gives away that the two-cell property 'descents for the ultraviolet': one has just to prove it at an arbitrary short imaginary time which is the same as arbitrary high temperature. Ignoring Planck scale uncertainties, etcetera, the form Eq. (3.13) has to become asymptotically exact for sufficiently small β, also in the presence of arbitrary interactions as long as they are not UV-singular! As we already noticed, this high temperature limit is rather tractable.

We now need to realize that we still have to take into account the 'remnant' of quantum statistics in the form of even permutations. Every even permutation can be written as a succession of exchanges of three particles $i, j, k \rightarrow j, k, i$

because these amount to two particle exchanges. When such an exchange does not cross a node (i.e. it resides inside the reach) the three particles are called 'connected'. By successions of three particle exchanges one can build up clusters of connected particles. All one has now to demonstrate is that a point $\mathbf{R}_t$ exists where *all* particles are connected in a single cluster, because this complete set of even permutations exhaust all permutations for a cell of one sign, because the odd permutations necessarily change the sign. One now needs a second property called tiling stating that when the particles are connected for the special point $\mathbf{R}_t$ this has also to be the case for all points in the cell. And tiling is proved by Ceperley for non-degenerate ground states and also for finite temperature. Actually due to the linearity of the Bloch equation, its fixed node solution is unique, and the tiling property in the high temperature limit will lead to the same property at any lower temperature.

Before we prove that the above holds for the high temperature limit density matrix, let us just dwell for a second on what this means for the winding properties of the constrained path integral. The even permutation requirement means that, as for the standard worldline pathintegrals, we have to connect the worldlines with each other at the temporal boundary, but now we have to take care that we single out those cycles corresponding with even (or three particle) exchanges. The 'maximal reach' just means that cycles containing worldlines that wind an arbitrary large number of times around the time axis *never encounter a node !* As noted before by Ceperley, this has the peculiar implication that in some non-obvious way the Fermi-gas has to know about Bose condensation. Since nodal constraints do allow for infinite windings there seems to be no 'force in the universe' that can forbid these infinite windings to happen and since the Cepereley path integral is probabilistic, when these infinite windings happen one has to accept it as Bose condensation. We will come back to this theme in a moment.

Following Mitas, one can now prove the two cell property of the high temperature limit using an inductive method. Assume that all N particles in the low β limit at a fixed $\mathbf{R_0}$ are connected in one cluster, to see what happens when an additional $N+1$ particle is added. Single out two other particles $N-1$, N and move these three particles away from the rest without crossing a node. Now we can profit from the fact that in the low β limit the density becomes factorizable: the determinant factors into a product of the determinant of the three special particles and the determinant of the rest. It is easy to show that the three particle determinant has the two cell property, proving that the N+1's particle is in the cluster of N particles. Since this is true for any N, the starting assumption that all particles in the cluster is hereby proven.

For free fermions, Mitas also proved the two nodal cell property for non-degenerate ground states using a similar induction procedure. The trick is to choose a special point $\mathbf{R}_t$ in the configuration space, at which one can easily show how all the particles are connected into a single cluster. Once proven for this single point, tiling ensures that the same is true for the entire nodal cell. Mitas

aligned the particles into lines and planes, thus forming some square lattice in the real space. This way the number of arguments of the wave functions is reduced and more importantly, the higher dimensional wave functions can be factorized into products of sine functions and the one dimensional wave functions, which are much easier to deal with than their higher dimensional counterparts. One distinct property of the 1 dimensional wave functions is that they are invariant under cyclic exchanges of odd numbers of particles, namely for N odd,

$$C^x_{+1}\Psi_{1D}(1,\cdots,N) = \Psi_{1D}(1,\cdots,N), \tag{3.17}$$

where C^x_{+1} represents the action to move every particle by one site in the $+x$ direction, with the last particle moved to the position of the first one, that is $1 \to 2, 2 \to 3, \cdots, N \to 1$.

Consider for example the non-degenerate ground state of 5 particles in 2 dimensions. For this state, it becomes straightforward to show that each group of the 3 near neighbors living in the real space square lattice are connected by products of four triplet exchanges, which are all performed along the 1 dimensional lines. Proven this, one can proceed as in the high temperature limit, by adding more particles to the lattice. And these newly added particles can be shown to be connected to the original particles' cluster by the similar method used for 5 particles. The only difference is that now one needs to consider the whole line of particles, on which the new particle is added, and thus a sequence of four cyclic exchanges, instead of the special triplet exchanges are required. Since for non-degenerate ground states, there are odd number of particles on each line, cyclic exchanges will not produce extra minus signs, thus leading to the same result as triplet exchanges. This completes the proof for 2 dimensions, and the high dimensional cases are essentially the same.

However, winding is a topological property that should be independent of representation. In the long time $\beta \to \infty$ limit the path integral contains the same information as the ground state wave function, and for the Fermi-gas we can actually easily determine the winding properties inside one of the nodal cells using the random permutation theory. This demonstrates that at zero temperature the Fermi-gas is indeed precisely equivalent to the Bose gas, within the nodal cell.

3.4.2 There is only room for winding at the bottom

The conclusion of the previous subsection is that the Ceperley wordlines can in principle become infinitely long because the topology of the reach allows them to become macroscopic. Does this mean that the zero-temperature order parameter of the Fermi-liquid is just an algebraic bose condensate of Ceperley wordlines characterized by a domination of the partition sum by macroscopic cycles? The two nodal cell topological property is a necessary but insufficient condition for this to be true. However, there are more reasons to believe that the Fermi-liquid has to be of this kind.

However the zero- and finite temperature Fermi-liquid are separated by a phase transition and it appears that only the winding sector of the Ceperley path integral can be responsible for this transition. The argument is simple and general. With regard to ordering dynamics the real space Ceperley path integral is governed by Boltzmannian principle and let us find out what 'substance' is available to form an order parameter. The nodal surface in isolation cannot be responsible, since it is an immaterial object that just governs the behavior of the 'Ceperley particles' . Henceforth, whatever its (singular) properties, these have to be reflected in the behavior of the matter. In principle one can imagine subtle topological changes occurring in the nodal surface but in the previous subsection we found this not to be the case in the Fermi-gas. Henceforth, searching for the thermodynamic singularity we should keep our eyes on the worldlines and these should be subjected to the generalities associated with bosonic matter. One source of thermodynamic singularity is that the system of bosons breaks the translational- and/or rotational symmetry of space, forming a crystal or some liquid crystal. Although the one dimensional Fermi-gas is such a crystal in disguise, it is impossible to hide a (partial) crystallization in higher dimensions: the higher dimensional Fermi-liquid is undoubtedly a true liquid. The worldlines have to be delocalized, but dealing with indistinguishable particles, being bosons or the 'even permuting' Ceperley particles, one has to account for an extra set of degrees of freedom: the reconnections at the temporal boundary. From a statistical physics perspective, Bose condensation appears as an order out of disorder phenomenon. Lowering temperature has the net effect of increasing the 'configurational entropy' associated with all possible ways of reconnecting worldlines, or either the appearances of cycles characterized by different windings. Worldlines get longer and thereby the length over which they can meander increases, and this in turn increases effectively the fugacity of long cycles. The more cycles can contribute, the larger the 'configurational entropy' associated with the cycles and this gain in space time 'configurational entropy' (physically the decrease of quantum zero point energy) causes eventually a flat distribution of the winding configurations, and in the Bose system this sets in at a sudden phase transition. Since all particles 'are part of the same wordline' the Bose condensate is macroscopically coherent. We learned that the reach allows the Ceperley particles to form infinite windings. We learn from the Bose condensate that at zero temperature only crystallization can prohibit the 'reconnection entropy' to take over, because the thermal de Broglie wavelength diverges. Henceforth, there does not seem to be any feature of the reach that can prohibit this to happen as well to the Ceperley worldlines at zero temperature.

There is a quite direct argument to support this view which was put forward by Ceperley some time ago [73,74]. As we already emphasized a number of times, on the canonical side the Fermi-liquid order manifests itself through the jump in the momentum distribution. Let us now turn to the zero temperature single

particle density matrix,

$$\begin{aligned} n(\mathbf{r}) &= \int d\mathbf{R}\rho(\mathbf{r}_1, \mathbf{r_2}, \cdots \mathbf{r}_N; \mathbf{r}_1 + \mathbf{r}, \mathbf{r_2}, \cdots \mathbf{r}_N; \infty) \\ &= \int \mathrm{d}\mathbf{k} e^{i\mathbf{k}\cdot\mathbf{r}} n_{\mathbf{k}}. \end{aligned} \tag{3.18}$$

In the boson condensate $n_B(\mathbf{r}) \to$ *constant* revealing the off-diagonal long-range order which is equivalent to the domination of infinite cycles. In the Fermi-liquid on the other hand,

$$n_F(\mathbf{r}) \simeq \frac{1}{(k_F r)^{d/2}} J_{d/2}(k_F r). \tag{3.19}$$

The oscillations governed by the Bessel function $J_{d/2}(k_F r)$ can be easily traced back to the size of the nodal pocket as discussed in a moment. However, the envelope function $(k_F r)^{-d/2}$ just behaves like the one particle density matrix of a Bose condensate showing off-diagonal long range order, like in the interacting Bose system in 1+1D at zero temperature. Relating this to the real space Ceperley path integral, this signals the presence of infinite cycles formed from Ceperley world lines.

Chapter 4

Stability of Quantum Critical Points: the Bosonic Story

4.1 Introduction

In this chapter, we start our exploration of the idea of quantum criticality. Much of the attention on quantum criticality has been focused on the finite temperature scaling properties [40, 80, 81]. Temperature is the only relevant scale in the quantum critical region above the QCP, bounded by the crossover line $T^* \sim |r|^{\nu z}$. The parameter r measures the distance to the QCP, ν is the correlation-length exponent in $\xi \sim r^{\nu}$ and z is the dynamical exponent in $\xi_\tau \sim \xi^z$. With the correlation length ξ and correlation time ξ_τ much larger than any other scale of the system, power law behavior is expected for many physical observables, e. g. the specific heat, magnetic susceptibility, and most notably resistivity. Clear deviations from the Fermi liquid predictions are experimentally detected, and these phases are commonly termed non-Fermi liquids. In many systems, the anomalous finite temperature scaling properties are asserted to result from the underlying zero temperature QCPs.

In this chapter, we would like to emphasize another aspect of quantum criticality, namely that it serves as a driving force for new exotic phenomena at extremely low temperatures and in extremely clean systems. One possibility is the appearance of new phases around the QCPs. It has been found in numerous experiments as one lowers temperature, seemingly inevitably in all the systems available, new phases appear near the QCP. Most commonly observed to date is

the superconducting phase. The phenomenon of a superconducting dome enclosing the region near the QCP is quite general (see Fig. 1). It has been identified in many heavy fermion systems [23,25,82], plausibly also in cuprates [83], even possibly in pnictides [84–89], and probably in organic charge-transfer salts [90–92]. Other examples include the nematic phase around the metamagnetic QCP in the bilayer ruthenate $Sr_3Ru_2O_7$ [93–96], the origin of which is still under intense debate [97–101]. The emerging quantum paraelectric - ferroelectric phase diagram is also very reminiscent [102, 103], as is the disproportionation-superconducting phase in doped bismuth oxide superconductors [104–109].

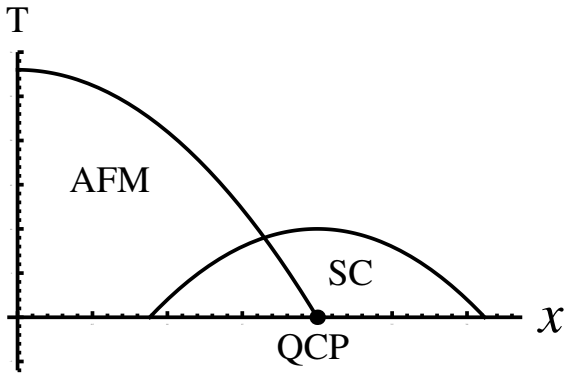

Figure 4.1: Illustration of the competing phases and superconducting dome. Here for concreteness, we consider the ordered phase to be an antiferromagnetic phase. x is the tuning parameter. It can be pressure, magnetic field or doping. The superconducting temperature usually has the highest value right above the QCP.

It has also been discovered recently that, as samples are becoming cleaner, on the approach to QCP we encounter first order transitions, and the new phases near the QCP are usually inhomogeneous and exhibit finite wavevector orderings (see [26, 110, 111] and references therein). For example, the heavy fermion compound $CeRhIn_5$ orders antiferromagnetically at low temperature and ambient pressure. As pressure increases, the Neel temperature decreases and at some pressure the antiferromagnetic phase is replaced by a superconducting phase through a first-order phase transition. There are also evidences for a competitive coexistence of the two phases within the antiferromagnetic phase, as in some organic charge-transfer superconductor precursor antiferromagnetic phases. Such coexistence was also observed in Rh-doped $CeIrIn_5$. The heavy fermion superconductor $CeCoIn_5$ has the unusual property that when a magnetic field is applied to suppress superconductivity, the superconducting phase transition becomes first-order below $T_0 \simeq 0.7K$. For the superconducting ferromagnet UGe_2, where superconductivity exists within the ferromagnetic state, the two magnetic transitions (ferromagnetic to paramagnetic and large-moment ferromagnetic to

small-moment ferromagnetic) are both first order [112–114]. Other examples of continuous phase transitions turning first-order at low temperatures include $CeRh_2Si_2$ [115,116], $CeIn_3$ [117], URhGe [118], $ZrZn_2$ [119] and MnSi [120]. The prevailing point of view seems to be that this happens only in a few cases and these are considered exceptions. Yet we are facing a rapidly growing list of these "exceptions", and we take the view here that they rather represent a general property of QCPs.

The point is that, on approach to the QCP, an interaction that was deemed irrelevant initially, takes over and dominates. For example it has been proposed recently that the superconducting instability, which is marginal in the usual Fermi liquids, becomes relevant near the QCP and leads to a high transition temperature [121]. Actually these instabilities are numerous and can vary, depending on the system at hand. However there seems to be a unifying theme of those instabilities. We suggest that QCPs are unstable precisely for the reasons we are interested in these points: extreme softness and extreme susceptibility of the system in the vicinity of QCPs. We regard the recently discovered first order transitions as indicators of a more fundamental and thus powerful phsyics. We are often prevented from reaching quantum criticality, and often the destruction is relatively trivial and certainly not as appealing and elegant as quantum criticality. We can draw an analogy from gravitational physics, where the naked singularities are believed to be prevented from happening due to many kinds of relevant instabilities. This is generally known as the "cosmic censorship conjecture" [122]. The recently proposed AdS/CFT correspondence [123–125], which maps a non-gravitational field theory to a higher dimensional gravitational theory, adds more to this story. Here researchers have begun to realize that the Reissner-Nordstrom black holes in AdS space, which should have a macroscopic entropy at zero temperature, are unstable to the spontaneous creation of particle-antiparticle pairs, and tend to collapse to a state with lower entropy [126,127].

There have appeared in the literature scattered examples of first-order quantum phase transitions at the supposed-to-be continuous QCPs [80,128–134], however it appears that the universality of this phenomenon is not widely appreciated. This universality is the main motivation for our work. We will systematically study the different possibilities for converting a continuous QPT to first order.

The first striking example how fluctuations of one of the order parameters can qualitatively change the nature of the transition comes from the Coleman-Weinberg model [135], where they showed how gauge fluctuations of the charged field introduce a first order transition. In this work it was shown that in dimension $d = 3$, for any weak coupling strength, one develops a logarithmic singularity, and therefore the effective field theory has a first-order phase transition. Subsequently, this result was extended to include classical gauge field fluctuations by Halperin, Lubensky and Ma [136], where a cubic correction to the free energy was found. Nontrivial gradient terms can also induce an inhomogeneous phase and/or glassy behavior [137].

A prototypical example for the competing phases and superconducting dome

is shown schematically in Fig.1. Below, we apply the renormalization group (RG) and scaling analysis to infer the stability if the QCP as a result of competition. We find in our analysis that the QCP is indeed unstable towards a first order transition as a result of competition. Obviously details of the collapse of a QCP and the resulting phase diagram depend on details of the nature of the fluctuating field and details of the interactions. We find that the most relevant parameters that enter into criterion for stability of a QCP are the strength of interactions between competing phases: we take this interaction to be repulsive between squares of the competing order parameters. When the two order parameters break different symmetries, the coupling will be between the squares of them. Another important factor that controls the phase diagram is the dynamical exponents z of the fields. The nature of the competition also depends on the classical or quantum character of the fields. Here by classical we do not necessarily mean a finite temperature phase transition, but rather that the typical energy scale is above the ultraviolet cutoff, and the finite frequency modes of the order parameters can be ignored, so that a simple description in terms of free energy is enough to capture the physics. We analyzed three possibilities for the competing orders:

i) *classical + classical*. Here we found that interactions generally reduce the region of coexistence, and when interaction strength exceeds some critical value, the second-order phase transitions become first order.

ii) *classical + quantum*. Here the quantum field is integrated out, giving rise to a correction to the effective potential of the classical order parameter. For a massive fluctuating field with $d + z \leqslant 6$, or a massless one with $d + z \leqslant 4$, the second-order quantum phase transition becomes first order.

iii) *quantum + quantum*. Here RG analysis was employed, and we found that in the high dimensional parameter space, there are generally regions with runaway flow, indicating a first-order quantum phase transition.

It has been proposed recently that alternative route to the breakdown of quantum criticality is through the basic collapse of Landau-Wilson paradigm of conventional order parameters and formation of the deconfined quantum critical phases ([138, 139]). This is a possibility that has been discussed for specific models and requires a different approach than the one taken here. We are not addressing this possibility.

The plan of this chapter is as follows. In section 4.2, we consider coupling two classical order parameter fields together. Both fields are characterized by their free energies and Landau mean field theory will be used. In section 4.3, we consider coupling a classical order parameter to a quantum mechanical one, which can have different dynamical exponents. The classical field is described by its free energy and the quantum field by its action; the latter is integrated out to produce a correction to the effective potential for the former. In section 4.4, we consider coupling two quantum mechanical fields together. With both fields described by their actions, we use RG equations to examine the stability conditions. In particular, we study in detail the case where the two coupled order parameters have different dynamical exponents, which, to our knowledge,

has not been considered previously. In the conclusion section, we summarize our findings. Details of the RG calculation for two quantum fields with different dynamical exponents are included in the Appendix 4.6.

4.2 Two competing classical fields

We consider in this section two competing classical fields. Examples are the superconducting order and antiferromagnetic order in $CeRhIn_5$ and Rh-doped $CeIrIn_5$, and the superconducting order and ferromagnetic order near the large-moment to small-moment transition in UGe_2. We will follow the standard textbook approach, and this case is presented as a template for the more complex problems studied later on.

We first study the problem at zero temperature. For simplicity, both of them are assumed to be real scalars. The free energy of the system consists of three parts, the two free parts F_ψ, F_M and the interacting part $F_{\rm int}$:

$$\begin{aligned} F =& F_\psi + F_M + F_{\rm int};\\ F_\psi =& \frac{\rho}{2}(\nabla\psi)^2 - \alpha\psi^2 + \frac{\beta}{2}\psi^4;\\ F_M =& \frac{\rho_M}{2}(\nabla M)^2 - \alpha_M M^2 + \frac{\beta_M}{2}M^4;\\ F_{\rm int} =& \gamma\psi^2 M^2. \end{aligned} \tag{4.1}$$

Here, by changing α, α_M, the system is tuned through the phase transition points. When the two fields are decoupled, with $\gamma = 0$, there will be two separated second-order phase transitions. Assume the corresponding values of the tuning parameter x at these two transition points are x_1 and x_2, we can parameterize α, α_M as $\alpha = a(x - x_1)$ and $\alpha_M = a_M(x_2 - x)$, where a, a_M are constants.

We would like to know the ground state of the system. Following the standard procedure, we first find the homogeneous field configurations satisfying $\frac{\partial F}{\partial \psi} = \frac{\partial F}{\partial M} = 0$, and then compare the corresponding free energy. It is easy to see that the above equations have four solutions, with $(|\psi|, |M|) = (0,0), (0, \sqrt{\alpha_M/\beta_M}), (\sqrt{\alpha/\beta}, 0), (\psi_*, M_*)$, where

$$\begin{aligned} \alpha\psi_*^2 =& \frac{\gamma' - \beta'_M}{\gamma'^2 - \beta'\beta'_M},\\ \alpha_M M_*^2 =& \frac{\gamma' - \beta'}{\gamma'^2 - \beta'\beta'_M}, \end{aligned} \tag{4.2}$$

and the rescaled parameters are $\gamma' = \gamma/\alpha\alpha_M, \beta' = \beta/\alpha^2, \beta'_M = \beta_M/\alpha_M^2$. When $\gamma = 0$, the fourth solution reduces to $(\psi_*, M_*) = (\sqrt{\alpha/\beta}, \sqrt{\alpha_M/\beta_M})$, with the two orders coexisting but decoupled. We are interested in the case where the two orders are competing, thus a relatively large positive γ.

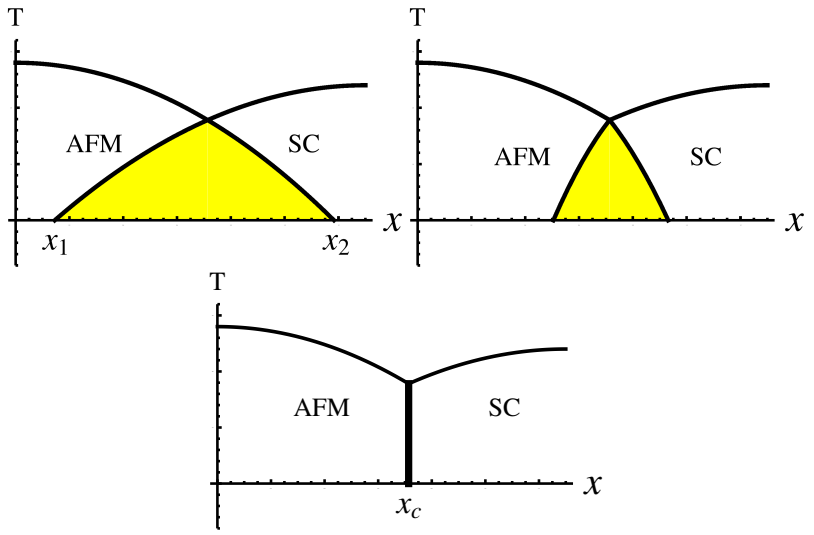

Figure 4.2: Illustration of the mean field phase diagram for two competing orders. Here for concreteness we consider antiferromagnetic and superconducting orders. The two orders coexist in the yellow region, whose area shrinks as the coupling increases from left to right. The left figure has $\gamma = 0$, the central one has $0 < \gamma < \sqrt{\beta\beta_M}$, and the right one has $\gamma > \sqrt{\beta\beta_M}$. When γ exceeds the critical value $\sqrt{\beta\beta_M}$, the two second-order phase transition lines merge and become first order (the thick vertical line).

For $x_1 < x < x_2$, we have $\alpha > 0, \alpha_M > 0$. The necessary condition for the existence of the fourth solution is $\gamma' > \beta', \beta'_M, \sqrt{\beta'\beta'_M}$ or $\gamma' < \beta', \beta'_M, \sqrt{\beta'\beta'_M}$. In this case, the configuration $(0,0)$ has the highest free energy $F[0,0] = 0$. For the configuration (ψ_*, M_*) with coexisting orders to have lower free energy than the two configurations with single order, one needs to have $\gamma' < \sqrt{\beta'\beta'_M}$, which reflects the simple fact that when the competition between the two orders is too large, their coexistence is not favored. Thus the condition for the configuration (ψ_*, M_*) to be the ground state of the system is $\gamma' < \beta'$ and $\gamma' < \beta'_M$. If $\gamma' > \min\{\beta', \beta'_M\}$, one of the fields has to vanish.

Next we observe that, for x near x_1, β'_M remains finite, $\alpha \sim (x - x_1)$, and γ' diverges as $1/(x - x_1)$, while β' diverges as $1/(x - x_1)^2$. So the lowest energy configuration is $\psi = 0$, $|M| = \sqrt{\alpha_M/\beta_M}$. Similarly, near x_2, the ground state is $(\sqrt{\alpha/\beta}, 0)$. The region with coexisting orders shrinks to

$$\frac{\gamma a_M x_2 + \beta_M a x_1}{\gamma a_M + \beta_M a} < x < \frac{\gamma a x_1 + \beta a_M x_2}{\gamma a + \beta a_M}. \tag{4.3}$$

For $\gamma < \sqrt{\beta\beta_M}$, this region has finite width. In this region, $(0,0)$ is the global

maximum of the free energy, $(0, \sqrt{\alpha_M/\beta_M}), (\sqrt{\alpha/\beta}, 0)$ are saddle points, and (ψ_*, M_*) is the global minimum. The phase with coexisting order is sandwiched between the two singly ordered phases, and the two phase transitions are both second-order. The shift in spin-density wave ordering and Ising-nematic ordering due to a nearby competing superconducting order has been studied recently by Moon and Sachdev [140, 141], where they found that the fermionic degrees of freedom can play important roles. The competition of magnetism and superconductivity in the iron arsenides was also investigated by Fernandes and Schmalian in [142]. They found that the phase diagram is sensitive to the symmetry of the pairing wavefunctions. It would be interesting to generalize our formalism to include all these effects.

For $\gamma > \sqrt{\beta\beta_M}$, this intermediate region with coexisting orders vanishes, and the two singly ordered phases are separated by a first-order quantum phase transition. The location of the phase transition point is determined by equating the two free energies at this point,

$$F\left[\sqrt{\frac{\alpha(x_c)}{\beta}}, 0\right] = F\left[0, \sqrt{\frac{\alpha_M(x_c)}{\beta_M}}\right], \tag{4.4}$$

which gives $x_c = (x_2 + Ax_1)/(1 + A)$, with $A = (a/a_M)\sqrt{\beta_M/\beta}$. The slope of the free energy changes discontinuously across the phase transition point, with a jump

$$\delta F^{(1)} \equiv \left| \left(\frac{dF}{dx}\right)_{x_c^+} - \left(\frac{dF}{dx}\right)_{x_c^-} \right| = \frac{aa_M}{\sqrt{\beta\beta_M}}(x_2 - x_1). \tag{4.5}$$

The size of a first-order thermal phase transition can be characterized by the ratio of latent heat to the jump in specific heat in a reference second-order phase transition [136]. A similar quantity can be defined for a quantum phase transition, where the role of temperature is now played by the tuning parameter x. We choose as our reference point $\gamma = 0$, where the two order parameters are decoupled. For $x < x_1$, one has $d^2F/dx^2 = -a_M^2/\beta_M$; for $x > x_2$, one has $d^2F/dx^2 = -a^2/\beta$; and $d^2F/dx^2 = -a_M^2/\beta_M - a^2/\beta$ for $x_1 < x < x_2$. We take the average of the absolute value of the two jumps to obtain

$$\delta F^{(2)} = \frac{1}{2}(a_M^2/\beta_M + a^2/\beta). \tag{4.6}$$

So the size of this first-order quantum phase transition is

$$\delta x = \frac{\delta F^{(1)}}{\delta F^{(2)}} = \frac{2\sqrt{\tilde{\beta}\tilde{\beta}_M}}{\tilde{\beta} + \tilde{\beta}_M}(x_2 - x_1), \tag{4.7}$$

with $\tilde{\beta} = \beta/a^2$ and $\tilde{\beta}_M = \beta_M/a_M^2$. It is of order $x_2 - x_1$, when $\tilde{\beta}$ and $\tilde{\beta}_M$ are not hugely different.

The above consideration can be generalized to finite temperature, by including the temperature dependence of all the parameters. Specially, there exists some temperature T^*, where $x_1(T^*) = x_2(T^*)$. In this way we obtain phase diagrams similar to those observed in experiments (see Fig. 4.2).

4.3 Effects of quantum fluctuations

In this section, we consider coupling an order parameter ψ to another field ϕ, which is fluctuating quantum mechanically. The original field ψ is still treated classically, meaning any finite frequency modes are ignored. For the quantum fields, in the spirit of Hertz-Millis-Moriya [143–145], we assume that the fermionic degrees of freedom can be integrated out, and we will only deal with the bosonic order parameters. This model may, for example, explain the first-order ferromagnetic to paramagnetic transition in UGe_2, where the quantum fluctuations of the superconducting order parameter are coupled with the ferromagnetic order parameter, which can be regarded as classical near the superconducting transition point.

We will integrate out the quantum field to obtain the effective free energy of a classical field. The partition function has the form

$$Z[\psi(\mathbf{r})] = \int \mathcal{D}\phi(\mathbf{r},\tau) \exp\left(-\frac{\mathcal{F}_\psi}{T} - S_\phi - S_{\psi\phi}\right). \tag{4.8}$$

The free energy is of the same form as in the previous section with $\mathcal{F}_\psi = \int d^d\mathbf{r} F_\psi$. Thus, in the absence of coupling to other fields, the system goes through a second-order quantum phase transition as one tunes the control parameter x across its critical value. We consider a simple coupling

$$S_{\psi\phi} = g \int d^d\mathbf{r} d\tau \psi^2 \phi^2. \tag{4.9}$$

The action of the ϕ field depends on its dynamical exponent z. We notice that such classical + quantum formalism has been used to investigate the competing orders in cuprates in [146].

The saddle point equation for ψ reads

$$\frac{\delta \ln Z[\psi(\mathbf{r})]}{\delta\psi(\mathbf{r})} = 0, \tag{4.10}$$

which gives

$$\left[-\alpha + \beta\psi^2(\mathbf{r}) - \frac{\rho}{2}\nabla^2 + g\langle\phi^2(\mathbf{r})\rangle\right]\psi(\mathbf{r}) = 0. \tag{4.11}$$

Here we have defined the expectation value,

$$\langle\phi^2(\mathbf{r})\rangle = \frac{1}{\beta}\int \mathcal{D}\phi(\mathbf{r}',\tau') \int_0^\beta d\tau \phi^2(\mathbf{r},\tau) \exp\left(-S_\phi - S_{\psi\phi}\right). \tag{4.12}$$

It can also be written in terms of the different frequency modes,

$$\begin{aligned}\langle\phi^2(\mathbf{r})\rangle =& T\sum_{\omega_n}\langle\phi(\mathbf{r},\omega_n)\phi(\mathbf{r},-\omega_n)\rangle \\ =& T\sum_{\omega_n}\int \mathcal{D}\phi(\mathbf{r}',\nu_s)\phi(\mathbf{r},\omega_n)\phi(\mathbf{r},-\omega_n)\exp\left(-S_\phi - S_{\psi\phi}\right).\end{aligned} \tag{4.13}$$

The quadratic term in S_ϕ is of the form

$$S_\phi^{(2)} = \sum_{\nu_s}\int d^d\mathbf{r}'\int d^d\mathbf{r}''\phi(\mathbf{r}',\nu_s)\chi_0^{-1}(\mathbf{r}',\mathbf{r}'',\nu_s)\phi(\mathbf{r}'',-\nu_s), \tag{4.14}$$

or more conveniently, in terms of momentum and frequency,

$$S_\phi^{(2)} = \sum_{\nu_s}\int \frac{d^d\mathbf{k}}{(2\pi)^d}\phi(\mathbf{k},\nu_s)\chi_0^{-1}(\mathbf{k},\nu_s)\phi(-\mathbf{k},-\nu_s). \tag{4.15}$$

So in the presence of translational symmetry, we find

$$\langle\phi^2\rangle = T\sum_{\omega_n}\int\frac{d^d\mathbf{k}}{(2\pi)^d}\frac{1}{\chi_0^{-1}(\mathbf{k},\omega_n)+g\psi^2}. \tag{4.16}$$

This leads to the 1-loop correction to the effective potential for ψ, determined by

$$\frac{\delta V_{\rm eff}^{(1)}[\psi]}{\delta\psi} = 2g\langle\phi^2\rangle\psi. \tag{4.17}$$

So far we have been general in this analysis. Further analysis requires us to make more specific assumptions about the dimensionality and dynamical exponents.

When the ϕ field has dynamical exponent $z=1$, its propagator is of the form

$$\chi_0(\mathbf{k},\omega_n) = \frac{1}{\omega_n^2+k^2+\xi^{-2}}. \tag{4.18}$$

A special case is a gauge boson, which has zero bare mass, and thus $\xi\to\infty$. This problem has been studied in detail by Halperin, Lubensky and Ma [136] for a classical phase transition (see also [147]), and by Coleman and Weinberg [135] for relativistic quantum field theory. Other examples are critical fluctuations associated with spin-density wave transitions and superconducting transitions in clean systems. We also note that Continentino and collaborators have used the method of effective potential to investigate some special examples of the fluctuation-induced first order quantum phase transition [80, 129–132].

Let us consider $T=0$, for which the summation $T\sum_{\omega_n}$ can be replaced by the integral $\int d\omega/(2\pi)$. We then get for the one-loop correction to the effective potential

$$\frac{\delta V_{\rm eff}^{(1)}[\psi]}{\delta\psi} = 2g\psi\int\frac{d\omega}{2\pi}\int\frac{d^d\mathbf{k}}{(2\pi)^d}\frac{1}{\omega^2+k^2+\xi^{-2}+g\psi^2}. \tag{4.19}$$

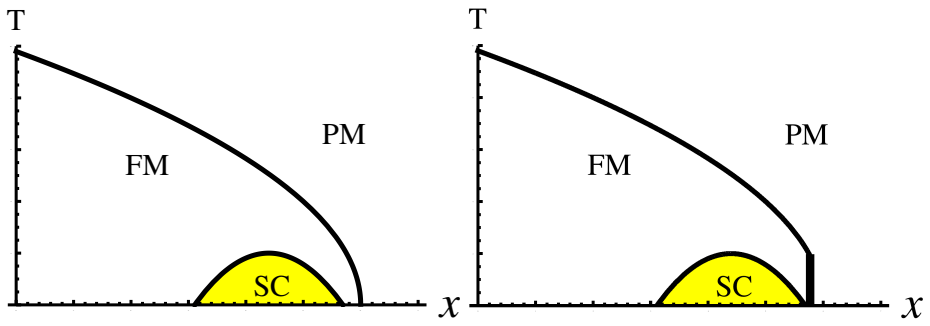

Figure 4.3: Schematic illustration of the fluctuation-induced first-order phase transition. Here, for concreteness, we consider ferromagnetic and superconducting orders. The ferromagnetic order is regarded as classical, while the superconducting one as quantum mechanical. At low temperatures, the second-order ferromagnetic to paramagnetic phase transition becomes first order (the thick vertical line), due to fluctuations of the superconducting order parameter.

Carrying out the frequency integral, we obtain for $d = 3$,

$$\frac{\delta V_{\rm eff}^{(1)}[\psi]}{\delta\psi} = \frac{g\psi}{2\pi^2}\int_0^\Lambda dk \frac{k^2}{\sqrt{k^2+\xi^{-2}+g\psi^2}}, \tag{4.20}$$

where an ultraviolet cutoff is imposed. Integrating out momentum gives

$$\frac{\delta V_{\rm eff}^{(1)}[\psi]}{\delta\psi} = \frac{g\psi}{4\pi^2}\left[\Lambda\sqrt{\Lambda^2+\xi^{-2}+g\psi^2} - (\xi^{-2}+g\psi^2)\ln\left(\frac{\Lambda+\sqrt{\Lambda^2+\xi^{-2}+g\psi^2}}{\sqrt{\xi^{-2}+g\psi^2}}\right)\right], \tag{4.21}$$

which can be simplified as

$$\frac{\delta V_{\rm eff}^{(1)}[\psi]}{\delta\psi} = \frac{g\psi}{4\pi^2}\left[\Lambda^2 + \frac{1}{2}(\xi^{-2}+g\psi^2) - (\xi^{-2}+g\psi^2)\ln\left(\frac{2\Lambda}{\sqrt{\xi^{-2}+g\psi^2}}\right)\right]. \tag{4.22}$$

Combined with the bare part,

$$V_{\rm eff}^{(0)}(\psi) = -\alpha\psi^2 + \frac{1}{2}\beta\psi^4, \tag{4.23}$$

we get the effective potential to one-loop order,

$$V_{\rm eff}(\psi) = -\hat{\alpha}\psi^2 + \frac{1}{2}\hat{\beta}\psi^4 - \frac{1}{16\pi^2}(\xi^{-2}+g\psi^2)^2\ln\left(\frac{2\Lambda}{\sqrt{\xi^{-2}+g\psi^2}}\right), \tag{4.24}$$

with the quadratic and quartic terms renormalized by $\hat{\alpha} = \alpha - g(4\Lambda^2 + \xi^{-2})/(32\pi^2)$ and $\hat{\beta} = \beta + 3g/(32\pi^2)$. When ϕ field is critical with $\xi \to \infty$, the third term is of the well-known Coleman-Weinberg form $\psi^4 \ln(2\Lambda/\sqrt{g\psi^2})$, which drives the second-order quantum phase transition to first order.

For ξ large but finite, we can expand the third term as a power series in $\xi^{-2}/(g\psi^2)$, and the effective potential is of the form

$$V_{\rm eff}(\psi) = -\bar{\alpha}\psi^2 + \frac{1}{2}\bar{\beta}\psi^4 - \frac{1}{16\pi^2}(2\xi^{-2}g\psi^2 + g^2\psi^4)\ln\frac{2\Lambda}{\sqrt{g\psi^2}}. \tag{4.25}$$

In addition to the Coleman-Weinberg term, there is another term of the form $\psi^2 \ln\psi$, and again we have also a first-order phase transition.

To study the generic case where the ϕ field is massive, we rescale the ψ field and cutoff, defining

$$u^2 \equiv \frac{g\psi^2}{\xi^{-2}}, \qquad \tilde{\Lambda} \equiv \frac{2\Lambda}{\xi^{-1}}. \tag{4.26}$$

The rescaled effective potential takes the form

$$\tilde{V}_{\rm eff}(u) = -\tilde{A}u^2 + \frac{1}{2}\tilde{B}u^4 - (1+u^2)^2 \ln\left(\frac{\tilde{\Lambda}}{\sqrt{1+u^2}}\right), \tag{4.27}$$

which can be further simplified as

$$\hat{V}_{\rm eff}(u) = -Au^2 + \frac{1}{2}Bu^4 + (1+u^2)^2\ln(1+u^2). \tag{4.28}$$

The above potential is plotted in Fig. 4.3. We notice that with large enough cutoff Λ, one generally has $B = \tilde{B} - \ln\tilde{\Lambda}$ large and negative. For $A < 1$, $u = 0$ is a local minimum. There are also another two local minima with $u^2 \equiv y$ a positive solution of equation

$$2(1+y)\ln(1+y) + (1+B)y + 1 - A = 0. \tag{4.29}$$

So we generally have a first-order quantum phase transition in this case (see Fig. 3 for a schematic picture).

With dynamical exponent $z = 2$, the propagator of ϕ field is

$$\chi_0(\mathbf{k}, \omega_n) = \frac{1}{|\omega_n|\tau_0 + k^2 + \xi^{-2}}. \tag{4.30}$$

Examples are charge-density-wave and antiferromagnetic fluctuations. In the presence of dissipation, superconducting transitions also have dynamical exponent $z = 2$.

So the one-loop correction to the effective potential at zero temperature becomes

$$\frac{\delta V_{\rm eff}^{(1)}[\psi]}{\delta\psi} = 2g\psi \int \frac{d\omega}{2\pi}\int \frac{d^d\mathbf{k}}{(2\pi)^d}\frac{1}{|\omega|\tau_0 + k^2 + \xi^{-2} + g\psi^2}. \tag{4.31}$$

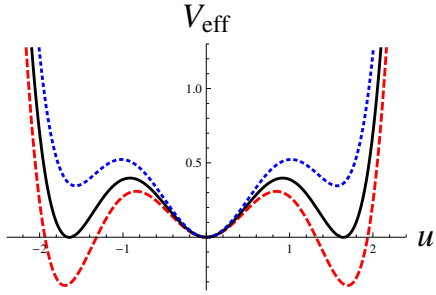

Figure 4.4: The effective potential as a function of the rescaled field u for various parameters in the case $d = 3, z = 1$. Here $V_{\text{eff}}(u) = -Au^2 + \frac{1}{2}Bu^4 + (1 + u^2)^2 \ln(1 + u^2)$, with $B = -5$, and $A = -0.25, -0.116, 0$ from top to bottom.

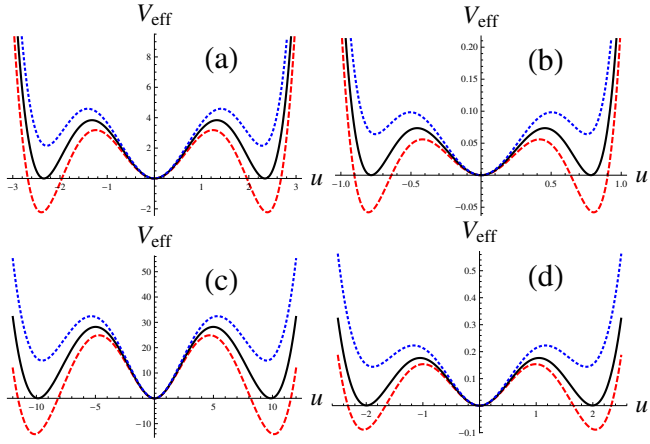

Figure 4.5: The effective potential as a function of the rescaled field u for (a) $d = 3, z = 2$, where we have plotted $V_{\text{eff}}(u) = -Au^2 + \frac{1}{2}Bu^4 + (1 + u^2)^{5/2} - 1$, with $B = -8$, and $A = -3, -2.597, -2.2$ from top to bottom; (b) $d = 3, z = 3$, where $V_{\text{eff}}(u) = -Au^2 + \frac{1}{2}Bu^4 + (1 + u^2)^3 \ln(1 + u^2)$, with $B = -10$, and $A = 0.1, 0.208, 0.3$ from top to bottom; (c) $d = 1, z = 2$, where we have plotted $V_{\text{eff}}(u) = -Au^2 + \frac{1}{2}Bu^4 - (1+u^2)^{3/2} + 1$, with $B = 0.1$, and $A = -5.3, -5.1413, -5$ from top to bottom; (d) $d = 1, z = 1$, where we have plotted $V_{\text{eff}}(u) = -Au^2 + \frac{1}{2}Bu^4 - (1 + u^2)\ln(1 + u^2)$, with $B = 0.3$, and $A = -1.45, -1.412, -1.39$ from top to bottom. All these plots are of similar shape. However, we notice that the scales are quite different.

The momentum integral is cutoff at $|\mathbf{k}| = \Lambda$, and correspondingly the frequency integral is cutoff at $|\omega|\tau_0 = \Lambda^2$. First, we integrate out frequency to obtain

$$\frac{\delta V_{\rm eff}^{(1)}[\psi]}{\delta\psi} = \frac{g\psi}{\pi^3\tau_0}\int_0^\Lambda dk k^2 \ln\left(1+\frac{\Lambda^2}{k^2+\xi^{-2}+g\psi^2}\right), \tag{4.32}$$

and then integrate out momentum, with the final result

$$\begin{aligned}\frac{\delta V_{\rm eff}^{(1)}[\psi]}{\delta\psi} = \frac{g\psi}{3\pi^3\tau_0}\Bigg[&\Lambda^3\ln\left(\frac{\xi^{-2}+g\psi^2+2\Lambda^2}{\xi^{-2}+g\psi^2+\Lambda^2}\right)+2\Lambda^3\\ &+2(\xi^{-2}+g\psi^2)^{3/2}\arctan\frac{\Lambda}{\sqrt{\xi^{-2}+g\psi^2}}\\ &-2(\xi^{-2}+g\psi^2+\Lambda^2)^{3/2}\arctan\frac{\Lambda}{\sqrt{\xi^{-2}+g\psi^2+\Lambda^2}}\Bigg].\end{aligned} \tag{4.33}$$

Up to order Λ^0, this is

$$\frac{\delta V_{\rm eff}^{(1)}[\psi]}{\delta\psi} = \frac{g\psi}{3\pi^3\tau_0}\left[\Lambda^3\left(2+\ln 2-\frac{\pi}{2}\right)+\frac{3\pi}{4}\Lambda(\xi^{-2}+g\psi^2)+\pi(\xi^{-2}+g\psi^2)^{3/2}\right]. \tag{4.34}$$

The first two terms just renormalize the bare α and β. When the ϕ field is critical, $\xi\to\infty$, the third term becomes of order ψ^5, and is thus irrelevant. When ξ is large but not infinite, we get the effective potential

$$V_{\rm eff}(\psi) = -\bar{\alpha}\psi^2+\frac{1}{2}\bar{\beta}\psi^4+\frac{g^{3/2}\xi^{-2}}{15\pi^2\tau_0}|\psi|^3+\frac{g^{5/2}}{15\pi^2\tau_0}|\psi|^5. \tag{4.35}$$

In addition to the ψ^5 term there is another term of order ψ^3, which may drive the second-order quantum phase transition to first order.

Let us consider a massive ϕ field. Carrying out the same rescaling as we made for $z=1$, we get the rescaled effective potential of the form

$$\hat{V}_{\rm eff}(u) = -Au^2+\frac{1}{2}Bu^4+(1+u^2)^{5/2}. \tag{4.36}$$

For large negative B, we obtain a first-order quantum phase transition (see Fig. 4.5(a)).

When the ϕ field has dynamical exponent $z=3$, e.g. for ferromagnetic fluctuations, its propagator is

$$\chi_0(\mathbf{k},\omega_n) = \frac{1}{\gamma\frac{|\omega_n|}{k}+k^2+\xi^{-2}}. \tag{4.37}$$

Thus the one-loop correction to the effective potential at $T=0$ is determined from

$$\frac{\delta V_{\rm eff}^{(1)}[\psi]}{\delta\psi} = 2g\psi\int\frac{d\omega}{2\pi}\int\frac{d^d\mathbf{k}}{(2\pi)^d}\frac{1}{\gamma\frac{|\omega|}{k}+k^2+\xi^{-2}+g\psi^2}, \tag{4.38}$$

with a momentum cutoff at $|\mathbf{k}| = \Lambda$, and a frequency cutoff at $\gamma|\omega| = \Lambda^3$. The frequency integral gives

$$\frac{\delta V_{\rm eff}^{(1)}[\psi]}{\delta\psi} = \frac{g\psi}{4\pi^4\gamma}\int_0^\Lambda dk k^3 \ln\left[1 + \frac{\Lambda^3}{k^3 + k(\xi^{-2} + g\psi^2)}\right], \tag{4.39}$$

and the momentum integral further leads to the result

$$V_{\rm eff}(\psi) = -\bar{\alpha}\psi^2 + \frac{1}{2}\bar{\beta}\psi^4 + \frac{1}{96\pi^4\gamma}(\xi^{-2} + g\psi^2)^3 \ln(\xi^{-2} + g\psi^2). \tag{4.40}$$

When ϕ is critical, $\xi \to \infty$, the third term is of the form $\psi^6 \ln\psi$, which is irrelevant. For finite ξ, there is also a term of the form $\psi^4 \ln\psi$, which will drive the second-order quantum phase transition to first order.

For general ξ, the rescaled effective potential reads

$$\hat{V}_{\rm eff}(u) = -Au^2 + \frac{1}{2}Bu^4 + (1+u^2)^3 \ln(1+u^2). \tag{4.41}$$

We define $x \equiv u^2$. To produce the energy barrier in a first-order transition, $d\hat{V}_{\rm eff}/dx = 0$ needs to have two distinct positive solutions. For A a freely tunable parameter, the condition for $-Bx + A = f(x) \equiv (1+x)^2(1+3\log(1+x))$ to have two distinct positive solutions is that $-B > \min[f'(x)] = f'(0) = 5$. So when the renormalized parameter satisfies the condition $B < -5$, we obtain a first-order quantum phase transition (see fig. 4.5(b)).

For a dirty metallic ferromagnet, the dynamical exponent is $z = 4$. In this case, with the propagator

$$\chi_0(\mathbf{k}, \omega_n) = \frac{1}{\gamma' \frac{|\omega_n|}{k^2} + k^2 + \xi^{-2}}, \tag{4.42}$$

the rescaled effective potential reads

$$\hat{V}_{\rm eff}(u) = -Au^2 + \frac{1}{2}Bu^4 - (1+u^2)^{7/2}. \tag{4.43}$$

Higher order terms need to be included at large u to maintain stability. When the ϕ field is critical, the third term is of order ϕ^7, which is irrelevant. When the ϕ field is massive but light, there will also be a term of order ϕ^5 which is again irrelevant. For general ϕ, in order for $u = 0$ to be a local minimum, we need to have $A < -7/2$. In this case, $\hat{V}'_{\rm eff}(u) = 0$ has only one positive solution. Thus we have a second-order quantum phase transition.

We can calculate the fluctuation-induced effective potential in other dimensions in the same way as above. For $d = 2, z = 1$, and also for $d = 1, z = 2$, with the rescaled field defined by $u^2 \equiv \frac{g\psi^2}{\xi^{-2}}$, the rescaled effective potential is of the form

$$\hat{V}_{\rm eff}(u) = -Au^2 + \frac{1}{2}Bu^4 - (1+u^2)^{3/2}. \tag{4.44}$$

When the ϕ field is critical, the third term becomes of order $-|\psi|^3$, of the Halperin-Lubensky-Ma type, thus the quantum phase transition is first-order. Generally when $A < -1.5, AB > -0.5, B(A+B) > -0.25$, $u = 0$ will be a local minimum of the rescaled effective potential $\hat{V}_{\rm eff}$, and there are two other local minima at nonzero u. Hence there is again a first-order quantum phase transition (see Fig. 4.5(c)). Otherwise there will be a second-order phase transition.

The effective potential in the case with $d = 2, z = 2$, and $d = 1, z = 3$ turns out be of the same form as that of $d = 3, z = 1$, as expected from the fact that both cases have the same effective dimension $d + z = 4$. The case $d = 2, z = 3$ is the same as $d = 3, z = 2$.

For $d = 1, z = 1$, the effective potential takes the form

$$\hat{V}_{\rm eff}(u) = -Au^2 + \frac{1}{2}Bu^4 - (1+u^2)\ln(1+u^2), \tag{4.45}$$

which leads to a first-order phase transition for $B < 1$ (see Fig. 4.5(d)). The third term reduces to $\psi^2 \ln \psi$ when ϕ is critical. In this case the quantum phase transition is always first order for any positive value of B.

In the table below, we list the most dangerous terms generated from integrating out the fluctuating fields. The second row in the table corresponds to the case where ϕ is critical or massless, and the third row has ϕ massive.

$d+z$	2	3	4	5	6	7
massless	$\psi^2 \ln \psi$	ψ^3	$\psi^4 \ln \psi$	ψ^5	$\psi^6 \ln \psi$	ψ^7
massive	$(\psi^2+1)\ln \psi$	$\psi^3 + \psi$	$\psi^2 \ln \psi$	ψ^3	$\psi^4 \ln \psi$	ψ^5

One can clearly see that in the massless case, the fluctuations are irrelevant when $d + z \geqslant 5$, while in the massive case, they are irrelevant for $d + z \geqslant 7$. Otherwise the second-order quantum phase transition can be driven to first order. The order of the correction is readily understood from the general structure of the integrals. With effective dimension $d + z$, in the massless case one has $\delta V/\delta\psi \sim \psi \int d^{d+z}k(1/k^2)$. Since $k^2 \sim \psi^2$, this gives the correct power $\delta V \sim \psi^{d+z}$. Replacing $g\psi^2$ by $g\psi^2 + \xi^{-2}$ and then carrying out the expansion in $\xi^{-2}/g\psi^2$, one gets for the massive case a reduction by 2 in the power. We also notice the even/odd effect in the effective potential: for $d + z$ even, there are logarithmic corrections. The case $d + z = 4$ can be easily understood, as the system is in the upper critical dimension, and logarithmic corrections are expected. We still do not have a simple intuitive understanding of the logarithm for $d + z = 2, 6$.

4.4 Two fluctuating fields

We consider in this section the case where the two coupled quantum fields are both fluctuating substantially. The partition function now becomes

$$Z = \int \mathcal{D}\psi(\mathbf{r},\tau) \int \mathcal{D}\phi(\mathbf{r},\tau) \exp\left(-S_\psi - S_\phi - S_{\psi\phi}\right). \tag{4.46}$$

We will use RG equations to determine the phase diagram of this system. When there is no stable fixed point, or the initial parameters lie outside the basin of attraction of the stable fixed points, the flow trajectories will show runaway behavior, which implies a first-order phase transition [147–151]. The spin-density-wave transitions in some cuprates and pnictides fall in this category [152–165].

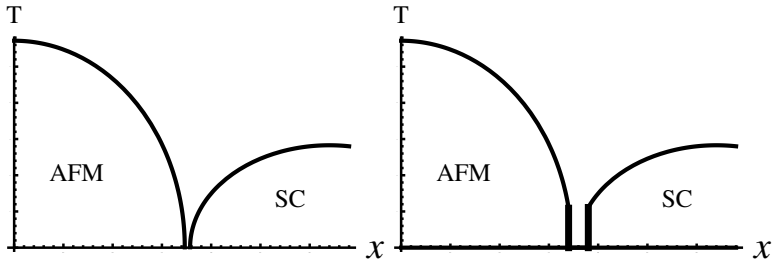

Figure 4.6: Illustration of the fluctuation-induced first-order phase transition in the case of two quantum fields. Here for concreteness we consider the antiferromagnetic order and superconducting order. At low temperatures, the phase transitions may become first order (the thick vertical lines), due to fluctuations.

We have considered in the previous sections coupling two single component fields, having in mind that this simplified model captures the main physics of competing orders. However, we will see below that when the quantum fluctuations of both fields are taken into account, the number of components of the order parameters do play important roles. So from now on we consider explicitly a n_1-component vector field $\boldsymbol{\psi}$ and a n_2-component vector field $\boldsymbol{\phi}$ coupled together. When both fields have dynamical exponent $z = 1$, the action reads

$$\begin{aligned} S_\psi &= \int d^d\mathbf{r}d\tau \left[-\alpha_1|\boldsymbol{\psi}|^2 + \frac{1}{2}\beta_1|\boldsymbol{\psi}|^4 + \frac{1}{2}|\partial_\mu\boldsymbol{\psi}|^2\right], \\ S_\phi &= \int d^d\mathbf{r}d\tau \left[-\alpha_2|\boldsymbol{\phi}|^2 + \frac{1}{2}\beta_2|\boldsymbol{\phi}|^4 + \frac{1}{2}|\partial_\mu\boldsymbol{\phi}|^2\right], \\ S_{\psi\phi} &= g\int d^d\mathbf{r}d\tau|\boldsymbol{\psi}|^2|\boldsymbol{\phi}|^2, \end{aligned} \tag{4.47}$$

where $\mu = 0, 1, \cdots, d$. This quantum mechanical problem is equivalent to a classical problem in one higher dimension. Then one can follow the standard procedure of RG: first decompose the action into the fast-moving part, the slow-moving part and the coupling between them. The Green's functions are $G_\psi = 1/(-2\alpha_1 + k^2 + \omega^2)$ and $G_\phi = 1/(-2\alpha_2 + k^2 + \omega^2)$. The relevant vertices are $\beta_1\psi_s^2\psi_f^2, \beta_2\phi_s^2\phi_f^2, g\psi_s^2\phi_f^2, g\psi_f^2\phi_s^2, g\psi_s\psi_f\phi_s\phi_f$. To simplify the notation we rescale the momentum and frequency according to $\mathbf{k} \to \mathbf{k}/\Lambda, \omega \to \omega/\Lambda$, so that they lie in the interval $[0, 1]$. The control parameters and couplings are rescaled according

to $\alpha_{1,2} \to \alpha_{1,2}\Lambda^2$, $\beta_{1,2} \to \beta_{1,2}\Lambda^{3-d}, g \to g\Lambda^{3-d}$. Afterwards we integrate out the fast modes with the rescaled momentum and frequency in the range $[b^{-1}, 1]$. Finally, we rescale the momentum and frequency back to the interval $[0, 1]$, thus $\mathbf{k} \to b\mathbf{k}, \omega \to b\omega$, and the fields are rescaled accordingly with $\psi \to b^{(d-1)/2}\psi, \phi \to b^{(d-1)/2}\phi$. Using an ϵ-expansion, where $\epsilon = 3 - d$, one obtains the set of RG equations to one-loop order,

$$\begin{aligned}
\frac{d\alpha_i}{dl} =& 2\alpha_i - \frac{1}{8\pi^2}[(n_i+2)\beta_i(1+2\alpha_i) + n_j g(1+2\alpha_j)], \\
\frac{d\beta_i}{dl} =& \epsilon\beta_i - \frac{1}{4\pi^2}[(n_i+8)\beta_i^2 + n_j g^2], \\
\frac{dg}{dl} =& g\left(\epsilon - \frac{1}{4\pi^2}\left[(n_1+2)\beta_1 + (n_2+2)\beta_2 + 4g\right]\right),
\end{aligned} \tag{4.48}$$

with index $i, j = 1, 2$, and $i \neq j$. These equations are actually more general than considered above. They also apply to generic models where two fields with the same dynamical exponent z are coupled together. Generally one has $\epsilon = 4 - d - z$, thus a quantum mechanical model with dynamical exponent z is equivalent to a classical model in dimension $d + z$.

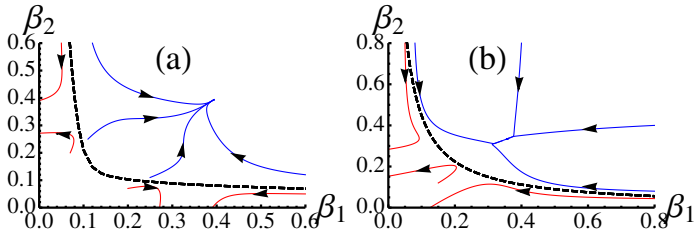

Figure 4.7: Plot of the RG trajectories in the $\beta_1 - \beta_2$ plane for two quantum fields with the same dynamical exponent below the upper critical dimension. Here we have chosen $\epsilon = 4 - d - z = 0.1$. The RG trajectories have been projected onto a constant g plane with $g = g^*$, and g^* the value of the coupling strength at the stable fixed point. (a) corresponds to the case $n_1 = n_2 = 1$, where the fixed point is at $\beta_1^* = \beta_2^* = g^* = 4\pi^2\epsilon/(n_1 + n_2 + 8) \simeq 0.3948$. (b) corresponds to the case $n_1 = 2, n_2 = 3$, where the fixed point is at $(\beta_1^*, \beta_2^*, g^*) = 4\pi^2\epsilon(0.0905, 0.0847, 0.0536) \simeq (0.3573, 0.3344, 0.2116)$. In both cases we found that, above some curve (the dashed lines), the RG trajectories flow to the corresponding stable fixed point, while below this curve, the RG trajectories show runaway behavior.

It is known that the above equations have six fixed points [166], four of which have the two fields decoupled, i.e., $g^* = 0$. They are the Gaussian-Gaussian point at $(\beta_1^*, \beta_2^*) = (0, 0)$, the Heisenberg-Gaussian point at $(\beta_1^*, \beta_2^*) = (4\pi^2\epsilon/(n_1 + 8), 0)$, the Gaussian-Heisenberg point at $(\beta_1^*, \beta_2^*) = (0, 4\pi^2\epsilon/(n_2 + 8))$, and the

decoupled Heisenberg-Heisenberg point at $(\beta_1^*, \beta_2^*) = (4\pi^2\epsilon/(n_1+8), 4\pi^2\epsilon/(n_2+8))$. The isotropic Heisenberg fixed point is at $\beta_1^* = \beta_2^* = g^* = 4\pi^2\epsilon/(n_1+n_2+8), \alpha_1^* = \alpha_2^* = \epsilon(n_1+n_2+2)/4(n_1+n_2+8)$. Finally there is the biconical fixed point with generally unequal values of β_1^*, β_2^*, and g^*. In the case, with $n_1 = n_2 = 1$, this is at $(\beta_1^*, \beta_2^*, g^*) = 2\pi^2\epsilon/9(1,1,3)$. For $n_1 = 2, n_2 = 3$, one has $(\beta_1^*, \beta_2^*, g^*) = 4\pi^2\epsilon(0.0905, 0.0847, 0.0536)$.

We find that there is always just one stable fixed point for $d + z < 4$, below the upper critical dimension [166]. The isotropic Heisenberg fixed point is stable when $n_1 + n_2 < n_c = 4 - 2\epsilon + O(\epsilon^2)$, the biconical fixed point is stable when $n_c < n_1 + n_2 < 16 - n_1 n_2/2 + O(\epsilon)$, and when $n_1 n_2 + 2(n_1 + n_2) > 32 + O(\epsilon)$, the decoupled Heisenberg-Heisenberg point is the stable one. When the initial parameters are not in the basin of attraction of the stable fixed point, one obtains runaway flow, strongly suggestive of a first-order phase transition. Consider for example $n_1 = 2, n_2 = 3$, where the biconical fixed point is stable. For two critical points not too separated, that is, $|\alpha_1 - \alpha_2|$ not too large, when $g > \sqrt{\beta_1\beta_2}$ the RG flow shows runaway behavior, and one gets a first-order quantum phase transition. The corresponding classical problem has been discussed in [167]. We notice the difference from the case with two competing classical fields, where one also obtains the same condition for the couplings $\gamma > \sqrt{\beta_1\beta_2}$ in order to have a first-order phase transition. There, the two ordered phases are required to overlap in the absence of the coupling, in other words, one needs to have $x_1 < x_2$. However, in the quantum mechanical case we are considering here, this is not necessary. We plot in Fig. 4.7 the RG trajectories for two cases (a) $n_1 = n_2 = 1$ and (b) $n_1 = 2, n_3 = 3$, where in both cases, below some curve, runaway behavior in the RG trajectories is found.

When $d + z = 4$, all the other fixed points coalesce with the Gaussian point, forming an unstable fixed point, thus leading to a first-order phase transition (see Fig. 4.8(a)). A similar model with an extra coupling and $n_1 = n_2 = 3$ has been discussed by Qi And Xu [133], where runaway flows were also identified. Another similar problem with $d = 2, z = 2$ was studied by Millis recently [134], where a fluctuation-induced first-order quantum phase transition was shown to occur. We also notice that in some situations, including fluctuations of the order parameter itself may drive the supposed-to-be first-order transitions to second order for both classical and quantum phase transitions [168–171].

For $d + z > 4$, the stabilities are interchanged. The Gaussian fixed point becomes the most stable one. So the basin of attraction of the stable fixed point changes. We found numerically that for a given coupling strength g, in the $\beta_1 - \beta_2$ plane, the RG trajectories show runaway behavior when the initial points lie below some curve (see Fig. 4.8(b)). That is, when the coupling between the two fields is strong enough, the QPTs become first order. Just above these curves, we found that the RG trajectories will enter the domain with negative β_1 or negative β_2, and then converge to the Gaussian fixed point. For β_1, β_2 large enough, the RG trajectories just converge to the Gaussian fixed point without entering the negative domain.

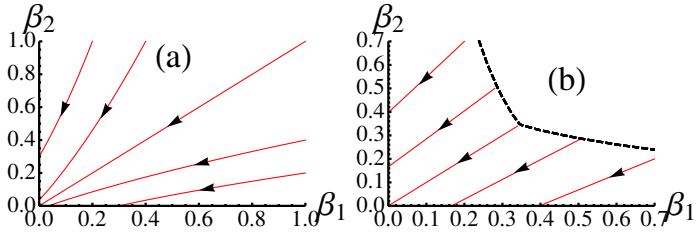

Figure 4.8: Plot of the RG trajectories in the $\beta_1 - \beta_2$ plane for two quantum fields with the same dynamical exponent in and above the upper critical dimension. The RG trajectories have been projected to a constant g plane. And we have chosen $n_1 = n_2 = 3$. (a) corresponds to the case exactly at the critical dimension with $\epsilon = 4 - d - z = 0$. In this case there is only one fixed point with $\beta_1^* = \beta_2^* = g^* = 0$, the Gaussian fixed point, which is unstable. We found runaway flows everywhere. (b) corresponds to the case above the critical dimension, where the Gaussian fixed point is the stable one. Here we have chosen $\epsilon = 4 - d - z = -0.1$. We found, below some curve (the dashed line), that the RG trajectories show runaway behavior.

4.4.1 Competing orders with different dynamical exponents

We consider next coupling a $z = 1$ field to another field with dynamical exponent $z = z_1 \geqslant 2$. To our knowledge, such models of two competing order parameters with different dynamical exponents have not been studied previously. The action now takes the form

$$\begin{aligned} S_\psi &= \int d^d\mathbf{k} d\omega \left(-\alpha_1 + \frac{k^2}{2} + \frac{\gamma_1}{2} \frac{|\omega|}{k^{z_1-2}} \right) |\boldsymbol{\psi}|^2 + \int d^d\mathbf{r} d\tau \frac{1}{2} \beta_1 |\boldsymbol{\psi}|^4, \\ S_\phi &= \int d^d\mathbf{r} d\tau \left[-\alpha_2 |\boldsymbol{\phi}|^2 + \frac{1}{2}\beta_2 |\boldsymbol{\phi}|^4 + \frac{1}{2} |\partial_\mu \boldsymbol{\phi}|^2 \right], \\ S_{\psi\phi} &= g \int d^d\mathbf{r} d\tau |\boldsymbol{\psi}|^2 |\boldsymbol{\phi}|^2. \end{aligned} \tag{4.49}$$

The RG analysis of such models is not an easy task. The conventional picture is that in d spatial dimensions, the quantum field theory of a bosonic field with dynamical exponent z is equivalent to a classical field theory in $d + z$ dimensions. This picture still holds when there are more than one field, but all the fields have the same dynamical exponent. However, when the coupled fields have different dynamical exponents, this picture is no longer valid: the fields are frustrated in choosing their effective dimensions. Technically, this problem arises in the RG analysis for example when one calculates the loop diagrams containing internal lines corresponding to fields with different dynamical exponents. If we

think more carefully about how one arrives at the conventional way of counting effective dimensions, we will find that one has to rescale the parameters to absorb the generally dimensionfull γ parameters, the presence of which ensures the frequency dependent terms in the action to have the right dimensions. We will show explicitly such rescaling below. With distinct dynamical exponents, one can no longer rescale out these γ parameters. They actually lead to dramatically different scaling behavior in the RG structure: there is now a line of fixed points.

The new parameter γ_1 has dimension $[\gamma_1] = L^{1-z}$, and its one-loop RG equation is simply

$$\frac{d\gamma_1}{dl} = (z-1)\gamma_1. \tag{4.50}$$

The Green's function for the ψ field becomes $G_\psi = 1/(-2\alpha_1 + k^2 + \gamma_1|\omega|/k^{z_1-2})$. The RG equations for the other parameters are modified accordingly,

$$\begin{aligned}
\frac{d\alpha_1}{dl} =& 2\alpha_1 - \frac{\Omega_d}{\pi\gamma_1}(n_1+2)\beta_1(\ln 2 + 2\alpha_1) - \Omega_{d+1}n_2 g(2+2\alpha_2),\\
\frac{d\alpha_2}{dl} =& 2\alpha_2 - \Omega_{d+1}(n_2+2)\beta_2(2+2\alpha_2) - \frac{\Omega_d}{\pi\gamma_1}n_1 g(\ln 2 + 2\alpha_1),\\
\frac{d\beta_1}{dl} =& \epsilon\beta_1 - \frac{2\Omega_d}{\pi\gamma_1}(n_1+8)\beta_1^2 - 2\Omega_{d+1}n_2 g^2,\\
\frac{d\beta_2}{dl} =& \epsilon\beta_2 - 2\Omega_{d+1}(n_2+8)\beta_2^2 - \frac{2\Omega_d}{\pi\gamma_1}n_1 g^2,\\
\frac{dg}{dl} =& g\left(\epsilon - \frac{2\Omega_d}{\pi\gamma_1}(n_1+2)\beta_1 - 2\Omega_{d+1}(n_2+2)\beta_2 - 8\frac{\Omega_d}{2\pi}\frac{2\gamma_1\ln\gamma_1 + \pi}{1+\gamma_1^2}g\right),
\end{aligned} \tag{4.51}$$

where $\epsilon = 3-d$ and $\Omega_d = 2\pi^{d/2}/(2\pi)^d\Gamma[d/2]$ is the volume of the d-dimensional unit sphere. The derivation of the above RG equations is included in the appendix. We notice from the above procedure that when the two fields have the same dynamical exponent $z > 1$, one can rescale the couplings to $\tilde{\beta}_1 = \beta_1/\gamma$, $\tilde{\beta}_2 = \beta_2/\gamma$, $\tilde{g} = g/\gamma$, and these new parameters satisfy the RG equations (4.48) with $\tilde{\epsilon} = 4-d-z$.

The presence of two different dynamical exponents obviously complicates the problem. It is generally expected that the modes with a larger dynamical exponent dominates the specific heat of the system, since they have a large phase space, while the modes with a smaller dynamical exponent may produce infrared singularities, since they have a smaller upper critical dimension [172]. In the absence of the coupling between the two fields, we have the RG equations

$$\begin{aligned}
\frac{d\tilde{\beta}_1}{dl} =& (4-d-z)\tilde{\beta}_1 - \frac{2\Omega_d}{\pi}(n_1+8)\tilde{\beta}_1^2,\\
\frac{d\beta_2}{dl} =& (3-d)\beta_2 - 2\Omega_{d+1}(n_2+8)\beta_2^2.
\end{aligned} \tag{4.52}$$

For $d = 3$, β_2 is marginal with an unstable fixed point, while $\tilde{\beta}_1$ is irrelevant and its Gaussian fixed point is stable.

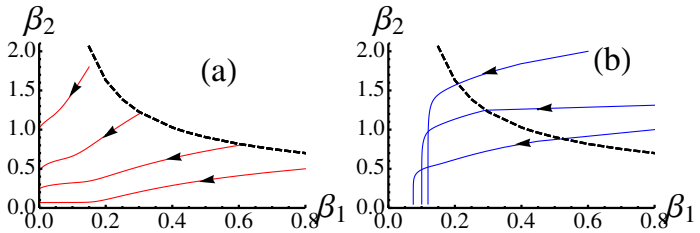

Figure 4.9: Plot of the RG trajectories in the $\beta_1 - \beta_2$ plane for two coupled quantum fields with different dynamical exponents. The RG trajectories have been projected to a constant g plane with $g = 1$. We have chosen the spatial dimension to be $d = 3$, the dynamical exponents $z_1 = 2, z_2 = 1$ and the number of field components $n_1 = n_2 = 3$. (a) shows the RG trajectories originating from the region below the dashed line, which flow to negative β_1 or negative β_2 regions. (b) shows the RG trajectories originating from the region above the dashed line, and those flow to the stable points on the positive axes of β_1, the location of which is sensitive to the initial value of the parameters.

Generally, for $z > 1$, if the initial value of γ_1 is nonzero, the absolute value of γ_1 will increase exponentially. The RG equation for β_2 becomes independent of other parameters,

$$\frac{d\beta_2}{dl} = \epsilon\beta_2 - 2\Omega_{d+1}(n_2 + 8)\beta_2^2. \tag{4.53}$$

We are interested in the case $\epsilon = 0$, for which β_2 is readily solved to be

$$\beta_2(l) = \frac{1}{\bar{\beta}_2^{-1} + 2\Omega_4(n_2 + 8)(l - l_{\rm cr})}, \tag{4.54}$$

with $\bar{\beta}_2$ taken at the crossover scale $l_{\rm cr}$ at which the β_2^2 term begins to dominate the g^2 term. Only the sign of $\bar{\beta}_2$ matters. If $\bar{\beta}_2 > 0$, as l increases, β_2 will decay to zero, flowing to its Gaussian fixed point. From the simplified RG equations for g,

$$\frac{dg}{dl} = -2\Omega_4(n_2 + 2)g\beta_2, \tag{4.55}$$

one can see that with a lower power in β_2, g drops to zero even more quickly than β_2. Taking β_2 as quasi-static when considering the evolution of g, one notices that g decays exponentially as $g(l) \sim \exp(-2\Omega_4(n_2 + 2)\beta_2 l)$. So $d\beta_1/dl$ also decays exponentially, and before β_2 goes to zero, β_1 already stabilizes to a finite value β_1^*, which depends on the initial value of β_1. Actually from the simplified RG equations for β_1, β_2, g with $1/\gamma_1$ set to zero, one can see directly that the

fixed points are at $\beta_2^* = g^* = 0$, with β_1^* any real number: we have a line of fixed points. When $\beta_1^* > 0$, there will be a second-order phase transition. When $\beta_1^* < 0$, the transition becomes first order (see Fig. 4.9).

If $\bar{\beta}_2 < 0$, the absolute value of β_2 will increase without bound. Subsequently g and β_1 also diverge, leading to runaway flows.

4.5 Conclusions

Quantum criticality in the presence of competing interactions is an important guiding concept that allows us to organize a framework for emergent states near QCPs. Here we investigated the stability of a quantum critical point in the presence of competing orders. We focused on a simple quadratic-quadratic interaction, where coupling between two competing phases is assumed to be of $g\psi^2\phi^2$ form. We find that QCPs are often unstable and transform into first order lines of transitions. The detailed scenario on how the instability develops depends on the precise nature of the competing interactions, dynamical exponents and strength of the coupling. The general trend we observe is that competing interactions, be they classical or quantum, often lead to the instability of QCPs. This instability in fact always occurs, in the cases we have investigated, if the coupling g is strong enough. We thus conclude that breakdown of QCPs is a ubiquitous phenomenon. The magnitude of the specific heat jump in some first order transitions (the *classical + classical* case) is of the same order as the specific heat released in a second order transition and these first order transitions are strong, and not weakly first order as found in Halperin-Lubensky-Ma. An immediate consequence of this breakdown is that we can expect spatially modulated inhomogeneous phases to be present near QCPs, given their propensity to turn into first order transitions. The wide likelihood identified here of first order transitions preempting a QCP leads us to anticipate the nucleation and metastability phenomena associated with such transitions [173]. Additionally, proximity to first-order transitions makes auxiliary fields (e. g. magnetic field, strain) and disorder very important over substantial parameter regions [174].

The broad similarities we pointed out between QCPs and AdS/CFT models offers an interesting possibility that in fact AdS models are also spatially inhomogeneous. More detailed analysis that allows breakdown of scaling, specific for AdS/CFT is suggested.

We derived the renormalization group equations for two coupled order parameters with different dynamical exponents. We found that there are a line of fixed points, which is quite different from the case where two order parameters have the same dynamical exponent. Very recently, there have appeared some interesting reports [172,175] investigating the effects of the presence of two order parameters with different dynamical exponents near the Pomeranchuk instability [176], as examples of multiscale quantum criticality. It would be interesting to see how the presence of two different dynamical exponents, and the coupling

between the corresponding order parameters, affect the scaling of resistivity, especially whether a linear-resistivity is possible, overcoming the "no-go" theorem for single parameter scaling [177].

In this chapter, we have confined ourselves to the framework of Hertz-Millis-Moriya [143–145], considering only the interplay of bosonic order parameters. It would also be interesting to study the electronic instabilities, to see whether the superconducting instabilities and Pomeranchuk instabilities are enhanced in fermionic quantum critical states. Fermi liquids, even with repulsive interactions, are unstable towards forming a superconducting state, due to the Kohn-Luttinger effect [178] resulting from the presence of a sharp Fermi surface. For the fermionic quantum critical states, the momentum distribution function may have only higher order singularities [179]. It would be interesting to check whether the Kohn-Luttinger effect is still active in this case.

4.6 Appendix: RG equations for two fields with different dynamical exponents

In this appendix, we will derive the RG equations of two competing orders with different dynamical exponents. We follow the notation of [180]. Our starting point is the action ((4.49)). First we count the dimensions of the field operators and all the parameters:

$$\begin{aligned}
[r] = [\tau] =& L, \\
[k] = [\omega] =& L^{-1}, \\
[\psi] = [\phi] =& L^{(1-d)/2}, \\
[\alpha_1] = [\alpha_2] =& L^{-2}, \\
[\beta_1] = [\beta_2] =& L^{d-3}, \\
[g] =& L^{d-3}, \\
[\gamma_1] =& L^{1-z}.
\end{aligned} \tag{4.56}$$

Then we decompose the action into slow and fast modes. The action for the slow modes reads

$$\begin{aligned} S^{(s)} =& S_{\psi}^{(s)} + S_{\phi}^{(s)} + S_{\psi\phi}^{(s)}, \\ S_{\psi}^{(s)} =& \int d^d\mathbf{k} d\omega \left(-\alpha_1 + \frac{k^2}{2} + \frac{\gamma_1}{2} \frac{|\omega|}{k^{z_1-2}} \right) |\boldsymbol{\psi}_s|^2 + \int d^d\mathbf{r} d\tau \frac{1}{2} \beta_1 |\boldsymbol{\psi}_s|^4, \\ S_{\phi}^{(s)} =& \int d^d\mathbf{r} d\tau \left[-\alpha_2 |\boldsymbol{\phi}_s|^2 + \frac{1}{2}\beta_2 |\boldsymbol{\phi}_s|^4 + \frac{1}{2} |\partial_\mu \boldsymbol{\phi}_s|^2 \right], \\ S_{\psi\phi}^{(s)} =& g \int d^d\mathbf{r} d\tau |\boldsymbol{\psi}_s|^2 |\boldsymbol{\phi}_s|^2. \end{aligned} \tag{4.57}$$

Since we will only consider RG to one-loop order, the interaction terms in the fast modes, the contraction of which leads to second-order diagrams, can be ignored. Thus we obtain the action for the fast modes,

$$\begin{aligned} S^{(f)} =& S_{\psi}^{(f)} + S_{\phi}^{(f)}, \\ S_{\psi}^{(f)} =& \int d^d\mathbf{k} d\omega \left(-\alpha_1 + \frac{k^2}{2} + \frac{\gamma_1}{2} \frac{|\omega|}{k^{z_1-2}} \right) |\boldsymbol{\psi}_f|^2, \\ S_{\phi}^{(f)} =& \int d^d\mathbf{r} d\tau \left[-\alpha_2 |\boldsymbol{\phi}_f|^2 + \frac{1}{2} |\partial_\mu \boldsymbol{\phi}_f|^2 \right], \end{aligned} \tag{4.58}$$

from which one can easily identify the Green's functions as

$$\begin{aligned} G_{ij}^f[\psi] =& \frac{\delta_{ij}}{-2\alpha_1 + k^2 + \gamma_1 \frac{|\omega|}{k^{z_1-2}}}, \\ G_{ij}^f[\phi] =& \frac{\delta_{ij}}{-2\alpha_2 + k^2 + \omega^2}. \end{aligned} \tag{4.59}$$

The coupling between the slow modes and fast modes takes the form

$$\begin{aligned} S_c = \int d^d\mathbf{r} d\tau \Bigg[& \sum_{ijkl} F_{ijkl} \left(3\beta_1 \psi_f^i \psi_f^j \psi_s^k \psi_s^l + 3\beta_2 \phi_f^i \phi_f^j \phi_s^k \phi_s^l \right) \\ & + g|\boldsymbol{\psi}_s|^2 |\boldsymbol{\phi}_f|^2 + g|\boldsymbol{\psi}_f|^2 |\boldsymbol{\phi}_s|^2 + 4g(\boldsymbol{\psi}_s \cdot \boldsymbol{\psi}_f)(\boldsymbol{\phi}_s \cdot \boldsymbol{\phi}_f) \Bigg], \end{aligned} \tag{4.60}$$

with the tensor $F_{ijkl} = \frac{1}{3}(\delta_{ij}\delta_{kl} + \delta_{ik}\delta_{jl} + \delta_{il}\delta_{jk})$.

Now we can integrate out the fast modes and see how the different parameters change accordingly. The effective action of the slow modes is determined by

$$\exp\left[-S_{\text{eff}}^{(s)} \right] = \exp\left[-S^{(s)} \right] \exp\left[-\langle S_c \rangle_f + \frac{1}{2} \langle S_c^2 \rangle_f^{\text{con}} \right]. \tag{4.61}$$

In the S_c^2 term we take a connected average, thus the superscript "con". The coefficients in the RG equations will depend on the different renormalization schemes. Here we will use the procedure that is most convenient for the problem at hand, similar in spirit to what was outlined in [181]. We integrate over the momentum interval $\Lambda/b < k < \Lambda$, which after rescaling $k \to k/\Lambda$, gives $b^{-1} < k < 1$. The frequency part is more complicated. We will introduce a cutoff when it is necessary, otherwise just integrate over the whole range $-\infty < \omega < \infty$. The main reason for us to choose this RG scheme is that in calculating the third correction to the coupling g, the two internal lines come from order parameters with different dynamical exponents, thus the two frequencies scale differently with momentum, and this RG scheme offers a simple and self-consistent treatment of the cutoffs.

γ_1 does not receive corrections up to first-order.

Figure 4.10: One-loop diagrams contributing to the first order correction of α_1. The solid lines represent the ψ fields, and the dashed lines represent the ϕ fields. The external lines are slow modes, and the internal lines are fast modes.

Two terms in the action (4.60) contribute to the first-order corrections of α_1. The coupling $\psi_s^2\psi_f^2$ leads to the correction

$$\delta^{(1)}S[\alpha_1] = 3\beta_1 \sum_{ijkl} F_{ijkl} \int_f \frac{d^{d+1}\mathbf{q}'}{(2\pi)^{d+1}} \langle \psi_f^i(\mathbf{q}')\psi_f^j(-\mathbf{q}')\rangle \int_s \frac{d^{d+1}\mathbf{q}}{(2\pi)^{d+1}} \psi_s^k(\mathbf{q})\psi_s^l(-\mathbf{q}). \tag{4.62}$$

Using the identity,

$$\sum_i F_{iikl} = \frac{n_1+2}{3}\delta_{kl}, \tag{4.63}$$

one obtains

$$\delta^{(1)}S[\alpha_1] = (n_1+2)\beta_1 \frac{\Omega_d}{2\pi} \int d\omega \int_{b^{-1}}^1 dk k^{d-1} \frac{1}{-2\alpha_1 + k^2 + \gamma_1 \frac{|\omega|}{k^{z_1-2}}} \int_s \frac{d^{d+1}\mathbf{q}}{(2\pi)^{d+1}} \boldsymbol{\psi}_s(\mathbf{q}) \cdot \boldsymbol{\psi}_s(-\mathbf{q}). \tag{4.64}$$

Assuming that the ψ field is near its critical point, thus α_1 is a small parameter, the Green's function can be expanded in terms of $-2\alpha_1$. The correction term

can be written as

$$\delta^{(1)}S[\alpha_1] = (n_1+2)\beta_1\frac{\Omega_d}{2\pi}(I_1+2\alpha_1 I_2)\int_s \frac{d^{d+1}\mathbf{q}}{(2\pi)^{d+1}}\boldsymbol{\psi}_s(\mathbf{q})\cdot\boldsymbol{\psi}_s(-\mathbf{q}), \tag{4.65}$$

where we have defined the series of functions

$$I_n = \int d\omega \int_{b^{-1}}^{1} dk k^{d-1}\frac{1}{\left(k^2+\gamma_1\frac{|\omega|}{k^{z_1-2}}\right)^n}. \tag{4.66}$$

Let us first calculate I_1. The frequency integral requires a cutoff. From dimensional analysis, we choose to integrate over the region $-1<\gamma_1\omega<1$, and obtain the result

$$I_1 = \frac{2}{\gamma_1}\int_{b^{-1}}^{1} dk k^{d+z_1-3}\ln\left(\frac{1+k^{z_1}}{k^{z_1}}\right). \tag{4.67}$$

To proceed further, we are required to specify the dimension and dynamical exponent. Consider $d=3, z_1=2$, where one has

$$I_1 = \frac{2}{3\gamma_1}\left[\ln 2 - b^{-3}\ln\left(\frac{1+b^{-2}}{b^{-2}}\right)+2(1-b^{-1})-2\arctan 1+2\arctan b^{-1}\right]. \tag{4.68}$$

Expanded to first order in $(1-b^{-1})$, it is simply

$$I_1 = \frac{2\ln 2}{\gamma_1}(1-b^{-1}). \tag{4.69}$$

For $d=2, z_1=2$, we obtain

$$I_1 = \frac{1}{\gamma_1}\left[2\ln 2-(1+b^{-2})\ln(1+b^{-2})+b^{-2}\ln b^{-2}\right], \tag{4.70}$$

which leads to the same result (4.69) when expanded to first order in $(1-b^{-1})$. This result can also be obtained more crudely by setting $k=1$ in the integrand of (4.67). I_2 can be calculated similarly, with the result

$$I_2 = \frac{2}{\gamma_1}(1-b^{-1}). \tag{4.71}$$

So the one-loop correction to α_1 coming from the coupling $\psi_s^2\psi_f^2$ is

$$\delta^{(1)}S[\alpha_1] = (n_1+2)\beta_1\frac{\Omega_d}{\pi\gamma_1}(1-b^{-1})(\ln 2+2\alpha_1)\int_s \frac{d^{d+1}\mathbf{q}}{(2\pi)^{d+1}}\boldsymbol{\psi}_s(\mathbf{q})\cdot\boldsymbol{\psi}_s(-\mathbf{q}), \tag{4.72}$$

We next calculate contributions from the coupling $\psi_s^2\phi_f^2$, which takes the form

$$\delta^{(2)}S[\alpha_1] = g\sum_{ijkl}F'_{ijkl}\int_f \frac{d^{d+1}\mathbf{q}'}{(2\pi)^{d+1}}\langle\phi_f^i(\mathbf{q}')\phi_f^j(-\mathbf{q}')\rangle\int_s \frac{d^{d+1}\mathbf{q}}{(2\pi)^{d+1}}\psi_s^k(\mathbf{q})\psi_s^l(-\mathbf{q}), \tag{4.73}$$

with $F'_{ijkl} = \delta_{ij}\delta_{kl}$. So we have simply the identity

$$\sum_i F'_{iikl} = n_2 \delta_{kl}, \tag{4.74}$$

which gives

$$\delta^{(2)} S[\alpha_1] = n_2 g \frac{\Omega_d}{2\pi} \int d\omega \int_{b^{-1}}^1 dk k^{d-1} \frac{1}{-2\alpha_2 + k^2 + \omega^2} \int_s \frac{d^{d+1}\mathbf{q}}{(2\pi)^{d+1}} \boldsymbol{\psi}_s(\mathbf{q}) \cdot \boldsymbol{\psi}_s(-\mathbf{q}). \tag{4.75}$$

Defining the new set of functions

$$I'_n = \int d\omega \int_{b^{-1}}^1 dk k^{d-1} \frac{1}{(k^2 + \omega^2)^n}, \tag{4.76}$$

one obtains

$$\delta^{(2)} S[\alpha_1] = n_2 g \frac{\Omega_d}{2\pi} (I'_1 + 2\alpha_2 I'_2) \int_s \frac{d^{d+1}\mathbf{q}}{(2\pi)^{d+1}} \boldsymbol{\psi}_s(\mathbf{q}) \cdot \boldsymbol{\psi}_s(-\mathbf{q}). \tag{4.77}$$

Here we integrate over frequencies in the range $-\infty < \omega < \infty$, and get

$$I'_1 = \pi \int_{b^{-1}}^1 dk k^{d-2}, \tag{4.78}$$

which is, to first order in $(1 - b^{-1})$,

$$I'_1 = \pi(1 - b^{-1}). \tag{4.79}$$

Similarly for I'_2 we have

$$I'_2 = \frac{\pi}{2} \int_{b^{-1}}^1 dk k^{d-4}, \tag{4.80}$$

thus

$$I'_2 = \frac{\pi}{2}(1 - b^{-1}). \tag{4.81}$$

Near $d = 3$, one has $\Omega_d/4 \simeq \Omega_{d+1}$. Grouping all these together, we obtain the second term in the correction to α_1 as

$$\delta^{(2)} S[\alpha_1] = n_2 g \Omega_{d+1} (1 - b^{-1})(2 + 2\alpha_2) \int_s \frac{d^{d+1}\mathbf{q}}{(2\pi)^{d+1}} \boldsymbol{\psi}_s(\mathbf{q}) \cdot \boldsymbol{\psi}_s(-\mathbf{q}). \tag{4.82}$$

The calculation of the first order corrections to α_2 is quite similar to that of α_1. There are again two terms contributing. The coupling $\psi_f^2 \phi_s^2$ gives rise to a term of the form

$$\delta^{(1)} S[\alpha_2] = g \sum_{ijkl} F'_{ijkl} \int_f \frac{d^{d+1}\mathbf{q}'}{(2\pi)^{d+1}} \langle \psi_f^i(\mathbf{q}') \psi_f^j(-\mathbf{q}') \rangle \int_s \frac{d^{d+1}\mathbf{q}}{(2\pi)^{d+1}} \phi_s^k(\mathbf{q}) \phi_s^l(-\mathbf{q}), \tag{4.83}$$

Figure 4.11: One-loop diagrams contributing to the first order correction of α_2. The solid lines represent the ψ fields, and the dashed lines represent the ϕ fields. The external lines are slow modes, and the internal lines are fast modes.

Summing over the field indices,

$$\sum_i F'_{iikl}\phi_s^k\phi_s^l = n_1|\boldsymbol{\phi}_s|^2, \tag{4.84}$$

we obtain

$$\delta^{(1)}S[\alpha_2] = n_1 g\frac{\Omega_d}{2\pi}\int d\omega\int_{b^{-1}}^1 dk k^{d-1}\frac{1}{-2\alpha_1 + k^2 + \gamma_1\frac{|\omega|}{k^{z_1-2}}} \int_s \frac{d^{d+1}\mathbf{q}}{(2\pi)^{d+1}}\boldsymbol{\phi}_s(\mathbf{q})\cdot\boldsymbol{\phi}_s(-\mathbf{q}), \tag{4.85}$$

which can be expanded as

$$\delta^{(1)}S[\alpha_2] = n_1 g\frac{\Omega_d}{2\pi}(I_1 + 2\alpha_1 I_2)\int_s \frac{d^{d+1}\mathbf{q}}{(2\pi)^{d+1}}\boldsymbol{\phi}_s(\mathbf{q})\cdot\boldsymbol{\phi}_s(-\mathbf{q}). \tag{4.86}$$

The result is

$$\delta^{(1)}S[\alpha_2] = n_1 g\frac{\Omega_d}{\pi\gamma_1}(1-b^{-1})(\ln 2 + 2\alpha_1)\int_s \frac{d^{d+1}\mathbf{q}}{(2\pi)^{d+1}}\boldsymbol{\phi}_s(\mathbf{q})\cdot\boldsymbol{\phi}_s(-\mathbf{q}). \tag{4.87}$$

The other term comes from the coupling $\phi_f^2\phi_s^2$. It has the form

$$\delta^{(2)}S[\alpha_2] = 3\beta_2\sum_{ijkl}F_{ijkl}\int_f \frac{d^{d+1}\mathbf{q}'}{(2\pi)^{d+1}}\langle\phi_f^i(\mathbf{q}')\phi_f^j(-\mathbf{q}')\rangle\int_s \frac{d^{d+1}\mathbf{q}}{(2\pi)^{d+1}}\phi_s^k(\mathbf{q})\phi_s^l(-\mathbf{q}). \tag{4.88}$$

We first sum over the field indices,

$$\sum_i F_{iikl}\phi_s^k\phi_s^l = \frac{n_2+2}{3}|\boldsymbol{\phi}_s|^2, \tag{4.89}$$

resulting in

$$\delta^{(2)}S[\alpha_2] = (n_2+2)\beta_2\frac{\Omega_d}{2\pi}\int d\omega \int_{b^{-1}}^{1} dk k^{d-1}\frac{1}{-2\alpha_2+k^2+\omega^2} \int_s \frac{d^{d+1}\mathbf{q}}{(2\pi)^{d+1}}\boldsymbol{\phi}_s(\mathbf{q})\cdot\boldsymbol{\phi}_s(-\mathbf{q}). \tag{4.90}$$

Expanding to first order in α_2, one has

$$\delta^{(2)}S[\alpha_2] = (n_2+2)\beta_2\frac{\Omega_d}{2\pi}(I_1'+2\alpha_2 I_2')\int_s \frac{d^{d+1}\mathbf{q}}{(2\pi)^{d+1}}\boldsymbol{\phi}_s(\mathbf{q})\cdot\boldsymbol{\phi}_s(-\mathbf{q}), \tag{4.91}$$

and the final result is

$$\delta^{(2)}S[\alpha_2] = (n_2+2)\beta_2\Omega_{d+1}(1-b^{-1})(2+2\alpha_2)\int_s \frac{d^{d+1}\mathbf{q}}{(2\pi)^{d+1}}\boldsymbol{\phi}_s(\mathbf{q})\cdot\boldsymbol{\phi}_s(-\mathbf{q}), \tag{4.92}$$

Figure 4.12: One-loop diagrams contributing to the first order correction of β_1. The solid lines represent the ψ fields, and the dashed lines represent the ϕ fields. The external lines are slow modes, and the internal lines are fast modes.

The first order correction to β_1 comes from two one-loop diagrams, one with two internal ψ_f lines, the other with two ϕ_f lines. The dependence of the internal lines on the external momenta and frequencies can be ignored here, since they are of higher order.

The first term with ψ_f internal lines is of the form

$$\delta^{(1)}S[\beta_1] = -(3\beta_1)^2\sum_{k_1k_2l_1l_2}\sum_{i_1i_2j_1j_2}F_{i_1j_1k_1l_1}F_{i_2j_2k_2l_2}\int_f\frac{d^{d+1}\mathbf{q}'}{(2\pi)^{d+1}}\langle\psi_f^{i_1}(\mathbf{q}')\psi_f^{i_2}(-\mathbf{q}')\rangle \langle\psi_f^{j_1}(\mathbf{q}')\psi_f^{j_2}(-\mathbf{q}')\rangle\int d^d\mathbf{r}d\tau\psi_s^{k_1}\psi_s^{k_2}\psi_s^{l_1}\psi_s^{l_2} + \text{ 2 permutations.} \tag{4.93}$$

Using the identity,

$$\sum_{ij}F_{ijk_1l_1}F_{ijk_2l_2} = \frac{1}{9}\left[(n_1+4)\delta_{k_1l_1}\delta_{k_2l_2}+2\delta_{k_1k_2}\delta_{l_1l_2}+2\delta_{k_1l_2}\delta_{k_2l_1}\right], \tag{4.94}$$

combined with the 2 other permutations of the external lines, the part containing the field component indices can be simplified as

$$\sum_{k_1k_2l_1l_2}\sum_{ij}F_{ijk_1l_1}F_{ijk_2l_2}\psi_s^{k_1}\psi_s^{k_2}\psi_s^{l_1}\psi_s^{l_2}+\ 2\text{ permutations}=\frac{n_1+8}{9}|\boldsymbol{\psi}_s|^4. \quad (4.95)$$

Thus the first correction to β_1 reads

$$\delta^{(1)}S[\beta_1]=-(n_1+8)\beta_1^2\frac{\Omega_d}{2\pi}\int d\omega\int_{b^{-1}}^1 dkk^{d-1}\frac{1}{(-2\alpha_1+k^2+\gamma_1\frac{|\omega|}{k^{z_1-2}})^2}\int d^d\mathbf{r}d\tau|\boldsymbol{\psi}_s|^4, \quad (4.96)$$

which is, to leading order of α_1,

$$\delta^{(1)}S[\beta_1]=-(n_1+8)\beta_1^2\frac{\Omega_d}{2\pi}I_2\int d^d\mathbf{r}d\tau|\boldsymbol{\psi}_s|^4. \quad (4.97)$$

Substituting the explicit expression for I_2, we get the result

$$\delta^{(1)}S[\beta_1]=-(n_1+8)\beta_1^2\frac{\Omega_d}{\pi\gamma_1}(1-b^{-1})\int d^d\mathbf{r}d\tau|\boldsymbol{\psi}_s|^4. \quad (4.98)$$

The second term has two ϕ_f internal lines, and takes the form

$$\begin{aligned}\delta^{(2)}S[\beta_1]=&-g^2\sum_{i_1i_2j_1j_2}\sum_{k_1k_2l_1l_2}F'_{i_1j_1k_1l_1}F'_{i_2j_2k_2l_2}\int_f\frac{d^{d+1}\mathbf{q}'}{(2\pi)^{d+1}}\langle\phi_f^{i_1}(\mathbf{q}')\phi_f^{i_2}(-\mathbf{q}')\rangle\\&\langle\phi_f^{j_1}(\mathbf{q}')\phi_f^{j_2}(-\mathbf{q}')\rangle\int d^d\mathbf{r}d\tau\psi_s^{k_1}\psi_s^{k_2}\psi_s^{l_1}\psi_s^{l_2}+\ 2\text{ permutations}.\end{aligned} \quad (4.99)$$

The part with the field component indices gives

$$\sum_{k_1k_2l_1l_2}\sum_{ij}F'_{ijk_1l_1}F'_{ijk_2l_2}\psi_s^{k_1}\psi_s^{k_2}\psi_s^{l_1}\psi_s^{l_2}+\ 2\text{ permutations}=n_2|\boldsymbol{\psi}_s|^4, \quad (4.100)$$

which further leads to the result

$$\delta^{(2)}S[\beta_1]=-n_2g^2\frac{\Omega_d}{2\pi}\int d\omega\int_{b^{-1}}^1 dkk^{d-1}\frac{1}{(-2\alpha_2+k^2+\omega^2)^2}\int d^d\mathbf{r}d\tau|\boldsymbol{\psi}_s|^4. \quad (4.101)$$

To leading order in α_2, it is

$$\delta^{(2)}S[\beta_1]=-n_2g^2\frac{\Omega_d}{2\pi}I_2'\int d^d\mathbf{r}d\tau|\boldsymbol{\psi}_s|^4, \quad (4.102)$$

or more explicitly,

$$\delta^{(2)}S[\beta_1]=-n_2g^2\Omega_{d+1}(1-b^{-1})\int d^d\mathbf{r}d\tau|\boldsymbol{\psi}_s|^4. \quad (4.103)$$

Figure 4.13: One-loop diagrams contributing to the first order correction of β_2. The solid lines represent the ψ fields, and the dashed lines represent the ϕ fields. The external lines are slow modes, and the internal lines are fast modes.

The first order correction to the β_2 term also comes from two diagrams. The first one has two ψ_f internal lines, and is of the form

$$\delta^{(1)}S[\beta_2] = -g^2 \sum_{i_1 i_2 j_1 j_2} \sum_{k_1 k_2 l_1 l_2} F'_{i_1 j_1 k_1 l_1} F'_{i_2 j_2 k_2 l_2} \int_f \frac{d^{d+1}\mathbf{q}'}{(2\pi)^{d+1}} \langle \psi_f^{i_1}(\mathbf{q}')\psi_f^{i_2}(-\mathbf{q}')\rangle \langle \psi_f^{j_1}(\mathbf{q}')\psi_f^{j_2}(-\mathbf{q}')\rangle \int d^d\mathbf{r}d\tau \phi_s^{k_1}\phi_s^{k_2}\phi_s^{l_1}\phi_s^{l_2} + \text{ 2 permutations.} \tag{4.104}$$

Summing over different field components, where one has

$$\sum_{k_1 k_2 l_1 l_2} \sum_{ij} F'_{ijk_1 l_1} F'_{ijk_2 l_2} \phi_s^{k_1}\phi_s^{k_2}\phi_s^{l_1}\phi_s^{l_2} + \text{ 2 permutations} = n_1 |\boldsymbol{\phi}_s|^4, \tag{4.105}$$

the first correction to the β_2 term is

$$\delta^{(1)}S[\beta_2] = -n_1 g^2 \frac{\Omega_d}{2\pi} \int d\omega \int_{b^{-1}}^{1} dk k^{d-1} \frac{1}{(-2\alpha_1 + k^2 + \gamma_1 \frac{|\omega|}{k^{z_1-2}})^2} \int d^d\mathbf{r}d\tau |\boldsymbol{\phi}_s|^4. \tag{4.106}$$

To first order in α_1, it is simply

$$\delta^{(1)}S[\beta_2] = -n_1 g^2 \frac{\Omega_d}{2\pi} I_2 \int d^d\mathbf{r}d\tau |\boldsymbol{\phi}_s|^4, \tag{4.107}$$

which can be written as

$$\delta^{(1)}S[\beta_2] = -n_1 g^2 \frac{\Omega_d}{\pi\gamma_1}(1 - b^{-1}) \int d^d\mathbf{r}d\tau |\boldsymbol{\phi}_s|^4. \tag{4.108}$$

The second diagram contains two ϕ_f internal lines, thus the correction reads

$$\delta^{(2)}S[\beta_2] = -(3\beta_2)^2 \sum_{k_1k_2l_1l_2} \sum_{i_1i_2j_1j_2} F_{i_1j_1k_1l_1}F_{i_2j_2k_2l_2} \int_f \frac{d^{d+1}\mathbf{q}'}{(2\pi)^{d+1}} \langle \phi_f^{i_1}(\mathbf{q}')\phi_f^{i_2}(-\mathbf{q}')\rangle \langle \phi_f^{j_1}(\mathbf{q}')\phi_f^{j_2}(-\mathbf{q}')\rangle \int d^d\mathbf{r}d\tau \phi_s^{k_1}\phi_s^{k_2}\phi_s^{l_1}\phi_s^{l_2} + \text{ 2 permutations.} \tag{4.109}$$

The summation over the field indices gives

$$\sum_{k_1k_2l_1l_2} \sum_{ij} F_{ijk_1l_1}F_{ijk_2l_2}\phi_s^{k_1}\phi_s^{k_2}\phi_s^{l_1}\phi_s^{l_2} + \text{ 2 permutations} = \frac{n_2+8}{9}|\boldsymbol{\phi}_s|^4. \tag{4.110}$$

Thus the second correction to β_2 reads

$$\delta^{(2)}S[\beta_2] = -(n_2+8)\beta_2^2\frac{\Omega_d}{2\pi}\int d\omega \int_{b^{-1}}^1 dk k^{d-1}\frac{1}{(-2\alpha_2+k^2+\omega^2)^2}\int d^d\mathbf{r}d\tau|\boldsymbol{\phi}_s|^4. \tag{4.111}$$

When the ϕ field is near its critical point, the above expression can be simplified to be

$$\delta^{(2)}S[\beta_2] = -(n_2+8)\beta_2^2\frac{\Omega_d}{2\pi}I_2'\int d^d\mathbf{r}d\tau|\boldsymbol{\phi}_s|^4, \tag{4.112}$$

which is

$$\delta^{(2)}S[\beta_2] = -(n_2+8)\beta_2^2\Omega_{d+1}(1-b^{-1})\int d^d\mathbf{r}d\tau|\boldsymbol{\phi}_s|^4. \tag{4.113}$$

There are three diagrams contributing to the first order corrections of the coupling g between the squares of the two fields. The first diagram has two ψ_f fields as internal lines. This term takes the form

$$\delta^{(1)}S[g] = -\frac{1}{2}\times 2\times 2(3\beta_1)g\sum_{k_1k_2l_1l_2}\sum_{i_1i_2j_1j_2}F_{i_1j_1k_1l_1}F'_{i_2j_2k_2l_2}\int_f\frac{d^{d+1}\mathbf{q}'}{(2\pi)^{d+1}} \langle\psi_f^{i_1}(\mathbf{q}')\psi_f^{i_2}(-\mathbf{q}')\rangle\langle\psi_f^{j_1}(\mathbf{q}')\psi_f^{j_2}(-\mathbf{q}')\rangle\int d^d\mathbf{r}d\tau\psi_s^{k_1}\psi_s^{l_1}\phi_s^{k_2}\phi_s^{l_2}. \tag{4.114}$$

The 1/2 comes from $(1/2)S_c^2$, and the two 2 factors come from the expansion in S_c^2 and the number of contractions in $\langle\psi_f\psi_f(x)\psi_f\psi_f(y)\rangle$. We first sum over the field indices,

$$\sum_{k_1k_2l_1l_2}\sum_{ij}F_{ijk_1l_1}F'_{ijk_2l_2}\psi_s^{k_1}\psi_s^{l_1}\phi_s^{k_2}\phi_s^{l_2} = \frac{n_1+2}{3}|\boldsymbol{\psi}_s|^2|\boldsymbol{\phi}_s|^2, \tag{4.115}$$

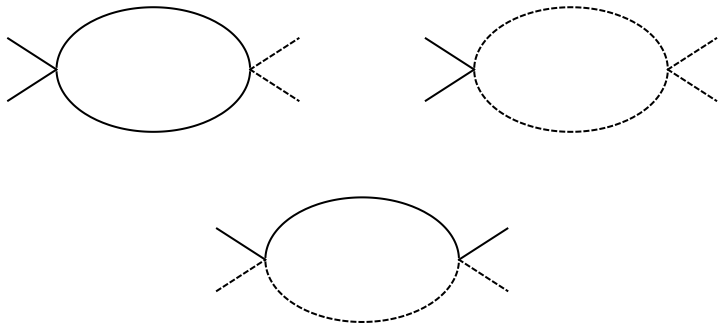

Figure 4.14: One-loop diagrams contributing to the first order correction of g. The solid lines represent the ψ fields, and the dashed lines represent the ϕ fields. The external lines are slow modes, and the internal lines are fast modes.

and then substitute the Green's functions,

$$\delta^{(1)}S[g] = -2\beta_1 g(n_1+2)\frac{\Omega_d}{2\pi}\int d\omega \int_{b^{-1}}^{1} dk k^{d-1} \frac{1}{(-2\alpha_1 + k^2 + \gamma_1 \frac{|\omega|}{k^{z_1-2}})^2} \int d^d\mathbf{r}d\tau |\boldsymbol{\psi}_s|^2 |\boldsymbol{\phi}_s|^2. \tag{4.116}$$

Keeping only the leading order term,

$$\delta^{(1)}S[g] = -2\beta_1 g(n_1+2)\frac{\Omega_d}{2\pi} I_2 \int d^d\mathbf{r}d\tau |\boldsymbol{\psi}_s|^2 |\boldsymbol{\phi}_s|^2, \tag{4.117}$$

one arrives at the result,

$$\delta^{(1)}S[g] = -2\beta_1 g(n_1+2)\frac{\Omega_d}{\pi\gamma_1}(1-b^{-1}) \int d^d\mathbf{r}d\tau |\boldsymbol{\psi}_s|^2 |\boldsymbol{\phi}_s|^2. \tag{4.118}$$

The internal lines of the second diagram are two ϕ_f fields. The corresponding correction term is now

$$\delta^{(2)}S[g] = -\frac{1}{2}\times 2\times 2(3\beta_2)g \sum_{k_1k_2l_1l_2}\sum_{i_1i_2j_1j_2} F_{i_1j_1k_1l_1}F'_{i_2j_2k_2l_2}\int_f \frac{d^{d+1}\mathbf{q}'}{(2\pi)^{d+1}} \langle\phi_f^{i_1}(\mathbf{q}')\phi_f^{i_2}(-\mathbf{q}')\rangle\langle\phi_f^{j_1}(\mathbf{q}')\phi_f^{j_2}(-\mathbf{q}')\rangle \int d^d\mathbf{r}d\tau \phi_s^{k_1}\phi_s^{l_1}\psi_s^{k_2}\psi_s^{l_2}. \tag{4.119}$$

The summation over field indices is similar to the first term,

$$\sum_{k_1k_2l_1l_2}\sum_{ij} F_{ijk_1l_1}F'_{ijk_2l_2}\phi_s^{k_1}\phi_s^{l_1}\psi_s^{k_2}\psi_s^{l_2} = \frac{n_2+2}{3}|\boldsymbol{\psi}_s|^2|\boldsymbol{\phi}_s|^2. \tag{4.120}$$

Thus the correction to the action is also similar,

$$\delta^{(2)}S[g] = -2\beta_2 g(n_2+2)\frac{\Omega_d}{2\pi}\int d\omega \int_{b^{-1}}^{1} dk k^{d-1}\frac{1}{(-2\alpha_2+k^2+\omega^2)^2}\int d^d\mathbf{r}d\tau|\boldsymbol{\psi}_s|^2|\boldsymbol{\phi}_s|^2, \tag{4.121}$$

which is, to leading order in α_2,

$$\delta^{(2)}S[g] = -2\beta_2 g(n_2+2)\frac{\Omega_d}{2\pi}I_2'\int d^d\mathbf{r}d\tau|\boldsymbol{\psi}_s|^2|\boldsymbol{\phi}_s|^2, \tag{4.122}$$

or

$$\delta^{(2)}S[g] = -2\beta_2 g(n_2+2)\Omega_{d+1}(1-b^{-1})\int d^d\mathbf{r}d\tau|\boldsymbol{\psi}_s|^2|\boldsymbol{\phi}_s|^2. \tag{4.123}$$

The third diagram has one ϕ_f internal line, and one ψ_f internal line. The correction takes the form

$$\begin{aligned}\delta^{(3)}S[g] = &-\frac{1}{2}(4g)^2\sum_{k_1k_2l_1l_2}\sum_{i_1i_2j_1j_2}F'_{i_1j_1k_1l_1}F'_{i_2j_2k_2l_2}\int_f\frac{d^{d+1}\mathbf{q}'}{(2\pi)^{d+1}}\\ &\langle\psi_f^{i_1}(\mathbf{q}')\psi_f^{i_2}(-\mathbf{q}')\rangle\langle\phi_f^{j_1}(\mathbf{q}')\phi_f^{j_2}(-\mathbf{q}')\rangle\int d^d\mathbf{r}d\tau\psi_s^{k_1}\phi_s^{l_1}\psi_s^{k_2}\phi_s^{l_2}.\end{aligned} \tag{4.124}$$

With the summation

$$\sum_{k_1k_2l_1l_2}\sum_{ij}F'_{ik_1jl_1}F'_{ik_2jl_2}\psi_s^{k_1}\phi_s^{l_1}\psi_s^{k_2}\phi_s^{l_2} = |\boldsymbol{\psi}_s|^2|\boldsymbol{\phi}_s|^2, \tag{4.125}$$

we obtain

$$\begin{aligned}\delta^{(3)}S[g] = -8g^2\frac{\Omega_d}{2\pi}\int d\omega\int_{b^{-1}}^{1}dk k^{d-1}\frac{1}{-2\alpha_2+k^2+\omega^2}\frac{1}{-2\alpha_1+k^2+\gamma_1\frac{|\omega|}{k^{z_1-2}}}\\ \int d^d\mathbf{r}d\tau|\boldsymbol{\psi}_s|^2|\boldsymbol{\phi}_s|^2.\end{aligned} \tag{4.126}$$

Assuming both fields are near their critical points, the above equation is approximately

$$\delta^{(3)}S[g] = -8g^2\frac{\Omega_d}{2\pi}I''\int d^d\mathbf{r}d\tau|\boldsymbol{\psi}_s|^2|\boldsymbol{\phi}_s|^2, \tag{4.127}$$

with the new function I'' defined as

$$I'' = \int_{-\infty}^{\infty}d\omega\int_{b^{-1}}^{1}dk k^{d-1}\frac{1}{k^2+\omega^2}\frac{1}{k^2+\gamma_1\frac{|\omega|}{k^{z_1-2}}}. \tag{4.128}$$

As mentioned before, here in our RG scheme, frequency is integrated over the whole real axes. In the two propagators, frequency scales differently with momentum. For the ψ field, $\gamma_1\omega \sim k^{z_1}$; for the ϕ field, $\omega \sim k$. And a finite cut-off

in frequency would lead to inconsistencies for such cases with miscellaneous dynamical exponents. Here the frequency integral gives

$$I'' = \int_{b^{-1}}^{1} dk k^{d+z_1-3} \frac{1}{\gamma_1^2 k^2 + k^{2z_1}} \left(-\gamma_1 \ln \frac{k^{2z_1-2}}{\gamma_1^2} + \pi k^{z_1-1} \right). \tag{4.129}$$

To leading order in $(1 - b^{-1})$, we have

$$I'' = \frac{1}{1+\gamma_1^2} (1 - b^{-1}) \left(2\gamma_1 \ln \gamma_1 + \pi \right). \tag{4.130}$$

This leads to the third term in the correction to the g term

$$\delta^{(3)} S[g] = -8g^2 \frac{\Omega_d}{2\pi} \frac{2\gamma_1 \ln \gamma_1 + \pi}{1+\gamma_1^2} (1 - b^{-1}) \int d^d \mathbf{r} d\tau |\boldsymbol{\psi}_s|^2 |\boldsymbol{\phi}_s|^2, \tag{4.131}$$

Now combining all the above results for the corrections of the different parameters, and carrying out the rescaling

$$\begin{aligned} \mathbf{r} &\to \mathbf{r}/b, \\ \tau &\to \tau/b, \\ \boldsymbol{\psi} &\to b^{(d-1)/2} \boldsymbol{\psi}, \\ \boldsymbol{\phi} &\to b^{(d-1)/2} \boldsymbol{\phi}, \end{aligned} \tag{4.132}$$

we obtain the RG equations

$$\begin{aligned} \gamma_1 &\to b^{z-1} \gamma_1, \\ -\alpha_1 &\to b^2 \left[-\alpha_1 + (n_1+2)\beta_1 \frac{\Omega_d}{\pi\gamma_1} (1 - b^{-1})(\ln 2 + 2\alpha_1) + n_2 g \Omega_{d+1} (1 - b^{-1})(2 + 2\alpha_2) \right], \\ -\alpha_2 &\to b^2 \left[-\alpha_2 + (n_2+2)\beta_2 \Omega_{d+1} (1 - b^{-1})(2 + 2\alpha_2) + n_1 g \frac{\Omega_d}{\pi\gamma_1} (1 - b^{-1})(\ln 2 + 2\alpha_1) \right], \\ \frac{\beta_1}{2} &\to b^{\epsilon} \left[\frac{\beta_1}{2} - (n_1+8)\beta_1^2 \frac{\Omega_d}{\pi\gamma_1} (1 - b^{-1}) - n_2 g^2 \Omega_{d+1} (1 - b^{-1}) \right], \\ \frac{\beta_2}{2} &\to b^{\epsilon} \left[\frac{\beta_2}{2} - n_1 g^2 \frac{\Omega_d}{\pi\gamma_1} (1 - b^{-1}) - (n_2+8)\beta_2^2 \Omega_{d+1} (1 - b^{-1}) \right], \\ g &\to b^{\epsilon} \left[g - 2\beta_1 g (n_1+2) \frac{\Omega_d}{\pi\gamma_1} (1 - b^{-1}) - 2\beta_2 g (n_2+2) \Omega_{d+1} (1 - b^{-1}) \right. \\ &\qquad \left. -8g^2 \frac{\Omega_d}{2\pi} \frac{2\gamma_1 \ln \gamma_1 + \pi}{1+\gamma_1^2} (1 - b^{-1}) \right], \end{aligned} \tag{4.133}$$

the differential form of which has been presented in equations (4.50, 4.51).

Chapter 5

Superconducting Instability in Quantum Critical Metals

5.1 Introduction

The 'mystery superconductors' of current interest share the property that their normal states are poorly understood 'non Fermi-liquids'. Experiments reveal that these are governed by a scale invariance of their quantum dynamics. The best documented examples are found in the heavy fermion (HF) systems [23, 25, 81, 82, 182–186]. As function of pressure or magnetic field one can drive a magnetic phase transition to zero temperature. On both sides of this quantum critical point (QCP) one finds Fermi-liquids characterized by quasiparticle masses that tend to diverge at the QCP. At the QCP one finds a 'strange metal' revealing traits of scale invariance, while at a 'low' temperature a transition follows most often to a superconducting state with a maximum T_c right at the QCP. It is widely believed that a similar 'fermionic quantum criticality' is governing the normal state in optimally doped cuprate high Tc superconductors. The best evidence is perhaps the 'Planckian' relaxation time observed in transport experiments $\tau_\hbar \simeq \hbar/(k_B T)$ [187, 188] indicating that this normal state has no knowledge of the scale E_F since in a Fermi-liquid $\tau = (E_F/k_B T)\tau_\hbar$. Very recently indications have been found that even the iron based superconductors might be governed by quantum critical normal states associated with a magnetic and/or structural zero temperature transition, giving rise to a novel scaling behavior of the electronic specific heat [189, 190].

The idea that superconductivity can be caused by a quantum phase transition involving a bosonic order parameter has a long history, starting with the marginal Fermi-liquid ideas of Varma [191] in the context of cuprates of the late 1980's and the ideas of spin-fluctuation driven heavy fermion superconductivity dating back to Lonzarich *et al.* [82]. The bulk of the large theoretical literature [192–227] dealing with this subject that evolved since then departs from an assumption dating back to the seminal work of Hertz in the 1970's [143]. This involves the nature of the ultraviolet: at some relatively short time scale where the electron system has closely approached a Fermi-liquid the influence of the critical order parameter fluctuations become noticable. The Fermi surface and Fermi energy of this quasiparticle system can then be used as building blocks together with the bosonic field theory describing the critical order parameter fluctuations to construct a perturbative framework dealing with the coupling between these fermionic- and bosonic sectors. The lowest order effect of this coupling is that the fermi gas of quasiparticles acts as a heat bath damping the bosonic order parameter fluctuations, with the effect that the effective space-time dimensionality of the bosonic field theory exceeds the upper critical dimension. These dressed order parameter fluctuations than 'back react' on the quasiparticle system causing 'singular' interactions in the Cooper channel, yielding in turn a rational for a generic 'high Tc' superconductivity at QCP's.

The crucial assumption in this 'Hertz philosophy' is that the fermion physics is eventually controlled by the Fermi gas. In the cases of empirical interest it is generally agreed that in the UV the interaction energies are much larger than the bare kinetic energies, while there is no obvious signature in the experiments for a renormalization flow that brings the system close to a weakly interacting fermion gas before entering the singular 'Hertz' critical regime. From the theoretical side, the introduction of this UV Fermi gas can be viewed as an intuitive leap. The only truly fermionic state of matter that is understood mathematically is the Fermi gas and its perturbative 'derivative' (the Fermi liquid): the fermion sign problem makes it impossible to address fermionic matter in general mathematical terms [228]. However, very recently the 'grib of the Fermi-gas' has started to loosen specifically in the context of fermionic critical matter. A first step in this direction is the demonstration of proof of principle that truly critical fermionic states of matter can exist that have no knowledge whatever of the statistical Fermi energy scale: the fermionic Feynman backflow wavefunction Ansatz [229]. The substantive development is the recent work addressing fermion physics using the string theoretical AdS/CFT correspondence. It appears that this duality between quantum field theory and gravitational physics is capable of describing Fermi-liquids that emerge from a manifestly strongly interacting, critical ultraviolet [230]. In another implementation, one finds an IR physics describing 'near' Fermi-liquids characterized by 'critical' Fermi surfaces [179] controlled by an emergent conformal symmetry implying the absence of energy scales like the Fermi-energy [231, 232].

This lengthy consideration is required to motivate the subject of this pa-

per: a phenomenological scaling theory for a Bardeen-Cooper-Schrieffer (BCS) type superconductivity starting from the postulate that the normal state is not a Fermi-liquid, but instead a truly conformal fermionic state of matter. With 'BCS type' we mean the following: we assume as in BCS that besides the electron system a bosonic modes are present that cause attractive electron-electron interactions. This 'glue' is retarded in the sense that the characteristic energy scale of this external bosonic system ω_B is small as compared to the ultraviolet cut-off scale of the quantum critical fermion system ω_c . Having a small Migdal parameter, the glue-electron vertex corrections can then be ignored and the the effects of the glue are described in terms of the Migdal-Eliashberg time dependent mean field theory, reducing to the static BCS mean field theory in the weak coupling limit [233]. All information coming from the electron system that is required for the pairing instability is encapsulated in the electronic pair susceptibility. Instead of using the Fermi gas pair susceptibility (as in conventional BCS), we rely on the fact that conformal invariance fixes the analytical form of this response function in terms of two free parameters: an overall UV cut-off scale (T_0) and the anomalous scaling dimension of the pair susceptibility, expressed in a dynamical critical exponent z and correlation function exponent η_p. The outcome is a scaling theory for superconductivity that is in essence very simple; much of the technical considerations that follow are dealing with details associated with modeling accurately the effects of the breaking of conformal invariance by temperature and the superconducting instability. This theory is however surprisingly economical in yielding phenomenological insights. Conventional BCS appears as a special 'marginal' case, and our main result is the generalized gap equation, Eq. (5.10). The surprise it reveals is the role of retardation: when the Migdal parameter ω_B/ω_c is small (where the mathematical control is best) we find at small coupling constants $\tilde{\lambda}$ a completely different behavior compared to conventional BCS: the gap magnitude Δ becomes similar to the glue energy ω_B. To illustrate the case with numbers, a moderate coupling to phonons like $\tilde{\lambda} = 0.3$ with a frequency $\omega_B = 50$ meV will yield rather independently of scaling dimensions a gap of 40 meV and a T_c of 100 Kelvin or so: these are numbers of relevance to cuprate superconductors!

The theory has more in store. Incorporating the motive that on both sides of the quantum critical point heavy Fermi liquids emerge from the quantum critical metal as in the heavy fermion systems, we show that the superconducting 'dome' surrounding the quantum critical point emerges naturally without changing the coupling to the bosonic glue. The form of this dome is governed by the correlation length, but we find via the pair susceptibility a direct relation with the effective mass of the quasiparticles of the Fermi-liquids. Last but not least, we analyze the orbital limiting upper critical magnetic field, finding out that pending the value of the dynamical critical exponent it can diverge very rapidly upon approaching the QCP, offering an explanation for the observations in the ferromagnetic URhGe heavy fermion superconductor [234].

The scaling phenomenology we present here is simple and obvious, but it ap-

pears to be overlooked so far. Earlier work by Balatsky [235], Sudbo [236] and Yin and Chakravarty [237] is similar in spirit but yet quite different. These authors depart from a Luttinger liquid type single particle propagators to compute the pair susceptibility from the bare fermion particle-particle loop. Although this leads to pair susceptibility similar (although not identical) to ours, it is conceptually misleading since in any non Fermi-liquid, there is no such simple relation between two-point and four-point correlators. This is particularly well understood for conformal field theories: for the higher dimensional cases the AdS/CFT correspondence demonstrates that two point CFT correlators are determined by kinematics in AdS while the four- and higher point correlators require a tree level computation [238–245]. More serious for the phenomenology, this older work ignores the role played by retardation; it is a-priori unclear whether one can construct a mathematically controlled scaling theory for BCS without the help of a small Migdal parameter.

The remainder of this chapter is organized as follows. In section 5.2 we review a somewhat unfamiliar formulation of the classic BCS theory that makes very explicit the role of the pair susceptibility. We then introduce the scaling forms for the pair susceptibilities as follow from conformal invariance. By crudely treating the modifications in the pair susceptibility at low energies associated with the presence of the pair condensate we obtain the new gap equation Eq. ((5.10)). This catches already the essence of the BCS superconductivity of quantum critical metals and we discuss its implications in detail. In section 5.3 we focus in on intricacies associated with determining the transition temperature. Conformal invariance is now broken and one needs to know the scaling functions in some detail. We use the exact results of 1+1 dimensional conformal field theory as a model to address these matters. In section 5.4 we turn to the harder problem of modeling the crossover from the large energy critical pair susceptibility to the low energy, zero temperature infrared that is governed by conventional Bogoliubov fermions, as needed to devise a more accurate zero temperature gap equation. The casual reader might want to skip both sections. The moral is that information on the cross-over behavior of the pair susceptibility is required that is beyond simple scaling considerations to address what happens when the conformal invariance is broken either by temperature (as of relevance to the value of T_c) or by the presence of the BCS condensate (of relevance for the zero temperature gap). The conclusion will be that although the gross behaviors are not affected, it appears to be impossible to compute numbers like the gap to T_c ratio accurately since these are sensitive to the details of the cross-over behaviors. In section 5.5 we explore the theory away from the critical point, assuming that cross-overs follow to heavy Fermi-liquids, where we address the origin of the superconducting dome. Finally, in section 5.6 we address the scaling behavior of the orbital limited upper critical field.

5.2 BCS theory and the scaling of the pair susceptibility

Let us first revisit the backbone of Migdal-Eliashberg theory. We need a formulation that is avoiding the explicit references to the Fermi gas of the text book formulation, but it is of course well known how to accomplish this. Under the condition of strong retardation and small couplings, the effects of the glue are completely enumerated by the gap equation [246] ignoring angular momentum channels (s,d waves, etcetera) for the time being,

$$1 - g\chi'_{\rm ret}(\vec{q}=0,\omega=0,\Delta,T) = 0, \tag{5.1}$$

where g is the effective coupling strength of the glue, while $\chi'_{\rm ret}$ is the zero frequency value of the real part of the retarded pair susceptibility at a temperature T in the presence of the gap Δ. This effective $\chi'_{\rm ret}$ also incorporates the effects of retardation. The textbooks with their focus on non-interacting electrons accomplish this in a rather indirect way, by putting constraints on momentum integrations. Retardation is however about time scales and the general way to incorporate retardation is by computing $\chi'_{\rm ret}$ by employing the Kramers-Kronig relation starting from the imaginary part of the full electronic pair susceptibility χ''_p. For a glue characterized by a single frequency ω_B,

$$\chi'_{\rm ret}(\omega=0) = 2\mathcal{P}\int_0^{2\omega_B} d\omega' \frac{\chi''_p(\omega')}{\omega'}. \tag{5.2}$$

with the full pair susceptibility given by the Kubo formula,

$$\chi_p(\vec{q},\omega) = -i\int_0^\infty dt e^{i(\omega+i\eta)t}\left\langle [b^\dagger(\vec{q},0), b(\vec{q},t)]\right\rangle, \tag{5.3}$$

associated with the pair operator $b^\dagger(\vec{q},t) = \sum_{\vec{k}} c^\dagger_{\vec{k}+\frac{\vec{q}}{2},\uparrow}(t) c^\dagger_{-\vec{k}+\frac{\vec{q}}{2},\downarrow}(t)$.

In the case of conventional superconductors the normal state is a Fermi-liquid, formed from (nearly) non-interacting quasiparticles. One can get away with a 'bare fermion loop' pair susceptibility. The specialty of this pair susceptibility is that its imaginary part is frequency independent at zero temperature. It extends up to the Fermi energy of the Fermi-liquid and from the unitary condition,

$$\int_0^\infty \chi''_p(\omega) d\omega = 1 \tag{5.4}$$

it follows that at zero temperature $\chi''(\omega) = N_0 = 1/(2E_F)$. In logarithmic accuracy the gap enters as the low frequency cut-off in Eq. (5.2) such that,

$$\chi'_{\rm ret}(\omega=0,\Delta,T=0) = \int_\Delta^{2\omega_B} \frac{d\omega'}{E_F\omega'} = \frac{1}{E_F}\log\frac{2\omega_B}{\Delta}, \tag{5.5}$$

and from Eq. (5.1) the famous BCS gap equation follows: $\Delta = 2\omega_B e^{-1/\lambda}$, where $\lambda = g/E_F$.

This formulation of BCS has the benefit that it makes very explicit that all the information on the electron system required for the understanding of the pairing instability is encoded in the pair susceptibility. This is in turn a bosonic response function of the electron system since it involves the response of two fermions, much like the dynamical susceptibilities associated with charge- or spin densities. In addition one needs the fact that the pair density is a non-conserved quantity, in the same sense as a staggered magnetization. When the quantum system is conformal (i.e. the zero temperature quantum critical metal) the analytical form of the dynamical pair susceptibility is fixed at zero temperature by the requirement of invariance under scale transformations [40],

$$\chi(\omega) = \lim_{\delta \to 0} Z''(-(\omega + i\delta)^2)^{-\frac{2-\eta_p}{2z}}, \tag{5.6}$$

as determined by the a-priori unknown unknown exponents η_p and z, the anomalous scaling dimension of the pair operator and the dynamical critical exponent, respectively. The normalization constant Z'' is via the unitarity condition Eq.(5.4) determined by the UV cut-off scale ω_c. Because we invoke a small Migdal parameter we are interested in the 'deep infrared' of the theory that is not very sensitive to the precise choice of this UV energy scale. A reasonable choice is the energy where the thermal de Broglie wavelength becomes of order of the electron separation, i.e. the Fermi energy of an equivalent system of non-interacting electrons. Defining $\alpha_p = \frac{2-\eta_p}{z}$ and using Eq. (5.4) with the cut-off scale ω_c, we find,

$$Z'' = \frac{1-\alpha_p}{\sin(\frac{\pi}{2}\alpha_p)} \frac{1}{\omega_c^{1-\alpha_p}}, \tag{5.7}$$

observing that $\alpha_p < 1$ in order for this function to be normalizable: this is the well known unitary bound on the operator dimensions. The real and imaginary parts of the zero temperature critical pair susceptibility are related by a phase angle $\frac{\pi}{2}\alpha_p$,

$$\chi(\omega) = \frac{Z''}{\omega^{\alpha_p}} \left(\cos(\frac{\pi}{2}\alpha_p) + i \sin(\frac{\pi}{2}\alpha_p) \right). \tag{5.8}$$

According to general conformal wisdoms, the pair operator is called irrelevant when $\alpha_p < 0$ such that χ" increases with frequency, relevant when $0 < \alpha_p < 1$ when χ'' decreases with frequency and marginal when $\alpha_p = 0$, such that χ_p'' is frequency independent, see Fig 1. From this scaling perspective, the Fermi liquid pair operator is just the special marginal case, and the BCS superconductor with its logarithmically running coupling constant falls quite literally in the same category as the asymptotically free quantum chromo dynamics in 3+1D and the Kondo effect. Another familiar case is the pair susceptibility derived from the 'Dirac fermions' of graphene [247, 248] and transition metal dichalcogenides [249, 250] characterized by $\alpha_p = -1$: in this 'irrelevant case' one needs a finite glue interaction to satisfy the instability criterium.

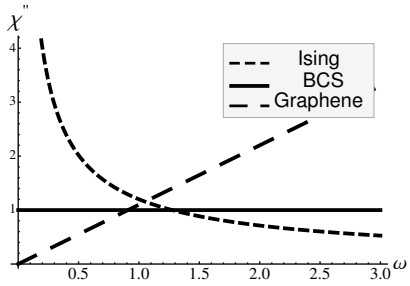

Figure 5.1: Illustration of the imaginary part of the pair susceptibility, comparing the relevant (Ising class), marginal (BCS case) and irrelevant (graphene class). The scaling exponent $\alpha_p = \frac{2-\eta_p}{z}$ is respectively $0 < \alpha_p < 1, \alpha_p = 0, \alpha_p < 0$. For the Ising class, the magnitude of the imaginary part of the pair susceptibility becomes larger and larger as one lowers the frequency. For the BCS case, the magnitude stays constant as the frequency is changed. For the graphene class, the magnitude decreases to zero in the low frequency infrared region.

The scaling behavior of the free fermion case is special and the pair operator in a general conformal fermionic state can be characterized by a scaling dimension that is any real number smaller than one. Obviously, the interesting case is the relevant one where $\alpha_p > 0$ (Fig.1). Let us here consider the zero temperature gap equation. In Eq. (5.6) we have already fully specified χ_p'' in the critical state. However, due to the zero temperature condensate the scale invariance is broken and the low frequency part of χ_p'' will now be dominated by an emergent BCS spectrum including a $s-$ or $d-$wave gap, Bogoliubov fermions and so forth. This will be discussed in detail in section V. Let us here introduce the gap in the BCS style by just assuming that the imaginary part of the pair susceptibility vanishes at energies less than Δ. Under this assumption the gap equation becomes,

$$1 - 2g \int_{\Delta}^{2\omega_B} \frac{d\omega}{\omega} \frac{Z'' \sin((\pi/2)\alpha_p)}{\omega^{(2-\eta_p)/z}} = 0, \tag{5.9}$$

evaluating the integral this becomes our 'quantum critical gap equation' ,

$$\Delta = 2\omega_B \left(1 + \frac{1}{\tilde{\lambda}} \left(\frac{2\omega_B}{\omega_c}\right)^{\alpha_p}\right)^{-\frac{1}{\alpha_p}}, \tag{5.10}$$

with

$$\tilde{\lambda} = 2\lambda \frac{1-\alpha_p}{\alpha_p}, \tag{5.11}$$

and $\lambda \equiv g/\omega_c$. The numerator $(1-\alpha_p)$ in $\tilde{\lambda}$ comes from the normalization constant Z'', while the denominator α_p from integrating over ω. Notice that λ has

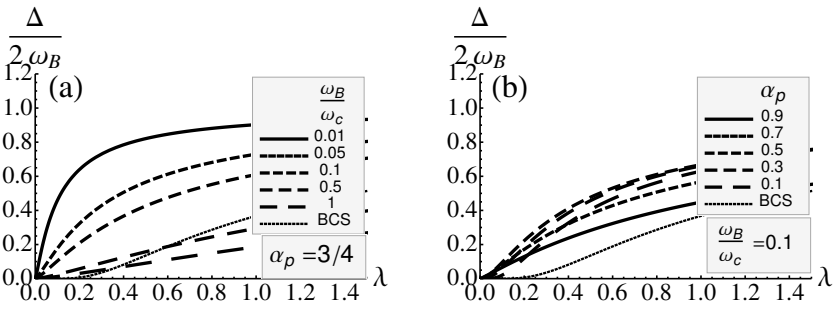

Figure 5.2: (a)The ratio of gap to retardation frequency $\Delta/(2\omega_B)$ as a function of glue strength λ for various retardation ranges ω_B/ω_c with fixed scaling dimension $\alpha_p = 3/4$. (b)The same plot, but with fixed retardation $\omega_B/\omega_c = 0.1$ and various scaling dimensions α_p. The dotted lines are the standard BCS result.

the same meaning of a conventional, say, dimensionless electron-phonon coupling constant. The dimensionful coupling constant g parametrizes the interaction strength between microscopic electrons and -lattice vibrations, and ω_c has the same status as the Fermi-energy in a conventional metal as the energy scale that is required to balance g. We argued earlier that ω_c is of order of the bare Fermi energy and therefore it make sense to use here values for e.g. the electron-phonon coupling constant as quoted in the LDA literature. Notice however that for a given λ the effective coupling constant $\tilde{\lambda}$ that appears in Eq. (5.10) is decreasing when α_p is becoming more relevant, i.e. when $\alpha_p \to 1$. From the frequency integral $\int d\omega\omega^{-(1+\alpha_p)}$, one would anticipate that the gap would increase for a more relevant pair susceptibility. The unitary condition imposes however an extra condition on the pair susceptibility. These two compensating effects lead to the important result that the gap is rather sensitive to the relevancy of the pair susceptibility. All what really matters is whether the pair susceptibility is relevant rather than marginal or irrelevant, and the degree of the relevancy is remarkably unimportant.

Eq.(5.10) is a quite different gap equation than the BCS one with its exponential dependence on the coupling λ. The multiplicative structure associated with the Fermi-liquid is scaling wise quite special, while Eq. (5.10) reflects directly the algebraic structure rooted in scale invariance. The surprise is that retardation acts quite differently when power laws are ruling. In Fig. (1) we show the dependence of the Δ/ω_B ratio on the coupling constant λ, both for different Migdal parameters and fixed α_p, as well as for various scaling dimensions and the Migdal parameter fixed. The comparison with the BCS result shows that drastic changes happen already for small scaling dimensions α_p especially in the small λ regime. Our equation actually predicts that the gap to glue frequency

ratio becomes of order one alrady for couplings that are as small as $\lambda = 0.1$ when the Migdal parameter is small. To place this in the context of high Tc superconductivity, let us assume that the pairing glue in the cuprates is entirely rooted in the 'glue peak' at $\omega_B \sim 50$meV that is consistently detected photoemission, tunneling spectroscopy and optical spectroscopy [251–253] . The electronic cut-off in the cuprates is likely of order $\omega_c = 0.5$ eV such that the Migdal parameter $\omega_B/\omega_c \simeq 0.1$. A typical gap value is 40 meV and we read off Fig. 1 that we need $\lambda = 0.45$ or 0.43 for $\alpha_p = 3/4, 1/4$ while using the BCS equation $\lambda = 1.1$! Taking this serious implies that in principle one needs no more than a standard electron-phonon coupling to explain superconductivity at a high temperature in cuprate superconductors. Of course this does not solve the problem: although one gets a high Tc for free it still remains in the dark how to form a fermionic quantum critical state with a high cut-off energy, characterized by a relevant pair susceptibility.

Eq.(5.10) is also very different from the gap equations obtained in the previous attempts to apply scaling theory to superconducting transition by Balatsky [235], Sudbo [236] and Yin and Chakravarty [237]. A crucial property of their results is that even in the relevant case one needs to exceed a critical value for λ to find a superconducting instability. The present scaling theory is in this regard a more natural generalization of BCS theory, where the standard BCS is just the 'marginal end' of the relevant regime where the Cooper instability cannot be avoided for attractive interactions. The previous approaches [235–237] start by considering the single particle spectral function, generalizing its analytic structure from simple poles to branch cuts. This way of thinking stems from the Fermi-liquid type assumption that the single particle Green's function is the only primary operator of the system, and all the higher point functions are secondary operators, to be determined by the single particle Green's function. But for critical systems, such assumptions are generally not to satisfied. It is well known for example from the AdS/CFT correspondence, that the four-point functions of strongly interacting conformal fields are much more complex than the combination of two-point functions [238–245]. Our basic assumption is that the pair susceptibility is by itself a primary operator subjected to conformal invariance which is the most divergent operator at the critical point.

5.3 Determining the transition temperature

Let us now turn to finite temperatures. A complicating fact is that temperature breaks conformal invariance, since in the euclidean formulation of the field theory its effect is that the periodic imaginary time acquires a finite compactification radius $R_\tau = \hbar/k_B T$. The pair susceptibility therefore acquires the finite size scaling form [40]

$$\chi(\omega) \equiv \chi(\vec{q} = 0, \omega) = Z T^{-(2-\eta_p)/z} \Phi\left(\frac{\omega}{T}\right), \tag{5.12}$$

where Φ is a universal scaling function and Z is a UV renormalization constant, while η_p and z are the anomalous scaling dimension of the pair operator and the dynamical critical exponent, respectively. At zero temperature this turns into the banch cut as shown in Eq.(5.6), while in the opposite high temperature or hydrodynamical regime ($\hbar\omega << k_BT$) it takes the form [40]

$$\chi(\omega) = Z' T^{-(2-\eta_p)/z} \frac{1}{1 - i\omega\tau_{rel}}, \tag{5.13}$$

where $\tau_{rel} \approx \hbar/k_BT$. The crossover from the hydrodynamical- (Eq. 5.6) to the high frequency coherent regime(Eq. 5.13) occurs at an energy $\sim k_BT$. The superconducting transition temperature is now determined by the gap equation through $1 - g\chi'_{\rm ret}(k_BT_c) = 0$. The problem is that χ'_{ret} is via the Kramers-Kronig transformation largely set by the cross-over regime in χ''_p. One needs the full solutions of the CFT's to determine the detailed form of Φ in this crossover regime and these are not available in higher dimensions.

In 1+1D these are however completely determined by conformal invariance, and for our present purposes these results might well represent a reasonable model since the gap equation is only sensitive to rather generic features of the cross-over behavior. Given the exponents η_p and z, the exact result for the finite temperature χ'' in 1+1D is well known [40],

$$\chi''(k,\omega) = Z \frac{\sinh(\frac{\omega}{2T})}{T^{2(1-2s)}} B(s+i\frac{\omega+k}{4\pi T}, s-i\frac{\omega+k}{4\pi T}) B(s+i\frac{\omega-k}{4\pi T}, s-i\frac{\omega-k}{4\pi T}), \tag{5.14}$$

with $1-2s = \frac{2-\eta_p}{2z}$. The temperature and frequency dependencies of this function for $k = 0$ are illustrated in Fig.(3). Indeed $\chi''(\omega) \to 0$ in a linear fashion with ω with a slope set by $1/T$, while for $\omega >> T$ the temperature dependence drops out, recovering the power law. The crossover occurs at $\omega \simeq 2k_BT/\hbar$ where $\chi''(\omega)$ has a maximum.

When temperature goes to zero the limiting form of the beta function becomes,

$$\lim_{u\to\infty} B(s+iu, s-iu) = \frac{2\pi}{\Gamma(2s)} e^{-\pi u} u^{2s-1}, \tag{5.15}$$

and the imaginary part of the pair susceptibility Eq. (5.14) acquires the power law form

$$\chi''(\omega) = \frac{2\pi^2 (4\pi)^{\alpha_p}}{[\Gamma(2s)]^2} Z \frac{1}{\omega^{\alpha_p}}. \tag{5.16}$$

Comparing this with Eq.(5.7) yields the normalization factor in terms of the cut-off scale

$$Z = \frac{[\Gamma(2s)]^2 (1-\alpha_p)}{2\pi^2 (4\pi)^{\alpha_p} \omega_c^{1-\alpha_p}}. \tag{5.17}$$

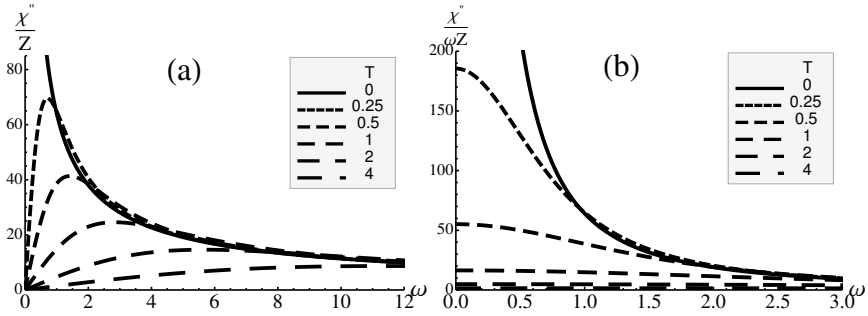

Figure 5.3: (a)Illustration of the imaginary part of the pair susceptibility $\chi''(k = 0, \omega, T)$ divided by the overall numerical factor Z, as a function of frequency ω for various temperatures. Here we've chosen $\alpha_p = 3/4$, so $s = 5/16$. (b) The same plot, but χ'' is further divided by ω. At zero temperature one has the power law scaling form. At finite temperature $\chi''(\omega)$ goes to zero, as ω goes to zero ($\chi''(\omega)/\omega \to$ constant, as $\omega \to 0$), and approaches the same power law behavior at large frequency. As one increases temperature, the maximum of $\chi''(\omega)$ goes down, and the corresponding ω_{max} shifts to larger frequency.

Combining Eq.'s (5.1),(5.2),(5.14),(5.17), we obtain the equation determining the critical temperature,

$$1 - \mathcal{C}'\lambda \left(\frac{2\omega_B}{\omega_c}\right)^{-\alpha_p} \left(\frac{T_c}{2\omega_B}\right)^{-\alpha_p} \mathcal{F}\left(\frac{2\omega_B}{T_c}\right) = 0, \tag{5.18}$$

where

$$\mathcal{F}(y) = \int_0^y \frac{dx}{x} \sinh(\frac{x}{2}) \left(\mathrm{B}(s + i\frac{x}{4\pi}, s - i\frac{x}{4\pi})\right)^2, \tag{5.19}$$

and $x = \omega/T$. The overall coefficient is

$$\mathcal{C}' = \frac{[\Gamma(2s)]^2(1-\alpha_p)}{\pi^2(4\pi)^{\alpha_p}}. \tag{5.20}$$

We plot in Fig.(4) the ratio of T_c to retardation frequency as function of glue strength, retardation and the scaling dimensions. One infers that the behavior of T_c is very similar to that of the zero temperature gap, plotted in Fig. (2). We observe that they are of the same order of magnitude $T_c \sim \Delta$, and this can be understood from the behavior of χ''/ω plotted in Fig.(3b). Since the large frequency behavior of $\chi''(\omega)/\omega$'s are the same for different temperatures, all what matters is the low frequency part. The gap imposes a cut-off for the zero temperature $\chi''(\omega)/\omega$, and its value is determined such that the area under this

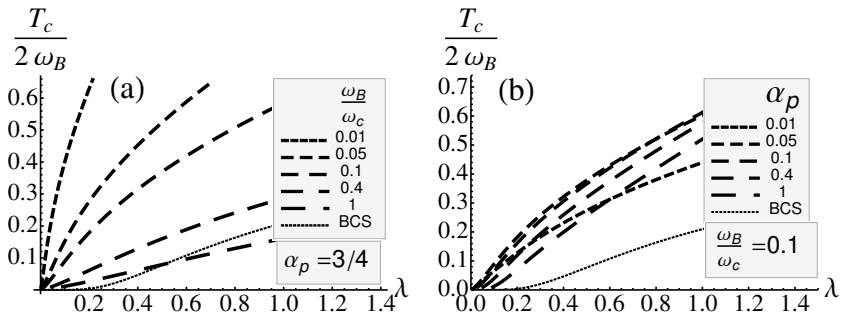

Figure 5.4: (a)The ratio of transition temperature to retardation frequency $T_c/(2\omega_B)$ as a function of glue strength λ for various retardation ranges ω_B/ω_c, with scaling dimension fixed $\alpha_p = 3/4$. (b)The same plot, but fix the retardation $\omega_B/\omega_c = 0.1$ while varying the scaling dimensions α_p. The dotted lines are the standard BCS result. The magnitude and dependence on glue strength and retardation are all similar to those of the gap.

curve including the low frequency cut-off, is the same as the area under the curve corresponding to T_c without a cut-off: by inspecting Fig.(3b) one infers directly that the gap and T_c will be of the same order. The same logic is actually at work in the standard BCS case. The finite temperature Fermi gas susceptibility is $\chi''(\omega) = \frac{1}{2E_F}\tanh(\frac{1}{4}\beta\omega)$ [246], and the familiar T_c equation follows,

$$1 - \lambda \int_0^{2\omega_B} \frac{d\omega}{\omega} \tanh(\frac{1}{4}\beta\omega) = 0, \tag{5.21}$$

such that $T_c \simeq 1.14\omega_B e^{-1/\lambda}$, of the same order as the BCS gap $\Delta = 2\omega_B e^{-1/\lambda}$. Now the effect of temperature is encoded in the tanh function. Although the Fermi-gas is not truly conformal, It is easy to check that this 'fermionic' tanh factor adds a temperature dependence to the χ'' that is nearly indistinguishable from what one obtains from the truly conformal marginal case that one obtains by setting $s = 1/2$ in Eq. (5.14).

We notice that conformal invariance imposes severe constraints on the finite temperature behavior of the pair susceptibility, thereby simplifying the calculation of T_c. In the 1+1-dimensional 'model' nearly everything is fixed by conformal invariance. The only free parameters that enter the calculation are the scaling dimension α_p, the cut-off scale ω_c and the glue quantities. As we will now argue the situation is actually much less straightforward for the zero temperature gap because this involves a detailed knowledge of the crossover to the physics of the superconductor ruling the low energy realms.

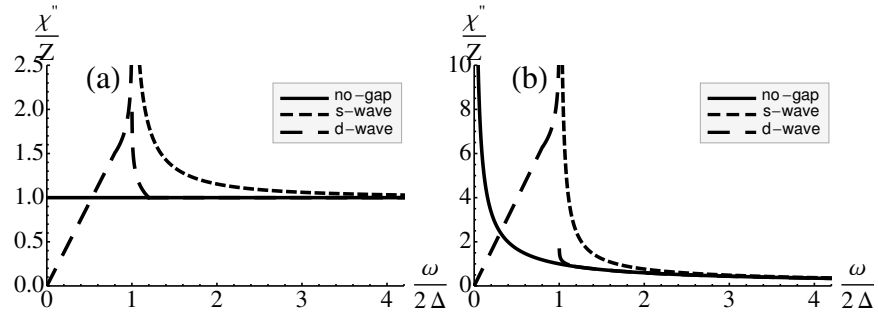

Figure 5.5: Illustration of the imaginary part of the pair susceptibility without a gap and in the presence of an s- and d- wave gap, for (a) the BCS case, and (b) the quantum critical case (here we've plotted using the parameter $\alpha_p = 3/4$). In the absence of gap, χ'' is a constant (for BCS) or has a simple power law behavior (for critical fermions). In the presence of a s-wave gap, the states below the gap are gapped out and there is a power law singularity right above the gap. When there is a d-wave gap, the low frequency part (way below the gap) is governed by a Dirac cone structure, thus a linear susceptibility, while near the gap a van Hove singularity is at work, leading to logarithmic divergences on both sides. The high frequency region for both s- and d-wave gap goes over to the case without a gap.

5.4 More about the gap equation

It is part of our postulate that when superconductivity sets in BCS 'normalcy' returns at low energies in the form of the sharp Bogoliubov fermions and so forth. Regardless the critical nature of the normal state, the scale invariance gets broken by the instability where the charge 2e Cooper pairs form, and this stable fixed point also dictates the nature of the low lying excitations. However, we are dealing with the same basic problem as in the previous section: in the absence of a solution to the full, unknown theory it is impossible to address the precise nature of the cross-over regime between the BCS scaling limit and the critical state at high energy. This information is however required to further improve the gap equation Eq. (5.10) of section II that was derived by crudely modeling χ'' in the presence of the superconducting condensate.

So much is clear that the crossover scale itself is set by the gap magnitude Δ. However, assuming that this affair has dealings with e.g. optimally doped cuprate superconductors, we can rest on experimental information: in optimally doped cuprates at low temperatures the coherent Bogoliubov fermions persist as bound states all the way to the gap maximum. Up to these energies it is therefore reasonable to assume that χ_p'' is determined by the bare fermion loops, and this regime has to be smoothly connected to the branch cut form of the χ_p'' at

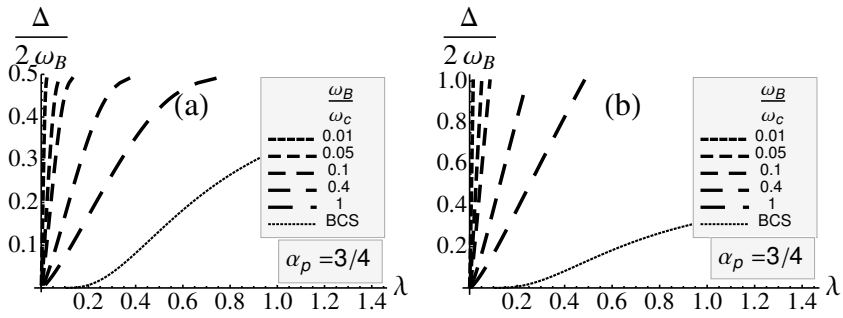

Figure 5.6: The ratio of the gap to retardation $\Delta/(2\omega_B)$ as a function of the glue strength λ, for various retardation ranges, with (a) a s-wave gap and (b) a d-wave gap. Here we've chosen $\alpha_p = 3/4$. The dotted lines are the standard BCS result. The dependence on glue strength and and retardation is similar but the magnitude of the gap is much enhanced compared to the previous treatment of gap as a simple IR cutoff. The d-wave case is enhanced even more.

higher energies. This implies that the standard BCS gap singularities have to be incorporated in our zero temperature pair susceptibility. As a final requirement, the pair susceptibility has to stay normalized according to Eq. (5.4), which significantly limits the modelling freedom.

Let us first consider the case of an isotropic s-wave gap singularity. The high frequency modes are still critical, and therefore the high frequency limit of the imaginary part of the pair susceptibility is determined by,

$$\lim_{\omega\to\infty} \chi''(\omega, \Delta, T = 0) = \frac{\mathcal{A}}{\omega^{\alpha_p}}. \tag{5.22}$$

In the presence of the superconducting condensate, the low energy modes below the gap have their energy raised above the gap, since we require $\chi''(\omega < \Delta, \Delta, T = 0) = 0$. The spectral weight is conserved according to Eq. (5.4), and since we assumed that the Bogoliubov excitations of the BCS fixed point survive at energies of order of the gap we need to incorporate a BCS s-wave type power law divergence right above the gap in the imaginary part of the pair susceptibility. The simplest function satisfying these conditions is,

$$\chi''(\omega, \Delta) = \mathcal{A}\frac{1}{\omega^{\alpha_p}} \left(\frac{\omega}{\sqrt{\omega^2 - (2\Delta^2)}} \right)^{1+\alpha_p} \Theta(\omega - 2\Delta), \tag{5.23}$$

with $\mathcal{A} = (1 - \alpha_p)\omega_c^{-(1-\alpha_p)}$ (see Fig.5b). We notice in passing that the BCS gap

corresponds to the case $\alpha_p = 0$,

$$\chi''_{\rm BCS}(\omega,\Delta) = \frac{1}{2E_F}\frac{\omega}{\sqrt{\omega^2-(2\Delta)^2}}\Theta(\omega-2\Delta). \tag{5.24}$$

The quantum critical gap equation for the s-wave superconductor now becomes,

$$1-2(1-\alpha_p)\lambda\left(\frac{2\omega_B}{\omega_c}\right)^{-\alpha_p}\left(\frac{\Delta}{\omega_B}\right)^{-\alpha_p}\int_1^{\frac{\omega_B}{\Delta}}\frac{dx}{(x^2-1)^{(1+\alpha_p)/2}} = 0. \tag{5.25}$$

Turning to the d-wave case the gap equation becomes necessarily a bit more complicated since we have to account for massless Bogolubiov fermions. At low frequencies $\omega << 2\Delta$ the pair susceptibility is now governed by free fermion loops and the Dirac-cone structure in the spectrum leads to a linear frequency dependence in the pair susceptibility, $\chi''(\omega) = \mathcal{A}_1\omega$. Near the gap, a logarithmic divergence is expected due to the Van Hove singularity, and therefore $\chi''(\omega) = \mathcal{A}_2 \log\frac{q_c+\sqrt{2\Delta-\omega+q_c^2}}{-q_c+\sqrt{2\Delta-\omega+q_c^2}}$ for $\omega < 2\Delta$, while $\chi''(\omega) = \mathcal{A}_3\log\frac{q_c+\sqrt{\omega-2\Delta+q_c^2}}{-q_c+\sqrt{\omega-2\Delta+q_c^2}}$ for $\omega > 2\Delta$, with q_c a cutoff. When the frequency is high compared to the gap scale, the pair susceptibility has the scaling form $\chi''(\omega) = \mathcal{A}_4\omega^{-\alpha_p}$. Matching these regimes at $2\Delta-\omega_1$ and $2\Delta+\omega_2$, with $0<\omega_1<2\Delta$ and $0<\omega_2<2\omega_B-2\Delta$, and assuming continuity of the pair susceptibility both below and above the gap (see Fig. 5b), we arrive at the gap equation for the d-wave case,

$$\begin{aligned}\frac{1}{2g} = \mathcal{A}_1(2\Delta-\omega_1) \quad &+ \quad \mathcal{A}_2\frac{q_c^2}{2\Delta}\int_0^{\omega_1/q_c^2}\frac{dx}{1-xq_c^2/(2\Delta)}\log\frac{1+\sqrt{x+1}}{-1+\sqrt{x+1}} \\ &+ \quad \mathcal{A}_3\frac{q_c^2}{2\Delta}\int_0^{\omega_2/q_c^2}\frac{dx}{1+xq_c^2/(2\Delta)}\log\frac{1+\sqrt{x+1}}{-1+\sqrt{x+1}} \\ &+ \quad \frac{\mathcal{A}_4}{\alpha_p}\left[(2\Delta+\omega_2)^{-\alpha_p}-(2\omega_B)^{-\alpha_p}\right].\end{aligned} \tag{5.26}$$

This contains a number of free parameters that are partially constrained by the spectral weight conservation. This however does not suffice to determine the gap uniquely. In the following we will make further choice of the parameters, to plot the gap. We choose the scaling dimension $\alpha_p = 3/4$, and the cut-off in the logarithm to be of order the square root of the gap, say $q_c/\sqrt{2\Delta} = 3$, the width of the logarithmic region to be 20 percent of the magnitude of the gap on both sides of the gap, that is $\omega_1/(2\Delta) = \omega_2/(2\Delta) = 0.2$, the coefficient of the high frequency part $\mathcal{A}_4 = 1/(4\omega_c^{3/4})$, and further define $\omega_1/q_c^2 = \omega_2/q_c^2 \equiv a$, $b \equiv \int_0^a dx \log\frac{1+\sqrt{x+1}}{-1+\sqrt{x+1}}$, $c \equiv \log\frac{1+\sqrt{a+1}}{-1+\sqrt{a+1}}$, $d \equiv \frac{4\times 1.2^{1/4}-1.2^{-3/4}\times 9b/c}{0.32+7.2b/c}$, thus the

corresponding d-wave gap equation reads,

$$1 - \frac{1}{2}\lambda\left(\frac{2\omega_B}{\omega_c}\right)^{-\frac{3}{4}}\left(\frac{\Delta}{\omega_B}\right)^{-\frac{3}{4}}(0.8d + 7.2\frac{d}{c}\int_0^a \frac{dx}{1-9x}\log\frac{1+\sqrt{x+1}}{-1+\sqrt{x+1}} + 9\frac{1.2^{-\frac{3}{4}}}{c}\int_0^a \frac{dx}{1+9x}\log\frac{1+\sqrt{x+1}}{-1+\sqrt{x+1}} + \frac{4}{3}(1.2^{-\frac{3}{4}} - (\frac{\Delta}{\omega_B})^{\frac{3}{4}})\ ) = 0, \quad (5.27)$$

We plot in Fig.(6) the behavior of the gap function in the s- and d-wave cases, to be compared with the outcomes Fig. (2) of the approach taken in section II where the gap simply entered as an IR cut-off scale, Eq. (5.9). One can see that in both cases the magnitude of the gap is enhanced by treating the singularity more carefully, while in the d-wave case this enhancement is even more pronounced than in the s-wave case. These effects can be understood in terms of the redistribution of the spectral weight, since the low frequency part is enhanced by the factor $1/\omega$ in the Kramers-Kronig frequency integral. The dependence of the gap on the glue strength and retardation does however not change significantly compared to what we found in section II, which can be understood from the fact that the gap depends on the combination $\lambda(2\omega_B/\omega_c)^{-\alpha_p}$. One also notices in Fig.(6) that the magnitude of the gap saturates already at small λ for modest retardation. This is an artifact of the modeling. In real system the power law (s-wave) or logarithmic (d-wave) spectral singularities will be damped (see e.g. [254–257]), and the endpoints at finite λ in Fig.(6) will turn into smooth functions..

The gap to T_c ratio is expected to be a number order unity number. However, it is quite sensitive to the details of the crossover regime between the high frequency critical behavior and the low frequency superconducting behavior as of relevance to the zero temperature gap. Numerically evaluating Eq.'s (5.18,5.25,5.27) we obtain gap to T_c ratio's as indicated in Fig. (7). Different from the Migdal-Eliasbergh case we find that these ratio's are rather strongly dependent on both the Migdal- and the coupling parameter, while the ratio becomes large for *small* coupling, in striking contrast with conventional strong coupling superconductivity. Invariably we find the ratio to be larger than the weak coupling BCS case, reflecting the strongly dissipative nature of quantum critical states at finite temperature that plays apparently a similar role as the 'pair-breaking' phonon heat bath in conventional superconductors.

5.5 Away from the critical points

Our scaling theory yields a simple and natural explanation for the superconducting domes surrounding the QCP's. This is usually explained in the Moriya-Hertz-Millis framework [143, 144, 258, 259] that asserts that the critical fluctuations of the bosonic order parameter turn into glue with singular strength while the Fermi-liquid is still in some sense surviving. We instead assert that the glue is some

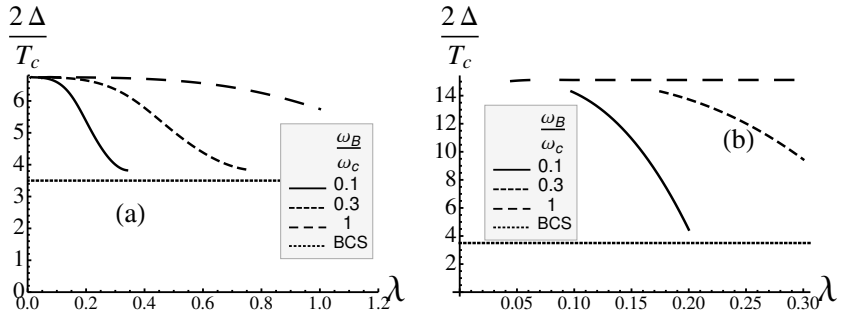

Figure 5.7: (a)The gap to T_c ratio $2\Delta/T_c$ as a function of glue strength λ for various retardation ranges ω_B/ω_c with fixed scaling dimension $\alpha_p = 3/4$, for s-wave pairing. The dotted line is the standard BCS result, where $2\Delta/T_c = 3.5$. (b) The same plot for d-wave pairing. The gap to T_c ratio decreases with increasing glue strength and retardation for both s- and d-wave gap. The ratios for different retardation ranges approach the same constant as $\lambda \to 0$.

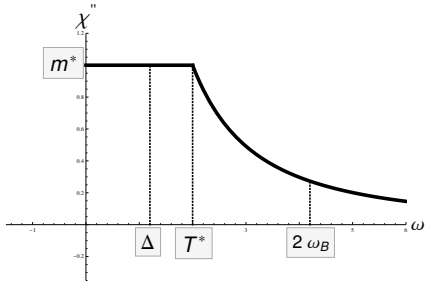

Figure 5.8: Illustration of the imaginary part of the pair susceptibility away from the critical point. For $\omega > T^*$, it has the critical scaling behavior, while for $\omega < T^*$, it retains the BCS form. T^* is the cross-over scale. The effective mass m^* is identified as the magnitude of the imaginary part of the pair susceptibility in the BCS region. The gap Δ acts as a low energy cut-off, and the retardation $2\omega_B$ as a high energy cut-off. When T^* lies between Δ and $2\omega_B$, as is the case shown above, both the critical modes and Fermi liquid modes contribute. When $\Delta > T^*$, only the critical modes contribute. When $2\omega_B < T^*$, only the Fermi liquid modes contribute.

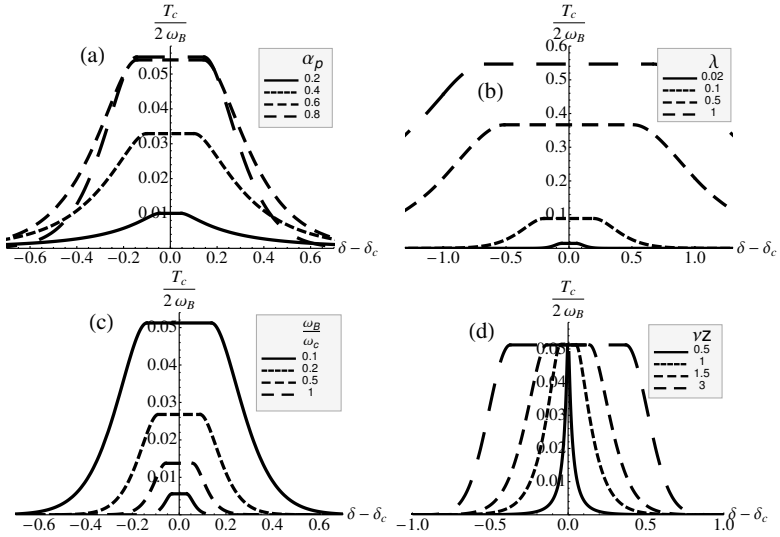

Figure 5.9: The ratio of T_c to retardation as a function of the distance away from criticality (a) for various scaling exponent α_p's with $\lambda = 0.06, \omega_B/\omega_c = 0.1, \nu z = 3/2$, (b) for various glue strength λ's with $\omega_B/\omega_c = 0.1, \nu z = 3/2, \alpha_p = 5/6$. (c) for various retardation over cut-off ω_B/ω_c's with $\lambda = 0.06, \nu z = 3/2, \alpha_p = 5/6$. (d) for various inverse Grüneisen exponent νz's with $\lambda = 0.06, \omega_B/\omega_c = 0.1, \alpha_p = 5/6$.

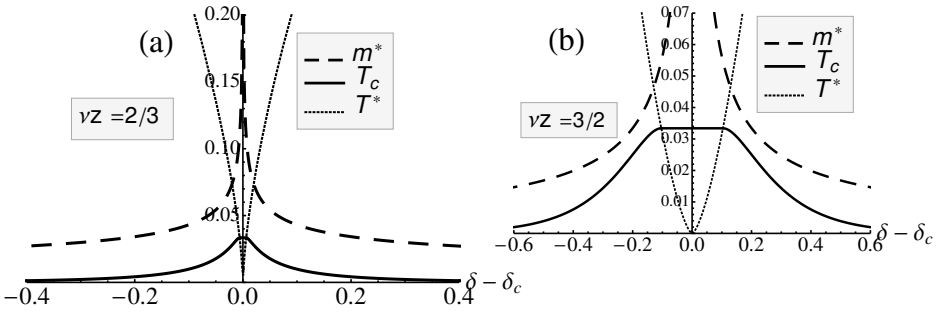

Figure 5.10: (a):The superconducting transition temperature T_c as a function of the distance from the critical point, for given crossover temperature T^* and retardation ω_B. The parameters are chosen as $z = 2, \nu = 1/3, \eta_p = 1, \lambda = 0.05, \omega_B/\omega_c = 0.1$. (b):The same plot for a different set of parameters $z = 3, \eta = 0.5, \nu = 1/2, \lambda = 0.05, \omega_B/\omega_c = 0.1$. In-between the two points $\delta_c \pm \tilde{\delta}$, at which the transition temperature coincides with the cross-over temperature $T_c(\delta_c \pm \tilde{\delta}) = T^*(\delta_c \pm \tilde{\delta})$, the critical temperature remains constant. For $T^* > 2\omega_B$, T_c decays exponentially. The schematic behavior of the effective mass m^* is also included. It diverges when approaching the critical point.

external agent (e.g., the phonons but not necessarily so) that is blind to the critical point, but the fermionic criticality boosts the SC instability at the QCP according to Eq. (5.10). By studying in detail the variation of the SC properties in the vicinity of the QCP it should be possible to test our hypothesis. The data set that is required is not available in the literature and let us present here a crude sketch of what can be done. In at least some heavy fermion systems [260] a rather sudden cross-over is found between the high temperature critical state and a low temperature heavy Fermi-liquid, at a temperature $T^* \sim |\delta - \delta_c|^{\nu z}$, with ν behaving like a correlation length exponent $\xi \sim |\delta - \delta_c|^{-\nu}$ as function of the zero temperature tuning parameter δ. Moving away from the QPT this means for the SC instability that an increasingly larger part of the frequency interval of χ'' below ω_B is governed by the Fermi-liquid 'flow' with the effect that T_c decreases. We can crudely model this by asserting that the imaginary part of the pair susceptibility acquires the critical form for $\omega > T^*$ and the Fermi-liquid form for $\omega < T^*$, while we impose that it is continuous at $\omega = T^*$. This model has the implication that the magnitude of χ'' in the Fermi-liquid regime is determined by T^* and η_p and we find explicitly that $N_0 \propto m^* \propto |\delta - \delta_c|^{-\nu(2-\eta_p)}$. We notice that this should not be taken literally, since this cross-over behavior can be a priori more complicated. In fact, from thermodynamic scaling it is known [261, 262] that $m^* \sim |\delta - \delta_c|^{\nu(d-z)}$. Fig. (8) would imply that $\alpha_p = 1 - d/z$. This is not

implied by scaling.

Given these assumptions, the gap equation away from the quantum critical point becomes,

$$1 - 2g\left(\int_{\Delta}^{T^*} \frac{d\omega}{\omega}\chi''_{\rm BCS}(\omega) + \int_{T^*}^{2\omega_B} \frac{d\omega}{\omega}\chi''_{\rm crit}(\omega)\right) = 0 \tag{5.28}$$

We are interested in the superconducting transition temperature, which has been shown in the previous section to be approximately the gap magnitude $T_c \simeq \Delta$. The imaginary part of the pair susceptibility in the critical region has still the power law form $\chi''_{\rm crit}(\omega) = Z''\sin(\alpha_p\pi/2)\omega^{-\alpha_p}$, while in the BCS region it is a constant determined by continuity at $\omega = T^*$ and therefore $\chi''_{\rm BCS}(\omega) = Z''\sin(\alpha_p\pi/2)(T^*)^{-\alpha_p}$.

Consequently we find in the regime $T_c < T^* < 2\omega_B$ the solution for the gap equation,

$$T_c = 2\omega_B x^{\nu z}\exp\left[\frac{1}{\alpha_p}\left(1 - x^{\nu(2-\eta_p)} - \frac{1}{\tilde{\lambda}}(\frac{2\omega_B}{\omega_c})^{\alpha_p}x^{\nu(2-\eta_p)}\right)\right], \tag{5.29}$$

where $x^{\nu z} = T^*/(2\omega_B)$. For $T^* < T_c$ a plateau is found since only the critical modes contribute to the pairing, while for $T^* > 2\omega_B$ the BCS exponent takes over since only the (heavy) Fermi-liquid quasiparticles contribute having as a consequence,

$$T_c = 2\omega_B\exp\left(-(\frac{2\omega_B}{\omega_c})^{\frac{2-\eta_p}{z}}\frac{x^{\nu(2-\eta_p)}}{\alpha_p\tilde{\lambda}}\right). \tag{5.30}$$

The outcomes are illustrated in Fig. (9,10). One notices in all cases that the dome shapes are concave with a tendency for a flat 'maximum'. This is automatically implied by our starting assumptions. When T_c is larger than T^* only the critical regime is 'felt' by the pairing instability and when this criterium is satisfied T_c does not vary, explaining the flat maximum. When T_c starts to drop below T^* the superconductivity gets gradually depressed because the Fermi-liquid regime increasingly contributes. Eventually, far out in the 'wings', one would still have superconductivity but with transition temperatures that become exponentially small. The domes reflect just the enhancement of the pairing instability by the critical fermion liquid relative to the Fermi-liquid.

The trends seen in Fig. 9 are easily understood. When the scaling dimension α_p is increasing, i.e. the pair operator is becoming more relevant, the maximum T_c increases while not much happens with the width of the dome (Fig. 9a), for the simple reason that the critical metal becomes more and more unstable towards the superconductor. When the coupling strength λ increases one finds in addition that the dome gets broader (Fig. 9b) because the 'contrast' between Fermi-liquid and quantum critical BCS is becoming less, illustrating the surprise that especially weakly coupled quantum critical superconductors are much better

than their traditional cousins. The same moral is found back when the Migdal parameter is varied (Fig. 9c), illustrating that at very strong retardation the differences are the greatest. Finally, in Fig. (9d) the evolution of the domes are illustrated when one changes the exponents relating T^* to the reduced coupling constant. We find that the dome changes from a quite 'box like' appearance to a 'peak' pending the value of νz. The mechanism can be deduced from Fig. 10, comparing the situation that the quantum critical 'wedge' is concave (fig. 10a, $\nu z < 1$) with a convex wedge (fig. 10b, $\nu z > 1$). Because T^* is varying more slowly in he latter case with the reduced coupling constant, the quantum critical regime becomes effectively broader with the effect that the quantum critical BCS keeps control over a wider coupling constant range. The trends in Fig.'s (9, 10) are quite generic and it would be interesting to find out whether by systematical experimental effort these behaviors can be falsified or confirmed.

5.6 The upper critical field

Another experimental observable that should be quite revealing with regard to scaling behavior is the orbital limiting upper critical field. The orbital limiting field is set by the condition that the magnetic length becomes of order of the coherence length, and the latter relates to the 'time like' T_c merely by the dynamical critical exponent z. In more detail, assuming a gap of the form [263],

$$\Delta(\vec{r}) = \Delta_0 \exp\left(-\frac{r^2}{2l^2}\right), \tag{5.31}$$

the linearized gap equation in the presence of an orbital limiting magnetic field becomes [27],

$$\frac{1}{\Omega^{d-1} g} = \int_{r_0}^{\infty} K_0(r,\beta) \exp\left(-\frac{r^2}{2l^2}\right) r^{d-1} dr, \tag{5.32}$$

where Ω^{d-1} is the volume of the $d-1$-dimensional unit sphere, l is the magnetic length related to the field by $H = \phi_0/(2\pi l^2)$ where $\phi_0 = hc/e$, while $K_0(r,\beta)$ is the real space pair susceptibility, which is the Fourier transform of χ' [264, 265]. For free fermions, the real space pair susceptibility is (see eg. [264]),

$$K_0(r,\beta) = \left(\frac{k_F}{2\pi r}\right)^{d-1} \frac{1}{v_F^2 \beta} \frac{1}{\sinh(\frac{2\pi r}{\beta v_F})}, \tag{5.33}$$

with a power law behavior $K_0(r,\beta) \sim r^{-d}$ at short distances or low temperatures where $r < \beta v_F$, and an exponential decay at large distances or high temperature. Let us consider critical fermions at $T = 0$, such that the pair susceptibility has the power law form $\chi(\omega) \sim \omega^{-(2-\eta)/z}$. The momentum dependence can be determined by replacing ω by k^z, such that $\chi(k) \sim k^{-(2-\eta)}$. It follows that the real space pair susceptibility has the power law form $K_0(r, T = 0) \sim$

$\int \chi(k)\exp(i\vec{k}\cdot\vec{r})d^d\vec{k} \sim r^{-(d-2+\eta_p)}$. Associate with the retardation a short distance cutoff r_0, and assume a scaling $2\omega_B/\omega_c = (r_0/a_c)^{-z}$, where a_c is the lattice constant. The magnetic length acts as a long distance cutoff and therefore,

$$\frac{1}{\Omega^{d-1}g} = \int_{r_0}^{l} \frac{\mathcal{C}_h}{r^{d-2+\eta_p}} r^{d-1} dr, \tag{5.34}$$

with the normalization factor $\mathcal{C}_h \simeq 2z(1-\alpha_p)\Omega^{-(d-1)}{\omega_c}^{-1}a_c^{-(2-\eta)}$, so that $(1/\Omega^{d-1})\int_{a_c} K_{\rm crit}(r) r^{d-1} dr \simeq \frac{1}{\omega_c}$, to give the right scale. The zero temperature upper critical field has then the same form as the one for T_c except for the occurrence of z,

$$\frac{2\pi H_{c2}(0)}{\phi_0 {r_0}^{-2}} \simeq \left(1 + \frac{1}{\tilde{\lambda}}\left(\frac{2\omega_B}{\omega_c}\right)^{\alpha_p}\right)^{-\frac{2}{2-\eta_p}}, \tag{5.35}$$

and it follows,

$$\frac{2\pi H_{c2}(0)}{\phi_0 {a_c}^{-2}} \simeq \left(\frac{T_c}{\omega_c}\right)^{2/z}. \tag{5.36}$$

In the BCS case one has $H_{c2}(0)/(\mathcal{B}\phi_0 k_F^2) = (T_c/E_F)^2$, with $\mathcal{B} \simeq 3.26$ for $d = 3$ [266]. The moral is obvious: in Lorentz-invariant ($z = 1$) systems the relation between H_{c2} and T_c is the same as for standard BCS, but when the normal state is governed by a universality class characterized by $z > 1$, $H_{c2}(0)$ will be amplified for a given T_c relative to conventional superconductors because $T_c/\omega_c, T_c/E_F \ll 1$.

Modeling the variation of H_{c2} in the vicinity of the QPT as in the previous paragraph, where the critical modes govern the short distance and BCS type behavior is recovered at large distance, while converting the cross-over temperature to a length scale r^*, by $T^*/\omega_c = (r^*/a_c)^{-z}$, we find that H_{c2} is determined by the equation,

$$\frac{1}{\Omega^{d-1}g} = \int_{r_0}^{r^*} \frac{\mathcal{C}_h}{r^{d-2+\eta_p}} r^{d-1} dr + \int_{r^*}^{l} \frac{\mathcal{C}'_h}{r^d} r^{d-1} dr, \tag{5.37}$$

with the matching condition $\mathcal{C}_h = (r^*)^{-2+\eta_p}\mathcal{C}'_h$. We find that one just has to replace the first two dynamic exponent z's in Eq. (5.29) by 2 while an extra factor of 2 has to be added to the second term in the exponent,

$$H_{c2} = \frac{\phi_0 a_c^{-2}}{2\pi} x^{2\nu}\left(\frac{2\omega_B}{\omega_c}\right)^{2/z} \exp\left[\frac{2}{2-\eta_p}\left(1 - x^{\nu(2-\eta_p)} - (\frac{2\omega_B}{\omega_c})^{\alpha_p}\frac{x^{\nu(2-\eta_p)}}{\tilde{\lambda}}\right)\right]. \tag{5.38}$$

In the region where only the Fermi-liquid quasiparticles contribute, the upper critical field has still an exponential form,

$$H_{c2} = \frac{\phi_0 a_c^{-2}}{2\pi}\left(\frac{2\omega_B}{\omega_c}\right)^{2/z} \exp\left[-2(\frac{2\omega_B}{\omega_c})^{\frac{2-\eta_p}{z}}\frac{x^{\nu(2-\eta_p)}}{(2-\eta)\tilde{\lambda}}\right]. \tag{5.39}$$

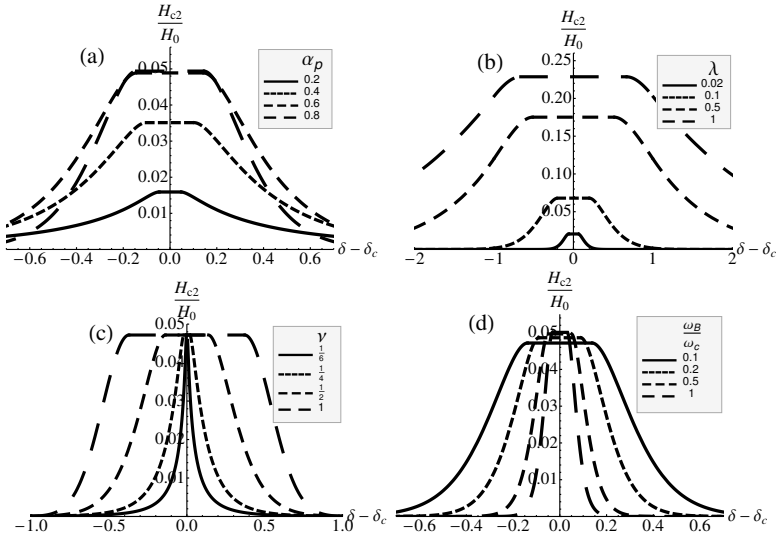

Figure 5.11: The upper critical field H_{c2} over $H_0 \equiv \phi_0 a_c^{-2}/(2\pi)$ as a function of the distance away from criticality (a) for various scaling exponent α_p's with $\lambda = 0.06, \omega_B/\omega_c = 0.1, \nu = 1/2, z = 3$, (b) for various glue strength λ's with $\omega_B/\omega_c = 0.1, \nu = 1/2, z = 3, \alpha_p = 5/6$, (c) for various ν's with $\lambda = 0.06, \omega_B/\omega_c = 0.1, \alpha_p = 5/6, z = 3$, (d) for various retardation ranges with $\lambda = 0.06, \nu = 1/2, z = 3, \alpha_p = 5/6$.

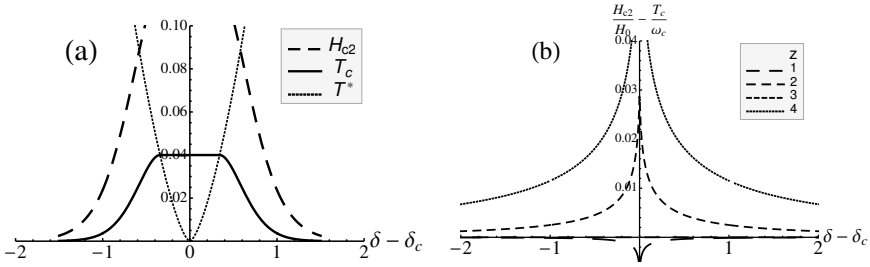

Figure 5.12: (a)Illustration of the different behavior of T_c and upper critical field H_{c2} as the quantum critical point is approached. H_{c2} increases much faster than T_c. Thus for a small T_c one can still have a large upper critical field. Here we plotted using the parameters $\lambda = 0.05, \omega_B/\omega_c = 0.1, \nu = 1/2, z = 3, \eta = -1$. (b) The difference $H_{c2}/H_0 - T_c/\omega_c$ as a function of the distance away from the critical point for different dynamical exponent z's. Here $H_0 \equiv \phi_0 a_c^{-2}/(2\pi)$, $\lambda = 0.06, \omega_B/\omega_c = 0.1, \nu z = 0.5, \alpha_p = 0.4$. For $z = 2$, the difference is 0. For $z = 3, 4$, the difference is positive and increases rapidly when approaching the critical point. For the case with $z = 1$, the difference is negative.

The dependence of H_{c2} on various parameters is shown in Fig. 11, and one infers that H_{c2} behaves in ways very similar T_c (Fig. 10). The interesting part is illustrated in Fig.(12b) where we plot $H_{c2}/H_0 - T_c/\omega_c$ as a function of the distance away from the critical point for different dynamical exponent z's, keeping all other quantities fixed, defining $H_0 \equiv \phi_0 a_c^{-2}/(2\pi)$. One infers that when $z > 2$, $H_{c2}/H_0 - T_c/\omega_c$ increases rapidly when approaching the critical point.

Using a 'ferromagnetic' dynamical exponent $z = 3$ and a Grüneisen exponent $1/\nu z = 2/3$ inspired on recent experiments [267,268] as well as theoretical considerations [143,144,179,186,258,259] we obtain the results in Fig. (12a). Compared to T_c, H_{c2} peaks much more strongly towards the QCP. This is in remarkable qualitative agreement with the recent results by Levy *et al.* on the behavior of the orbital limiting field in URhGe exhibiting a ferromagnetic QCP [234], where the highest T_c is about 0.5 K [118], while the upper critical field exceeds 28 T. It has also been observed in noncentrosymmetric heavy fermion superconductors $CeRhSi_3$ [269, 270] and $CeIrSi_3$ [271, 272], where the Pauli limiting effect is suppressed due to lack of inversion center of the crystal structures and the orbital limiting effect plays the main role of pair breaking. Near the quantum critical points, H_{c2} can be as high as about 30 K, although the zero field T_c is of order 1K [273, 274]. This class of experiments can be understood in our framework as resulting from the change of the scaling relation between H_{c2} and T_c. (See also [275] for a tentative explanation from the customary Hertz-Millis-Moriya perspective.)

5.7 Conclusions

Perhaps the real significance of the above arguments is no more than to supply a cartoon, a metaphor to train the minds on thinking about pairing instabilities in non Fermi-liquids. This scaling theory has the merit of being mathematically controlled, given the starting assumptions of the 'retarded glue' and conformal invariance. The Migdal parameter plays an identical role as in conventional BCS theory to yield a full control over the glue-fermion system dynamics, while we trade in Fermi-liquid principle for the even greater powers of scale invariance. The outcomes are gap and Tc equations where the standard BCS/Eliasberg equations show up as quite special cases associated with the marginality of the pair operators of the Fermi gas. The difficulty is of course to demonstrate that these starting assumptions have dealings with either nature itself and/or microscopic theories of electron systems where they should show up as emergent phenomena at low energy. However, the same objections apply to much of the current thinking regarding superconducting instabilities at quantum critical points with their implicit referral to a hidden Fermi gas. In such considerations there is an automatism to assume that eventually the superconductivity has to be governed by Eliashberg type equations. At the least, the present analysis indicates that such equations are not divine as long as the Fermi-liquid is not detected di-

rectly. Stronger, in line with the present analysis one might wish to conclude that superconducting instabilities will be generically more muscular in any non-Fermi-liquid. The Fermi-liquid is singular in the regard that its degrees of freedom are stored in the Fermi-sea, and this basic physics is responsible for the exponential smallness of the gap in terms of the coupling constant. This exponential smallness should be alien to any non Fermi-liquid.

How about experiment? Scaling theories have a special status in physics because they guide the analysis of experimental data in terms of a minimal a-priori knowledge other than scale invariance. The present theory has potentially the capacity to produce high quality empirical tests in the form of scaling collapses. However, there is a great inconvenience: one has to be able to vary the glue coupling strength, retardation parameters and so forth, at will to test the scaling structure of the equations. These are parameters associated with the materials themselves, and one runs into the standard difficulty that it is impossible to vary these in a controlled manner. What remain are the rather indirect strategies discussed in the last two sections: find out whether hidden relations exist between the detailed shape of the superconducting and the crossover lines; are there scaling relations between H_{c2} and T_c as discussed in the last section? We look forward to experimental groups taking up this challenge.

There appears to be one way to interrogate our starting assumptions in a very direct way by experiment. Inspired by theoretical work by Ferrell [276] and Scalapino [277], Anderson and Goldman showed quite some time ago [278] that the dynamical pair susceptibility can be measured directly using the AC Josephon effect – see also [279, 280], for a recent review see ref. [281]. It would be interesting to find out whether this technique can be improved to measure the pair susceptibility over the large frequency range, 'high' temperatures and high resolution to find out whether it has the conformal shape. It appears to us that the quantum critical heavy fermion superconductors offer in this regard better opportunities than e.g. the cuprates given their intrinsically much smaller energy scales. This will be the topic of next chapter.

In conclusion, exploiting the motives of retardation and conformal invariance we have devised a phenomenological scaling theory for superconductivity that generalizes the usual BCS theory to non Fermi-liquid quantum critical metals. The most important message of this simple construction is that it demonstrates the limitations of the usual Fermi-liquid BCS theory. The exponential smallness of the gap in the coupling is just reflecting the 'asymptotic freedom' of the Fermi-liquid, and this is of course a very special case within the landscape of scaling behaviors. Considering the case that the pair operator is relevant, we find instead an 'algebraic' gap equation revealing that at weak couplings and strong retardation the rules change drastically: as long as the electronic UV cut-off and the glue energy are large, one can expect high T_c's already for quite weak electron-phonon like couplings. If our hypothesis turns out to be correct, this solves the problem of superconductivity at a high temperature although it remains to be explained why quantum critical normal states can form with the required properties. It

is however not straightforward to device a critical test for our hypothesis. The problem is the usual one that pair susceptibilities, λ's or $\alpha^2 F$'s, and so forth cannot be measured directly and one has to rely on imprecise modelling. However, it appears to us that 'quantum critical BCS superconductivity' works so differently from the Fermi-liquid case that it eventually should be possible to nail it down in the laboratory. We hope that the sketches in the above will form a source of inspiration for future work.

Chapter 6

Measuring the Pair Susceptibility Directly

6.1 Introduction

Dynamical correlation functions provide crucial insights for the understanding of strongly correlated electron systems. By measuring the wavevector- and frequency-dependent magnetic susceptibility, inelastic neutron scattering has become one of the most powerful tools in characterizing magnetism. In these experiments, the beam of scattering external particles couple to the order parameter of the system, in the case of magnetism the spin density of the sample, and the resulting differential scattering cross-section is a direct measure of the autocorrelation function of the order parameter.

For superconductivity, one would ideally also like to measure the susceptibility associated with the order parameter. However, the superconducting pairing order parameter Δ is off-diagonal in particle number space, $\Delta \sim \langle c_\downarrow c_\uparrow \rangle$, and nature does not endow us with an external electromagnetic field that couples directly to the order parameter, like it does for magnetism. A probe of the 'pairing' susceptibility thus always requires an *indirect* measurement.

Such an indirect probe has been known for 40 years. Based on the Josephson effect, in which the order parameters of two superconductors are coupled to each other, in 1970 Ferrell [276] and Scalapino [277] suggested a superconductor-insulator-normal (SIN) tunneling setup in which a strong superconductor acts as an effective external probe for a normal metallic state above its superconducting transition temperature T_c; the fluctuating pair field of the metal is coupled to

the rigid pair-field of the strong superconductor, and this leads to an additional contribution to the total tunneling current, on top of the well-known SIN-junction quasiparticle current. This additional tunneling current is proportional to the imaginary part of the pair(ing) susceptibility of the pairing order parameter of the metallic state (see also [282]).

This scheme has been used to study the pair fluctuations near the superconducting transition temperature. A divergence in the pair susceptibility is universally expected as the phase transition is approached, and a 'relaxational' peak characteristic for Gaussian fluctuations was indeed confirmed experimentally very early on in the work by Goldman and collaborators [278] in aluminum and lead (i.e., conventional s-wave materials), and much more recent also in junctions of d-wave cuprates [283].

Up to now, all the efforts on the pair tunneling experiments have been confined to the region *near* T_c. The pair susceptibility at higher temperatures may have been ignored because for conventional Fermi liquids it is expected to be boring. The main purpose of this chapter is to make it clear to experimentalists that with the recent advances in unconventional superconductivity, especially for systems near the quantum critical points (QCPs), it has become worthwhile to measure the dynamic pair susceptibility away from the transition temperature. The basic point is that the frequency and temperature dependence of the pair susceptibility further away from T_c actually contains important information about the normal state properties of the non-Fermi liquid materials. Such information is vital for the understanding of both the exotic pairing mechanism in such systems and the underlying non-Fermi liquid parent state. Experimentalists have been able to measure the single particle properties of these systems using ARPES and STM, as well as the properties in the particle-hole channel, using for example INS, ESR. However, a direct probe in the particle-particle channel is still lacking, though its importance is obvious, since pairing itself happens in the particle-particle channel. We would like to convince the reader that the pair tunneling experiment actually provides such a highly desired Cooper channel probe .

We will calculate the pair susceptibility for different scenarios of the pairing mechanism for quantum critical metals. Although there exists no proper microscopic description for quantum critical materials, right at the quantum critical point the rules of criticality nevertheless come to our aid, in the sense that we can work with effective models without the need for a microscopic description. We will consider several limiting cases of the whole manifold of possible effective theories. One class of models assumes the separation of the electronic part and the glue part, in which one scenario further assumes that the glue part becomes critical in the quantum critical state; another assumes the electronic part to be critical. The former is best represented by the quantum critical γ-model investigated by Chubukov and collaborators [284]. The latter is the quantum critical BCS (QC-BCS) model that was explored by two of the present authors [121]. There also exist another class of models which do not distinguish between the electronic part and the glue part, only dealing with the bosonic order parameters,

while incorporating scale invariance at high temperature and high frequency. This is the holographic superconductors proposed by Hartnoll, Herzog and Horowitz, for which the superconductor is effectively described by a gravitational theory in one dimension higher [126,285]. We will calculate the dynamic pair susceptibility for these models, in addition to the conventional Fermi liquid BCS model, which is used as a reference point. To our knowledge, this has not been done before. The previous investigations have been focusing on the superconducting transition temperature, for which only the information at zero frequency is needed. The equations we will be solving for the pair correlation functions can be viewed as the finite frequency generalizations of the heavily investigated gap equations, which lie at zero frequency.

In order to experimentally distinguish the various scenarios it is necessary to measure the pair susceptibility away from T_c; to be more precise, a reduced temperature $\tau = (T - T_c)/T_c > 1$ is required. To access such a temperature window clearly demands that the strong superconductor has a significantly larger transition temperature than the quantum critical material of interest. This suggest to consider probing a heavy fermion material at its quantum critical point, where both quantum critical behavior and relatively low T_c ($\simeq 1\,\mathrm{K}$) are expected. The strong side superconductor should have $T_c > 10\mathrm{K}$ to allow for a practical temperature window.

The supposed d-wave symmetry of the order parameter in most materials of interest presents both a challenge and an opportunity. The calculations in this chapter presume s-wave symmetry, but hold equally well for d-wave after projection in the relevant channel. The only real requirement is a non-zero Josephson coupling, in other words a non-zero dc Josephson current at $T = 0$. There is also no hard requirement for the type of interface; a planar junction, point contact, or scanning tunneling tip interface all qualify in essence (for the results in this chapter we work in the tunneling regime). The relaxational peak has been observed in d-wave to d-wave planar junction at very high temperatures 60–80K [283], providing both experimental proof of principle and great promise for lower temperature experiments.

For all the models to be considered in this chapter, we assume a mean field type superconducting phase transition. This is likely true for the quantum critical materials we are interested: optimally doped cuprates and heavy fermions. For underdoped cuprates phase fluctuations are expected to play an important role as well; these are not captured by the current analysis.

The core of this chapter is devoted to numerically determine the pair susceptibility for the three models, as function of frequency and temperature. We will use Eliashberg-like equations throughout this chapter. Eliashberg theory is a fully dynamical theory, where the momentum dependence is assumed to be relatively smooth, and the crucial information is in the frequency dependent part. The solution of these Eliashberg-like equations can only be determined numerically. We extract from the particular parameter sets the general features of the different models. Our main result is summarized graphically in Fig. (6.4) where we

plot the pair susceptibility $\chi_p(\omega, T)$ for the three distinct models (using typical parameters) at the same scale.

The remainder of this chapter is organized as follows. In section 6.2, we give a brief introduction to the tunneling experiment proposed by Ferrell and Scalapino, and realized by Goldman and more recently by Bergeal et al. . In section 6.3 and section 6.4, we turn to theory. Three different models are reviewed in section 6.3, all of which assume electron-glue dualism. These different models are presented in a unified framework using Eliashberg-type integral equations. In section 6.4, we first review the basic idea of the holographic superconductors and then we outline how the pair susceptibility can be calculated by solving the equation of motion for a scalar field. The main results are analyzed in section 6.5. Section 6.6 is devoted to proposing a realistic experiment, including the candidate materials and experimental setup.

6.2 The pair tunneling experiment

The formal definition of the pair susceptibility is as follows,

$$\chi_p(\mathbf{q}, \omega) = -i \int_0^\infty dt e^{i\omega t - 0^+ t} \langle \big[b^\dagger(\mathbf{q}, 0), b(\mathbf{q}, t) \big] \rangle, \tag{6.1}$$

where $b^\dagger(\mathbf{q}, t) = \sum_{\mathbf{k}} c^\dagger_{\mathbf{k}+\mathbf{q}/2,\uparrow}(t) c^\dagger_{-\mathbf{k}+\mathbf{q}/2,\downarrow}(t)$, and $c^{(\dagger)}_{\mathbf{k},\sigma}$ the usual annihilation (creation) operators for electrons with momentum $\mathbf{k}$ and spin σ. For a non-interacting Fermi gas the pair susceptibility can be calculated directly in terms of single particle Green's functions, and gives $\chi_p''(\omega) = \frac{\pi}{2} N(\frac{\omega}{2}) \tanh \frac{\omega}{4T}$. For interacting non-Fermi liquid materials the pair susceptibility is a true two-particle property containing particle-particle pair channel information.

It was realized by Ferrell [276] and worked out further by Scalapino [277] that the pair susceptibility is observable in the tunneling current of an SIN junction. They considered the tunneling regime, i.e., large insulating barrier and consequently small tunneling amplitude γ. In this regime the tunneling current can be calculated perturbatively in the tunneling amplitude. The lowest non-zero contribution to the tunneling current is the well-known linear response result of single quasiparticles tunneling between normal metal and superconductor, of order $|\gamma|^2 \sim R_N$, where R_N is the resistance of the entire junction in a normal state (i.e, NIN junction). This famous, and by now textbook result was observed in the pioneering experiments of Giaever and predicts that at zero temperature (for s-wave superconductor) $I_{\text{tun}} R_N = \sqrt{V^2 - \Delta^2}\, \theta(V - \Delta)$; at finite temperatures there is an exponential suppression of the tunneling current at bias voltages below the gap Δ.

To order $|\gamma|^2$ only isolated quasiparticles can give a non-zero tunneling current. However, at order $|\gamma|^4$ it is possible for Cooper pairs to tunnel, and Cooper pairs are not constraint by the quasiparticle gap Δ. This is what Ferrell and

Scalapino predicted, that there is a contribution to the tunneling current from tunneling Cooper pairs of order $|\gamma|^4$, on top of the quasiparticle tunneling current (contributing at order $|\gamma|^2$ and $|\gamma|^4$). On the normal metal side, this tunneling process corresponds precisely to the imaginary part of the pair susceptibility $\chi_p''(\mathbf{q}=0,\omega)$ where $\hbar\omega = 2eV_{\rm bias}$ [277].

Up to order $|\gamma|^4$, the tunneling current in a SIN is of the form,

$$I_{\rm tun}(V) = I_{\rm qp}(V) + I_{\chi_p''}(V), \tag{6.2}$$

$$I_{\chi_p''}(V) \propto \chi_p''(2eV/\hbar). \tag{6.3}$$

The proportionality factor obviously includes the factor $|\gamma|^4$, but also local densities of state of both S and N materials and effective junction area; since these factors are highly sample-dependent, the overall magnitude of the pair susceptibility contribution to the tunneling current will generally be an experimental fitting parameter. Note that this higher order Cooper pair tunneling process is a second order Josephson effect: if at low temperaturers the regular dc Josephson effect can be observed (i.e., a finite supercurrent at zero bias in SIS configuration), then the higher order tunneling Cooper pair process is likely to occur in the SIN configuration at finite bias.

The pair susceptibility can also be probed at non-zero wave vector $\mathbf{q}$, by applying a magnetic field parallel to the interface surface, which creates the necessary momentum offset of the tunneling pairs [277]. In this chapter we are only concerned with zero momentum $\mathbf{q} = 0$, and we restrict to this case from now on.

The experimental challenge is thus to fabricate a junction that has a discernable second order Josephson tunneling effect. The imaginary part of the pair susceptibility can then be determined up to an unknown overall proportionality factor from the tunneling I-V-curve by subtracting the quasiparticle tunneling current contribution. One may worry that the pair susceptibility signal, of order $|\gamma|^4$, will be so small that it will always drown in the quasiparticle tunneling current signal of order $|\gamma|^2$. There are two reasons why this will likely not be a problem at all: (i) there exist exact expressions for the quasiparticle tunneling current through the Blonders-Tinkham-Klapwijk 'BTK'- formula [286] which has been generalized to d-wave superconductors as well [287]; therefore the quasiparticle tunneling current can be subtracted with rather high precision. And (ii), the quasiparticle tunneling current is rather featureless and suppressed for bias voltages below the gap; close to T_c the pair susceptibility signal is extremely enhanced for $V \ll \Delta$. The true experimental challenge lies in extending the temperature range in which $\chi_p''(\omega)$ can be detected from the total tunneling current to temperatures $(T - T_c)/T_c > 1$.

Goldman and collaborators demonstrated that the proposal by Ferrell and Scalapino is indeed observable in experiment [278]; they considered planar junctions between conventional s-wave superconductors and normal metals, e.g., a aluminum ($T_c \approx 2$K) – aluminum-oxide – lead ($T_c \approx 7$K) NIS interface; this

setup sets an upper bound to the reduced temperature $\tau = (T - T_c)/T_c$ of $\sim (7-2)/2 = 2.5$. They measured tunneling current I-V-curves similar to the ones plotted in Fig. 6.1. They observed a discernable peak with a quasi-Lorentzian line-shape up to $T \approx 3$K (reduced temperature $\tau \approx 0.5$), and at temperature close to T_c, namely at $0.01 < \tau < 0.05$ they found the peak to lie at bias voltage $\omega_{\max} \simeq 8k_B(T - T_c)/\hbar\pi$.

Bergeal et al. recently managed to observe the pair susceptibility at a SIN interface for d-wave materials [283]; they devised a planar junction of an underdoped cuprate ($T_c \approx 60$K) and optimally doped cuprate ($T_c \approx 90$K). This configuration naturally constraints reduced temperature τ to be smaller than 0.5. There are more differences compared with the experiments by Goldman. Instead of directly measuring the tunneling current Bergeal et al. observed the differential conductance. Also, they did not use a generalized BTK formula to subtract the quasiparticle current (instead they noticed that microwave radiation suppressed to peak, and they used this to set the background). The experiment by Bergeal et al. was designed to verify a theoretical prediction by Janko et al. for phase fluctuations in underdoped cuprates [288]; Janko et al. predicted a resonance, instead Bergeal et al. found relaxational behavior. The temperature at which Bergeal et al. performed their experiments are actually rather favorable for our intended target: if the pair susceptibility can be detected at temperatures $T > 60$K the signal should be substantially sharper for temperatures below 10 K, while at the same time allowing reduced temperature to be large. Furthermore, Bergeal et al. observed the relaxational peak that we expect for all different models considered in this chapter. Whether to measure the tunneling current directly or the differential conductance is an experimental trade-off, in principle they carry the same information.

6.3 Pairing mechanisms with electron-glue dualism

The pairing mechanism in quantum critical metals is still under intense debate. Different scenarios have been proposed. It is vital to have an experimental tool to test these scenarios directly. Since superconductivity, i.e., pairing, happens in the Cooper channel, it is surely desirable to be able to measure the Cooper channel directly. Such an experiment has been described in detail in the previous section. The central object that will be measured in such tunneling experiments is the imaginary part of the full dynamical pairing susceptibility. In this section, we will introduce several different scenarios of superconductivity for quantum critical metals. We intend to use these scenarios to represent the different limits of the whole manifold of theories. We study in detail the frequency and temperature evolution of the pair susceptibility in these scenarios. The whole formalism is presented in this section, and the numerical results will be analyzed in the next section.

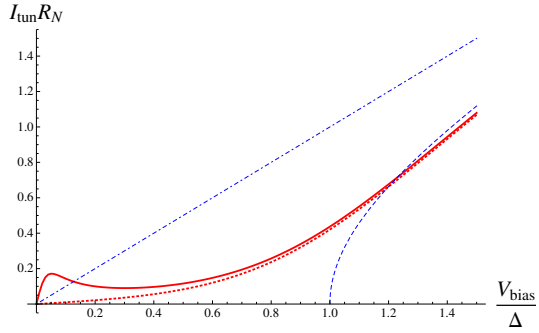

Figure 6.1: Sketch of typical tunneling current $I_{\text{tun}}(V)$ (solid line) as measured in experiments by Goldman. At a temperature $T = \Delta/4$ the usual quasiparticle current for a SIN tunneling junction is given by the dotted line. The difference between the total tunneling current and the quasiparticle current is the pair susceptibility $\chi_p''(\omega = 2eV)$: characterized by a small peak at a relatively low voltage. For reference are plotted as well the zero temperature quasiparticle current (dashed line) and the high temperature linear Ohmic behavior (dotdashed line).

Let us look at the pair susceptibility. The full pair susceptibility contains contributions from all forms of interactions. The general strategy is to separate it into two parts: the electronic part and the glue part. The electronic part is non-singular down to extremely low temperatures. The Coulomb interaction is included in this part. The bosonic glue mediates an attractive electron-electron interaction. It may arise from the coupling of the electrons to lattice distortions. It can also be the collective excitations of the electrons themselves. In some heavy fermion compounds in the vicinity of magnetic quantum phase transitions, magnetic fluctuations may act as glue for superconductivity. For some superconductors, like cuprates, it is questionable whether the glue part is even relevant, since it has a much lower energy scale than that of the electronic interaction, say U and J [289]. We will see later on that in some scenarios the peculiarity of the quantum critical states can lead to the surprising result that even a weak glue can have tremendous effect on superconductivity.

The glue is generally retarded in the sense that its characteristic energy scale ω_b is small compared to the ultraviolet cut-off scale of the electronic part ω_c. With a small Migdal parameter ω_b/ω_c, the electron-glue vertex corrections can then be ignored and the effects of the glue are described by the Migdal-Eliashberg time-dependent mean field theory. And we have the Bethe-Salpeter equation (see Fig. 6.2),

$$\chi(k,k';q) = \chi_0(k,k';q) + u^2 \sum_{k_1,k_2} \chi_0(k,k_1;q) D(k_2-k_1) \chi(k_2,k';q), \qquad (6.4)$$

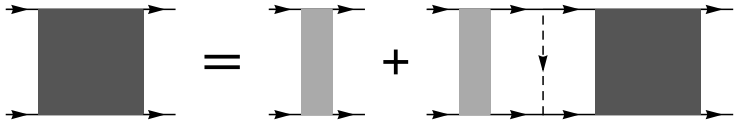

Figure 6.2: Feynman diagram of the Cooper channel Bethe-Salpeter equation. The dark gray square represents the four-point correlation function in the Cooper channel and the light gray rectangle is the corresponding electronic part. The solid lines stand for the electron propagator and the dashed line is the glue propagator.

where $\chi(k,k';q)$ represents the full four-point correlation function with incoming momenta/frequencies $(-k,k+q)$ and outgoing momenta/frequencies $(-k',k'+q)$ and $\chi_0(k,k';q)$ is the corresponding electronic part; $D(p)$ is the glue propagator and u the electron-glue coupling strength taken to be constant below the ultraviolet cut-off scale. The momentum and frequency are grouped in a single symbol here, i.e., four-vector notation $q=(\mathbf{q},\omega)$. The pair susceptibility is obtained from the four-point correlation function by performing a summation over the relative momenta/frequencies, $\chi_p(q)=\sum_{k,k'}\chi(k,k';q)$.

Further simplification can be made by assuming that the pairing problem in quantum critical metals can still be treated within the Eliashberg-type theory, with the electronic vertex operator χ_0 and the glue propagator D strongly frequency dependent, but no substantial momentum dependence. The glue part will only appear in the form of a frequency-dependent pairing interaction $\lambda(\Omega)=\int d^d\mathbf{q}D(\mathbf{q};\Omega)$. A partial summation over the outgoing momenta/frequencies gives the vertex operator $\Gamma(k;q)=\sum_{k'}\chi(k,k';q)$. Also performing the integration over the relative momentum in Γ_0, and taking the total momentum to be vanishing, i.e. $\Gamma_0(\nu;\omega)=\int d\mathbf{k}\Gamma_0(\mathbf{k},\nu;\mathbf{q}=0,\omega)$, we arrive at the final form of the Bethe-Salpeter equation with only (imaginary) frequency arguments,

$$\Gamma(i\nu;i\Omega) \;=\; \Gamma_0(i\nu;i\Omega) \;+\; \mathcal{A}\,\Gamma_0(i\nu;i\Omega)\sum_{\nu'}\lambda(i\nu' \;-\; i\nu)\Gamma(i\nu';i\Omega). \quad (6.5)$$

A further frequency summation over ν yields the pair susceptibility $\chi_p(i\Omega,\mathbf{q}=0)=\sum_\nu\Gamma(i\nu;i\Omega)$ at imaginary frequency $i\Omega$; analytic continuation $i\Omega\to\omega+i\eta$ will give the desired pair susceptibility at real frequency $\chi_p(\omega)$.

The superconducting transition happens when the real part of the full pair susceptibility at $\omega=0$ diverges. The gap equation is the $\omega=0$ limit of the Bethe-Salpeter equation,

$$\Gamma(i\nu)=\Gamma_0(i\nu)+\mathcal{A}\,\Gamma_0(i\nu)\sum_{\nu'}\lambda(i\nu'-i\nu)\Gamma(i\nu'), \quad (6.6)$$

with $\Gamma(i\nu)=\Gamma(i\nu;i\Omega=0)$.

The Bethe-Salpeter equation (6.5) can be solved either by iteration or by direct matrix inversion. The transition temperature T_c is determined by setting the determinant of the kernel equal to zero at zero Matsubara frequency. We will compare three different approaches to pairing in the remainder of this section.

6.3.1 Fermi liquid BCS

We first present as point of reference the case of Fermi liquid BCS. We consider a free Fermi gas, interacting via a normal glue, say an Einstein phonon. The electronic part of the pair susceptibility is simply the convolution of single-particle Green's functions,

$$\chi_0(\mathbf{q}, i\Omega) = \frac{T}{N} \sum_{\mathbf{k},n} G\left(-\mathbf{k}, -i\nu_n\right) G\left(\mathbf{k}+\mathbf{q}, i\nu_n + i\Omega\right). \tag{6.7}$$

For this model, we ignore the self-energy correction, and use the free fermion Green's function $G(\mathbf{k}, i\omega) = 1/(i\omega_n - \varepsilon_{\mathbf{k}})$. The imaginary part of the bare pair susceptibility has the simple form $\chi_0''(\omega) = \frac{1}{\omega_c} \tanh\left(\frac{1}{4}\beta\omega\right)$ at $\mathbf{q} = 0$. Here the Fermi energy acts as the ultraviolet cut-off, with $\omega_c = \frac{2}{\pi N(0)} \simeq E_F$. The bare vertex operator reads

$$\Gamma_0(i\nu_n, i\Omega) = \frac{2T}{\omega_c(2\nu_n + \Omega)} \left[\theta(\nu_n + \Omega) - \theta(-\nu_n)\right], \tag{6.8}$$

with $\theta(x)$ the Heaviside step function. $\Gamma_0(i\nu_n, i\Omega)$ vanishes in the interval $-\Omega < \nu_n < 0$, and decays as $1/\nu_n$ for ν_n large. It is symmetric under the transformation $\nu_n \to -\Omega - \nu_n$. This symmetry can be made more explicit by writing $\Gamma_0(i\nu_n, i\Omega)$ in terms of the relative frequencies $\tilde{\nu}_n = \Omega/2 + \nu_n$,

$$\Gamma_0(i\nu_n, i\Omega) = \frac{T}{\omega_c \tilde{\nu}_n} \left[\theta(\frac{\Omega}{2} + \tilde{\nu}_n) - \theta(\frac{\Omega}{2} - \tilde{\nu}_n)\right]. \tag{6.9}$$

For $i\Omega = 0$, $\Gamma_0(i\nu_n, i\Omega)$ is simply $T/(\omega_c|\nu_n|)$. A BCS-type paring interaction

$$\lambda(\nu' - \nu) = \begin{cases} g/\mathcal{A} & \text{for } |\tilde{\nu}|, |\tilde{\nu}'| < \omega_b, \\ 0 & \text{otherwise,} \end{cases} \tag{6.10}$$

leads to the gap equation

$$1 - g \sum_{|\nu| < \omega_b} \Gamma_0(i\nu_n, \Omega = 0) = 0, \tag{6.11}$$

which gives immediately for the Fermi liquid BCS model an exponentially small transition temperature $T_c \simeq \omega_b \exp\left(-1/\lambda\right)$, with $\lambda = gN(0)$.

We also note that the BCS-type paring interaction (6.10) leads to a simple RPA form for the full pair susceptibility,

$$\chi(\omega) = \frac{\chi_0(\omega)}{1 - g\chi_0(\omega)}, \tag{6.12}$$

where retardation enters through the bare pair susceptibility, $\chi_0(\omega) = \sum_{|\tilde{\nu}|<\omega_b} \Gamma_0(\nu;\omega)$.

However, for the subsequent numerical calculation of the full dynamical pair susceptibility, we will instead use the pairing interaction from a single Einstein phonon,

$$\lambda(i\Omega) = \frac{g}{\mathcal{A}} \frac{\omega_b^2}{\omega_b^2 + \Omega^2}, \tag{6.13}$$

which has the nice property that it is smooth and nonsingular for all frequencies, and does not give extra artificial features in the result.

6.3.2 The Critical Glue Model

Now we will start to consider the new models proposed for quantum critical metals that go beyond the conventional Fermi liquid BCS theory. In this subsection, we will present one class of scenarios that attribute the novelty of unconventional superconductivity in such systems to the peculiar behavior of the glue when approaching the QCP. The glue part is assumed to become critical near the QCP, while the electronic part is still kept a conventional fermion bubble, though with self-energy corrections. We will call such scenarios the critical glue model.

This class of scenarios are arguably best represented by the models introduced by Chubukov and collaborators [284], where they assume that pairing is mediated by a gapless boson, and the pairing interaction is of the power-law form

$$\lambda(i\Omega) = \left(\frac{\Omega_0}{|\Omega|}\right)^{\gamma}. \tag{6.14}$$

Here the exponent γ parameterizes the different models, and it is usually assumed to take values between 0 and 1. For example, an antiferromagnetic QCP gives rise to a pairing interaction with $\gamma = 1/2$, and a ferromagnetic QCP has $\gamma = 1/3$. The pairing interaction has a singular frequency dependence, which makes the pairing problem in such models qualitatively different from that of the Fermi liquid BCS model. The coupling strength is absorbed in the single scale-full parameter Ω_0.

The electronic part of the pair susceptibility is assumed to be still just the convolution of the single particle Green's functions, i.e., of the same form as Eq. (6.7). But now the massless boson also contributes a nontrivial self-energy, $\Sigma(i\omega_n) = i\omega_n \left(\Omega_0/|\omega_n|\right)^{\gamma} S(\gamma, n)$, where $S(\gamma, n) = |n + 1/2|^{\gamma-1} \left[\zeta(\gamma) - \zeta(\gamma, |n + \frac{1}{2}| + \frac{1}{2})\right]$, with $\zeta(\gamma)$ the Riemann zeta function and $\zeta(\gamma, n)$ the generalized Riemann zeta

function. Let us define $Z(\omega_n) = 1 + (\Omega_0/|\omega_n|)^\gamma S(\gamma, n)$. The bare pair susceptibility thus reads

$$\chi_{p,0}(i\Omega) = \frac{T}{N}\sum_{\mathbf{k},\nu_n} \frac{1}{-i\nu_n Z(-\nu_n) - \xi_{\mathbf{k}}} \frac{1}{i(\nu_n+\Omega)Z(\nu_n+\Omega) - \xi_{\mathbf{k}}}. \tag{6.15}$$

And the corresponding bare vertex operator becomes

$$\Gamma_0(i\nu_n, i\Omega) = \frac{2T}{\omega_c[(\nu_n+\Omega)Z(\nu_n+\Omega) + \nu_n Z(-\nu_n)]} \times \\ [\theta((\nu_n+\Omega)Z(\nu_n+\Omega)) - \theta(-\nu_n Z(-\nu_n))]\,. \tag{6.16}$$

With the glue becoming critical, the only scale in such models is Ω_0. And the superconducting transition temperature is proportional to Ω_0, with a model-dependent coefficient, $T_c = A(\gamma)\Omega_0$.

6.3.3 Quantum Critical BCS

In this subsection we will consider another scenario for superconductivity in quantum critical metals, which is orthogonal to the critical glue mode presented in the last subsection. In this approach, the novelty of unconventional superconductivity in such systems is attributed solely to the critical behavior of the electronic part, with the glue part assumed featureless. Hereafter this approach will be dubbed quantum critical BCS (QCBCS) scenario [121].

According to its behavior in the scaling limit, the electronic part of the pair susceptibility $\chi_{p,0}$ was classified into three different categories: marginal, relevant and irrelevant. The prototype of the marginal case is the free Fermi gas, for which the imaginary part of the bare pair susceptibility $\chi''_{p,0}$ is essentially constant at low temperatures. In the QCBCS scenario, the quantum critical metals were assumed to fall into another category tagged as relevant, i.e., $\chi''_{p,0}$ increases when going to lower frequency or lower temperature. More spectral weight is accumulated at lower energy scales, where pairing is more effective. Thus it is much easier to get superconductivity in such models. The gap equation becomes algebraic, and even a weak glue can give rise to a high temperature superconductor. The basic logic behind such construction is the empirical fact the quantum critical metals are more susceptible than Fermi liquid metals. When approaching the QCP, an interaction that was deemed irrelevant initially, takes over and dominates, replacing the QCP by a new stable phase.

A massless boson, as was considered in the critical glue model, modifies the electronic part of the pair susceptibility through self-energy corrections, giving a nice example of an irrelevant pair susceptibility, i.e., $\chi''_{p,0}$ decreases when going to lower frequency or lower temperature. We emphasize that this does not necessarily imply that the critical glue model is ineffective in producing pairing. The massless boson is providing self-energy corrections to single particle Green's

functions and inducing an attractive interaction between electrons at the same time. The two effects compensate, and it is actually possible to produce a high transition temperature.

Coming back to the QCBCS scenario, at zero temperature, the imaginary part of the bare pair susceptibility has the scaling form $\chi''_{p,0}(\omega) \sim \omega^{-\alpha_p}$, with the exponent α_p parameterizing different models; $\alpha_p = 0$, i.e., $\chi''_{p,0}(\omega)$ constant, corresponds to the marginal case. When $\alpha_p > 0$, $\chi''_{p,0}$ increases at lower frequency, describing a relevant pair susceptibility; $\alpha_p < 0$ corresponds to the irrelevant case.

Aiming at the dynamical pairing susceptibility, let us now consider the QCBCS scenario at finite temperature. Temperature breaks conformal invariance and in the euclidean formulation of field theory the imaginary time direction is compactified, leading to the finite size scaling form of the bare pair susceptibility,

$$\chi_{p,0}(\omega, T) = \frac{Z}{T^{\alpha_p}} \mathcal{F}\left(\frac{\omega}{T}\right), \tag{6.17}$$

with the exponent $0 < \alpha_p < 1$, Z a UV renormalization constant and $\mathcal{F}$ a scaling function. The upper bound on α_p stems from unitarity requirements. At zero temperature, this turns into the branch cut as shown above, $\chi_0 \sim \omega^{-\alpha_p}$, while in the opposite high temperature or hydrodynamical regime ($\hbar\omega \ll k_B T$) it takes the form

$$\chi_{p,0}(\omega, T) = \frac{Z'}{T^{\alpha_p}} \frac{1}{1 - i\omega\tau_{\rm rel}}, \tag{6.18}$$

where $\tau_{\rm rel} \approx \hbar/k_B T$.

One example of such a scaling function $\mathcal{F}(\omega/T)$ that possesses the above two limiting forms at low and high temperatures is the following one, borrowed from exact solutions in $1+1$-dimensional conformal field theory,

$$\mathcal{F}''(y) = \sinh(\frac{y}{2}) B^2(s + i\frac{y}{4\pi}, s - i\frac{y}{4\pi}), \tag{6.19}$$

where B is the Euler beta function, and $s = 1/2 - \alpha_p/4$. Another example that results in such a scaling function is a simple generalization of the free fermion vertex operator (6.9),

$$\Gamma_0(i\nu_n, i\Omega) = \frac{(1-\alpha)T}{\omega_c^{1-\alpha} \mathrm{sgn}(\tilde{\nu}_{\rm n}) |\tilde{\nu}_n|^{\alpha+1}} \left[\theta(\frac{\Omega}{2} + \tilde{\nu}_n) - \theta(\frac{\Omega}{2} - \tilde{\nu}_n)\right]. \tag{6.20}$$

One can check that this vertex operator actually leads to a relevant pair susceptibility with $\alpha_p = \alpha$, a power-law tail at high frequency, and the linear hydrodynamic behavior at low frequency. There is a peak at frequencies of order the temperature. We will use this latter one to calculate the full pair susceptibility.

Combining the BCS-type pairing interaction (6.10) and the above vertex operator (6.20) one arrives at an algebraic gap equation characteristic of the QCBCS scenario,

$$1 - 2g \frac{1-\alpha_p}{\omega_c^{1-\alpha_p}} \int_{T_c}^{\omega_b} \frac{d\nu}{\nu^{\alpha_p+1}} = 0, \tag{6.21}$$

As in the Fermi liquid BCS case, we will also use the smooth and nonsingular pairing 'Einstein phonon' interaction (6.13) to calculate the dynamical pair susceptibility in the QCBCS scenario.

6.4 Holographic superconductors

The three different models we considered in the last section all assume the separation of the electronic part and the glue part. There also exist another class of models for which superconductivity is "glueless" and instead driven by the extreme instability of the zero temperature critical state itself. This class of models are based upon the AdS/CFT correspondence of string theory and are called "holographic superconductors" (HS). The simplest model to obtain a holographic superconductor with quite similar behavior to real superconductors was first built in [285, 290] through Einstein gravity which is minimally coupled to a Maxwell field and a charged complex scalar with a potential term. The system is described by the action

$$\mathcal{S}=\int d^4x\sqrt{-g}\Big[R+\frac{6}{L^2}-\frac{1}{4}F_{\mu\nu}F^{\mu\nu}-m^2\Psi^*\Psi-(\nabla^\mu\Psi-iqA^\mu\Psi)^*(\nabla_\mu\Psi-iqA_\mu\Psi)\Big]. \tag{6.22}$$

Here we consider the superconductor to be 2+1 dimensional. A generalization to 3+1 dimension is straightforward.

Below some critical temperature T_c, the charged black hole solutions develop a nonzero static scalar field outside the horizon, which is usually called a nontrivial hair. There are two possible reasons for this instability on the gravity side. One is that the effective mass for the scalar field is $m^2_{\text{eff}}=m^2+q^2g^{tt}A_t^2$. Since the last term is negative, there is a chance that m^2_{eff} becomes sufficiently negative near the horizon to destabilize the scalar field. Furthermore, as one lowers the temperature of a charged black hole, it becomes closer to extremal which means that g_{tt} is closer to developing a double zero at the horizon. So at low temperatures, $|g^{tt}|$ is large and instability becomes strong. Another reason for the instability comes from the fact that at low temperatures the horizon geometry of the near extremal RN black hole has an AdS_2 near-horizon throat. Then an asymptotically stable negative mass squared scalar field can become unstable because the Breitenlohner-Freedman (BF) bound is different for the near horizon AdS_2 and the asymptotic AdS_4. This gives the chance that we can have the condensate even for uncharged scalar field with $q=0$.

The combined effects of these two mechanisms lead the charged black holes to develop scalar hair at low temperatures. According to the AdS/CFT dictionary, on the dual field theory side there is a global U(1) symmetry which corresponds to the U(1) gauge symmetry on the gravity side. From the point of view of the dual field theory, this $U(1)$ symmetry is broken below T_c at a finite charged density because of the condensation of the charged scalar. The complex scalar Ψ

corresponds to the scalar operator of the order parameter $\mathcal{O}$ of the dual field theory. In the following, we focus on the normal state of holographic superconductor which is described by RN-AdS black hole

$$ds^2 = -f(r)dt^2 + \frac{dr^2}{f(r)} + r^2(dx^2+dy^2), \tag{6.23}$$

$$f(r) = r^2 - \frac{1}{r}\left(r_+^3 + \frac{\rho^2}{4r_+}\right) + \frac{\rho^2}{4r^2}, \tag{6.24}$$

$$A = \rho\left(\frac{1}{r_+} - \frac{1}{r}\right)dt, \tag{6.25}$$

The black hole is characterized by two parameters, the location of the horizon r_+ and the charge density ρ. They are related to the mass and charge of RN-AdS black hole respectively. The Hawking temperature of the black hole, which is identified as the temperature of the dual field theory in the AdS/CFT duality, is $T = (3r_+/4\pi)[1-\rho^2/(12r_+^4)]$. When $r\to\infty$, $A_t \to \mu - \rho/r$. Here μ and ρ are identified as the chemical potential and the charge density of the dual field theory respectively. In the following, we fix the charge density to be $\rho_0 = 1$.

Since the dual operator of Ψ is the order parameter, the two-point retarded Green's function of the dual operator for the fluctuation of Ψ gives the pair susceptibility,

$$\chi(\mathbf{k},\omega) = G^R_{\mathcal{O}^\dagger\mathcal{O}}(\mathbf{k},\omega). \tag{6.26}$$

We will calculate the two-point retarded Green's function for the fluctuation of Ψ in the normal phase above the transition temperature T_c, i.e. our calculation is in the RN-AdS black hole background. We consider the zero momentum mode of $\delta\Psi$ and expand it as $\delta\Psi(r,x,t) = \psi(r)e^{-iwt}$. The equation of motion for $\psi(r)$ is

$$\psi'' + \left(\frac{f'}{f} + \frac{2}{r}\right)\psi' + \left(\frac{(w+qA_t)^2}{f^2} - \frac{m^2}{f}\right)\psi = 0. \tag{6.27}$$

Since we are interested in the retarded Green's function, we impose the infalling boundary condition in the near horizon geometry [291], i.e.

$$\psi(r) \simeq (r-r_+)^{-i\frac{w}{4\pi T}} \quad \text{as } r\to r_+. \tag{6.28}$$

Near the boundary, the scalar field goes as

$$\psi(r) \simeq \frac{\psi_-}{r^{\triangle_-}} + \frac{\psi_+}{r^{\triangle_+}} \quad \text{as } r\to\infty, \tag{6.29}$$

where $\triangle_\pm = \frac{3}{2} \pm \nu$ with $\nu = \sqrt{9+4m^2}/2$.

In 3+1 dimensional gravity theory in asymptotical AdS_4 spacetime, the BF bound for the scalar is $m^2 \geq -9/4$, so ν is always non-negative. For $\nu = 0$, the two terms $\psi_\pm$ will be degenerate and a new logarithmic term appears. We will not consider this case for simplicity. For $\nu \in (0,1]$, both modes $\psi_\pm$ are

normalizable. We can choose either ψ_+ or ψ_- as the source and treat the other as the corresponding response, and the dual operators are $\mathcal{O}_-$ and $\mathcal{O}_+$ respectively. We can calculate the retarded Green's function for the two operators respectively [291, 292],

$$G^R_{\mathcal{O}^\dagger_- \mathcal{O}_-} \sim \frac{\psi_-}{\psi_+}, \qquad G^R_{\mathcal{O}^\dagger_+ \mathcal{O}_+} \sim \frac{\psi_+}{\psi_-}. \tag{6.30}$$

When $w/T \to \infty$, the Green's function approaches the form in pure AdS_4 spactime, i.e. $G^R_{\mathcal{O}^\dagger_- \mathcal{O}_-} \sim 1/w^{2\nu}$ and $G^R_{\mathcal{O}^\dagger_+ \mathcal{O}_+} \sim w^{2\nu}$. For $\nu > 1$, only ψ_+ is normalizable. We can only take ψ_- as the source and treat ψ_+ as the corresponding response. The dual operator is $\mathcal{O}_+$ and we can calculate the retarded Green's function for it as above.

We notice from the equation of motion (6.27) and the infalling boundary condition (6.28) for ψ, the holographic superconductor has the symmetry $\chi_q(\omega) = \chi^*_{-q}(-\omega)$. For $q \neq 0$, one generally has $\chi''_q(\omega) \neq -\chi''_q(-\omega)$, and only for very high temperatures, the symmetry $\chi''(\omega) = -\chi''(-\omega)$ is restored. For the three models we considered in the last section, one always has $\chi''(\omega) = -\chi''(-\omega)$. We regard this as an artifact of the present minimal model of holographic superconductors. It would be interesting to see how the particle-hole symmetry can emerge in such holographic models.

6.5 Evolution of the full pair susceptibility

Using a SIN tunneling junction, experimentalists can measure the imaginary part of the full dynamical pair susceptibility χ''_p in the normal state of the quantum critical metals. In this section we investigate in detail theoretically the temperature and frequency evolution of $\chi''_p(\omega, T)$ for the three different scenarios introduced in the last section. We intend to use these models as templates that can be compared with future experimental results. Let us imagine what the experimentalists will do. They will take a sample, say some heavy fermion compound, tune it to the critical state by applying pressure or doping, scan the tunneling current for various bias voltages at different temperatures, and finally subtract the quasiparticle contributions to get the pair tunneling part. The superconducting transition temperature is fixed for this particular sample. So in our calculation, we will choose some particular sets of parameters, i.e., retardation scale, glue strength, etc., so that the three different models produce the same T_c. The overall magnitude of the measured $\chi''_p(\omega, T)$ depends on the details of the tunneling junction and is therefore difficult to predict on an absolute scale. The good news is that the difference of the various models also lies in the pattern of the relative change of the amplitude with frequency and temperature. So in the following study, we will normalize the amplitude with respect to its value at some particular reference temperature and frequency, and consider the quantity $\chi''_p(\omega, T)/\chi''_p(\omega^*, T^*)$.

For the three models with electron-glue dualism, we have formulated the equations in Matsubara frequency. Generically though, to obtain the real-frequency dynamical pair susceptibility, a crucial step is the analytic continuation, i.e., the replacement $i\Omega \to \omega + i\delta$, which is generally a non-trivial procedure. We choose the method of Padé approximants. Historically the Padé approximant analytic continuation method is based on continued fractions but the method of matrix inversion actually works much faster. Although the Padé approximant method is uncontrolled it seems to work very well in our case, probably because the pair susceptibility is a very smooth function with only a single characteristic peak/feature. Furthermore, our calculation has no statistical noise (it is not quantum Monte-Carlo), and in principle we can improve the precision arbitrarily by (i) increasing matrix size, (ii) increasing numerical precision in all steps, and (iii) increasing the number of Padé points $i\Omega_n$, until computational resources run out.

With the form of $\Gamma_0(i\nu_n; i\Omega)$ and $\lambda(i\Omega)$ specified as in Eqs. (6.8,6.16,6.20) and (6.13,6.14), we proceed to solve the Bethe-Salpeter equation (6.5) for the three different models, using matrix inversion to get $\Gamma(i\nu_n; i\Omega)$. Then we sum over ν_n and arrive at the imaginary frequency pair susceptibility $\chi(i\Omega)$, the analytic continuation of which, by the method of Padé approximants, gives the final result for the dynamical pair susceptibility $\chi_p(\omega)$.

For holographic superconductors, we solve the differential equation 6.27 with the boundary condition 6.28 near the horizon, and then extract the two coefficients $\psi_\pm$ near the boundary. The ratio of the two gives the pair susceptibility.

Figure 6.4 displays the temperature and frequency evolution of the imaginary part of the full dynamical pair susceptibility $\chi_p''(\omega, T)$ for the four different models in a false-color plot. Here the UV cut-off scale is set to $\omega_c \equiv 1$. The exponents, coupling strengths and retardation scales are tuned to give the same $T_c = 0.01$ for all three models with electron-glue dualism. For Fermi liquid BCS, the parameters are $\omega_b = 0.2$, $g = 0.3667545$. For the critical glue model, $\gamma = 1/3$, $\Omega_0 = 0.00267089$ (matrix size is 1000, number of Padé points is 16). For quantum critical BCS, $\alpha = 1/2$, $\omega_b = 0.2$, $g = 0.2131115$. For holographic superconductor, $T_c = 0.1468$. For all the four models, the horizontal axis is normalized with respect to T_c. The labeling ω should be understood as $\omega/(100T_c)$.

There is stunning difference for the four different scenarios. For FLBCS, there is a clear division of a core part and an external part. The core part corresponds to the peak, which dies out quickly away from T_c. The external part comes from the electronic pair susceptibility. Extrapolating the 'external' contours from high temperatures to lower temperatures, one finds that they converge to a single point. This convergence is readily read off from the bare pair susceptibility $\chi_{p,0} \sim \tanh(\omega/4T)$, the contours of which converge to $T = 0$, or $\tau = -1$.

The contours of the full pair susceptibility in QCBCS, HS and CG are all self-similar. However in CG, they are of elliptic shape, which is totally different from the corresponding bare one. This is clear sign that the effects of the critical glue persists even at high temperatures. In QCBCS and HS, the contours of the

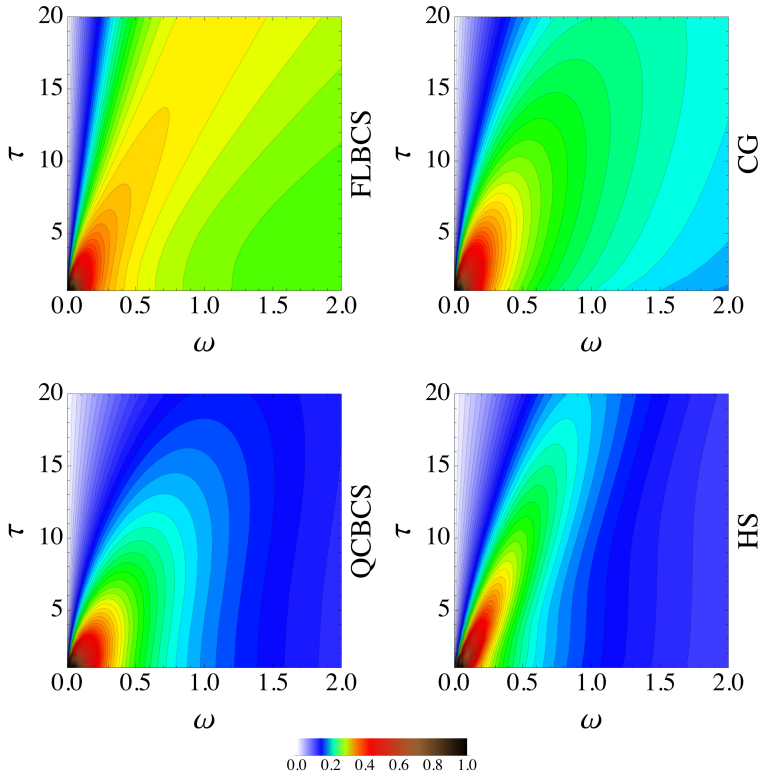

Figure 6.3: The imaginary part of the full pair susceptibility as function of frequency and temperatures for the three different models. Here we plot $\chi''(\omega,\tau)/\chi''(\omega_{\max},\tau=1)$. $\tau=(T-T_c)/T_c$ goes from 1 to 20. Frequency is normalized in terms of T_c, and the horizontal axis represents $\omega/(200T_c)$.

full pair susceptibility have the shape of a mountain with cliff on the right and they are quite similar to those of the bare ones, meaning that the electronic part dominates away from T_c.

Next we will consider linecuts of $\chi_p''(\omega,T)$ at various fixed temperatures. The gross feature is that for all the models considered, except the holographic superconductors with very small charge q, above T_c, $\chi_p''(\omega)$ always has just one peak. As temperature increases, the peak becomes broader, with the peak location moving to higher frequency, and the peak height decreasing. However the different models show subtle differences in the way how the peak changes with temperature. We will proceed to characterize the peak evolution, first near T_c and then away from T_c.

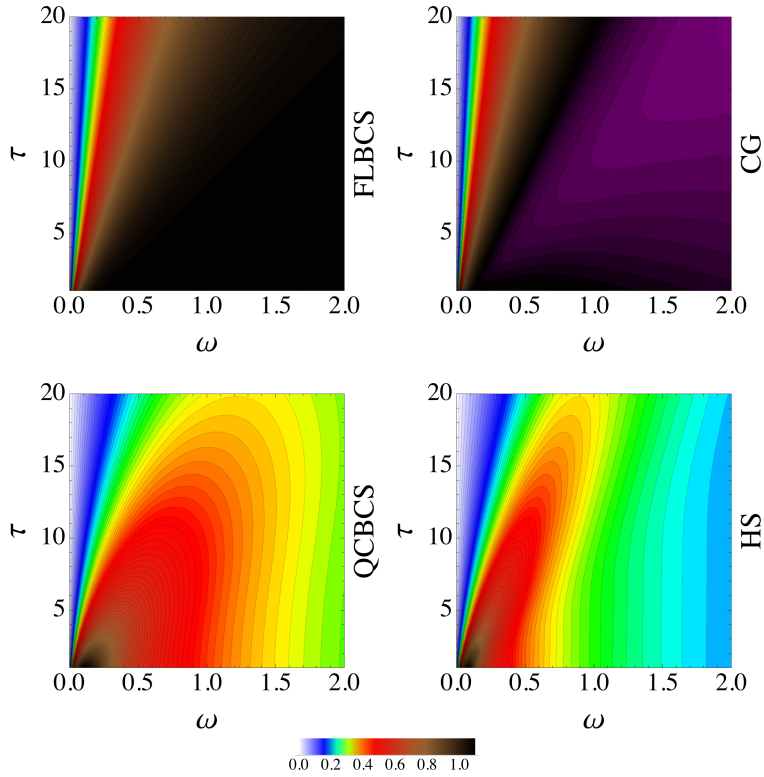

Figure 6.4: The imaginary part of the bare pair susceptibility as function of frequency and temperatures for the three different models. For holographic superconductor, we plot the corresponding result in Schwarzschild-AdS background.

For holographic superconductors with q near zero, we find that on top of the conformal peak, which has its origin from the asymptotic AdS geometry and thus insensitive to temperature, another peak gradually builds up as one approaches T_c. And in the temperature range $T_c < T \lesssim 5T_c$, we observe a peak-dip-hump structure plus the conformal tail at high frequencies.

The behavior of the pair susceptibility near T_c characterizes the nature of the superconducting transition. Here in the three models with electron-glue dualism, aiming at optimally doped cuprates as well as heavy fermion systems, we assume a mean field type transition, ignoring phase fluctuations altogether. The pairing fluctuations near T_c are thus diffusive in nature, and the pair susceptibility has a diffusive pole

$$\chi_p(\omega) \propto -N(0)T_c \frac{1}{i\omega - \tau_{\mathrm{GL}}^{-1}}. \tag{6.31}$$

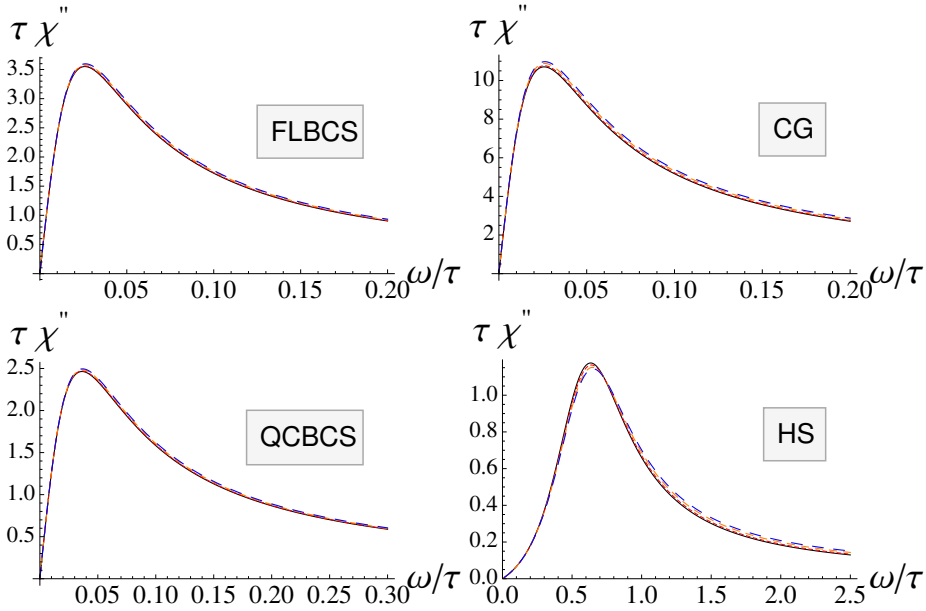

Figure 6.5: Scaling collapse of the imaginary part of the full pair susceptibility near T_c for the four different models: FLBCS, CG, QCBCS and Holographic superconductor. In each figure, we have plotted 4 different temperatures $T/T_c = 1.01, 1.03, 1.07, 1.1$.

Here the characteristic relaxation rate $\tau_{\rm GL}^{-1}$, stemming from pair breaking effects, can be determined from a Ginzburg-Landau calculation [277, 282]. Assuming preformed pairs above T_c would lead to a propagating nature for the pairing fluctuations and thus a different form of $\chi_p(\omega)$. But as already mentioned, we will not consider this possibility here. The proportionality factor in Eq. (6.31) is model dependent and for FLBCS is $8k_B/\lambda^2\pi\hbar$.

The immediate consequence of the diffusive pole in Eq. (6.31) is that near T_c the imaginary part of the pair susceptibility has a quasi-Lorentzian line-shape, i.e., a typical relaxational peak,

$$\chi_p''(\omega) \propto \frac{N(0)}{\tau} \frac{\omega\,\tau_{\rm GL}}{1+(\omega\,\tau_{\rm GL})^2}, \tag{6.32}$$

independent of the particular pairing mechanism. Here we have defined the reduced temperature $\tau = (T - T_c)/T_c$.

The peak evolution thus shows universal quasi-Lorentzian peak behavior near T_c for these three models. The peak location is at $\omega_{\rm max} \simeq \tau_{\rm GL}^{-1} \propto (T - T_c)$, which goes to 0 linearly as $T \to T_c$. The peak height is $\chi''_{p,\rm max} \propto N(0)T_c/(T - T_c)$,

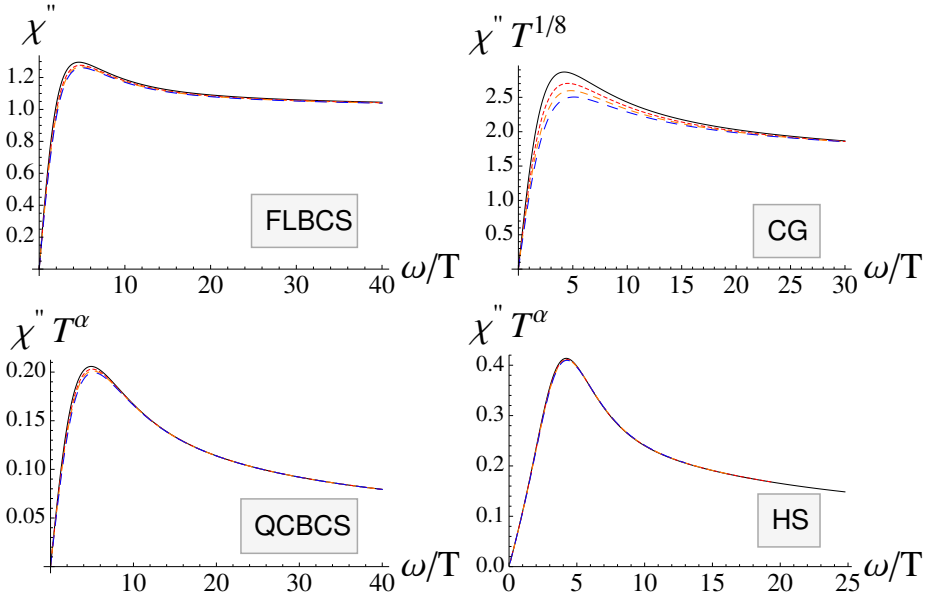

Figure 6.6: Scaling collapse of the imaginary part of the full pair susceptibility at high temperatures for the four different models: FLBCS, CG, QCBCS and holographic superconductor (from top to bottom). In each figure, we have plotted 4 different temperatures: $T/T_c = 11, 14, 17, 21$.

which diverges as $(T - T_c)^{-1}$ when $T \to T_c$. The full width at half maximum of the peak width is $\omega_{\rm wid} = 2\sqrt{3}\,\omega_{\rm max}$, which also vanishes linearly as $T \to T_c$. The fact that peak width and the peak location move together is a robust property of the peak and is used as self consistency check of our numerical calculations.

Above we wrote $\omega_{\rm max} \simeq \tau_{\rm GL}^{-1}$, and this was meant literally: in our numerical results we never find the *exact* relation $\omega_{\rm max} = \frac{8k_B}{\pi\hbar}(T - T_c)$. Instead, we find deviations from this result up to 10 percent for the FLBCS and CG models, and up to factor 3 difference for the QCBCS model. So, although the relaxational peak itself is universal for these three models, the precise location of the peak $\omega_{\rm max}$ does have some model-dependent information. Furthermore, the peak location $\omega_{\rm max}$ can be measured experimentally *without fitting , i.e., parameter free.* Unfortunately, the precise value of $\omega_{\rm max}$ depends also on non-universal parameters such as the glue coupling strengthλ. The only conclusive outcome that may arise is that if $\omega_{\rm max}$ *differs* from $\tau_{\rm GL}^{-1}$ by a factor of 1.5 or more, then the FLBCS and CG models are very improbable.

For holographic superconductor, as one approaches T_c, the pair susceptibility

becomes of the form

$$\chi_p(\omega) = \frac{\chi^{(0)}}{1 - i\omega\tau_1 - \omega\tau_2}, \tag{6.33}$$

where $\chi^{(0)}$ is frequency independent and diverges when approaching T_c. τ_1, τ_2 are real numbers and both of them diverge as $T \to T_c$, $\tau_1 = A_1/(T - T_c), \tau_2 = A_2/(T - T_c)$. The ratio A_1/A_2 is of order 1 even at T_c. In addition to the obvious frequency asymmetry, one can see the difference of the holographic superconductor with the other three models from the shape of the peak at positive frequencies near T_c (Fig. 6.5).

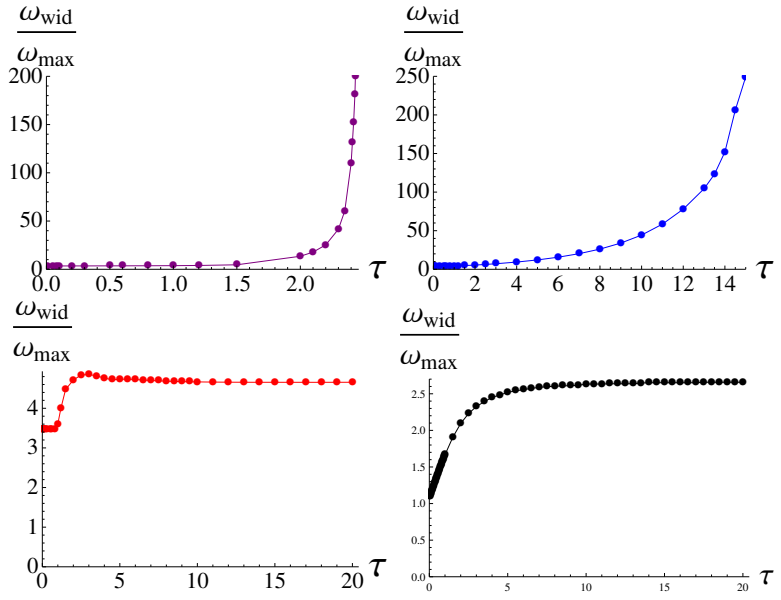

Figure 6.7: Evolution of the ratio of the peak width and peak location for Fermi liquid BCS (top left), Critical Glue (top right), QCBCS (bottom left) and holographic superconductor (bottom right).

Away from T_c, the pair susceptibility probes the normal state properties of the system, revealing the particular underlying pairing mechanisms. Different models give different predictions for the behavior of $\chi_p''(\omega)$ and the pair tunneling measurement can be used to further distinguish between the different models. The results for the four models introduced in the last section are shown in Figs. 6.6, 6.7.

The basic picture is that for the quantum critical BCS and holographic superconductors, the relaxational peak will cross over to the quantum critical peak originated from the electronic part of the pair susceptibility, while for Fermi liquid BCS and critical glue model, the peak simply dies out, and $\chi_p''(\omega)$ becomes

more and more flat at higher and higher temperatures. We plot in Fig. 6.6 the scaling collapse of the pair susceptibility. Scale invariance is spoiled by perturbative corrections in the critical glue model, and it does not have a good scaling collapse. The best-fit exponent actually changes as one fits different frequency ranges. All the other three models do have ω/T scaling. Another obvious feature one can read off from Fig. 6.6 is that the pair susceptibility in QCBCS and HS is more peaky than the other two models.

Such difference can be shown quantitatively by extracting the evolution of the peak location, peak height and peak width. The most revealing quantity is the ratio of the peak width and peak location (Figs. 6.7). For FLBCS and CG, the width and also the ratio grows exponentially at higher temperatures. For QCBCS and holographic superconductors, both the peak width and peak location increases linearly with temperature, and they are locked together again at high temperature, as they were in the region near T_c. We can see clearly in the ratio of the two, the crossover from one region dominated by the relaxational peak to a plateau dominated by the quantum critical peak. The behavior of the peak height in QCBCS and holographic superconductor is also quite different from the other two models. At high temperature, the peak height tends to a constant in FLBCS and CG, while for QCBCS and holographic superconductor it decays as power-law with exponent α_p, $\chi''_{p,\max} \sim T^{-\alpha_p}$. These will be the smoking gun evidences for QCBCS/HS.

6.6 Outlook: towards a realistic experiment

We have proposed to use the the second-order Josephson effect in SIN junctions to measure the pair susceptibility of the quantum critical metals. There are two possible experimental approaches using modern thin-film preparations and STM/STS techniques with a superconducting tip. Recently there has been significant progress employing multi-target pulsed laser deposition (PLD) to grow epitaxial layers of complex (ternary, quarternary , etc.) compounds [283]. Here the grand challenge would be to form a a tunnel junction between a high-temperature superconductor (HTS) and a heavy-fermion superconductor(HFS). For example, as proof of principal we suggest YBCO with $T_c = 90K$ and $CeIrIn_5$ with $T_c = 0.4K$ and the quantum critical region persisting to about 30K, both probably d-wave superconductors. With the enormous spread in transition temperatures one could thereby reach τ-values of about 70 over a wide range of frequencies ω at the lower temperatures. The advantage of HF-$CeIrIn_5$ is that around ambient pressures the superconducting dome is surrounded by regime of quantum critical behavior [293].

A second innovative method, now in development, is the scanning tunneling (STM/STS) measurement which has just been demonstrated as striking effective in probing the gap formations of URu_2Si_2 [294, 295]. We would suggest using a superconducting tip formed from the HTS either by etching down a single crystal

or gluing tiny crystallites of YBCO to a normal Ir or Pt tip. Such scanning experiments have never been attempted between a HTS and the cleaved surface of a HFS, e.g. $CeIrIn_5$, another grand challenge for the heavy fermion community. Stimulated by our pair-susceptibility calculations, we hope the experimentalists will evaluate the above possibilities in their efforts toward novel thin film and tunneling investigations.

Chapter 7

Conclusions

We have been battling with the signful fermions in this thesis. We have not really gotten very far with the microscopic approach. The reformulation of the Anderson-Higgs mechanism for bosonic systems and the understanding of its absence in fermionic systems from the worldline perspective are interesting stories by themselves [Chapter 2]. The Mott-insulator picture of the free fermion nodal structure deepens our understanding of fermionic statistics [Chapter 3]. However, we are still far from a satisfying general understanding of the fermion sign problem. Probably we theorists should be more modest. It can be that there is actually no way to solve the sign problem once and for all. The NP hardness of this problem already tells us that a mathematically rigorous approach is impossible, which is not necessarily bad news: it hints strongly at surprising new discoveries. The task of theorists is thus to find the prototype, be it in the form of a wavefunction, an effective field theory, or even using the language of string theory, to model emergent phenomena.

From this point of view, the natural question to ask is whether the different worldline theories and different nodal structures can serve as prototypes of new forms of matter. A scalar field theory on the worldline represents a bosonic particle. Inclusion of Grassmann fields changes the statistics to become fermionic. Different statistics are encodes in the different field content of the 0+1-dimensional worldline field theory. Along this line of thinking, it would be interesting to see whether it is possible to construct a more complex worldline field theory that can represent fermions without double occupancy, as appears in the t-J model. Such particles have essentially different statistics as compared to conventional fermions. When the extra worldline fields are gapped, they can be integrate out,

leaving us with a normal fermionic particle. In this way the second-order phase transition in the worldline field theory may explain the continuous nature of the transition from the usual fermions to the projected fermions in the t-J model.

In order to understand Mott physics from the worldline formalism, we also need a better way of dealing with the effect of the lattice. The essence of the existence of the lattice is that the number of available states is greatly reduced. This is a necessary condition for the electrons to experience jamming and produce a Mott insulating state. Pictorially the effect of the lattice can be modeled by replacing the point particles by finite size hard core spheres. And the Mott transition corresponds to the jamming transition of such spheres.

A generalization of the 0+1-dimensional worldline field theory to 1+1-dimensional worldsheet would lead to string theory. Having in mind the equivalence of the Anderson-Higgs mechanism and infinite winding, an obvious question to ask is what happens when the strings have long windings. Here one considers a finite density of strings. And to calculate the free energy of this system, one needs to sum over all possible permutations of the initial or finial string configurations. Such a string condensation will backreact to the space-time geometry, and will have important cosmological implications.

We do learn important lessons from wrestling with the fermion nodal structure. The traditional way to understand the different phases of matter is to use symmetry properties of the wave functions. The nodal structure provides a more topological perspective. Wen and collaborators have used the pattern of zeros of the wave functions to characterize the topological order in fractional quantum Hall states [296–298]. There the nodes are at discrete points where two particles coincide. The pattern of zeros describes how fast the wavefunction approaches to zero near the nodes.

The number of nodal cells is an adiabatic invariant for quantum-mechanical systems [299]. We have seen in Chapter 3 that for the Fermi gas, there are two nodal cells. The immediate consequence is that for the Fermi liquid, which can be adiabatically continued to the Fermi gas, there should also be just two nodal cells. This number can be used to characterize the different phases of interacting fermions. In the Mott insulating state, the particles localize and the number of nodal cells is expected to be $N!$, with N the total number of particles. So as the repulsion between the particles increases, and the metallic Fermi liquid ground state is driven to become a Mott insulator, there must be a phase transition in-between to open up more nodal cells. One can imagine that the initial nodal hypersurface becomes more and more wrinkled, as we approach the critical point, and eventually topology changes and more nodal cells are created. At the critical point, the nodal hypersurface has to be scale invariant, thus a fractal structure [229]. This process can happen smoothly, and a second-order phase transition is plausible. It's still not clear to us what is the universality class of this transition. The problem is how to make such intuitive pictures into concrete mathematical equations, and calculate the normal state properties of the system at finite temperatures.

A less ambitious project is to simply do perturbation theory around the Fermi gas. We already have some preliminary results on this problem. The Feynman rules in such first-quantized formalism have been constructed and in principle everything that can be done in the conventional second-quantized formalism can also be done using the worldline language. The partition function and all the correlation functions can be expressed in terms of the N-particle density matrix. The question is what can we learn by doing this. What we can hope for is to write down a sign-free perturbation theory for fermions. From the perturbation corrected density matrix, we can read off the perturbed nodal surface. And then we can carry out the constrained path integral using the new nodal constraints, which will produce a new density matrix. Such a process can be repeated untill the result converges to some fixed point. We can see clearly from this process the difference of the fermionic RG from the usual bosonic RG. The geometric nodal hypersurface provides new dimensions for the parameter space, arising from the constraints on the paths. A natural question to ask at this point is what are the possible fixed-point nodal surfaces. One possible geometry is the one corresponding to free fermions, a $dN-1$-dimensional hypersurface that divides the whole dN-dimensional configuration space into 2 parts. Another possible geometry is the one corresponding to Mott insulators with infinitely large Hubbard U. This fixed-point geometry is simply the whole dN-dimensional space with several discrete points deleted. A more interesting fixed-point geometry is the fractal nodal surface [229]. With such a fractal boundary, one may expect to have "multifractal" behavior in the physical observables, i.e. scaling behavior with a continuous spectrum of exponents.

The macroscopic approach has been more rewarding up to now. The simple scaling theory of superconductivity we proposed for quantum critical metals [Chapter 5] turns out to have surprising connections with other pursuits of strongly correlated electron systems. One such connection is with the numerical work on the two dimensional Hubbard model. The Hubbard model is now accepted as the de facto model for cuprates. Numerical calculations of the Hubbard model strongly support the idea of a finite-doping QCP separating the low-doping region, found to be a non-Fermi liquid, from a higher doping Fermi liquid region. In the vicinity of the QCP, calculations also show that for a wide range of temperatures, the doping and temperature dependence of the single-particle properties are consistent with marginal Fermi liquid behavior. The critical doping seems to be in close proximity to the optimal doping for superconductivity as found both in the context of the Hubbard and t-J models. This proximity already indicates that a QCP enhances pairing, though the detailed mechanism is largely unknown.

We have been working together with Jarrell's group, using the dynamical cluster approximation to understand the proximity of the superconducting dome to the QCP in the Hubbard model [300]. The full pairing susceptibility is decomposed into the bare susceptibility, which is constructed from the dressed one-particle Green's function, and the vertex function. The d-wave channel is found to be the most divergent one. The bare pair susceptibility and the vertex

function are then projected to the d-wave channel. At critical doping, as one lowers the temperature, the magnetic susceptibility saturates, the charge susceptibility is strongly enhanced, and the d-wave pairing susceptibility diverges at a certain temperature. An interesting result is that the d-wave pairing vertex falls monotonically with increasing doping. And it changes smoothly across the critical doping. In contrast, the bare d-wave pairing susceptibility exhibits significantly different features close to and away from the QCP. In the underdoped region, it saturates at low temperatures. In the overdoped region, it displays the normal Fermi liquid type log divergence. However at the critical doping, it diverges more quickly with decreasing temperature, roughly following the power-law behavior $1/\sqrt{T}$. Decomposing the pairing vertex into different channels, it is also found that as the QCP is approached, the pairing originates predominantly from the spin channel. The basic observation of the Hubbard model is that pairing in the critical region is due to an algebraic temperature-dependence of the bare pair susceptibility rather than an enhanced d-wave pairing vertex, supporting our QCBCS picture of superconductivity in such systems.

Another interesting connection is with the newly developed string theoretical approach to condensed matter systems. A class of superconductors have been constructed theoretically, which have a mathematical description in terms of charged black holes with nontrivial 'hair' [285]. This approach is based on the idea of the AdS/CFT correspondence, which states that the strong coupling limit of a gauge theory can be described by a weak coupling gravitational theory in one dimension higher and with negative cosmological constant [123–125]. In the gravitational description, black holes will play the role of temperature. Superconductivity follows from the spontaneous breaking of the U(1) symmetry, i.e. the formation of a non-zero condensate. On the gravity side, such condensates correspond to static non-zero fields outside the black holes, usually called black holes 'hair'. In AdS space, the negative cosmological constant plays the role of a confining box, and the charged particles pair-created from the vacuum via the Schwinger effect will be confined to the region near the horizon, producing the black hole 'hair'. A coupled system of gravity, Maxwell field and a charged scalar is enough to produce a superfluid/superconducting condensate. Due to the asymptotic AdS background, the pairing susceptibility in such models will automatically have a power-law behavior at high frequency. Near zero frequency, it also displays the usual hydrodynamic behavior. So this class of models can be looked upon as a more sophisticated way of incorporating scaling in the presence of superconductivity, along the same line as our QCBCS approach. In Chapter 5, we have used as a toy model the scaling function from 1+1 dimensional CFT. The AdS/CFT approach will provide us with the truly high dimensional scaling functions.

The big theme that emerges from this thesis is the instability of QCPs. It is by now an empirical fact based on experiments that the quantum critical metals are more susceptible than normal metals and superconductors. States of matter that can not be constructed from stable states like normal metals or supercon-

ductors can be built near the QCPs. We still do not have a good theoretical understanding of this fact. The general reasoning is that since the QCP is a highly degenerate state, a tiny perturbation may make it unstable. Chapter 5 of this thesis is based on such logic, where we incorporate this idea in a scaling theory of superconductivity. For the Fermi liquid, the superconducting instability is driven by a marginally relevant four-point interaction between excitations about the Fermi surface. The exponential form of the gap equation follows from the marginal nature of the interaction. One may speculate that in quantum critical metals, the superconducting instability becomes truly relevant, resulting in the algebraic gap equation of Chapter 5.

A more difficult question is, for particular materials which perturbation will finally dominate and determine the fate of the QCP. In many materials, superconductivity seems to be a plausible end of QCPs. We have seen another possibility in Chapter 4 that, in the presence of competing orders, the second-order phase transitions may become first order at low temperatures, with the immediate consequence that spatially modulated inhomogeneous phases are expected to be present near the QCPs. Other examples include the nematic phase around the metamagnetic QCP in the bilayer ruthenate $Sr_3Ru_2O_7$ [93–96]. A better understanding of this problem will provide theoretical guidance for the search for exotic materials in systems involving QCPs.

Bibliography

[1] J. Zaanen, Nature **440**, 1118 (2006).

[2] A. F. M. Imada and Y. Tokura, Rev. Mod. Phys. **70**, 1039 (1998).

[3] H. V. Löhneysen, A. Rosch, M. Vojta, and P. Wölfle, Reviews of Modern Physics **79**, 1015 (2007).

[4] F. Kagawa, K. Miyagawa, and K. Kanoda, Nature **436**, 534 (2005).

[5] S. V. Kravchenko and M. P. Sarachik, Reports on Progress in Physics **67**, 1 (2004).

[6] J. Zaanen, Nature **422**, 569 (2003).

[7] A. Damascelli, Z. Hussain, and Z. Shen, Reviews of Modern Physics **75**, 473 (2003).

[8] S. A. Kivelson, I. P. Bindloss, E. Fradkin, V. Oganesyan, J. M. Tranquada, A. Kapitulnik, and C. Howald, Reviews of Modern Physics **75**, 1201 (2003).

[9] P. Abbamonte, A. Rusydi, S. Smadici, G. D. Gu, G. A. Sawatzky, and D. L. Feng, Nature Physics **1**, 155 (2005).

[10] M. Troyer and U. Wiese, Phys. Rev. Lett. **94**, 17201 (2005).

[11] J. G. Bednorz and K. A. Müller, Z. Phys. B: Condens. Matter **64**, 189 (1986).

[12] P. A. Lee, N. Nagaosa, and X. G. Wen, Rev. Mod. Phys. **78**, 17 (2006).

[13] J. Zaanen, G. A. Sawatzky, and J. W. Allen, Phys. Rev. Lett. **55**, 418 (1985).

[14] F. C. Zhang and T. M. Rice, Phys. Rev. B **37**, 3759 (1988).

[15] N. E. Hussey, J. Phys: Cond. Mat. **20**, 123201 (2008).

[16] C. Jaudet, J. Levallois, A. Audouard, D. Vignolles, B. Vignolle, R. Liang, D. A. Bonn, W. N. Hardy, N. Hussey, L. Taillefer, and C. Proust, Physica B **404**, 354 (2009).

[17] J. Zaanen and B. J. Overbosch, arXiv:0911.4070v1 [cond-mat.str-el] (unpublished).

[18] F. Steglich, J. Aarts, C. D. Bredl, W. Lieke, D. Meschede, W. Franz, and H. Schäfer, Phys. Rev. Lett. **43**, 1892 (1976).

[19] H. R. Ott, H. Rudigier, Z. Fisk, and J. L. Smith, Phys. Rev. Lett. **50**, 1595 (1983).

[20] H. v. Löhneysen, T. Pietrus, G. Portisch, H. G. Schlager, A. Schröder, M. Sieck, and T. Trappmann, Phys. Rev. Lett. **72**, 3262 (1994).

[21] P. Coleman, in *Handbook of Magnetism and Advanced Magnetic Materials*, edited by H. Kronmuller and S. Parkin (John Wiley and Sons, Hoboken, New Jersey, 2007), Vol. 1, p. 95.

[22] S. Doniach, Physica B **91**, 231 (1977).

[23] P. Gegenwart, Q. Si, and F. Steglich, Nature Physics **4**, 186 (2008).

[24] H. Shishido, R. Settai, H. Harima, and Y. Ōnuki, J. Phys. Soc. Jpn. **74**, 1103 (2005).

[25] G. R. Stewart, Rev. Mod. Phys. **73**, 797 (2006).

[26] C. Pfleiderer, Rev. Mod. Phys. **81**, 1551 (2009).

[27] A. A. Abrikosov, L. P. Gorkov, and I. E. Dzayloshinskii, *Methods of Quantum Field Theory in Statistical Physics* (Dover, New York, 1963).

[28] J. van Wezel, J. van den Brink, and J. Zaanen, Physical Review Letters **94**, 230401 (2005).

[29] M. Salmhofer and C. Honerkamp, Progress of Theoretical Physics **105**, 1 (2001).

[30] N. Mannella, W. L. Yang, X. J. Zhou, H. Zheng, J. F. Mitchell, J. Zaanen, T. P. Devereaux, N. Nagaosa, Z. Hussain, and Z. Shen, Nature **438**, 474 (2005).

[31] J. M. Luttinger, Physical Review **119**, 1153 (1960).

[32] M. Oshikawa, Physical Review Letters **84**, 3370 (2000).

[33] S. Weinberg, *The Quantum Theory of Fields* (Cambridge University Press, Cambridge, UK, 2000).

[34] R. P. Feynman, Phys. Rev. **91**, 1291 (1953).

[35] R. P. Feynman, Phys. Rev. **91**, 1301 (1953).

[36] H. Kleinert, *Path Integrals in Quantum Mechanics, Statistics, Polymer Physics, and Financial Markets* (World Scientific, Singapore, 2009).

[37] S. Bund and A. M. J. Schakel, Modern Physics Letters B **13**, 349 (1999).

[38] D. M. Ceperley, Reviews of Modern Physics **67**, 279 (1995).

[39] D. M. Ceperley and E. L. Pollock, Physical Review Letters **56**, 351 (1986).

[40] S. Sachdev, *Quantum Phase Transitions* (Cambridge University Press, New York, 1999).

[41] W. Meissner and R. Ochsenfeld, Naturwissenschaften **21**, 787 (1933).

[42] J. R. Schrieffer, *Theory Of Superconductivity* (Perseus Books, Massachusetts, 1999).

[43] L. N. Cooper, Phys. Rev. **104**, 1189 (1956).

[44] J. Bardeen, L. N. Cooper, and J. R. Schrieffer, Phys. Rev. **108**, 1175 (1957).

[45] J. Bardeen, L. N. Cooper, and J. R. Schrieffer, Phys. Rev. **106**, 162 (1957).

[46] P. W. Anderson, Phys. Rev. **110**, 827 (1958).

[47] P. W. Anderson, Phys. Rev. **130**, 439 (1963).

[48] R. P. Feynman, Phys. Rev. **90**, 1116 (1953).

[49] R. P. Feynman, Phys. Rev. **91**, 1291 (1953).

[50] E. L. Pollock and D. M. Ceperley, Phys. Rev. B **36**, 8343 (1987).

[51] D. M. Ceperley, Rev. Mod. Phys. **67**, 279 (1995).

[52] P. W. Higgs, Phys. Lett. **12**, 132 (1964).

[53] P. W. Higgs, Phys. Rev. **145**, 1156 (1966).

[54] P. W. Higgs, Phys. Rev. Lett. **13**, 508 (1964).

[55] G. 't Hooft and M. J. G. Veltman, Nucl. Phys. **B44**, 189 (1972).

[56] G. 't Hooft, Nucl. Phys. **B33**, 173 (1971).

[57] G. 't Hooft, Nucl. Phys. **B35**, 167 (1971).

[58] S. Weinberg, Phys. Rev. Lett. **19**, 1264 (1967).

[59] S. L. Glashow, J. Iliopoulos, and L. Maiani, Phys. Rev. **D2**, 1285 (1970).

[60] E. Farhi and L. Susskind, Phys. Rept. **74**, 277 (1981).

[61] A. J. Leggett, *The Quantum Liquids: Bose Condensation and Cooper Pairing in Condensed-Matter Systems* (Oxford University Press, Oxford, 2006).

[62] G. C. Wick, A. S. Wightman, and E. P. Wigner, Phys. Rev. **88**, 101 (1952).

[63] A. F. Andreev, Phys. Rev. B **68**, 155419 (2003).

[64] J. Zaanen, F. Kruger, J. H. She, D. Sadri, and S. I. Mukhin, Iranian Journal of Physics Research **8**, 39 (2008).

[65] V. L. Goncharov, Izvestia Akad. Nauk. SSSR **8**, 3 (1944).

[66] V. L. Goncharov, Trans. Amer. Math. Soc. **19**, 1 (1962).

[67] M. R. Schafroth, Phys. Rev. **100**, 463 (1955).

[68] F. A. Berezin and M. S. Marinov, Ann. Phys. **104**, 336 (1977).

[69] C. Schubert, Phys. Rept. **355**, 73 (2001).

[70] P. A. M. Dirac, *Lectures on Quantum Mechanics* (Dover Publications, New York, 2001).

[71] M. Henneaux and C. Teitelboim, *Quantization of gauge systems* (Princeton University Press, Princeton, New Jersey, 1992).

[72] L. Brink, P. Di Vecchia, and P. S. Howe, Nucl. Phys. **B118**, 76 (1977).

[73] D. M. Ceperley, J. Stat. Phys. **63**, 1237 (1991).

[74] D. M. Ceperley, in *Monte Carlo and Molecular Dynamics of Condensed Matter Systems*, edited by K. Binder and G. Ciccotti (Editrice Compositori, Bologna, Italy, 1996).

[75] D. M. Ceperley, Physical Review Letters **69**, 331 (1992).

[76] G. Baskaran and P. W. Anderson, Phys. Rev. B **37**, 580 (1988).

[77] J. B. Kogut, Reviews of Modern Physics **51**, 659 (1979).

[78] J. Zaanen, Z. Nussinov, and S. I. Mukhin, Annals of Physics **310**, 181 (2004).

[79] L. Mitas, Physical Review Letters **96**, 240402 (2006).

[80] M. A. Continentino, *Quantum Scaling in Many-Body Systems* (World Scientific, Singapore, 2001).

[81] H. von Löhneisen, A. Rosch, M. Vojta, and P. Wölfle, Rev. Mod. Phys. **79**, 1015 (2007).

[82] N. D. Mathur, F. M. Grosche, S. R. Julian, I. R. Walker, D. M. Freye, R. K. W. Haselwimmer, and G. G. Lonzarich, Nature **394**, 39 (1998).

[83] S. Sachdev, Rev. Mod. Phys. **75**, 913 (2003).

[84] J. Zhao, Q. Huang, C. de la Cruz, S. Li, J. W. Lynn, Y. Chen, M. A. Green, G. F. Chen, G. Li, Z. Li, J. L. Luo, N. L. Wang, and P. Dai, Nature Mater. **7**, 953 (2008).

[85] R. H. Liu, G. Wu, T. Wu, D. F. Fang, H. Chen, S. Y. Li, K. Liu, Y. L. Xie, X. F. Wang, R. L. Yang, L. Ding, C. He, D. L. Feng, and X. H. Chen, Phys. Rev. Lett. **101**, 087001 (2008).

[86] S. Margadonna, Y. Takabayashi, M. T. McDonald, M. Brunelli, G. Wu, R. H. Liu, X. H. Chen, and K. Prassides, Phys. Rev. B **79**, 014503 (2009).

[87] J. Chu, J. G. Analytis, C. Kucharczyk, and I. R. Fisher, Phys. Rev. B **79**, 014506 (2009).

[88] N. Ni, M. E. Tillman, J. Yan, A. Kracher, S. T. Hannahs, S. L. Bud'ko, and P. C. Canfield, Phys. Rev. B **78**, 214515 (2008).

[89] F. L. Ning, K. Ahilan, T. Imai, A. S. Sefat, R. Jin, M. A. McGuire, B. C. Sales, and D. Mandrus, J. Phys. Soc. Jpn. **78**, 013711 (2009).

[90] D. S. Chow, F. Zamborszky, B. Alavi, D. J. Tantillo, A. Baur, C. A. Merlic, and S. E. Brown, Phys. Rev. Lett. **85**, 1698 (2000).

[91] M. Itoi, M. Kano, N. Kurita, M. Hedo, Y. Uwatoko, and T. Nakamura, J. Phys. Soc. Jpn. **76**, 053703 (2007).

[92] M. Itoi, C. Araki, M. Hedo, Y. Uwatoko, and T. Nakamura, J. Phys. Soc. Jpn. **77**, 023701 (2007).

[93] A. J. S. S. A. Grigera, R. S. Perry, M. Chiao, S. R. Julian, G. G. Lonzarich, S. I. Ikeda, Y. Maeno, A. J. Millis, and A. P. Mackenzie, Science **294**, 329 (2001).

[94] S. A. Grigera, P. Gegenwart, R. A. Borzi, F. Weickert, A. J. Schofield, R. S. Perry, T. Tayama, T. Sakakibara, Y. Maeno, A. G. Green, *et al.*, Science **306**, 1154 (2004).

[95] R. A. Borzi, S. A. Grigera, J. Farrell, R. S. Perry, S. J. S. Lister, S. L. Lee, D. A. Tennant, Y. Maeno, and A. P. Mackenzie, Science **315**, 214 (2007).

[96] A. W. Rost, R. S. Perry, J. Mercure, A. P. Mackenzie, and S. A. Grigera, Science **325**, 1360 (2009).

[97] H. Kee and Y. B. Kim, Phys. Rev. B **71**, 184402 (2005).

[98] A. M. Berridge, A. G. Green, S. A. Grigera, and B. D. Simons, Phys. Rev. Lett. **102**, 136404 (2009).

[99] S. Raghu, A. Paramekanti, E. Kim, R. A. Borzi, S. Grigera, A. P. Mackenzie, and S. A. Kivelson, Phys. Rev. B **79**, 214402 (2009).

[100] W. Lee and C. Wu, Phys. Rev. B **80**, 104438 (2009).

[101] M. H. Fischer and M. Sigrist, Phys. Rev. B **81**, 064435 (2010).

[102] R. Roussev and A. J. Millis, Phys. Rev. B **67**, 014105 (2003).

[103] S. E. Rowley, L. J. Spalek, R. P. Smith, M. P. M. Dean, G. G. Lonzarich, J. F. Scott, and S. S. Saxena, arXiv:0903.1445v1 [cond-mat.str-el] (unpublished).

[104] R. J. Cava, B. Batlogg, J. Krajewski, R. C. Ferrel, L. W. Rupp, A. E. White, W. F. Peck, and T. W. Kometani, Nature **332**, 814 (1988).

[105] L. F. Mattheiss, E. M. Gyorgy, and D. W. Johnson, Phys. Rev. B **37**, 3745 (1988).

[106] S. Pei, J. D. Jorgensen, B. Dabrowski, D. G. Hinks, D. R. Richards, A. W. Mitchell, J. M. Newsam, S. K. Sinha, D. Vaknin, and A. J. Jacobson, Phys. Rev. B **41**, 4126 (1990).

[107] J. B. Goodenough, Phase Transitions **22**, 79 (1990).

[108] P. B. Allen and V. N. Kostur, Z. Phys. B: Condens. Matter **104**, 613 (1997).

[109] I. B. Bischofs, V. N. Kostur, and P. B. Allen, Phys. Rev. B **65**, 115112 (2002).

[110] C. Pfleiderer, J. Phys: Cond. Mat. **17**, S987 (2005).

[111] R. Jaramillo, Y. Feng, J. C. Lang, Z. Islam, G. Srajer, P. B. Littlewood, D. B. McWhan, and T. F. Rosenbaum, Nature **459**, 405 (2009).

[112] S. S. Saxena, P. Agarwal, K. Ahilan, F. M. Grosche, R. K. W. Haselwimmer, M. J. Steiner, E. Pugh, I. R. Walker, S. R. Julian, P. Monthoux, G. G. Lonzarich, A. Huxley, I. Sheikin, D. Braithwaite, , and J. Flouquet, Nature **406**, 587 (2000).

[113] A. Huxley, I. Sheikin, E. Ressouche, N. Kernavanois, D. Braithwaite, R. Calemczuk, and J. Flouquet, Phys. Rev. B **63**, 144519 (2001).

[114] C. Pfleiderer and A. D. Huxley, Phys. Rev. Lett. **89**, 147005 (2002).

[115] T. Graf, J. D. Thompson, M. F. Hundley, R. Movshovich, Z. Fisk, D. Mandrus, R. A. Fisher, and N. E. Phillips, Phys. Rev. Lett. **78**, 3769 (1997).

[116] R. Movshovich, T. Graf, D. Mandrus, J. D. Thompson, J. L. Smith, and Z. Fisk, Phys. Rev. B **53**, 8241 (1996).

[117] S. Kawasaki, M. Yashima, Y. Kitaoka, K. Takeda, K. Shimizu, Y. Oishi, M. Takata, T. C. Kobayashi, H. Harima, S. Araki, H. Shishido, R. Settai, and Y. Onuki, Phys. Rev. B **77**, 064508 (2008).

[118] F. Lévy, I. Sheikin, B. Grenier, and A. D. Huxley, Science **309**, 1343 (2005).

[119] M. Uhlarz, C. Pfleiderer, and S. M. Hayden, Phys. Rev. Lett. **93**, 256404 (2004).

[120] C. Pfleiderer, P. Böni, T. Keller, U. K. Rößler, and A. Rosch, Science **316**, 1871 (2007).

[121] J. She and J. Zaanen, Phys. Rev. B **80**, 184518 (2009).

[122] R. Penrose, Riv. Nuovo Cimento **1**, 252 (1969).

[123] J. Maldacena, Adv. Theor. Math. Phys. **2**, 231 (1998).

[124] E. Witten, Adv. Theor. Math. Phys. **2**, 253 (1998).

[125] S. S. Gubser, I. R. Klebanov, and A. M. Polyakov, Phys. Lett. B **428**, 105 (1998).

[126] S. A. Hartnoll, C. P. Herzog, and G. T. Horowitz, Journal of High Energy Physics **12**, 015 (2008).

[127] S. Sachdev, arXiv:1006.3794v3 [hep-th] (unpublished).

[128] D. Belitz, T. R. Kirkpatrick, and T. Vojta, Rev. Mod. Phys. **77**, 579 (2005).

[129] M. A. Continentino and A. S. Ferreira, Physica A **339**, 461 (2004).

[130] A. S. Ferreira, M. A. Continentino, and E. C. Marino, Sol. St. Comm. **130**, 321 (2004).

[131] A. S. Ferreira, M. A. Continentino, and E. C. Marino, Phys. Rev. B **70**, 174507 (2004).

[132] A. S. Ferreira and M. A. Continentino, J. Stat. Mech. P05005 (2005).

[133] Y. Qi and C. Xu, Phys. Rev. B **80**, 094402 (2009).

[134] A. J. Millis, Phys. Rev. B **81**, 035117 (2010).

[135] S. Coleman and E. Weinberg, Phys. Rev. D **7**, 1888 (1973).

[136] B. I. Halperin, T. Lubensky, and S. K. Ma, Phys. Rev. Lett. **32**, 292 (1974).

[137] Z. Nussinov, I. Vekhter, and A. V. Balatsky, Phys. Rev. B **79**, 165122 (2009).

[138] T. Senthil, A. Vishwanath, L. Balents, S. Sachdev, and M. P. A. Fisher, Science **303**, 1490 (2004).

[139] T. Senthil, L. Balents, S. Sachdev, A. Vishwanath, and M. P. A. Fisher, Phys. Rev. B **70**, 144407 (2004).

[140] E. G. Moon and S. Sachdev, Phys. Rev. B **80**, 035117 (2009).

[141] E. G. Moon and S. Sachdev, arXiv:1005.3312v4 [cond-mat.supr-con] (unpublished).

[142] R. M. Fernandes and J. Schmalian, Phys. Rev. B **82**, 014521 (2010).

[143] J. A. Hertz, Phys. Rev. B **14**, 1165 (1976).

[144] A. J. Millis, Phys. Rev. B **48**, 7183 (1993).

[145] T. Moriya, *Spin Fluctuations in Itinerant Electron Magnetism* (Springer-Verlag, Berlin, New York, 1985).

[146] Y. Zhang, E. Demler, and S. Sachdev, Phys. Rev. B **66**, 094501 (2002).

[147] J. H. Chen, T. C. Lubensky, and D. R. Nelson, Phys. Rev. B **17**, 4274 (1978).

[148] E. Domany, D. Mukamel, and M. E. Fisher, Phys. Rev. B **15**, 5432 (1977).

[149] J. Rudnick, Phys. Rev. B **18**, 1406 (1978).

[150] H. H. Iacobson and D. J. Amit, Annals of Physics **133**, 57 (1981).

[151] J. Cardy, *Scaling and renormalization in Statistical Physics* (Cambridge University Press, Cambridge, UK, 1996).

[152] J. M. Tranquada, B. J. Sternlieb, J. D. Axe, Y. Nakamura, and S. Uchida, Nature **375**, 561 (1995).

[153] Y. Ando, K. Segawa, S. Komiya, and A. N. Lavrov, Phys. Rev. Lett. **88**, 137005 (2002).

[154] N. Doiron-Leyraud, C. Proust, D. LeBoeuf, J. Levallois, J. Bonnemaison, R. Liang, D. A. Bonn, W. N. Hardy, and L. Taillefer, Nature **447**, 565 (2007).

[155] S. A. Kivelson, E. Fradkin, and V. J. Emery, Nature **393**, 550 (1998).

[156] E. Fradkin, S. A. Kivelson, M. J. Lawler, J. P. Eisenstein, and A. P. Mackenzie, arXiv:0910.4166v2 [cond-mat.str-el] (unpublished).

[157] C. de la Cruz, Q. Huang, J. W. Lynn, J. Li, W. R. II, J. L. Zarestky, H. A. Mook, G. F. Chen, J. L. Luo, N. L. Wang, and P. Dai, Nature **453**, 899 (2008).

[158] C. Xu, M. Muller, and S. Sachdev, Phys. Rev. B **78**, 020501(R) (2008).

[159] C. Fang, H. Yao, W. F. Tsai, J. P. Hu, and S. A. Kivelson, Phys. Rev. B **77**, 224509 (2008).

[160] Q. Huang, Y. Qiu, W. Bao, M. A. Green, J. W. Lynn, Y. C. Gasparovic, T. Wu, G. Wu, and X. H. Chen, Phys. Rev. Lett. **101**, 257003 (2008).

[161] C. Krellner, N. Caroca-Canales, A. Jesche, H. Rosner, A. Ormeci, and C. Geibel, Phys. Rev. B **78**, 100504(R) (2008).

[162] J. Yan, A. Kreyssig, S. Nandi, N. Ni, S. L. Bud'ko, A. Kracher, R. J. McQueeney, R. W. McCallum, T. A. Lograsso, A. I. Goldman, and P. C. Canfield, Phys. Rev. B **78**, 024516 (2008).

[163] J. Zhao, W. Ratcliff, J. W. Lynn, G. F. Chen, J. L. Luo, N. L. Wang, J. Hu, and P. Dai, Phys. Rev. B **78**, 140504(R) (2008).

[164] A. I. Goldman, D. N. Argyriou, B. Ouladdiaf, T. Chatterji, A. Kreyssig, S. Nandi, N. Ni, S. L. Bud'ko, P. C. Canfield, and R. J. McQueeney, Phys. Rev. B **78**, 100506(R) (2008).

[165] M. D. Prato, A. Pelissetto, and E. Vicari, Phys. Rev. B **74**, 144507 (2006).

[166] J. M. Kosterlitz, D. R. Nelson, and M. E. Fisher, Phys. Rev. B **13**, 412 (1976).

[167] S. Murakami and N. Nagaosa, J. Phys. Soc. Jpn. **69**, 2395 (2000).

[168] F. Fucito and G. Parisi, J. Phys. A: Math. Gen. **14**, L499 (1981).

[169] D. Belitz and T. R. Kirkpatrick, Phys. Rev. Lett. **89**, 247202 (2002).

[170] P. Jakubczyk, Phys. Rev. B **79**, 125115 (2009).

[171] P. Jakubczyk, W. Metzner, and H. Yamase, Phys. Rev. Lett. **103**, 220602 (2009).

[172] M. Zacharias, P. Wölfle, and M. Garst, Phys. Rev. B **80**, 165116 (2009).

[173] P. C. Hohenberg and J. B. Swift, Phys. Rev. E **52**, 1828 (1995).

[174] K. Yonemitsu, A. R. Bishop, and J. Lorenzana, Phys. Rev. B **47**, 12059 (1993).

[175] M. Garst and A. V. Chubukov, Phys. Rev. B **81**, 235105 (2010).

[176] I. Pomeranchuk, Sov. Phys. JETP **8**, 361 (1958).

[177] P. Phillips and C. Chamon, Phys. Rev. Lett. **95**, 107002 (2005).

[178] W. Kohn and J. M. Luttinger, Phys. Rev. Lett. **15**, 524 (1965).

[179] T. Senthil, Phys. Rev. B **78**, 035103 (2008).

[180] A. Altland and B. Simons, *Condensed Matter Field Theory* (Cambridge University Press, Cambridge, UK, 2006).

[181] I. Herbut, *A Modern Approach to Critical Phenomena* (Cambridge University Press, Cambridge, UK, 2007).

[182] J. Zaanen, Science **319**, 5867 (2008), and references therein.

[183] P. Coleman, C. Pépin, Q. Si, and R. Ramazashvili, J. Phys: Cond. Mat. **13**, 723 (2001).

[184] P. Coleman and A. J. Schofield, Nature **433**, 226 (2005).

[185] S. Paschen, T. Lühmann, S. Wirth, P. Gegenwart, O. Trovarelli, C. Geibel, F. Steglich, P. Coleman, and Q. Si, Nature **432**, 881 (2004).

[186] Q. Si, S. Rabello, K. Ingersent, and J. L. Smith, Nature **413**, 804 (2001).

[187] D. van der Marel, H. J. A. Molegraaf, J. Zaanen, Z. Nussinov, F. Carbone, A. Damascelli, H. Eisaki, M. Greven, P. H. Kes, and M. Li, Nature **425**, 271 (2003).

[188] R. A. Cooper, Y. Wang, B. Vignolle, O. J. Lipscombe, S. M. Hayden, Y. Tanabe, T. Adachi, Y. Koike, M. Nohara, H. Takagi, C. Proust, and N. E. Hussey, Science **323**, 603 (2009).

[189] S. L. Bud'ko, N. Ni, and P. C. Canfield, Phys. Rev. B **79**, 220516 (2009).

[190] J. Zaanen, Phys. Rev. B **80**, 212502 (2009).

[191] C. M. Varma, P. B. Littlewood, S. Schmitt-Rink, E. Abrahams, and A. E. Ruckenstein, Phys. Rev. Lett. **63**, 1996 (1989).

[192] P. Monthoux, D. Pines, and G. G. Lonzarich, Nature **450**, 1177 (2007).

[193] A. V. Chubukov and S. Sachdev, Phys. Rev. Lett. **71**, 169 (1993).

[194] C. M. Varma, Z. Nussinov, and W. van Saarloos, Phys. Rep. **361**, 267 (2002).

[195] N. E. Bonesteel, I. A. McDonald, and C. Nayak, Phys. Rev. Lett. **77**, 3009 (1996).

[196] V. Galitski and S. Sachdev, Phys. Rev. B **79**, 134512 (2009).

[197] A. V. Chubukov and J. Schmalian, Phys. Rev. B **72**, 174520 (2005).

[198] A. V. Chubukov and A. M. Tsvelik, Phys. Rev. B **76**, 100509 (2007).

[199] A. Abanov, A. V. Chubukov, and A. M. Finkel'stein, Euro. Phys. Lett. **54**, 488 (2001).

[200] A. Abanov, A. V. Chubukov, and J. Schmalian, Euro. Phys. Lett. **55**, 369 (2001).

[201] A. V. Chubukov, A. M. Finkel'stein, R. Haslinger, and D. K. Morr, Phys. Rev. Lett. **90**, 077002 (2003).

[202] P. Krotkov and A. V. Chubukov, Phys. Rev. Lett. **96**, 107002 (2006).

[203] P. Krotkov and A. V. Chubukov, Phys. Rev. B **74**, 014509 (2006).

[204] A. Abanov, A. V. Chubukov, and M. R. Norman, Phys. Rev. B **78**, 220507 (2008).

[205] D. V. Khveshchenko and W. F. Shively, Phys. Rev. B **73**, 115104 (2006).

[206] E. G. Moon and S. Sachdev, Phys. Rev. B **80**, 035117 (2009).

[207] Z. Fisk and D. Pines, Nature **394**, 22 (1998).

[208] I. I. Mazin and D. J. Singh, Phys. Rev. Lett. **79**, 733 (1997).

[209] P. Monthoux and G. G. Lonzarich, Phys. Rev. B **59**, 14598 (1999).

[210] D. Fay and J. Appel, Phys. Rev. B **22**, 3173 (1980).

[211] A. Millis, S. Sachdev, and C. M. Varma, Phys. Rev. B **37**, 4975 (1988).

[212] M. Franz and A. J. Millis, Phys. Rev. B **58**, 14572 (1998).

[213] R. Roussev and A. J. Millis, Phys. Rev. B **63**, 140504 (2001).

[214] K. B. Blagoev, J. R. Engelbrecht, and K. S. Bedell, Phys. Rev. Lett. **82**, 133 (1999).

[215] Z. Wang, W. Mao, and K. Bedell, Phys. Rev. Lett. **87**, 257001 (2001).

[216] P. B. Allen and R. C. Dynes, Phys. Rev. B **12**, 905 (1975).

[217] F. Marsiglio and J. P. Carbotte, Phys. Rev. B **33**, 6141 (1986).

[218] J. P. Carbotte, Rev. Mod. Phys. **62**, 1027 (1990).

[219] D. J. Scalapino, E. Loh, and J. E. Hirsch, Phys. Rev. B **34**, 8190 (1986).

[220] L. N. Bulaevskii and M. V. Zyskin, Phys. Rev. B **42**, 10230 (1990).

[221] T. R. Kirkpatrick, D. Belitz, T. Vojta, and R. Narayanan, Phys. Rev. Lett. **87**, 127003 (2001).

[222] K. G. Sandeman, G. G. Lonzarich, and A. J. Schofield, Phys. Rev. Lett. **90**, 167005 (2003).

[223] P. Strack, S. Takei, and W. Metzner, Phys. Rev. B **81**, 125103 (2010).

[224] D. T. Son, Phys. Rev. D **59**, 094019 (1999).

[225] O. V. Dolgov and E. G. Maksimov, Sov. Phys. Usp. **25**, 688 (1982).

[226] O. Dolgov, I. Mazin, A. Golubov, S. Savrasov, and E. Maksimov, J. Phys: Cond. Mat. **20**, 434226 (2008).

[227] R. Combescot, Euro. Phys. Lett. **43**, 701 (1997).

[228] M. Troyer and U. Wiese, Phys. Rev. Lett. **94**, 17201 (2005).

[229] F. Krüger and J. Zaanen, Phys. Rev. B **78**, 035104 (2008).

[230] M. Cubrovic, J. Zaanen, and K. Schalm, Science **325**, 439 (2009).

[231] H. Liu, J. McGreevy, and D. Vegh, arXiv:0903.2477[hep-th] (unpublished).

[232] T. Faulkner, H. Liu, J. McGreevy, and D. Vegh, arXiv:0907.2694[hep-th] (unpublished).

[233] J. R. Schrieffer, *Theory Of Superconductivity* (Perseus Publishing, Massachusetts, 1971).

[234] F. Levy, I. Sheikin, and A. Huxley, Nature Physics **3**, 460 (2007).

[235] A. Balatsky, Philos. Mag. Lett. **68**, 251 (1993).

[236] A. Sudbo, Phys. Rev. Lett. **74**, 2575 (1995).

[237] L. Yin and S. Chakravarty, Int. J. Mod. Phys. B **10**, 805 (1996).

[238] W. Muck and K. S. Viswanathan, Phys. Rev. D **58**, 041901 (1998).

[239] D. Freedman, S. Mathur, A. Matusis, and L. Rastelli, Phys. Lett. B **452**, 61 (1999).

[240] E. D'Hoker and D. Freedman, Nucl. Phys. B **544**, 612 (1998).

[241] H. Liu, Phys. Rev. D **60**, 106005 (1998).

[242] E. D'Hoker and D. Z. Freedman, Nucl. Phys. B **550**, 261 (1998).

[243] E. D'Hoker, D. Z. Freedman, S. D. Mathur, A. Matusis, and L. Rastelli, Nucl. Phys. B **562**, 353 (1999).

[244] G. Chalmers and K. Schalm, Nucl. Phys. B **554**, 215 (1998).

[245] G. Chalmers and K. Schalm, Phys. Rev. D **61**, 046001 (1999).

[246] P. B. Allen, in *Modern Trends in the Theory of Condensed Matter*, edited by A. Pekalski and J. Przystawa (Springer-Verlag, Berlin, New York, 1980).

[247] B. Uchoa and A. H. C. Neto, Phys. Rev. Lett. **98**, 146801 (2007).

[248] N. B. Kopnin and E. B. Sonin, Phys. Rev. Lett. **100**, 246808 (2008).

[249] A. H. C. Neto, Phys. Rev. Lett. **86**, 4382 (2001).

[250] B. Uchoa, G. G. Cabrera, and A. H. C. Neto, Phys. Rev. B **71**, 184509 (2005).

[251] J. Lee, K. Fujita, K. McElroy, J. A. Slezak, M. Wang, Y. Aiura, H. Bando, M. Ishikado, T. Masui, J.-X. Zhu, A. V. Balatsky, H. Eisaki, S. Uchida, and J. C. Davis, Nature **442**, 546 (2006).

[252] A. Damascelli, Z. Hussain, and Z. X. Shen, Rev. Mod. Phys. **75**, 473 (2003).

[253] E. van Heumen, E. Muhlethaler, A. Kuzmenko, H. Eisaki, W. Meevasana, M. Greven, and D. van der Marel, Phys. Rev. B **79**, 184512 (2009).

[254] I. E. Dzyaloshinskii, J. Phys. I France **6**, 119 (1996).

[255] V. Y. Irkhin, A. A. Katanin, and M. I. Katsnelson, Phys. Rev. B **64**, 165107 (2001).

[256] V. Y. Irkhin, A. A. Katanin, and M. I. Katsnelson, Phys. Rev. Lett. **89**, 076401 (2002).

[257] A. N. Rubtsov, M. I. Katsnelson, A. I. Lichtenstein, and A. Georges, Phys. Rev. B **79**, 045133 (2009).

[258] T. Moriya and T. Takimoto, J. Phys. Soc. Jpn. **64**, 960 (1995).

[259] C. Pepin, Phys. Rev. Lett. **94**, 066402 (2005).

[260] J. Custers, P. Gegenwart, H. Wilhelm, K. Neumaier, Y. Tokiwa, O. Trovarelli, C. Geibel, F. Steglich, C. Pépin, and P. Coleman, Nature **424**, 524 (2003).

[261] L. Zhu, M. Garst, A. Rosch, and Q. Si, Phys. Rev. Lett. **91**, 066404 (2003).

[262] J. Zaanen and B. Hosseinkhani, Phys. Rev. B **70**, 060509 (2004).

[263] A. K. Rajagopal and R. Vasudevan, Phys. Lett. **23**, 539 (1966).

[264] R. G. Dias and J. M. Wheatley, Phys. Rev. B **50**, 13887 (1994).

[265] A. J. Schofield, Phys. Rev. B **51**, 11733 (1995).

[266] E. Helfand and N. R. Werthamer, Phys. Rev. B **147**, 288 (1966).

[267] R. Kuchler, N. Oeschler, P. Gegenwart, T. Cichorek, K. Neumaier, O. Tegus, C. Geibel, J. A. Mydosh, F. Steglich, L. Zhu, and Q. Si, Phys. Rev. Lett. **91**, 066405 (2003).

[268] Y. Tokiwa, T. Radu, C. Geibel, F. Steglich, and P. Gegenwart, Phys. Rev. Lett. **102**, 066401 (2009).

[269] N. Kimura, K. Ito, K. Saitoh, Y. Umeda, H. Aoki, and T. Terashima, Phys. Rev. Lett. **95**, 247004 (2005).

[270] Y. Muro, M. Ishikawa, K. Hirota, Z. Hiroi, N. Takeda, N. Kimura, and H. Aoki, J. Phys. Soc. Jpn. **76**, 033706 (2007).

[271] I. Sugitani, Y. Okuda, H. Shishido, T. Yamada, A. Thamizhavel, E. Yamamoto, T. D. Matsuda, Y. Haga, T. Takeuchi, R. Settai, and Y. Ōnuki, J. Phys. Soc. Jpn. **75**, 043703 (2006).

[272] Y. Okuda, Y. Miyauchi, Y. Ida, Y. Takeda, C. Tonohiro, Y. Oduchi, T. Yamada, N. D. Dung, T. D. Matsuda, Y. Haga, T. Takeuchi, M. Hagiwara, K. Kindo, H. Harima, K. Sugiyama, R. Settai, and Y. Ōnuki, J. Phys. Soc. Jpn. **76**, 044708 (2007).

[273] N. Kimura, K. Ito, H. Aoki, S. Uji, and T. Terashima, Phys. Rev. Lett. **98**, 197001 (2007).

[274] R. Settai, Y. Miyauchi, T. Takeuchi, F. Lévy, I. Siieikin, and Y. Onuki, J. Phys. Soc. Jpn. **77**, 073705 (2008).

[275] Y. Tada, N. Kawakami, and S. Fujimoto, Phys. Rev. Lett. **101**, 267006 (2008).

[276] R. A. Ferrell, J. Low Temp. Phys. **1**, 423 (1969).

[277] D. J. Scalapino, Phys. Rev. Lett. **24**, 1052 (1970).

[278] J. T. Anderson and A. M. Goldman, Phys. Rev. Lett. **25**, 743 (1970).

[279] H. Takayama, Prog. Theor. Phys. (Japan) **46**, 1 (1971).

[280] K. Yoshihiro and K. Kajimura, Phys. Lett. **32A**, 71 (1970).

[281] A. M. Goldman, Journal of Superconductivity and Novel Magnetism **19**, 317 (2006).

[282] A. Larkin and A. Varlamov, *Theory of Fluctuations in Superconductors* (Oxford University Press, Oxford, 2005).

[283] N. Bergeal, J. Lesueur, M. Aprili, G. Faini, J. P. Contour, and B. Leridon, Nature Physics **4**, 608 (2008).

[284] E.-G. Moon and A. Chubukov, Journal of Low Temperature Physics **161**, 263 (2010).

[285] S. A. Hartnoll, C. P. Herzog, and G. T. Horowitz, Phys. Rev. Lett. **101**, 031601 (2008).

[286] G. E. Blonder, M. Tinkham, and T. M. Klapwijk, Phys. Rev. B **25**, 4515 (1982).

[287] Y. Tanaka and S. Kashiwaya, Phys. Rev. Lett. **74**, 3451 (1995).

[288] B. Janko, I. Kosztin, K. Levin, M. R. Norman, and D. J. Scalapino, Phys. Rev. Lett. **82**, 4304 (1999).

[289] P. W. Anderson, Science **316**, 1705 (2007).

[290] S. S. Gubser, Phys. Rev. D **78**, 065034 (2008).

[291] D. T. Son and A. O. Starinets, Journal of High Energy Physics **0209**, 042 (2002).

[292] J. McGreevy, arXiv:0909.0518 [hep-th] (unpublished).

[293] S. Kambe, H. Sakai, Y. Tokunaga, and R. E. Walstedt, Phys. Rev. B **82**, 144503 (2010).

[294] P. Aynajian, E. H. da Silva Neto, C. V. Parker, Y. Huang, A. Pasupathy, J. Mydosh, and A. Yazdani, Proceedings of the National Academy of Science **107**, 10383 (2010).

[295] A. R. Schmidt, M. H. Hamidian, P. Wahl, F. Meier, A. V. Balatsky, J. D. Garrett, T. J. Williams, G. M. Luke, and J. C. Davis, Nature **465**, 570 (2010).

[296] X. G. Wen and Z. Wang, Phys. Rev. B **78**, 155109 (2008).

[297] M. Barkeshli and X. G. Wen, Phys. Rev. B **82**, 24530 (2010).

[298] Y. M. Lu, X. G. Wen, Z. Wang, and Z. Wang, Phys. Rev. B **81**, 115124 (2010).

[299] M. Robnik, Phys. Lett. **80A**, 117 (1980).

[300] S.-X. Yang, H. Fotso, S.-Q. Su, D. Galanakis, E. Khatami, J.-H. She, J. Moreno, J. Zaanen, and M. Jarrell, Phys. Rev. Lett. **106**, 047004 (2011).

Samenvatting

De veel-deeltjessystemen om ons heen, gecreëerd door de natuur of door de mens, bestaan uit elektronen. Elektronen zijn fermionen. De fermionische golffunctie verandert van teken wanneer twee fermionen van plaats verwisseld worden. Dus als we een kwantummechanische som over alle veel-deeltjestoestanden uitvoeren, dan tellen we termen op met zowel positief als negatief teken, en het netto resultaat zal hevig oscilleren. Dit leidt tot het beruchte fermionische mintekenprobleem, dat zo complex is als zijn kan, genaamd niet-deterministisch polynomiaal (NP) moeilijk in wiskundige termen. Het minteken-probleem verhindert in het algemeen een wiskundig exacte oplossing van het veel-deeltjessysteem.

Verrassend genoeg zijn er verscheidene wisselwerkende fermionische systemen, bijvoorbeeld normale metalen en ^{3}He bij lage temperaturen, die op een bevredigende manier beschreven kunnen worden met een fenomenologische theorie van Landau, gebaseerd op de aanname van adiabatische verbondenheid met het vrije Fermi gas. Echter, in de afgelopen decennia is er meer en meer experimenteel bewijs verzameld waarbij het erop lijkt dat het Landau paradigma het begeven heeft en de helse fermionische mintekens vrij spel hebben. Deze exotische materialen bevinden zich meestal nabij een nultemperatuur-faseovergang naar een andere stabiele fase. Geassocieerd met dit singuliere punt worden abnormale schalingseigenschappen voortdurend waargenomen in een eindig gebied van het fasediagram. Dit is de motivatie van het idee van kwantumkritikaliteit, om te proberen de vreemde eigenschappen van het systeem bij eindige temperatuur te beschrijven in termen van lage-energie vrijheidsgraden van de grondtoestand.

In dit proefschrift verkennen we de minteken-volle fermionische wereld. In hoofdstuk 2 en 3 bestuderen we het fermionische minteken-probleem in het wereldlijn padintegraal formalisme, waarin het minteken-probleem het meest transparant is. In hoofdstukken 4 tot en met 6 analyseren we het idee van kwantum kritikaliteit. We leggen de nadruk op de instabiliteiten van de kwantum-kritische punten (KKPen) bij lage temperaturen, alwaar exotische nieuwe fases ontstaan.

In hoofdstuk 2 presenteren we een simpele oefening met minteken-volle wereldlijn-padintegralen. We leggen met behulp van dit formalisme het mechanisme achter het Anderson-Higgs effect voor een gas van geladen bosonen met een achtergrond magnetisch veld uit, and vervolgens gebruiken we deze methode om de afwezigheid van dit effect voor een gas van fermionen te bewijzen.

In dit formalisme wordt de fermionische statistiek gecodeerd door het gebruik van aanvullende Grassmann coördinaten op een manier die leidt tot manifeste wereldlijn-supersymmetrie. Deze extra symmetrie is de spil om de afwezigheid van het effect voor geladen fermionen te demonstreren.

In hoofdstuk 3 beginnen we het fermionische minteken-probleem op te pakken in het wereldlijn-formalisme. Het inzichtelijke werk van Ceperley om fermionische padintegralen the construeren in termen van begrensde wereldlijnen wordt herhaald. In deze representatie worden de mintekens geassocieerd met de Fermi-Dirac statistiek op zelfconsistente wijze vertaald naar een geometrische begrenzingstructuur, het nodale hyperoppervlak, die werkt op een effectieve bosonische dynamica. Werkend met de padintegraal in impuls-ruimte laten we zien het Fermi gas begrepen kan worden door analogie met een Mott isolator in een harmonische val.

In hoofdstuk 4 verkennen we de instabiliteiten van KKPen die ontstaan door competitie tussen de bosonische orde-parameters. De fases nabij KKPen worden verondersteld om of klassiek of kwantummechanisch te zijn en worden aangenomen afstotend te wisselwerken via een kwadraat-kwadraat wisselwerking. We ontdekken dat voor willekeurige dynamische exponent en voor willekeurige dimensionaliteit een voldoende sterke wisselwerking KKPen instabiel maakt, en dat deze de overgangen naar eerste-orde dringt. We stellen voor dat deze instabiliteit en het begin van eerste-orde overgangen leidt tot ruimtelijk inhomogene toestanden in praktische materialen nabij vermoedelijke KKPen.

In hoofdstuk 5 onderzoeken we de instabiliteit van fermionische vrijheidsgraden nabij KKPen. In het bijzonder bestuderen we de instabiliteit in het deeltje-deeltje kanaal, en we presenteren een simpele fenomenologische schalingstheorie voor supergeleiding in kwantumkritische metalen. Onder de aanname dat de normale toestand een sterk-wisselwerkende kwantumkritische toestand van fermionen is, stellen we voor dat de paringssusceptibiliteit relevant wordt, in plaats van de marginale BCS-vorm, met het effect dat de paringsinstabiliteit veel sterker wordt. Zelfs met een zwakke wisselwerking kunnen we een hoge overgangstemperatuur krijgen vergelijkbaar met wat in echte materialen wordt gevonden. We bediscussiëren ook de gedraging van het orbitaal-gelimiteerde hogere kritisch magnetisch veld als functie van de nultemperatuur koppelingsconstante. Vergeleken met de variatie in de overgangstemperatuur zou het kritisch veld een grotere variatie kunnen laten zien afhankelijk van de waarde van de dynamische kritische exponent.

In hoofdstuk 6 stellen we voor om een tweede-orde Josephson-effect te gebruiken als directe detector van het Cooper-kanaal van kwantumkritische metalen, om het probleem van onconventionele supergeleiding in zulke systemen te belichten. Om experimentatoren van sjablonen te voorzien, berekenen we de paringssusceptibiliteit voor verscheidene verschillende scenario's. De evolutie van de piekstructuur in het imaginaire deel van de susceptibiliteit wordt in detail onderzocht. We ontdekken dat modellen die aannemen dat elektronen zich in een kritische normale toestand bevinden substantieel verschillen van het Fermi

vloeistof BCS-model en zijn moderne uitbreidingen.

Summary

The many-body systems around us, created by nature or by humans, consist of electrons. Electrons are fermions. The fermion wavefunction changes sign when any two fermions are interchanged. So when we do a quantum-mechanical summation over all the many-particle states, we are adding terms with both positive and negative signs, and the result will be highly oscillatory. This leads to the infamous fermion sign problem, which is as hard as it can be, called non-deterministic polynomial-time (NP) hard in mathematical terms. The sign problem generally impedes a mathematically exact solution of the many-body systems.

Surprisingly, several strongly interacting fermionic systems, e.g. normal metals and ^{3}He at low temperatures, can be satisfactorily described by a phenomenological theory of Landau based on the assumption of adiabatic connectivity to the free Fermi gas. However more and more experimental evidences are accumulating in the last few decades, pointing towards the breakdown of the Landau paradigm and release of fermion signs from hell. These exotic materials usually lie on the verge of a zero temperature phase transition to another stable phase. Associated with such a singular point, anomalous scaling behaviors are constantly observed in a finite region of the phase diagram. This motivates the idea of quantum criticality, trying to describe the strange finite temperature properties of the system in terms of the low energy degrees of freedom of the ground state at zero temperature.

We explore the signful fermionic world in this thesis. In Chapter 2 and 3, we study the fermion sign problem in the worldline path integral formalism, in which the sign problem is most transparent. In Chapter 4 through 6, we explore the idea of quantum criticality. We focus on the instabilities of the quantum critical points (QCPs) at low temperatures, where exotic new phases appears.

In Chapter 2, we present a simple exercise of the signful worldline path integrals. We explain in this formalism the mechanism behind the Anderson-Higgs effect for a gas of charged bosons in a background magnetic field, and then use the method to prove the absence of the effect for a gas of fermions. In this formalism, the fermionic statistics are encoded via the inclusion of additional Grassmann coordinates in a manner that leads to a manifest worldline supersymmetry. This extra symmetry is key in demonstrating the absence of the effect for charged fermions.

In Chapter 3, we start to tackle the fermion sign problem in the worldline formalism. The insightful work of Ceperley in constructing fermionic path integrals in terms of constrained worldlines is reviewed. In this representation, the minus signs associated with Fermi-Dirac statistics are self consistently translated into a geometrical constraint structure, the nodal hypersurface, acting on an effective bosonic dynamics. Working with the path integral in momentum space, we then show that the Fermi gas can be understood by analogy to a Mott insulator in a harmonic trap.

In Chapter 4, we explore the instabilities of QCPs arising from the competition between the bosonic order parameters. The phases near QCPs are assumed to be either classical or quantum and assumed to repulsively interact via quadratic-quadratic interactions. We find that for any dynamical exponents and for any dimensionality strong enough interaction renders QCPs unstable, and drives transitions to become first order. We propose that this instability and the onset of first-order transitions lead to spatially inhomogeneous states in practical materials near putative QCPs.

In Chapter 5, we explore the instability of the fermionic degrees of freedom near QCPs. In particular, we study the instability in the particle-particle channel, and present a simple phenomenological scaling theory for superconductivity in the quantum critical metals. Asserting that the normal state is a strongly interacting quantum critical state of fermions, we propose that the pairing susceptibility becomes relevant, instead of the BCS marginal form, which has the effect that the pairing instability becomes much stronger. Even with a weak attractive interaction, we can get a high transition temperature comparable to what is found in real materials. We also discuss the behavior of the orbital-limited upper critical magnetic field as a function of the zero-temperature coupling constant. Compared to the variation in the transition temperature, the critical field might show a much stronger variation pending the value of the dynamical critical exponent.

In Chapter 6, we propose to use the second order Josephson effect as a direct probe of the Cooper channel of quantum critical metals, to shed light on the problem of unconventional superconductivity in such systems. To provide templates for experimentalists, we calculate the pair susceptibility for several different scenarios. The evolution of the peak structure in the imaginary part of the susceptibility is investigated in detail. We find that models assuming the electrons are in a critical normal state differ substantially from the Fermi liquid BCS model and its modern extensions.

Publications

1. *Pacifying the Fermi-liquid: battling the devious fermion signs*,
   J. Zaanen, F. Krueger, J.-H. She, D. Sadri, S. I. Mukhin, Iranian Journal of Physics Research **8**, 39 (2008), arXiv:0802.2455 [cond-mat.other][Chapter 3].

2. *Statistics, Condensation and the Anderson-Higgs Mechanism: The Worldline Path Integral View*,
   Jian-Huang She, Darius Sadri, Jan Zaanen, Phys. Rev. B **78**, 144504 (2008) [Chapter 2].

3. *BCS Superconductivity in Quantum Critical Metals*,
   Jian-Huang She, Jan Zaanen, Phys. Rev. B **80**, 184518 (2009)[Editor's Suggestion] [Chapter 5].

4. *Stability of Quantum Critical Points in the Presence of Competing Orders*,
   Jian-Huang She, Jan Zaanen, Alan R. Bishop, Alexander V. Balatsky, Phys. Rev. B **82**, 165128 (2010)[Editor's Suggestion] [Chapter 4].

5. *Proximity of the Superconducting Dome and the Quantum Critical Point in the Two-Dimensional Hubbard Model*,
   S.-X. Yang, H. Fotso, S.-Q. Su, D. Galanakis, E. Khatami, J.-H She, J. Moreno, J. Zaanen, M. Jarrell, Phys. Rev. Lett. **106**, 047004 (2011).

6. *Observing the Origin of Superconductivity in Quantum Critical Metals*,
   J.-H. She, B. J. Overbosch, Y. Liu, Y.-W. Sun, J. A. Mydosh, J. Zaanen, to appear [Chapter 6].

Curriculum Vitae

I was born in Rudong, China, on the 7^{th} of July 1981. After finishing primary school and high school there, I started my undergraduate studies at the Department of Modern Physics, University of Science and Technology of China, in 1999. I majored in theoretical physics, and the diploma work with which I graduated in summer of 2003, "Review of Seiberg-Witten duality in N=2 supersymmetric gauge theories" was supervised by Prof. Si-Cong Jing. During the undergraduate studies, I started to be exposed to research, first in a high energy theory group, where I reviewed the proton spin problem, then in a quantum information group, getting involved in the research of many body entanglement, and finally in a condensed matter theory group, working on the transport problem of semiconductors.

In September 2003, as a master student, I joined the string theory group of Prof. Miao Li at the Institute of Theoretical Physics, Chinese Academy of Science, in Beijing. During my master studies, I worked on the interplay of string theory and cosmology. I published 6 papers and gave several talks about my work both in the institute and in other universities.

In May 2007, I began my Ph.D. studies under the supervision of Prof. Jan Zaanen at the Instituut-Lorentz for theoretical physics in Leiden. This thesis contains the main results of the research during this period. In the summer of 2010, I spent three months working at Los Alamos National Lab in the group of Prof. Sasha Balatsky and Prof. Alan Bishop. As a graduate student, I presented my work through talks and posters at several conferences in the Netherlands, Japan, England and the United States. During my Ph.D, I was twice teaching assistant for a course in condensed matter physics for master students.

Acknowledgements

This thesis would not have been possible without the contributions and encouragements of the many people around me. First I would like to thank my supervisor Jan Zaanen, who has supported me thoughout my thesis with his insight and enthusiasm whilst allowing me the room to work out problems in my own way. I had great fun working with him.

I am indebted to Sergei Mukhin, Sasha Balatsky, Alan Bishop and John Mydosh. Part of this thesis came out of collaborations with them and discussions with them have been wonderful experiences in my life. I would also like to thank Koenraad Schalm and Duncan Haldane, with whom I have had the privilege to work with during my Ph.D study. I enjoyed helpful conversations with David Santiago, Peter Denteneer, Hans van Leeuwen, Bas Edixhoven and Frans Oort.

It is such a great pleasure for me to have this chance thank my collaborators and friends ('comrades'): Frank Krüger, Darius Sadri and Bas Overbosch. We had been working together so enthusiastically on nodes and then on the pair susceptibility problem. I am grateful to all the Stripe Club members: Aron Beekman, Andrej Mesaroš, Daniel Abel, Mihailo Čubrović, Vladimir Juričić, Louk Rademaker, Kai Wu, Yan Liu and Ya-Wen Sun, for creating a productive intellectual atmosphere around me. In particular I thank Daniel Abel for being an active member of the nodal club, and thank Yan Liu and Ya-Wen Sun for contributions to the last chapter of this thesis. Special thanks to Bas Overbosch for translating the summary into Dutch, and Aron Beekman for checking the grammar.

I thank Fran, Marianne and Trudy for the motherly help during the last four years. I thank everybody in Institute Lorentz for making it like a family.

I am grateful to my friends: Xin Wang and Qing-Jing Yang, Jiong-Wei Wang and Xiao-Xun Yang, Jian-Wei Wang and Simon Haller, Lin-Hua Jiang and Hua Pan, Jun-Jun Shan and Hai-Yan Liu, Wei Xu and Ai-Ying He, Jun Wang and Ying Zhao, Jun Wang and Jin-Feng Shen, Guo-Cai Dong and Nan Li, Peng Yang, Keke Liu, Karine Bot, Xi Jin and especially Pang Gong and Xiao Shuaige.

I thank my parents and parents-in-law for their deep love and constant support during my study. I thank my wife Zhen and my daughter Ninyee, without whom all these would have been meaningless.